NASA CR-134810
MDC G5979

DESIGN AND EVALUATION OF THERMODYNAMIC VENT/SCREEN BAFFLE CRYOGENIC STORAGE SYSTEM

Final Report
June 1975

by E. C. Cady

MCDONNELL DOUGLAS ASTRONAUTICS COMPANY
5301 BOLSA AVENUE
HUNTINGTON BEACH, CALIFORNIA 92647

prepared for

NATIONAL AERONAUTICS AND SPACE ADMINISTRATION

NASA Lewis Research Center
Contract NAS3-17801

1. Report No. NASA CR-134810	2. Government Accession No.	3. Recipient's Catalog No
4. Title and Subtitle Design and Evaluation of Thermodynamic Vent/Screen Baffle Cryogenic Storage System		5. Report Date June 1975
		6. Performing Organization Code
7. Author(s) E. C. Cady		8. Performing Organization Report No. MDC G5979
		10. Work Unit No.
9. Performing Organization Name and Address McDonnell Douglas Astronautics Company 5301 Bolsa Avenue Huntington Beach, California 92647		11. Contract or Grant No. NAS 3-17801
		13. Type of Report and Period Covered Final; 1/3/74 to 6/30/75
12. Sponsoring Agency Name and Address NASA Lewis Research Center, Cleveland, Ohio		14. Sponsoring Agency Code
15. Supplementary Notes Project Manager, John C. Aydelott, NASA Lewis Research Center, Cleveland, Ohio.		

16. Abstract

A comprehensive analytical program was performed to compare an integrated thermodynamic vent/screen baffle orbital cryogenic propellant storage and transfer system with other concepts. The screen systems were found to be 20% to 29% lighter in weight than a propulsively accelerated Tug-scale LH_2/LO_2 resupply module. The screen systems were compared with small-scale supercritical storage systems for the Space Shuttle fuel cell reactant and life support system fluid supply and were lighter by up to 556 kg (1225 lb) for the extended 30-day mission. When compared with high-pressure gas storage for the Spacelab atmosphere supply, the screen system saved 79% of the inert system weight for the 30-day mission. An experimental program found that heat flux rates up to 9,450 watts/m^2 (3,000 Btu/hr-ft^2) degraded the LH_2 bubble point performance of eight screens by a maximum of 12.5%. No effects of helium pressurant, screen material, or LH_2 superheat were observed.

17. Key Words (Suggested by Author(s))		18. Distribution Statement	
Cryogenic propellants Propellant acquisition Orbital storage Screen characteristics Thermodynamic vent			
19. Security Classif. (of this report) Unclassified	20. Security Classif. (of this page) Unclassified	21. No. of Pages 172	22. Price*

* For sale by the National Technical Information Service, Springfield, Virginia 22151

NASA-C-168 (Rev. 6-71)

PREFACE

This report was prepared by McDonnell Douglas Astronautics Company under Contract NAS3-17801. The contract is administered by the National Aeronautics and Space Administration, Lewis Research Center, Cleveland, Ohio. The NASA Project Manager for the contract is Mr. John C. Aydelott. This is the final report on the contract and it summarizes the technical effort expended from 3 January 1974 to 30 June 1975.

CONTENTS

SYMBOLS

A, B	Experimentally determined constants
a	Screen surface area to unit volume ratio (1/m)
A	Area (m^2)
b	Screen thickness (m)
C	Constant
C_p	Specific heat at constant pressure (joule/gm-°K)
D	Diameter (m)
e	Roughness dimension (m)
f	Friction factor, $\frac{H_f 2 g_c}{\frac{L}{Dh} V^2}$, $\frac{H \epsilon^2 D g_c}{V^2 Qb}$
F	Thrust (N)
g	Acceleration level (g's)
g_c	Gravitational constant (9.806 m/sec^2)
Gr	Grashof number, $\frac{g \beta \Delta T X^3 \rho^2}{\mu^2}$
h	Heat transfer coefficient (joule/m^2-sec-°K)
H	Head loss (m)
J	Energy conversion factor (0.102 kg-m/joule)
K	Thermal conductivity (joule/m-sec-°K)
L	Length (m)
ℓ	Insulation thickness (m)
N	Number of pleats
Nu	Nusselt number, $\frac{hD}{K}$
P	Power (watt)
Pr	Prandl number, $\frac{C_p \mu}{K}$

PRECEDING PAGE BLANK NOT FILMED

ΔP	Pressure loss (N/m^2)
$\dot{q}$	Heat flux ($watt/m^2$)
Q	Screen tortuosity factor (1.0 for square weave, 1.3 for Dutch weave)
$\dot{Q}$	Volumetric flow rate (m^3/sec), heating rate (watt)
r	Radius (m)
R	Screen radius (m)
Ra	Rayleigh number, Gr • Pr
Re	Reynolds number, $\frac{\rho V D_h}{\mu}$, $\frac{\rho V}{\mu a^2 D}$
S	Annulus spacing, channel height (m)
t	Time (sec)
t, t'	Wall thickness (m)
T	Temperature (°K)
V	Fluid approach velocity (m/sec)
$\overline{V}$	Volume (m^3)
$\dot{W}$	Weight flow rate (kg/sec)
W	Weight (kg)
X	Thickness (m), characteristic dimension (m)
α, β	Experimentally determined constants
Δ	Differential
ϵ	Screen void fraction
η	Efficiency
μ	Viscosity ($N\text{-}sec/m^2$)
ν	Kinematic viscosity (m^2/sec)
ρ	Density (kg/m^3)
σ	Surface tension (dyne/cm), Stefan-Boltzmann constant
ϕ'	Constant in equation (1), reflects deviation of screen pore from ideal circular pore

Subscripts

COND	Conduction
f	Frictional, fluid
h	Hydraulic
HEX	Heat exchanger
i	Inside
j	Mixer jet
RAD	Radiation
s	Through the screen, standpipe
t	Tank
tube	Tube
T	Total

DESIGN AND EVALUATION OF THERMODYNAMIC VENT/SCREEN BAFFLE CRYOGENIC STORAGE SYSTEM

By E. C. Cady
McDonnell Douglas Astronautics Company

SUMMARY

A comprehensive analytical program was performed to compare an integrated thermodynamic vent system (TVS) and wall screen liner (WSL) orbital cryogenic propellant storage and transfer system with other systems. Both a pumped TVS and a cooled-shield TVS, integrated with both a full WSL and a multiple-channel partial WSL, were studied. When compared with a Tug-scale (70.8 m^3 (2,500 ft^3) LH_2 tank and 21.24 m^3 (750 ft^3) LO_2 tank) propulsively accelerated resupply module, the pumped TVS/WSL was 20% lighter and the cooled-shield TVS/partial WSL was 29% lighter for a 3-day coast, 17-hour transfer mission. For a multiple-restart acquisition mission, the cooled-shield TVS/WSL was 8% heavier but potentially more reliable than the propulsively settled restart system.

The screen systems were compared with small-scale (~0.5 m^3) supercritical cryogen storage systems for life support reactant supply, and were up to 40% more efficient in terms of the ratio of delivered reactant to total system weight for 30-day to 200-day orbital coast missions. For the Space Shuttle fuel cell reactant supply system, use of a cooled-shield TVS/WSL saved about 139 kg (306 lb) for the baseline 7-day mission and about 556 kg (1225 lb) for the 30-day extended mission, compared to the current supercritical design.

The screen systems were compared with the high-pressure gas storage system for the Spacelab atmosphere makeup supply. It was found that a cooled-shield TVS/WSL would save 349 kg (700 lb) out of 442 kg (975 lb) of inert system weight for a 30-day mission.

Detail design of a 51-cm (20-inch) diameter LN_2 tank with a full pleated WSL for NASA LeRC Zero-Gravity Facility experiments was accomplished.

An experimental program was performed which studied the effects of heat transfer on the LH_2 bubble point of eight screens ranging from 325 x 2300 to 120 x 120. It was found that heat flux up to 9450 watt/m^2 (3000 Btu/hr-ft^2) resulted in a maximum bubble point degradation of 12.5%. No observable effects of gaseous helium pressurant (compared to GH_2 pressurant), screen material (aluminum compared to stainless steel), or LH_2 superheat were noted.

INTRODUCTION

Future space missions will require cryogenic fluid storage and expulsion subsystems capable of providing efficient long-term subcritical storage, and predictable low-g liquid expulsion for reliable multiple low-g propulsive stage main-engine restarts, auxiliary propulsion, life support systems, and in-orbit propellant transfer. Capillary systems using fine-mesh screens have been developed and shown to control fluid behavior for a wide variety of noncryogenic fluids in orbit (ref. 1). However, to achieve similar expulsion success with cryogenic propellants during orbital storage and transfer, heat and mass transfer effects must also be controlled.

A number of techniques have been proposed to achieve the required thermal control. One concept uses a dual-screen liner and is designed to hold the cryogen off the tank wall to provide liquid-free venting (ref. 2). This approach is relatively heavy and relies on passive gravity-dependent thermal control, which has not been demonstrated in low gravity. Passive systems for thermal control, based on thermodynamic phase conversion and using a wall-mounted heat exchanger, have been proposed to intercept and remove the heat entering the cryogen tank (ref. 3). Active thermodynamic vent systems (TVS), using a pump and compact heat exchanger, have been developed by NASA (refs. 4, 5). Use of a pump entails a potential decrease in system reliability, but results in fluid-dynamic and heat-transfer processes that are not significantly gravity-dependent and which have been satisfactorily demonstrated in ground tests.

Proper integration of a thermodynamic vent system with a single-wall screen liner (WSL) for liquid acquisition could provide a simply constructed, reliable, and proven solution to the problems of low-gravity cryogenic propellant storage, outflow, and resupply. Further, optimization of the thermodynamic vent system and single-wall screen liner configuration and flow characteristics could provide the critically required thermal and fluid dynamic control in the cryogen tank during inflow.

This integrated TVS and WSL acquisition system was studied by McDonnell Douglas Astronautics Company (MDAC) under NASA Contract NAS3-15846 from July 1972 to August 1973 to determine the system fluid dynamic feasibility and general optimum design characteristics for LH_2 at 34.5 N/cm^2 (50 psia) (ref. 6).

The overall system concept studied is shown schematically in Figure 1. The system consists of two major components, a complete WSL and a pump-driven TVS. The annulus between the screen and the tank wall remains full of liquid at all times and serves two functions. First, it provides liquid communication from the outflow line to the bulk propellant in the tank which, although its orientation in the tank is unknown, will certainly be in contact with the tank screen liner because of the wetting characteristics of cryogens. This communication allows outflow and propellant transfer in low gravity. Second, the annulus provides the flow path for pumped cryogen, which absorbs tank incident heating, flows through the standpipe, and rejects the absorbed heat to the TVS.

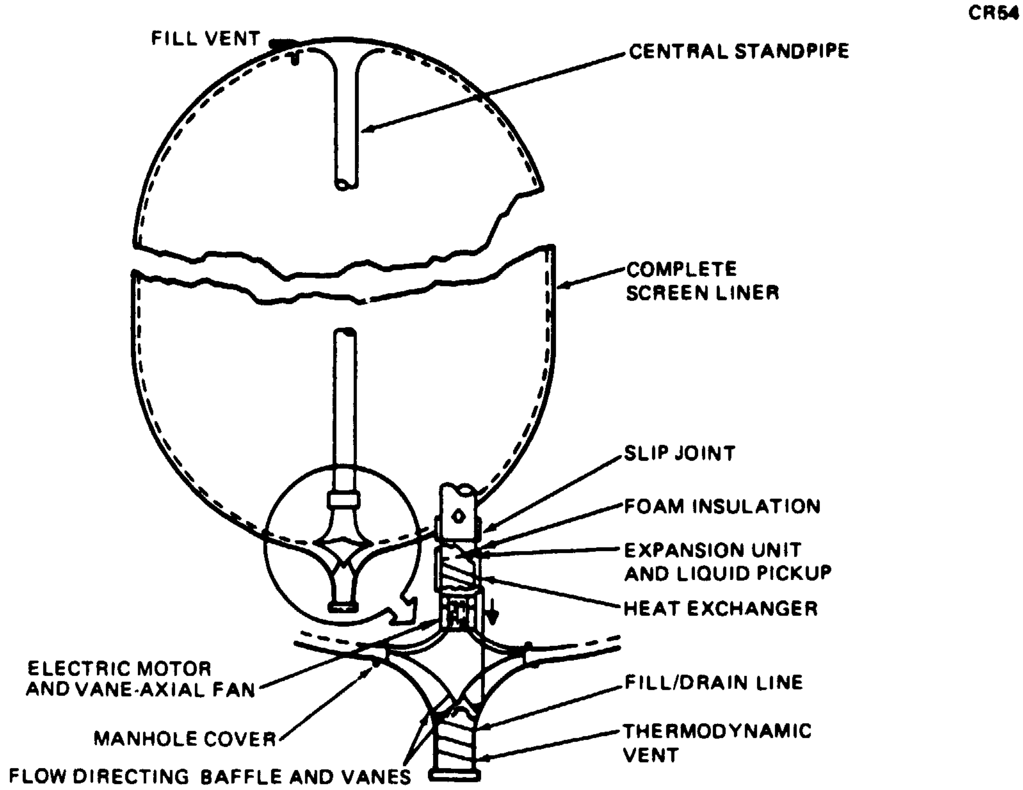

Figure 1. Conceptual Tank Design

The NAS3-15846 study verified that the TVS/WSL system was fluid-dynamically feasible for LH_2 storage at 34.5 N/cm^2 (50 psia), and determined the optimum (lowest system weight) design characteristics for six tanks ranging from 141.6 m^3 (5,000 ft^3) with L/D = 4 to 1.416 m^3 (50 ft^3) with L/D = 1.

The 18-month program described in this report continued the work performed under Contract NAS3-15846 by performing analyses and experiments to determine if the integrated TVS/WSL system was competitive, compared to accelerated or supercritical systems, for orbital LH_2/LO_2 acquisition and transfer systems. The original contract consisted of four tasks plus reporting. Two new tasks were added in September 1974. The six tasks performed under Contract NAS3-17801 are described here.

In Task I, the TVS/WSL storage system was evaluated parametrically for use with liquid oxygen (LO_2) at 34.5 N/cm^2 (50 psia). A range of spherical tank sizes — 0.1416, 1.416, and 14.16 m^3 (5, 50, and 500 ft^3) was optimized for minimum weight using the screen characteristics, correlations, and analyses developed under Contract NAS3-15846 for 30- and 300-day missions with a range of outflow rates, TVS flow rates, and g-levels.

In Task II, three storage and transfer concepts were structurally optimized and compared for both a 70.8-m^3 (2,500-ft^3) LH_2 tank and a 21.24-m^3 (750-ft^3) LO_2 tank for two different storage and transfer missions. These were the TVS/WSL system with either a full or partial WSL, a zero-heat-leak shield/WSL system with either a full or partial WSL, and an acceleration-settled Tug propellant transfer module.

In Task III, three storage and transfer concepts were structurally optimized and compared for LH_2 and LO_2 tanks, each with a capacity of 0.5 m^3 (17.5 ft^3), for 30- and 300-day environmental control and life support (EC/LS) fluid storage and transfer missions. These were the TVS/WSL system with either a full or partial WSL, a zero-heat-leak shield/WSL system with either a full or partial WSL, and a supercritical storage and transfer module.

In Task IV, a 51-cm (20-inch) diameter spherical tank containing screen channels and suitable for testing in the NASA LeRC Zero-Gravity Facility was designed in detail. The design specifications and requirements were defined by NASA and included the requirements that the experimental tank system, containing the screen acquisition system, be interchangeable with an unbaffled tank which is a part of an existing Zero-Gravity Facility experimental test package.

In Task V, thermal/structural optimizations were performed for LH_2 and LO_2 tanks sized to meet the requirements of an advanced manned space transportation system, and an advanced manned space laboratory module for supplying fuel cell reactants and maintaining a habitable environment. The TVS/WSL was designed in sufficient detail to be compared with the Space Shuttle supercritical fuel cell reactant and life support fluid supply system and the Spacelab gaseous nitrogen and oxygen atmosphere supply system, on the basis of weight.

In Task VI, an experimental program using LH_2 was performed to determine the effects of heat transfer and pressurizing gas on the static retention capability of eight screens. Gaseous helium and hydrogen were used as pressurants. A range of heat transfer rates was used to simulate those encountered with warm gas pressurization of cryogenic storage systems employing screen baffles.

This report is not organized by task: rather it is divided into an Analytical Studies section covering Tasks I, II, III, and V, and a Heat Transfer Effects Experimental Study section covering Task VI. The Task IV design effort is described in Appendix A.

ANALYTICAL STUDIES

The basic objective of all of the analysis work described in this section was to compare the TVS/WSL system on the basis of weight with currently accepted methods of orbital storage and transfer such as propulsion-accelerated transfer, supercritical storage, and high-pressure gas. The previous study (Contract NAS8-15846, ref. 6) showed that a significant weight penalty in additional boiloff over long missions may be incurred by the TVS pump, together with potentially decreased reliability. For this reason, the use of a cooled-shield TVS was also analyzed. A cooled shield is a thin metallic shield with attached coolant tubes, which is integrated with a multilayer insulation (MLI) system and completely surrounds the tanks. The shield acts as a boiler for vented liquid and intercepts all of the heat flux to the tank through the MLI; however, heat through heat shorts (supports, plumbing, etc.) may not be intercepted and must be carefully controlled to allow proper TVS operation.

A basic ground rule in these analyses was that the thermal protection system was not changed from the baseline systems, with the exception of the high-pressure gas storage and the cooled-shield systems. For the supercritical systems, cooled shields were already employed, not as boilers, but as gas superheaters. For some of these, modifications were required to the thermal control system to allow proper operation of the cooled-shield TVS, as described below.

Parametric Evaluation of the TVS/WSL for Liquid Oxygen

The analytical tools and computer programs necessary for these analyses were all developed under Contract NAS3-15846 (ref. 6) and were used directly. As in the previous study, it was assumed for this task that each tank was an adiabatic system at 34.5 N/cm^2 (50 psia) with oxygen vapor and liquid as the only contained fluids. The characteristics of the three tankage systems to be studied are shown in Table 1a. Baffle diameters were arbitrarily selected based on the previous study (ref. 6) and resulted in a puddle residual of less than 0.1 percent. Shown in Table 1b are the pertinent properties of 34.5 N/cm^2 LO_2.

The correlations developed for LH_2 under Contract NAS3-15846 were corrected for use with LO_2. The screen bubble points, determined with 34.5 N/cm^2 (50 psia) LH_2, are characterized by the bubble point equation (see symbols list):

$$H = \frac{\phi' \sigma}{g \rho D} \qquad (1)$$

It was assumed that the ϕ' obtained for saturated LH_2 at 34.5 N/cm^2 (50 psia) was appropriate for LO_2 at 34.5 N/cm^2. Since both fluids were saturated cryogens (zero contact angle) with low surface tension values, it was reasonable to assume that their behavior within the screen pores would be similar and that the values of ϕ' would be comparable. The bubble point for LO_2 was, therefore, predicted from the fluid properties of surface tension, σ, and

PRECEDING PAGE BLANK NOT FILMED

TABLE 1a. – TANKAGE SYSTEM CHARACTERISTICS

Tank	Volume $m^3(ft^3)$	L/D	Tank Diameter m(ft)	Baffle Diameter m(ft)	Tank Wall Area $m^2(ft^2)$	Gap Width - cm (in.) for Residual of				
						1%	2%	3%	4%	5%
1	14.16 (500)	1	3.00 (9.85)	0.732 (2.4)	28.3 (305)	0.51 (0.20)	0.99 (0.39)	1.50 (0.59)	2.01 (0.79)	2.52 (0.99)
2	1.416 (50)	1	1.39 (4.57)	0.366 (1.2)	6.1 (65.6)	0.231 (0.091)	0.465 (0.183)	0.696 (0.274)	0.930 (0.366)	1.161 (0.457)
3	0.1416 (5)	1	0.646 (2.12)	0.1525 (0.5)	1.31 (14.1)	0.108 (0.043)	0.216 (0.085)	0.325 (0.128)	0.432 (0.170)	0.541 (0.213)

TABLE 1b. – LO_2 PROPERTIES

At saturation: $34.5\ N/cm^2 = 104°K$ (50 psia = 187°R)
$\rho = 1065\ kg/m^3$ ($66.5\ lb/ft^3$)

$\mu = 0.000146\ N\text{-}sec/m^2$ (0.000098 lb/ft-sec)

$h_{fg} = 1.95 \times 10^5$ joule/kg (84 Btu/lb)

$K = 0.1315$ joule/m-sec-°K (0.075 Btu/hr-ft-°R)

$\sigma = 10$ dyne/cm (0.00069 lb/ft)

density, ρ. The surface tension of LO_2 (ref. 7) was 10 dyne/cm (6.9×10^{-4} lb/ft) at 34.5 N/cm^2. The density of LO_2 (ref. 7) was 1065 kg/m^3 (66.5 lb/ft^3) at 34.5 N/cm^2. Therefore, comparing the static bubble point head, H, for 34.5 N/cm^2 LO_2 with 34.5 N/cm^2 LH_2 gave:

$$H_{LO_2} = \frac{\sigma LO_2}{\sigma LH_2} \frac{\rho LH_2}{\rho LO_2} H_{LH_2} = \frac{10}{1.13} \frac{(64.1)}{(1065)} H_{LH_2} = 0.532\, H_{LH_2} \qquad (2)$$

The values of H_{LO_2} tor the 10 screens previously studied (ref. 6) are shown in Table 2. Reference 8 indicated that these 10 scre~ns were suitable for use in the 3 tanks studied; therefore, these 10 screens were used in this analysis. The screen flow-through loss correlation determined previously (ref. 6) is:

$$H = \alpha \frac{Qba^2}{\epsilon^2 g_c} \frac{\mu}{\rho} V + \beta \frac{Qb}{\epsilon^2 D g_c} V^2 = AV + BV^2 \qquad (3)$$

From equation (3), the head loss parameter, A, varies as μ/ρ (or kinematic viscosity), while B is independent of fluid properties. Thus, comparing A and B for 34.5 N/cm^2 LO_2 with 34.5 N/cm^2 LH_2 gave:

$$A_{LO_2} = \frac{\mu_{LO_2}\, \rho_{LH_2}}{\mu_{LH_2}\, \rho_{LO_2}} A_{LH_2} = \frac{14.6 \times 10^{-5}}{0.96 \times 10^{-5}} \frac{(64.1)}{(1065)} A_{LH_2} = 0.916\, A_{LH_2}$$

$$B_{LO_2} = B_{LH_2} \qquad (4)$$

The channel flow-loss correlation relates friction factor and Reynolds number (both of which already include fluid properties) with a roughness parameter based on the screen shute wire size. Thus, the only correction required of the channel flow (annulus) correlation was inclusion of the proper fluid properties. The values for the screen performance parameters for use with 34.5 N/cm^2 LO_2 are summarized in Table 2.

Analysis of Screen Pore Size and Wall Spacing. – The conditions for which the annulus spacing was studied for each screen in each tank are:

A. Acceleration: 10^{-2}, 10^{-3}, 10^{-4}, and 10^{-5} g.

B. Inflow rate: 1% of tank volume/minute.

C. Outflow rate: 1 and 0.01% of tank volume/minute.

D. Pump-mixer flow rate: 1 and 0.1% of tank volume/minute.

TABLE 2. – SCREEN PERFORMANCE PARAMETERS

Screen	Bubble Point, m (ft) LO_2	Flow-Through Parameters		Roughness, ϵ cm (in.)	Weight kg/m^2 ($lb/100\ ft^2$)
		A	B (ft)		
325 x 2300	0.2562 (0.841)	1.042	0.6919 (2.27)	0.00127 (0.0005)	0.532 (10.9)
200 x 1400	0.1797 (0.589)	0.81	0.6126 (2.01)	0.00203 (0.0008)	0.908 (18.6)
720 x 140	0.094 (0.309)	0.148	0.2627 (0.862)	0.00546 (0.00215)	0.693 (14.2)
165 x 800	0.0653 (0.214)	0.0989	0.0805 (0.264)	0.00254 (0.001)	0.796 (16.3)
50 x 250	0.0363 (0.119)	0.0412	0.0631 (0.207)	0.00572 (0.00225)	1.133 (23.2)
24 x 110	0.0179 (0.0588)	0.0141	0.1554 (0.51)	0.01334 (0.00525)	3.1 (63.5)
500 x 500	0.0876 (0.287)	0.0507	0.04267 (0.140)	0.00254 (0.001)	0.166 (3.4)
150 x 150	0.0245 (0.080)	0.093	0.01347 (0.0442)	0.0066 (0.0026)	0.342 (7.0)
60 x 60	0.0122 (0.0401	0.00535	0.02761 (0.0906)	0.01905 (0.0075)	1.167 (23.9)
40 x 40	0.0090 (0.0297)	0.00263	0.01497 (0.0491	0.0254 (0.01)	1.362 (27.9)

Again, annulus spacings from 1 to 5% of tank volume see Table 1a) and the worst condition of flow were studied. It was shown in ref. 6 that the worst flow condition was outflow against gravity at the maximum flow rate. The analysis described in ref. 6 was used to study each tank, screen, and g-level, resulting in plots of safety factor (ratio of screen bubble point to total flow head losses) as a function of puddle residual. As shown in Figure 2 for the 14.16-m^3 (500-ft^3) tank, the four finest screens had adequate performance (defined as a safety factor of 2) using a 1% annulus at 10^{-2} g's. Seven of the 10 screens showed adequate performance in the 1% annulus at 10^{-3} g's, and the remaining 3 (24 x 110, 60 x 60, and 40 x 40) had adequate performance in the 2% annulus at 10^{-3} g's. For the 1.416-m^3 (50-ft^3) tank, as shown in Figure 3, 6 of the 10 screens had adequate performance in the 1% annulus at 10^{-2} g's, and the remaining 4 had adequate performance in the 1% annulus at 10^{-3} g's.

Figure 4 shows that 7 of the 10 screens had adequate performance in the 0.1416-m^3 (5-ft^3) tank in the 1% annulus at 10^{-2} g's. Two of the 3 remaining screens also had adequate performance at 10^{-2} g's, but with larger annulus gaps (2% for the 24 x 110 and 4% for the 60 x 60). Only the 40 x 40 screen did not have adequate performance at 10^{-2} g's, but would have adequate performance at 10^{-3} g's.

Again, as was the case for the LH_2 tanks (ref. 6), the lightest practical screens, giving adequate performance with minimum screen weight, were the 325 x 2300 and 150 x 150 (see Table 2). Therefore, these two screens were carried along through the pump-mixer and tankage optimization tasks.

Determination of Pump-Mixer Power Requirements. – The same techniques for standpipe optimization and pump-mixer characterization used previously (ref. 6) were used for this study. The hydrostatic head was not included in the total TVS pump power because this head was recovered for TVS flow down the standpipe and the standpipe/pump-mixer optimization was independent of g-level. Definition of the optimum standpipe size is shown as the circles in Figures 5, 6, and 7 for the three tanks and for the two missions and TVS flow rates.

It was shown in the preliminary analysis described in ref. 8 that there was an insignificant difference between an aluminum and a stainless steel standpipe in the LO_2 tank. This was because the high density of LO_2 forced the standpipe residual weight and the pump boiloff weight to be dominant, and the standpipe weight was second-order in effect. Thus, the differences due to standpipe material were minimized. For the final system study discussed in ref. 8, there was only a 4.5-kg (10-lb) weight difference out of 454 kg (1000 lb) total weight (1.0%) for an aluminum standpipe compared to a stainless steel standpipe in the 14.16-m^3 (500-ft^3) tank. Similar results were found for the other tanks. Therefore, only the stainless steel standpipe was studied for the LO_2 tank systems.

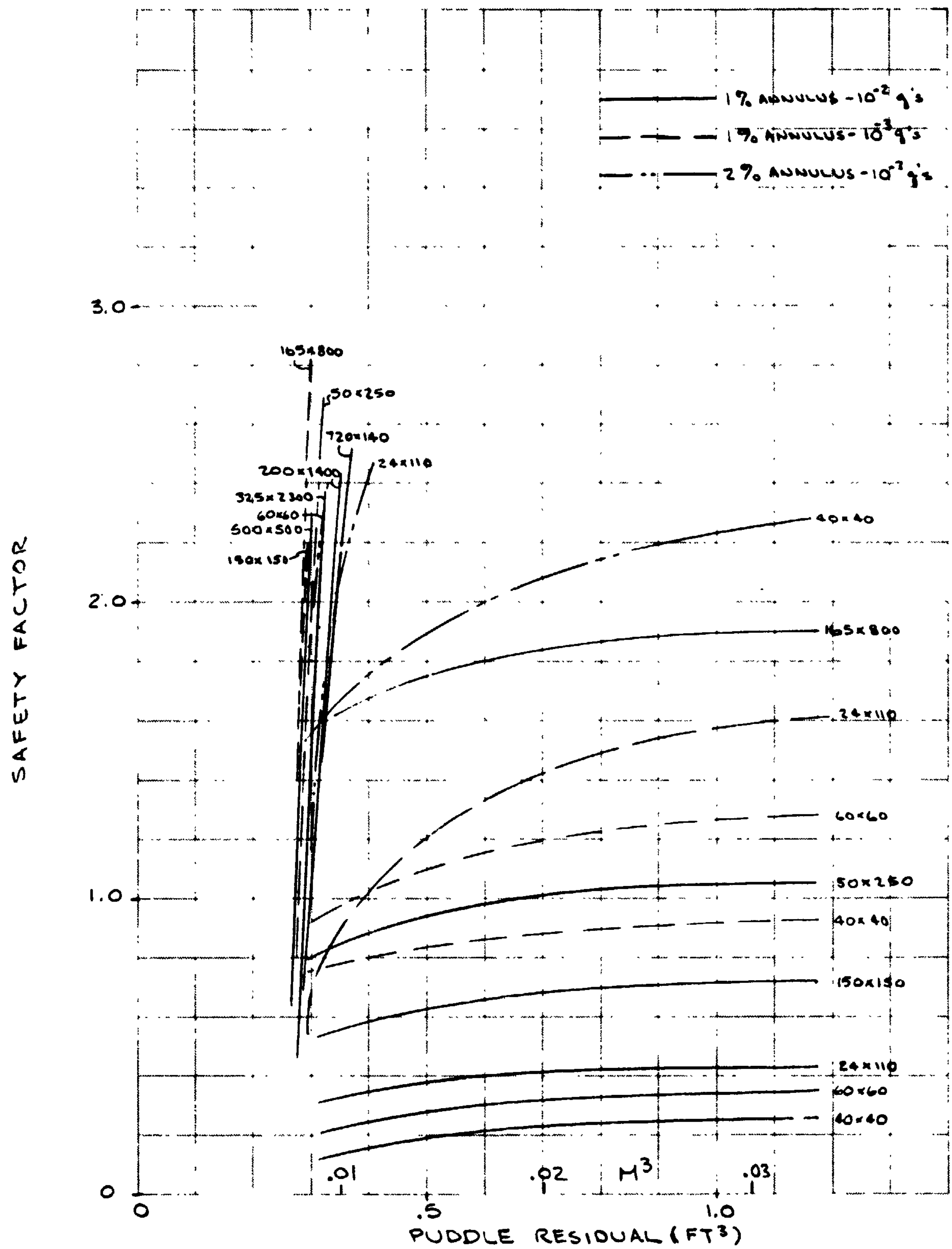

Figure 2. Screen Performance for Outflow from 14.16-m^3 (500-ft^3) LO_2 Tank

CR54

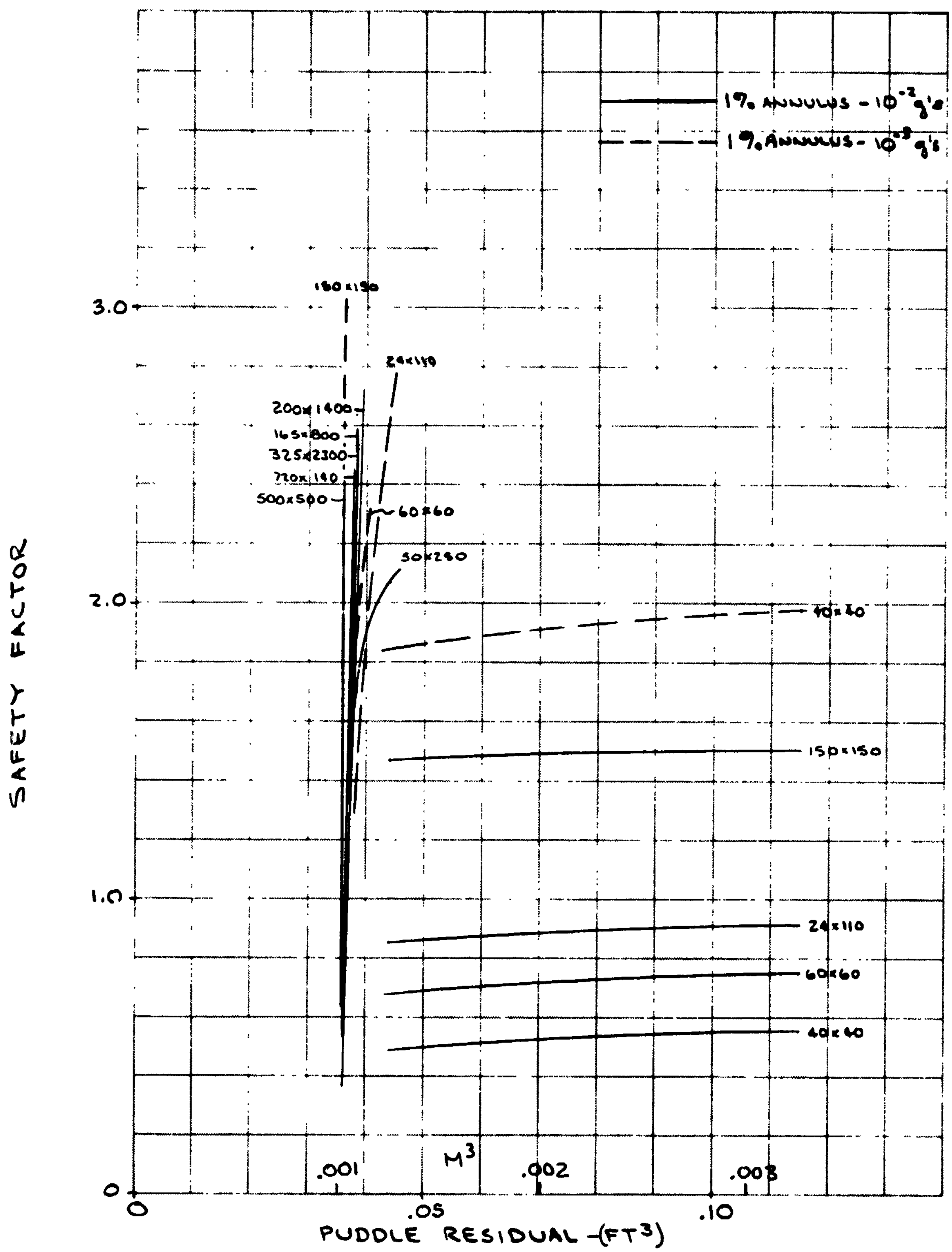

Figure 3. Screen Performance for Outflow From 1.416-m^3 (50-ft^3) LO_2 Tank

CR54

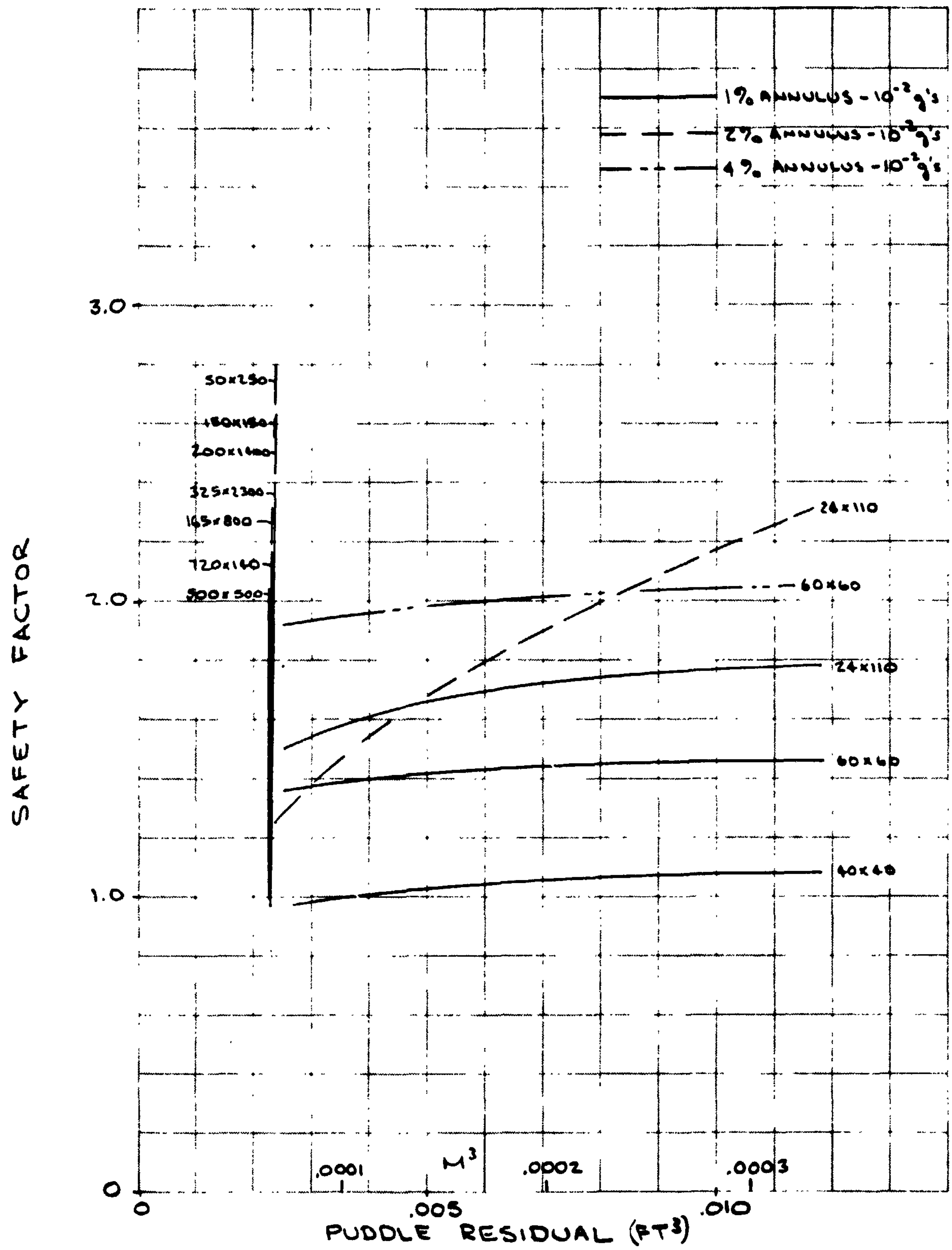

Figure 4. Screen Performance for Outflow from 0.1416-m³ (5-ft³) LO2 Tank

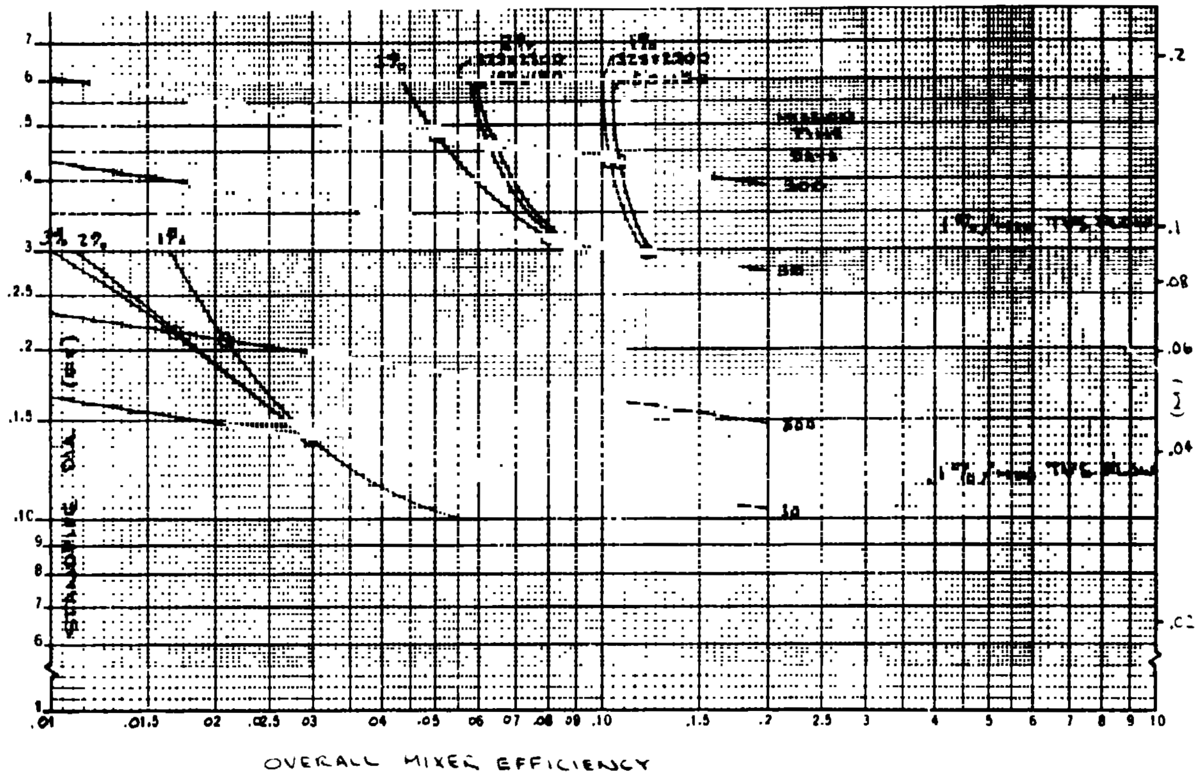

Figure 5. Determination of Optimum Standpipe Diameter for 14.16-m^3 (500-ft^3) LO_2 Tank

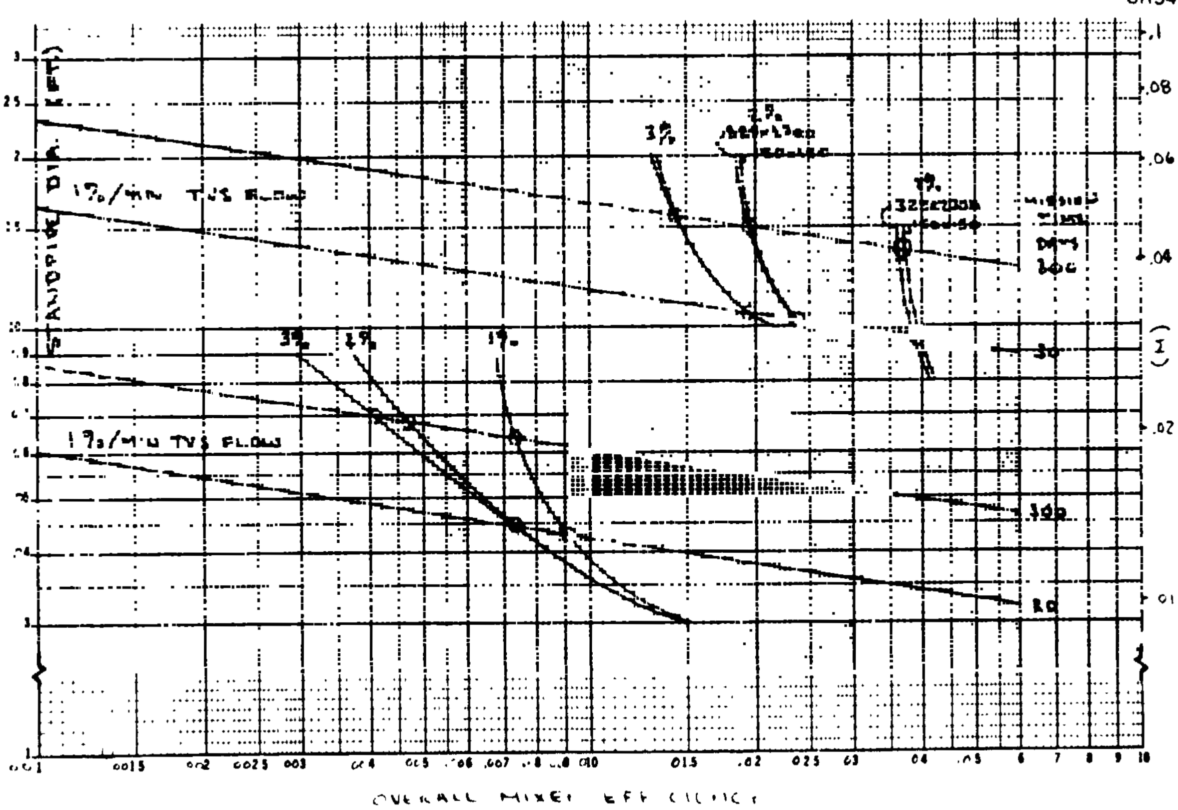

Figure 6. Determination of Optimum Standpipe Diameter for 1.416-m^3 (50-ft^3) LO_2 Tank

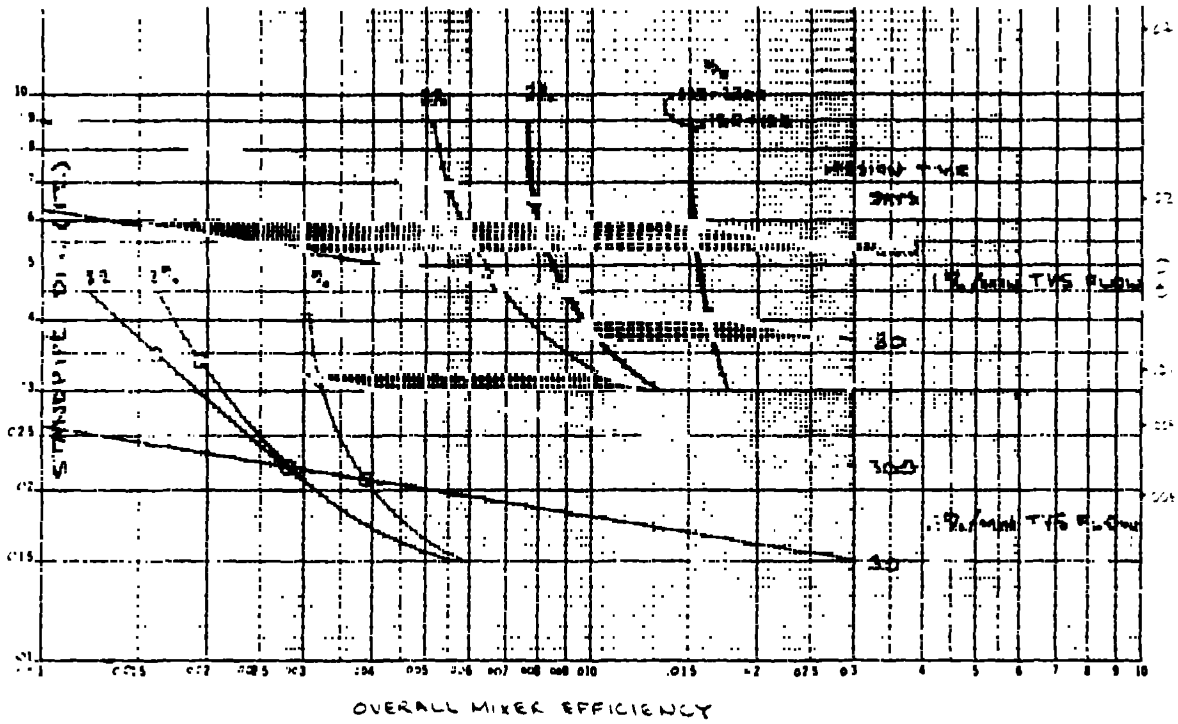

Figure 7. Determination of Optimum Standpipe Diameter for 0.1416-m^3 (5-ft^3) LO_2 Tank

In determining the pump-mixer characteristics, it was assumed that the same pump and motor efficiency characteristics were appropriate because the mixers were vane-axial fans operating at a very low power level. Thus, the total efficiency correlation used in ref. 6 was used in this study. However, the weight of the LO_2 pump-mixer was greater than for an LH_2 pump-mixer. This was because in order to assure safe motor operation in LO_2, the stator was sealed in a can pressurized with helium above the LO_2 pressure. The rotor was free to operate with LO_2 lubricated bearings with no safety hazard. This concept has been extensively studied and developed by Pesco Products (now Sundstrand Corporation), and an appropriate revised motor weight correlation was obtained from Sundstrand (ref. 9). Sundstrand estimated that the weight of the sealed LO_2 motor would be 10% greater than the weight of the LH_2 motor of the same size. This increase had an insignificant effect on system weight since the largest motor in this study weighed on the order of 0.1 kg.

A more serious problem resulted from the very small power requirements for these mixers. Mr. G. H. Caine of Sundstrand (ref. 9) made the following expert observations regarding small electric-motor-driven pumps:

A. The smallest low-head-rise LH_2 pump for destratification made by Pesco was rated at 7 watts, but was actually tested at ~ 1 watt by General Dynamics/Convair by reducing both voltage and frequency to about one third of their design values.

B. The smallest physical dimension of a pump made by Pesco, which was operated at very high RPM, was a diameter of about 2 cm (0.07 ft).

C. The lowest practical power level for normal use is about 1 watt; this limit is imposed by starting torque requirements caused by possible contamination (a particle between moving parts). As an example, an electric clock usually draws a minimum of 1 watt for the same reason.

D. The limit of 1 watt is basically a reliability limit and represents the limit of Pesco experience.

E. Below 1 watt, losses such as bearing, windage, friction, and stray (gap) losses become very significant, especially for LO_2 pumps with "canned" stators and larger gap losses. The values of 2-3% efficiency obtained are probably realistic.

F. With very clean systems, and with the natural filtration efficiency of the screen liner, a practical minimum, within the reach of current technology, would be 0.1 watt input power. Again, this minimum is a reliability limit imposed by potential contamination, not necessarily a fabrication limit. These tiny machines would have to be fabricated under a microscope, and motor weights of 4 to 5 grams (0.01 lb) would not be unrealistic.

G. Pumps of 0.1 watt input power would require development. A significant problem in such development would be accurate determination of very low pump head and flowrate, and especially efficiency.

Based on these observations, a minimum input power of 0.1 watt was assumed in this and all subsequent analyses.

Selection of Optimum Tankage Design. – Using the optimum standpipe size determined from Figures 5 to 7, the optimum system weight analysis was performed using the analysis developed previously (ref. 6) for the full range of flow conditions, mission times, and tank sizes. Figure 8 shows the optimization for the 14.16 m^3 (500-ft^3) tank for the 300-day mission. The effect of the high density LO_2 residual forced the minimum weight system toward the minimum annulus gap (1.2% for the 325 x 2300 screen and 1.4% for the 150 x 150 screen). Figure 8 shows that screen weight differences also disappear because of the LO_2 weight dominance. For the 30-day mission for the 500-ft^3 tank, shown in Figure 9, the extreme dominance of the annulus residual forced the minimum weight system to the minimum annulus gap – as was the case for the LH_2 tank study (ref. 6). Figure 10 shows that for the 1.416-^{3} (50-ft^3) tank, the minimum weight occurs at a 1.5% annulus for both the 325 x 2300 and 150 x 150 screens for the 300-day mission, while for the 30-day mission the minimum annulus gap is again optimum. Similarly, Figure 11 shows that for the 0.141-m^3 (5-ft^3) tank for the 300-day mission, the minimum weight occurs at a 2.0% annulus for both the 325 x 2300 and 150 x 150 screens.

CR54

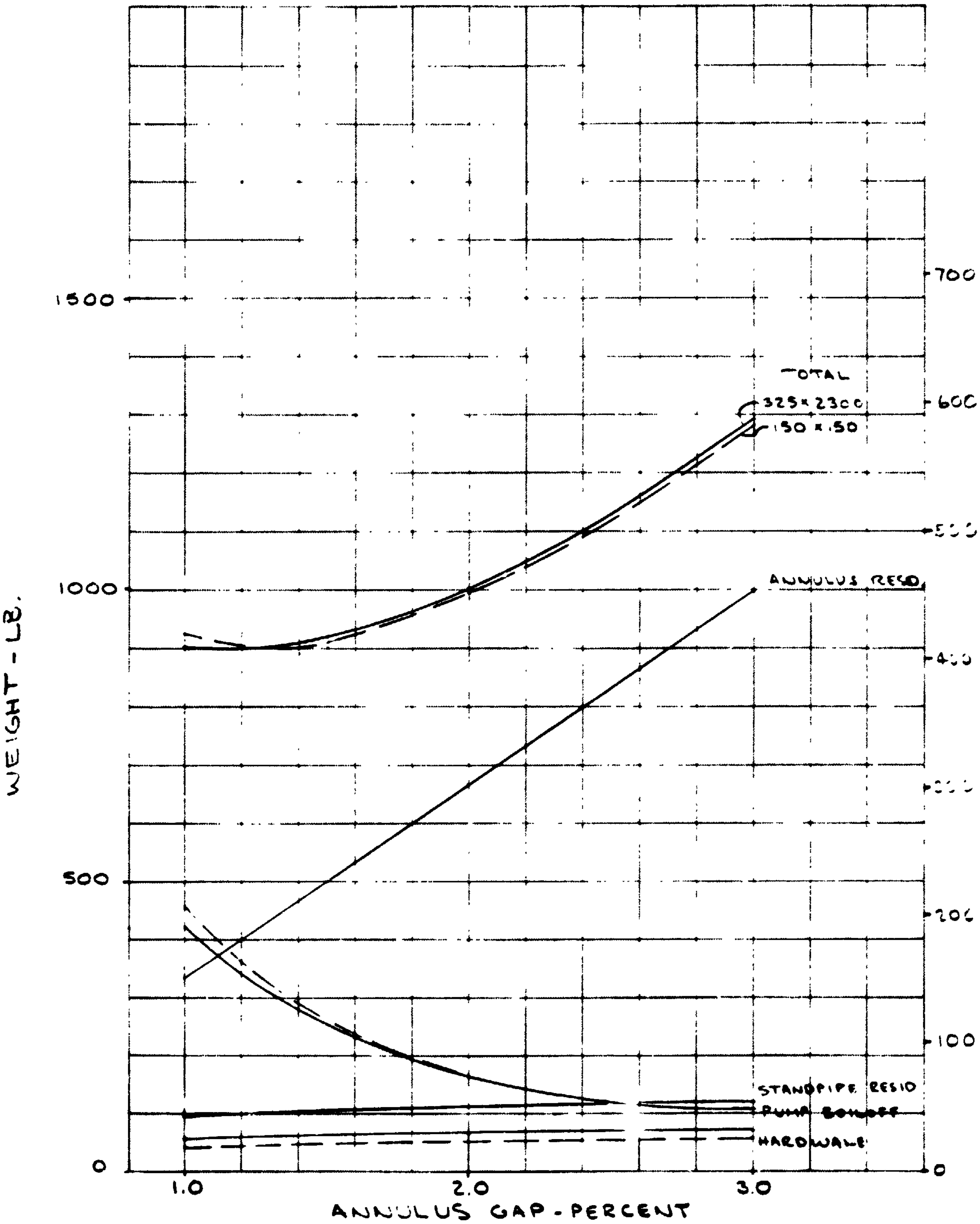

Figure 8. Optimum Annulus Gap for 300-Day Storage in the 14.16-m^3 (500-ft^3) LO_2 Tank

CR54

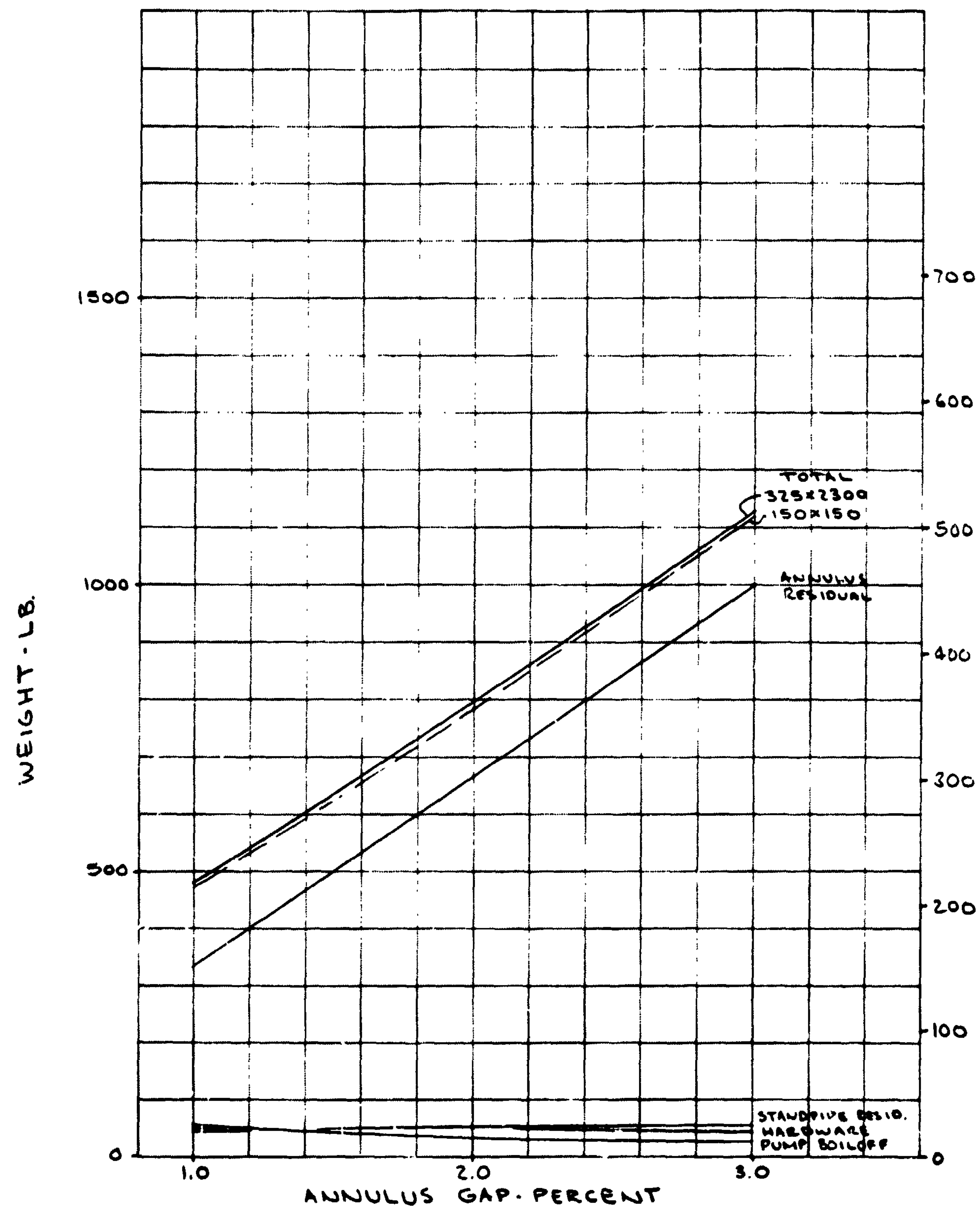

Figure 9. Optimum Annulus Gap for 30-Day Storage in the 14.16-m^3 (500-ft^3) LO_2 Tank

CR64

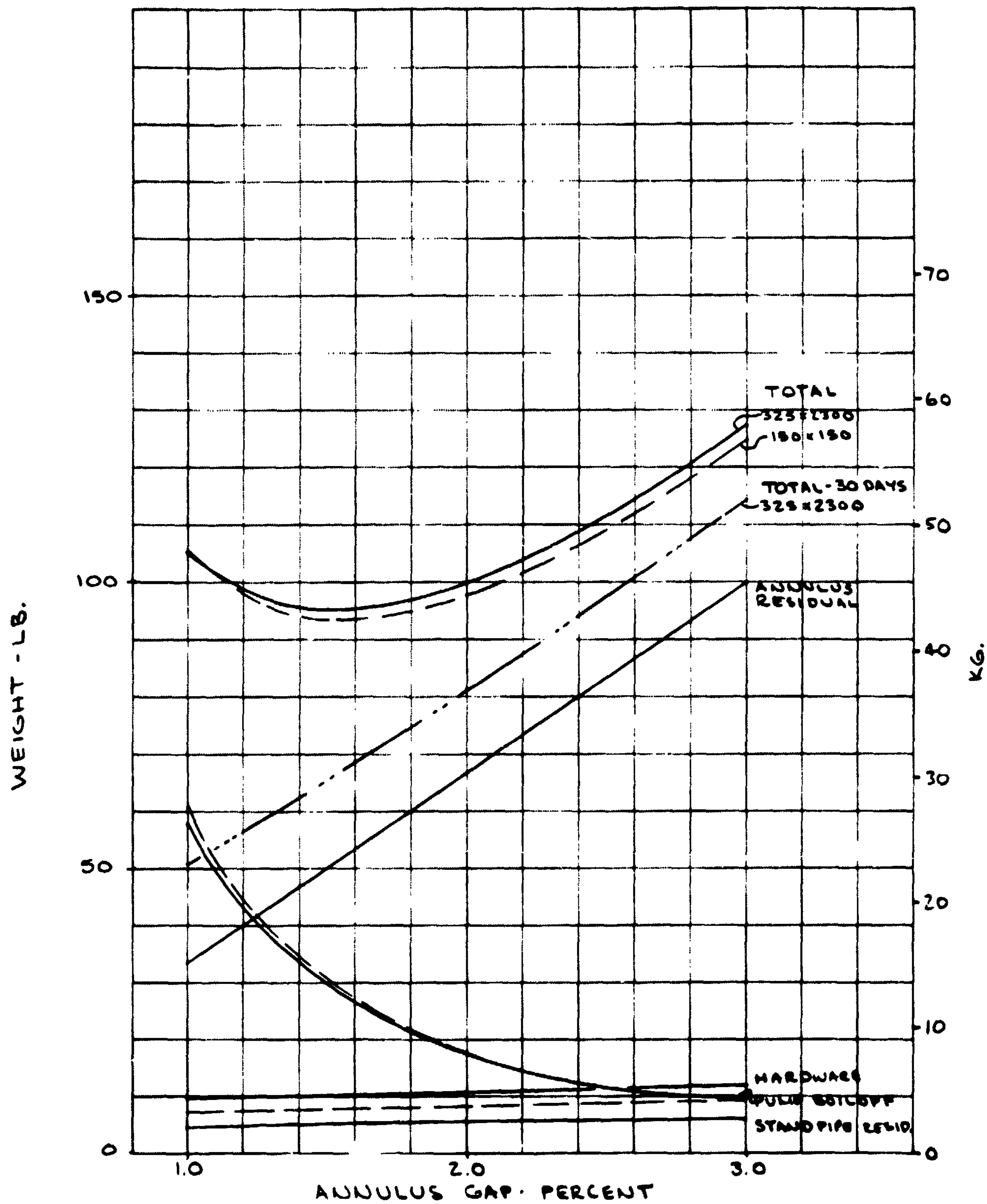

Figure 10. Optimum Annulus Gap for 300 (and 30-) Day Storage in the 1.416-m^3 (50-ft^3) LO_2 Tank

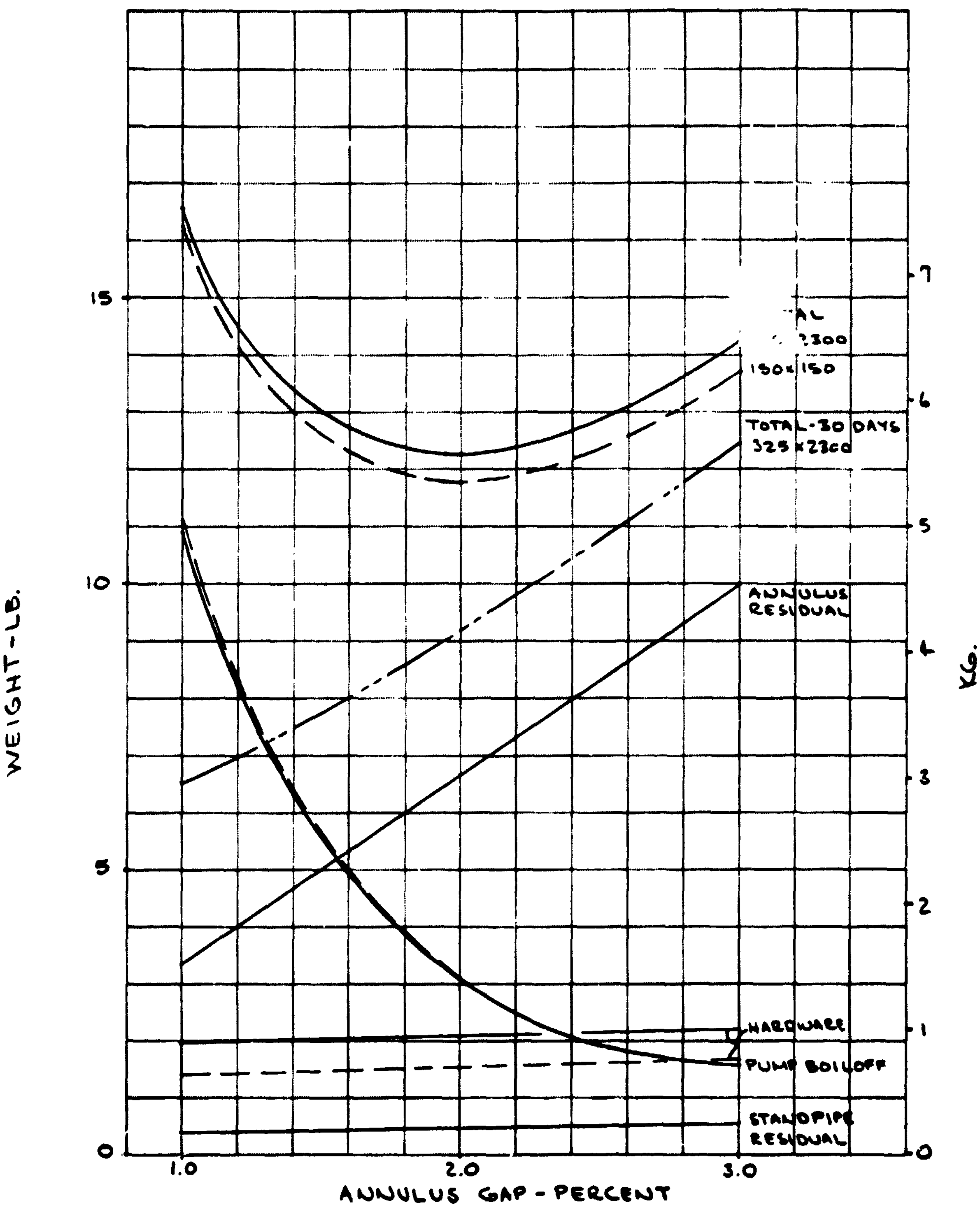

Figure 11. Optimum Annulus Gap for 300 (and 30-) Day Storage in the 0.1416-m^3 (5-ft^3) LO_2 Tank

Figures 8 through 11 were for a TVS flowrate of 1% tank volume/minute; Figure 12 shows that the minimum annulus is optimum for a TVS flowrate of 0.1% tank volume/minute for the 500-ft^3 tank for 300-day mission. The results for low flow rates were the same for the smaller tanks, and were also the case for the LH_2 tanks (ref. 6).

The outflow performance for each tank and screen at the minimum weight annulus gap for the 300-day mission was determined as a function of g-level and shown in Figure 13. For all of the tanks, the 325 x 2300 screen had adequate performance at g-levels up to 10^{-2} g's. For the 14.16-m^3 (500-ft^3) tank, the maximum g-level at which the 150 x 150 screen gave adequate performance was about 3.5 x 10^{-3} g's, and for the 1.416-m^3 (50-ft^3) tank, about 7.8 x 10^{-3} g's.

The general conclusions which can be drawn are similar to those drawn for the LH_2 tanks (ref. 6); the 325 x 2300 screen gave optimum performance for the larger tanks and g-levels – the 150 x 150 screen would give optimum performance for the smaller tanks or for lower g-levels. Again, for all of the LO_2 tanks, the pump power levels were so low that it was not clear that the pump/motors could be built or that the predicted efficiencies could be achieved. This question was explored further in subsequent studies described below.

Tug-Scale Transfer System

The physical and operational characteristics of the baseline Tug-Scale Propulsion Module (TSPM) are described in ref. 10. The TSPM is an acceleration-settled propellant transfer or propulsive stage which includes a 70.8-m^3 (2500-ft^3) LH_2 tank, a 21.24-m^3 (750-ft^3) LO_2 tank, a structural shroud, tank wall-mounted heat exchanger TVS and MLI/purge systems, propulsion module, pressurization system, and suitable plumbing lines and other hardware.

Two missions were studied: (1) 3-day storage in orbit at less than 10^{-5} g followed by propellant transfer at 0.1% of tank volume/minute and; (2) 7-day storage in synchronous equatorial orbit, 6-burn Tug mission with acquisition outflow at 0.06% of tank volume/second for engine start. The Tug mission is shown in Table 3 which indicates the timeline and propellant use for each mission phase.

Tug-Scale Propulsion Module; 3-Day Transfer Mission. – For the TSPM, the principal weight penalties were the propulsion module weight, the settling propellant weight, and the propellant residual weight. The weights for thruster propellant consumption were based on accelerating a total mass of 32,800 kg (72,420 lb), which included the TSPM, the total propellant weight of 22,300 kg (49,160 lb) of LO_2 and 4,600 kg (10,140 lb) of LH_2, and the Tug to which the propellant was to be transferred. The small gaseous oxygen-hydrogen thrusters were assumed to achieve a specific impulse of 350 seconds. The time required to empty the tank (the outflow capability) is a function of the applied g-level or, for a given system weight, the thrust

CR54

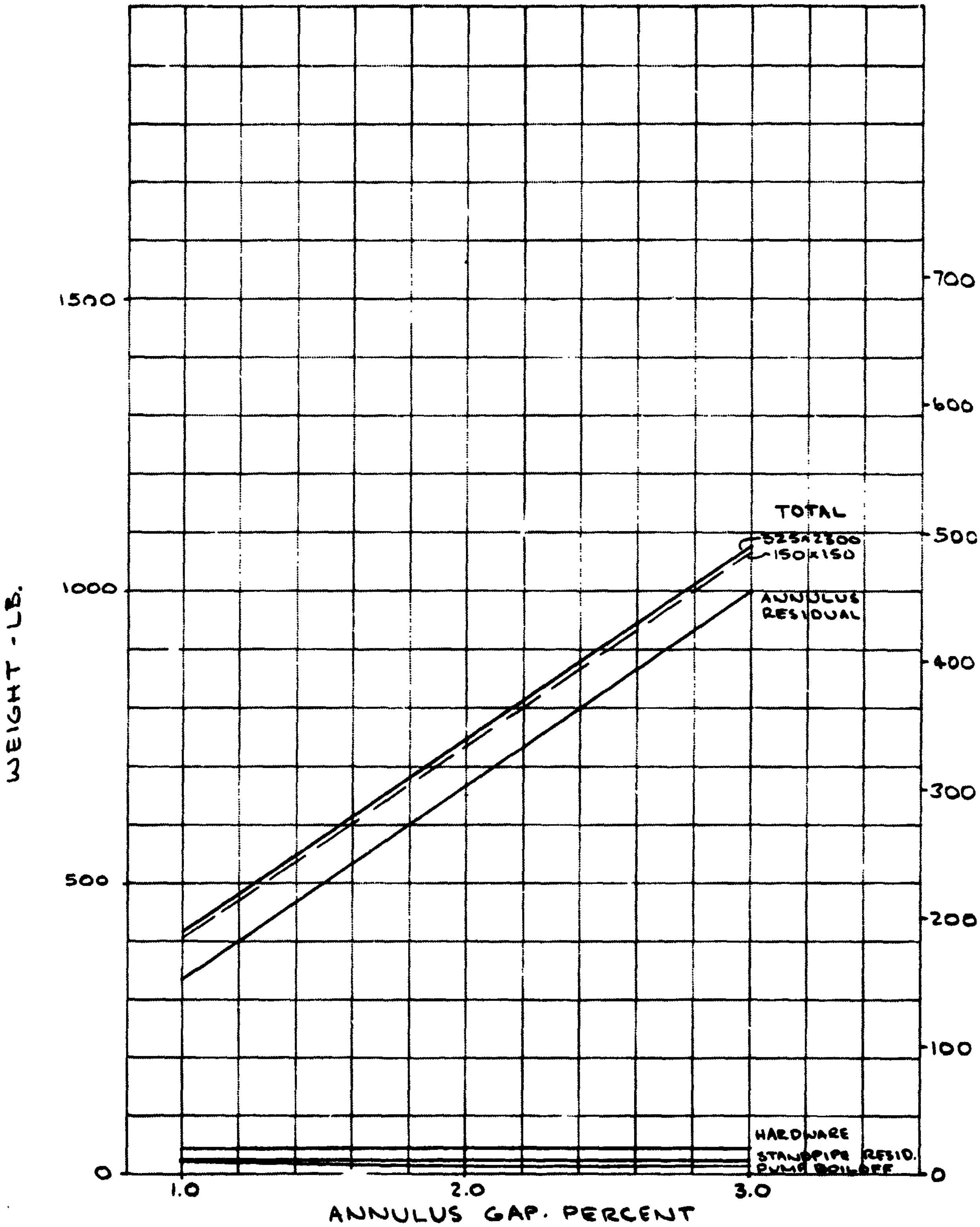

Figure 12. Optimum Annulus Gap for 300-Day Storage in the 14.16-m^3 (500-ft^3) LO_2 Tank at 0.1% TVS Flowrate

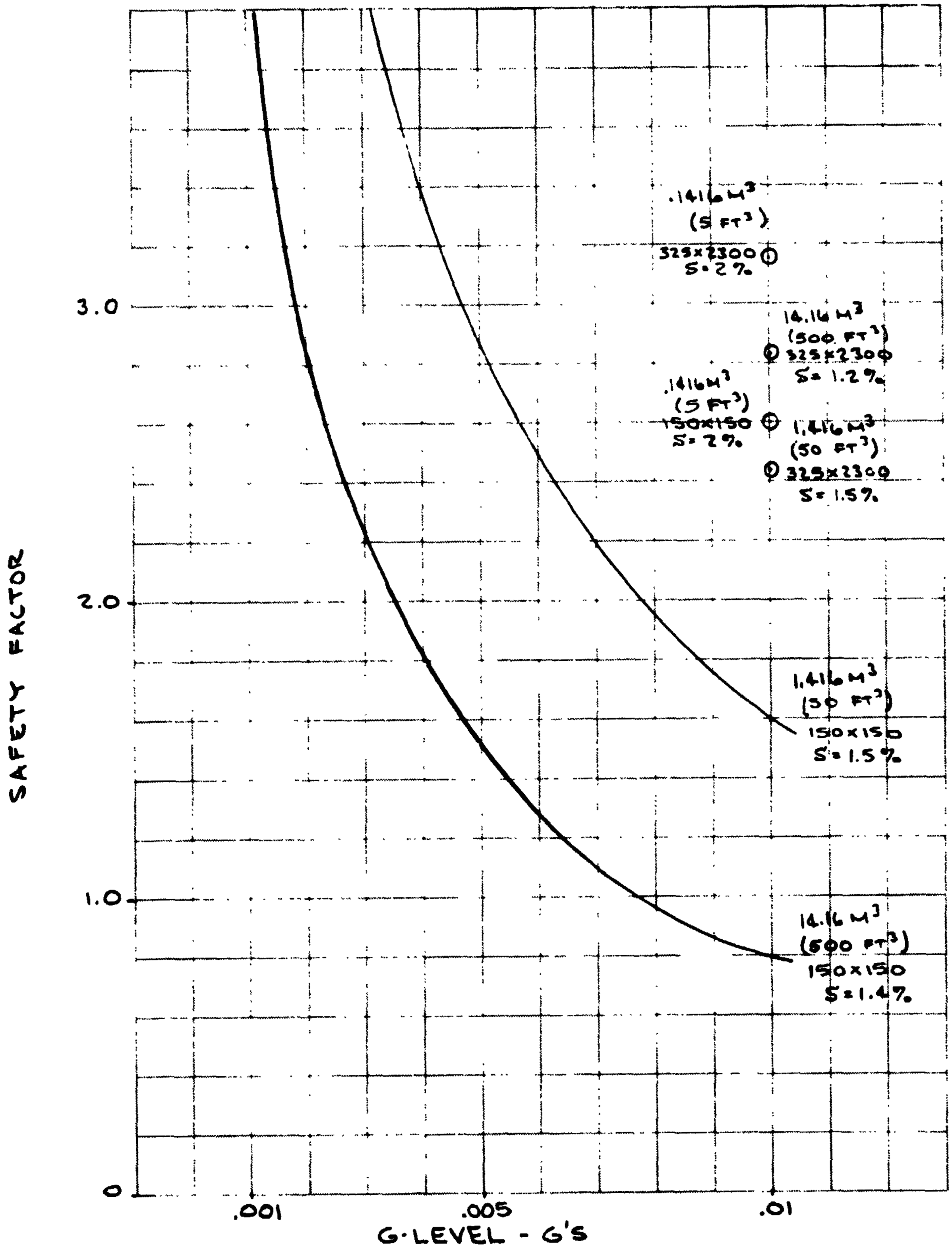

Figure 13. Outflow Performance at Optimum Annulus Gap(s) for Three LO_2 Tanks

TABLE 3. – SYNCHRONOUS EQUATORIAL ORBIT - DEPLOYMENT MISSION
REPRESENTATIVE MISSION R-1D

Event	Sequence No.	Time (hr)		Tug Main Engine						
				Full Thrust ΔV m/sec			Burn Time** (min)	LH_2 Propellant kg(lb)	LO_2 Propellant kg(lb)	Total Propellant kg(lb)
		Δ	Total	Ideal	Gravity Loss*	Total				
Shuttle Liftoff			0							
Shuttle Burnout	1		0.14							
Coast to 100 nmi (185 km)	1-2a	0.73								
Shuttle Insert	2a		0.87							
Coast to 160 nmi (296 km)	2a-2	0.76								
Circularize	2		1.63							
Tug Deploy and Coast	2-3	173.11								
Phasing Orbit Insert	3		174.74	556	14	570	4.1	521	3,124	3,645
Coast to TOI	3-4	1.92								
Transfer Orbit Insert	4		176.66	1896	49	1945	9.9	1257	7,544	8,801
Coast to Sync Orbit	4-5	5.27								
Mission Orbit Insert	5		181.93	1783	3	1786	6.1	775	4,648	5,423
Deploy Payload	5-6	11.15								
Transfer Orbit Insert	6		193.08	1782	1.5	1783.5	2.8	356	2,134	2,490
Coast to POI	6-7	5.27								
Phasing Orbit Insert	7		198.35	1134	3	1137	1.3	165	991	1,156
Coast	7-8	3.02								
Circularize for Rendevous	8		201.37	1313	2	1315	1.1	140	838	978
Shuttle Rendez. and Coast	8-9	4.53								
Shuttle Deorbit	9		205.90							
Touchdown	10		206.60							
								3214	19,279	22,493
								(7084)	(42,503)	(49,587)

* Based on 66,720-N (15,000-lb) thrust engine

** Burn time – 66,720-N (15,000-lb) main engine

ORIGINAL PAGE IS
OF POOR QUALITY

of the settling engines. The residual left in the tank results because of vapor pull-through near the end of the low-g draining, which is also a function of applied g-level. It was originally specified that the LO_2 tank was to be spherical. However, ref. 10 claimed that using a conical bottom in the LO_2 tank would save 272 kg (600 lb) of LO_2 residual at 10^{-4} g. Therefore, in our study, a conical-bottomed LO_2 tank was assumed in order to use the data on residual versus g-level provided by ref. 10. However, the TSPM was penalized for the additional LO_2 tank weight incurred by using a conical bottom. The tanks were sized based on high-strength aluminum alloy, 2219-T87, using monocoque construction without reinforcement (except where welding occurs), and designed with a factor of 1.5 on the yield strength. The TSPM tankage parameters are shown in Table 4. The additional weight penalty for the conical tank was 72.5 kg (160 lb) (a spherical LO_2 tank would weigh 71.6 kg or 158 lb). The tank pressures assumed were 17.25 N/cm^2 (25 psia) for the LH_2 tank and 19.3 N/cm^2 (28 psia) for the LO_2 tank. The propellant characteristics and properties are shown in Table 5.

The TSPM tanks included a wall-mounted heat exchanger TVS which used boiling vented H_2 to cool the LH_2 tank and then used the vented H_2 as superheated vapor to cool the LO_2 tank, keeping it vent-free. In order to evaluate the venting penalty, define the TVS design, and optimize the MLI design, the heat leak to the tanks was analyzed. This heat leak consisted of that conducted through the tank supports and that conducted through the plumbing lines and supports. It was determined from ref. 10 that the tank supports were made of S-glass-filament-wound composite tubes, assumed to be 1.27-cm (0.5-inch) diameter by 0.05-cm (0.02-inch) wall for the LH_2 tank and 1.27-cm (0.5-inch) by 0.1-cm (0.04-inch) wall for the LO_2 tank. As scaled from the drawings in ref. 10, there were 24 supports 1.22 m (48 inch) long and 8 supports 0.81 m (32 inch) long for the LH_2 tank, and 24 supports 1.07 m (42 inch) long for the LO_2 tank. The total conductive heat leak down the supports (assuming the supports are insulated and that radiation down the tube interior is blocked) is shown in Table 6. The plumbing line lengths were also scaled from these drawings, and the line sizes were given in ref. 10. It was assumed that the lines were thin-walled stainless-steel tubing and valved close to the tank, so that the lines are only full of vapor, and the conductivity along the entire line and vapor lengths and through the plumbing supports constitute the only heat leakage. This requires that these lines be insulated with foam, vacuum jackets, or MLI to prevent radiation heat leak to the cold portions of the lines near the tank. The lines and their heat leak are also shown in Table 6. It was assumed that the line supports doubled the conductive heat leak along the line.

The TVS wall-mounted heat exchanger design must be such that the vented H_2 is boiled in the tubing on the H_2 tank wall. To provide a temperature gradient for heat transfer, and maximize tube spacing, the vented H_2 is expanded to a lower pressure ($\sim$3.45 N/cm^2) and temperature ($\sim$17.2°K) and boiled at essentially constant pressure until the vent fluid is heated back to nearly 22°K. The total enthalpy change available is 5.12×10^5 joule/kg (220 Btu/lb); however, because of the problem of insufficient temperature

TABLE 4. — TSPM TANKAGE CHARACTERISTICS

Propellant	Volume $m^3 (ft)^3$	L/D	Diameter m(ft)	Tank Wall Area m^2 (ft^2)	Tank Pressure N/cm^2 (psia)	Wall Thickness cm(in.)	Weight kg (lb)
LH_2	70.8 (2500)	2	3.78 (12.4)	89.6 (965)	17.25 (25)	0.127 (0.05) 0.063** (0.025**)	249 (548)
LO_2	21.24 (750)	1*	3.78 (12.4)	48.8 (525)	19.3 (28)	0.198 (0.078) 0.071** (0.028**)	144 (318)

* 90-degree conical bottom

** Spherical portion of tank

TABLE 5. – TSPM PROPELLANT PROPERTIES

	LH_2	LO_2
Tank Pressure - N/cm^2 (psia)	17.25 (25)	19.3 (28)
Temperature – °K (°R)	22.14 (39.86)	96.79 (174.23)
Density – kg/m^3 (lb/ft^3)	68.4 (4.27)	1105.4 (69)
Conductivity – joule/m-sec-°K (Btu/hr-ft-°R)	0.114 (0.066)	0.142 (0.082)
Viscosity – $N\text{-}sec/m^2$ (lb/ft-sec)	1.13×10^{-5} (0.76×10^{-5})	16.74×10^{-5} (11.25×10^{-5})
Surface Tension – dyne/cm (lb/ft)	1.61 (1.11×10^{-4})	11.67 (8.05×10^{-4})
Heat of Vaporization – joule/kg (Btu/lb)	4.34×10^5 (186.7)	2.05×10^5 (88)
Tank Volume – m^3 (ft^3)	70.8 (2,500)	21.24 (750)
Propellant Quantity – kg (lb) (initial - 5% ullage)	4,600 (10,141)	22,300 (49,163)

TABLE 6. – TSPM TANK HEAT LEAK

	Diameter (cm)	Length (m)	$Q_{Conduction}$ (watt)	Q_{Vapor} (watt)	$Q_{Support}$ (watt)
Tank Supports					
LH_2	1.27	1.22, -81	0.0436		
LO_2	1.27	1.07	0.0442		
Plumbing					
LH_2					
Transfer	3.81	7.11	0.0173	0.0006	0.0173
Pressurization	1.90	7.11	0.0086	0.0001	0.0086
Fill/Drain	7.62	1.65	0.1488	0.0094	0.1488
Emergency Vent	7.62	8.13	0.0302	0.0018	0.0302
Purge and Press.	2.54	8.13	0.0101	0.0002	0.0101
			0.2150	0.0121	0.2150
LO_2					
Transfer	3.81	2.03	0.0483	0.0010	0.0483
Pressurization	1.90	2.03	0.0242	0.0003	0.0242
Fill/Drain	7.62	7.11	0.0276	0.0012	0.0276
Emergency Vent	7.62	11.43	0.0172	0.0007	0.0172
Purge/Vent	2.54	11.43	0.0057	0.0001	0.0057
			0.1230	0.0033	0.1230
Mixer					
LH_2	2.54	-	(0.1)		
LO_2	2.54	-	(0.1)		

gradient near 22°K, and the problem of reduced heat transfer following transition to mist flow in the vent tube, only 85% of this enthalpy change is considered available, or 4.35×10^5 joule/kg (187 Btu/lb). In the LO_2 tank heat exchanger, the H_2 is assumed heated from 54.5°K (98°R) (to avoid freezing of the LO_2) to 96.6°K (174°R), or an enthalpy increase of 4.89×10^5 joule/kg (210 Btu/lb). For the LH_2 tank, the maximum wall temperature gradient could exceed 5°K, and for the LO_2 tank, the mean wall temperature gradient could exceed 21°K. Even in low gravity these large temperature gradients could set up stable cold and warm stratified regions leading eventually to boiling in the warm regions, unless the propellants are mixed. Therefore, it was assumed that a mixer would have to be used to assure that the wall-mounted heat exchanger performed properly. The criteria for mixing to break up existing stratified layers have been well established (refs. 11 and 12), but no criteria exist for continuous mixing in low gravity of wall-bound temperature cells. It is clear, however, that to minimize effects of wall heat transfer (which requires a larger wall heat exchanger) and minimize boiloff due to mixer input power, the size of the mixer should be minimized. Therefore, the design approach was to provide the smallest feasible mixer (~0.1 watt, 2.5 cm diameter) (ref. 13) and check the destratification performance against accepted criteria from refs. 11 and 12.

For an input power of 0.1 watt, the fluid power is 0.00255 watt (at an overall efficiency of 2.55%) and the mixer must only provide a velocity head (in low gravity) of $V_j^2/2g$ (where V_j is the mixer exit velocity) and a volumetric flow of V_jA_j. Equating the head and flow to the fluid power gives $V_j = 0.53$ m/sec (1.73 ft/sec) for H_2 and $V_j = 0.21$ m/sec (0.69 ft/sec) for O_2. The mixer (jet) Reynolds number, Re_j, for these velocities is 81,000 for H_2 and 35,000 for O_2.

From ref. 11, a criterion was developed for the critical jet Reynolds number. The critical jet Reynolds number was defined as the value where the buoyant force becomes unimportant when compared to the inertial forces. For a Reynolds number greater than this critical value, the system may be assumed to mix completely and increasing the jet Reynolds number further simply decreases the mixing time required. Below this critical Reynolds number, the buoyant forces may be strong enough to limit the degree of mixing.

The maximum value of this critical Reynolds number is given by

$$Re_j^{\,2} = 0.912 \left(\frac{D}{H}\right)^{2/3} Pr^{-2/3}\, Gr^{2/3} \tag{5}$$

This criterion was established by assuming that the mixing jet must possess enough energy at the free surface to overcome the buoyant force, and move the hot liquid at the surface to the bottom of the tank. Using this jet Reynolds number as the critical value, the mixing jet should easily penetrate the stratified layer where the momentum due to the pump is always greater than the free convection momentum, and the liquid kinetic energy due to the pump is always greater than the free convection kinetic energy.

The values of G_r used for our cases was based on the maximum temperature differences and the tank dimensions. This criterion gave a required Re_j of 3800 for H_2 and 2100 for O_2, which are substantially below the values of Re_j for the minimum mixer size. Clearly, even the smallest available mixer has adequate power (used continuously) to provide sufficient mixing and destratification in 10^{-5} g.

The mixing parameters were also checked against the dimensionless mixing time correlations (based on large tank test data) of ref. 12. For the LH_2 tank, the time for the 0.1-watt mixer to reduce the stratification to 5% of its initial value was 2.72 hours, and for the LO_2 tank, 6.73 hours.

(The LO_2 tank time is probably conservative, since a conical tank should mix faster.) Both of these times are short relative to total mission time and, thus, continuous mixing can easily be accomplished using the minimum size mixer.

With the total tank heat leak defined as shown in Table 6, the tank insulation was optimized and the vent rate defined. The insulation system consisted of MLI applied to both the LH_2 and LO_2 tanks. The MLI was assumed to be embossed, perforated, aluminized Kapton film. It was assumed to be applied in a series of panels with 12 layers each and with staggered seams, and to be built up at 23 layers/cm. MLI performance was assumed to be characterized by effective conductivity, $K = 8.65 \times 10^{-5}$ joule/m-sec-°K (5×10^{-5} Btu/hr-ft-°R) for the LH_2 tank and $K = 10.9 \times 10^{-5}$ joule/m-sec-°K (6.3×10^{-5} Btu/hr-ft-°R) for the LO_2 tank (ref. 14). MLI density was assumed (for 2.5-cm thickness) to be 0.7 kg/m^2 (0.145 lb/ft^2) (ref. 14). The MLI was assumed supported on the propellant tanks with hollow posts molded from epoxy and fiberglass and bonded to foam-filled phenolic honeycomb pads bonded to the tank surface.

In order to purge the MLI effectively from the back side (for loaded ascent), a 2.5-cm annulus was assumed to be provided between the propellant tank and the insulation. An internal purge manifold was located in this annulus, and it distributed purge gas at balanced pressure throughout the annulus, permitting even flow through the MLI. The MLI was assumed spaced away from the tank surface on an aluminum wire mesh supported by the foam-honeycomb pads. The aluminum mesh was assumed to be of 20-mesh 0.009 wire weighing 0.18 kg/m^2 (0.037 lb/ft^2) with the mesh installed in stretch-formed segments with cutouts provided for all MLI penetrations. An external tension membrane of Nomex mesh was assumed to be provided to contain the MLI during purge and preconditioning operation, when backside pressure forces are being exerted, and to protect the insulation surface from mechanical damage. The MLI thickness for each tank and mission was optimized based on minimization of the insulation weight and boiloff weight, as described in ref. 6. The optimum MLI parameters are shown in Table 7. The optimum vent rate for the H_2 tank, when used to cool the O_2 tank, gives the minimum O_2 MLI thickness, as shown in the table.

With the MLI heat flux defined and by defining the internal heat transfer coefficients, the wall-mounted heat exchanger designs for the H_2 and O_2 tanks can be defined. The mean velocity near the tank wall due to the mixer flow, based on flow area ratio, was 0.00003 m/sec (0.0001 ft/sec) for the H_2, resulting in an internal wall heat transfer coefficient of 0.154 joule/m^2-sec-°K (0.0272 Btu/hr-ft^2-°R). For the O_2 tank the velocity at the wall was 0.000012 m/sec (0.00004 ft/sec), and the corresponding heat transfer coefficient was 0.965 joule/m^2-sec-°K (0.017 Btu/hr-ft^2-°R). From ref. 10, the tube size for the wall-mounted heat exchanger was given as 1.27-cm (0.5-inch) diameter, which, for a single pass and based on the vent flow rates shown, gave tube-side heat transfer coefficients as shown in Table 8. The equations defining the required spacing for the wall-mounted heat exchanger with internal heat transfer, arranged so that the net heat transfer to the fluid is zero, were developed in ref. 15. The equation for the tube spacing, D_o, is:

TABLE 7. – OPTIMUM MLI PARAMETERS FOR TSPM

Tank	Mission	MLI Thickness cm (in.)	MLI Weight kg (lb)	$\dot{Q}/A$ watt/m^2 (Btu/hr-ft^2)	Vent Rate kg/hr (lb/hr)	Vent Heat Capacity watt (Btu/hr)
LH_2	3-day	2.08 (0.82)	52.0 (114.7)	0.969 (0.3075)	0.73 (1.6)	87.6 (299)
	7-day	3.53 (1.39)	88.2 (194.5)	0.572 (0.1813)	0.43 (0.95)	52.1 (178)
LO_2	3-day	0.84 (0.33)	11.4 (25.1)	2.011 (0.638)	0.73 (1.6)	98.4 (336)
	7-day	1.42 (0.56)	19.3 (42.6)	1.188 (0.377)	0.43 (0.95)	58.6 (200)

TABLE 8. — WALL-MOUNTED HEAT EXCHANGER DESIGN DATA

Tank	Mission	Tank Internal Heat Transfer Coeff h_f joule/m^2-sec-°K (Btu/hr-ft^2-°R)	Tube Internal Heat Transfer Coeff h_i joule/m^2-sec-°K (Btu/hr-ft^2-°R)	Tank Wall Thickness cm (in)	Tube Spacing, D_o cm (ft)	Tube Weight kg (lb)
LH_2	3-day	0.154 (0.0272)	82.5 (14.54)	0.127 (0.05)	160.0 (5.25)	4.7 (10.4)
	7-day	0.154 (0.0272)	54.35 (9.58)	0.127 (0.05)	222.0 (7.28)	3.4 (7.5)
LO_2	3-day	0.096 (0.017)	120.3 (21.2)	0.198 (0.078)	427.0 (14.0)	1.1 (2.4)
	7-day	0.096 (0.017	79.15 (13.95)	0.198 (0.078	602.0 (19.75)	1.1 (2.4)

NOTE: K_t = 31.1 joule/m-sec-°K at 22°K (18 Btu/hr-ft-°R at 40°R)

= 65.7 joule/m-sec-°K at 94.4°K (38 Btu/hr-ft-°R at 170°R)

$$\frac{D_o}{\tanh N} + \frac{2\sqrt{h_f K_t t}}{\pi D_{tube} h_i} D_o = \frac{2\sqrt{h_f K_t t}\left(T_f - T_{HEX} + \frac{\dot{Q}/A}{h_f}\right)}{\dot{Q}/A} \tag{6}$$

where

$$N = \frac{D_o}{2}\sqrt{\frac{h_f}{K_t t}} \tag{7}$$

Equations (6) and (7) are solved iteratively to find D_o. The values of D_o are shown in Table 8 together with the wall-mounted heat exchanger weights. The heat flux to the tank wall and the temperature gradients in the wall may cause boiling within the tank, depending on the point of incipient boiling, which is of the order of 0.005°K for H_2 and 0.05°K for O_2. However, other areas of the propellant will be subcooled, and when mixed with the vapor bubbles, will result in zero net thermal increase in the tank.

An analysis was performed to define the settling propellant weight penalty. For the 3-day transfer mission, the propellant residual decreases with increasing ACS-imposed g-level, but the ACS propellant required increases. Thus, there is a point of minimum propellant penalty (including residual plus ACS propellant) for any given g-level. Figure 14 shows the required propulsion module propellant and propellant residual weight as a function of total draining time and g-level for the TSPM, taken from data in ref. 10. The sum of the propulsion module propellant and residual is shown in Figure 14 as the short curved lines, with the circles indicating the minimum-weight transfer time for a given g-level. The long dashed line is the locus of minimum total propellant weight versus transfer time over a g-level range of 10^{-1} to 10^{-5}.

For the three-day mission with outflow at 0.1% of tank volume/minute, the required transfer time is 1,000 minutes, or 16.67 hours, and the mininum propellant penalty, from Figure 14, is 435 kg (960 lb). For the three-day mission, transfer in 16.67 hours will require 4.8×10^{-5} g. The required thrust is

$$F = 4.8 \times 10^{-5}\ (9.8)\ (32800) = 15.5\ \text{N}\ (3.5\ \text{lb})$$

and the thruster propellant consumption is

$$W = \frac{15.5\ \text{N}}{350\ \text{sec}} \frac{(60,000\ \text{sec})}{9.8\ \text{m/sec}^2} = 272\ \text{kg}\ (600\ \text{lb})$$

The total propellant residual is 163 kg (360 lb).

In order to provide balanced thrust, the use of two 7.75-N (1.75- lb) thrust motors is required. In order to obtain the maximum performance

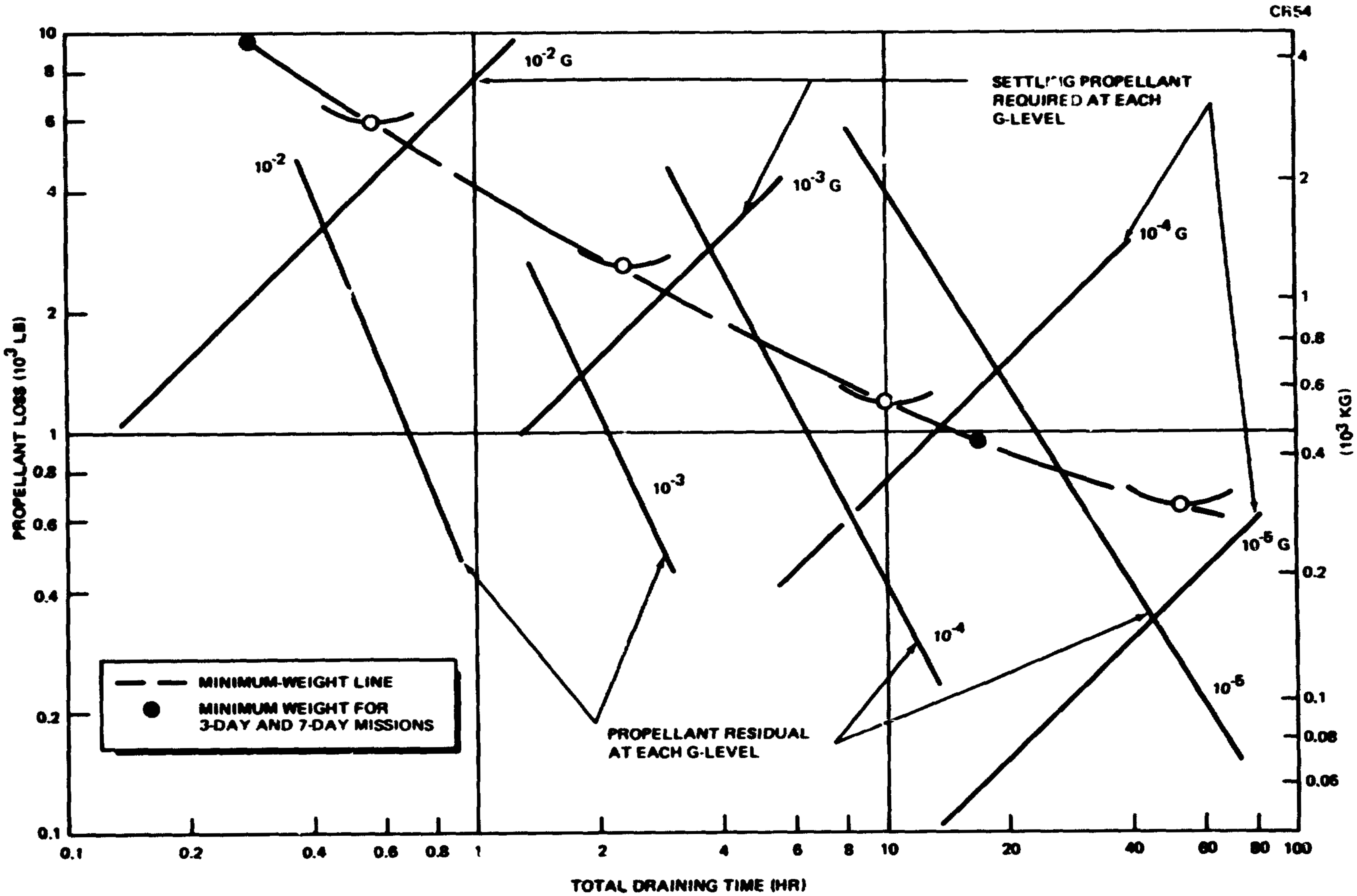

Figure 14. Propellant Penalty Versus Draining Time for TSPM

of 350 sec-I_{sp}, O_2/H_2 propellants were assumed in ref. 10. This selection was based primarily upon the high performance achievable and upon the system simplicity and commonality which is a result of using the same propellants as used for the primary systems of the TSPM and the user vehicle.

Selection of the baseline design for the liquid/vapor interface control propulsion system for logistic operations required evaluation of several possible design options. The major alternatives considered are summarized as follows: user vehicle or TSPM mounted thrusters, existing attitude propulsion systems (APS) or new propulsion systems and thrusters, single or multiple thrusters, and propellant selection among cold gas, storable monopropellant, storable bipropellant, and O_2/H_2.

The propellant transfer propulsion system operational requirements developed in ref. 10 are:

Continuous thrust (hours)	17
Design life (missions)	50
Total life requirements (hours)	850
Minimum acceleration (g)	4.8×10^{-5}
Thrust level (Newtons) total	15.5 (3.5 lb)

At the present time, most operational thrusters have a demonstrated firing life of less than one hour and in most cases only a few minutes. Some exceptions exist such as a 16-hour demonstration test conducted on a small hydrazine monopropellant thruster using test facility tankage and plumbing.

Other low thrust (millipound level) systems have the potential of unlimited life, but in the thrust range under consideration here, highly qualified systems are not yet available. Apollo N_2O_4/MMH and N_2O_4/A-50 bipropellant reaction control systems have been run continuously for up to six hours, and on a cumulative life basis up to 12 hours. The projected life capability of advanced O_2/H_2 systems has been predicted to be about 1,000 hours based on tests conducted under NASA-LeRC Contract NAS3-14352.

Since the TSPM returns to earth with the Shuttle Orbiter after each in-orbit transfer operation, the opportunity exists for frequent maintenance of any systems installed in the module assembly, if required. If the propulsion system used for propellant transfer operations is placed on the user vehicles, the maintenance-free life requirement is extremely high.

Based upon the above requirements, it was concluded that insufficient extended life data exist on propulsion components to risk installation of the propulsion systems for liquid/vapor interface control on the user vehicles. It also follows that this propulsion system function should not be combined with the existing user vehicles APS for the same reason.

The selected baseline configuration incorporates separate linear acceleration of the user vehicle/TSPM for liquid/vapor interface control, connected user/logistic module ullage for receiver tank thermodynamic control, gas pump in the ullage return line for liquid expulsion, and turbopump heat-exchanger supercritical system for NPSP control of both propellants and to feed the gaseous oxygen-hydrogen acceleration thrusters.

The system components required to support the fluid transfer operation are incorporated into the TSPM configuration. Concentration of this equipment in the TSPM eliminates the payload penalty associated with transporting component weight on Tug payload placement missions, eliminates the need for in-space maintenance of components, and eliminates or minimizes the configurational impact upon the user vehicles.

Details of the system configuration and operation, taken from ref. 10, are as follows. The propellants are stored cryogenics (i.e., LO_2 and LH_2) which are isolated at low pressure. Figure 15 presents a schematic of a typical system. The engines operate from two charged accumulators one of which stores GH_2, the other GO_2. When the system is activated, GH_2 and GO_2 flow to the engines and the gas generators where they are ignited. The gas generators drive the turbopump and provide heat to vaporize the pumped cryogenics which are stored in the accumulators. The system "bootstraps" and is self-propagating. The system shuts down when the gas supply is shut off.

Key numbers 1 through 4 of Figure 15 represent the fluid transfer elements of the TSPM/user vehicle interface. Key numbers 27 through 35 represent the fluid elements required to interface the tank with the Orbiter. The Orbiter interface will provide for all the "in the bay operations", including the fill, vent, and drain functions on the ground, and the vent and emergency dump function for boost operations.

After the TSPM has been deployed, TSPM to user docking completed, the fluid interface connections verified, and the orbiter separated from the TSPM/user, the fluid transfer cycle is initiated.

The propellant transfer functions of the baseline configuration are as follows. The two gas generator assemblies 38 and valves 39 and 43 will be energized open, causing LO_2 and LH_2 to flow into the gas generator driving the LH_2 and LO_2 turbopumps 45 and 41. High pressure LO_2 and LH_2 from the turbopumps is passed through the heat exchangers 40 and 44 to the accumulators 42 and 37. The pressure level of the accumulators is maintained in the operating band by cycling the turbopumps as required. After operational pressure level is established in the accumulators, the propellant valves in the thrusters are energized open and thrust is generated for use in cross-plane linear acceleration. Recharging of the accumulators will occur while propellant is settled such that liquid can be delivered to turbopumps 41 and 45. Zero-g starting of the thrusting system can be accomplished by drawing gas from the accumulators which could have been charged on the ground through ground fill valves 56 and 57.

Propellant tank NPSP is provided by routing pressurized oxygen and hydrogen gas from the accumulators to the respective tank pressure-control valves 13 and 24. Three-way valves 8 and 21 are positioned to interconnect the ullages of the receiver and logistic tanks during the initial NPSP pressurization cycle. After tank pressure levels within the NPSP requirements of the receiver vehicle have been established, valves 8 and 21 are repositioned to route gas from the receiver through the pump to the logistic tanks. The pumps are energized and the transfer flow control valves 6 and 15 are positioned for chill-down flow rates. After chill down is accomplished, valves 6 and 15 are positioned for the design transfer flow rates. Valves 6 and 15 are

CR54

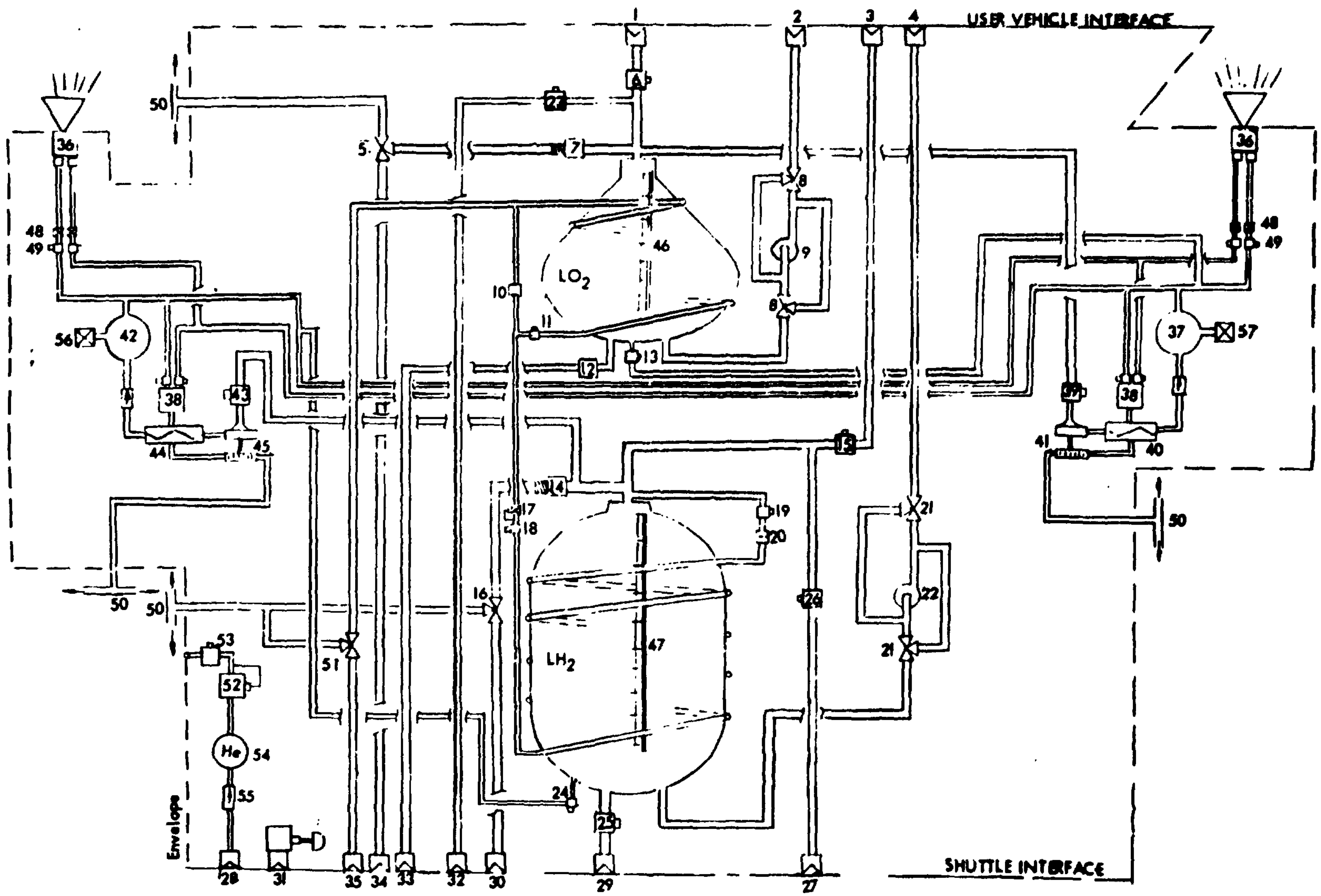

Figure 15. TSPM Systems Schematic

modulating valves and provide the flow control required for chill down and 10-to-1 throttling capability used during the final portion of the propellant transfer cycle to improve the tank feedout characteristics.

The gas pumps and valve clusters also have the capability of reverse propellant flow for detanking the user for emergency or abnormal conditions.

At the conclusion of the transfer cycle, pumps 9 and 22 are shut down and valves 6 and 15 are closed. The independent operational mode is established for the TSPM and user vehicle propellant systems. The cross-plane thrusters will remain in operation until the TSPM and user vehicle reach the closest point with the Orbiter parking plane. At this time the linear acceleration thrusters will be shut down and rendezvous operation with the Orbiter will be initiated.

Some APS stationkeeping may be required during the 3-day coast, but the requirement for having charged accumulators to bootstrap for thrusting and transfer may require that a separate APS stationkeeping system be used. Evaluation of system integration is beyond the scope of this analysis — rather the entire propulsion module weight of 56.6 kg (125 lb), as defined in ref. 10, will be assessed only to the TSPM system. The pressurization system components described above were defined in ref. 10 and their weights, plus the weight of the required plumbing lines, of 24.8 kg (54.7 lb) for the pressurization system and 91.5 kg (201.8 lb) for the transfer/fill system, are common to both the TSPM and to the TVS/WSL. The total weight summary for the TSPM is compared to the TVS/WSL system described in a later section.

<u>TVS/WSL System; 3-Day Transfer Mission.</u> — The TVS/WSL system was analyzed to optimize the system characteristics for the 3-day (88.67 hours including transfer time) coast mission with transfer at 0.1% tank volume/minute. The tankage characteristics are shown in Table 9.

The LH_2 tank pressure was again assumed at 17.25 N/cm^2 (25 psia) and the LO_2 pressure at 19.3 N/cm^2 (28 psia), so the screen bubble points and flow characteristics were modified to these conditions. Because the tankage is of aluminum, aluminum screens were used for the WSL rather than 304 stainless steel screens.

The finest mesh aluminum screen that can be built is 200 x 1400 Dutch twill (the reason for this is that aluminum wire finer than about 0.004 cm (0.0016 inches) in diameter cannot be drawn). This screen was selected because it has the maximum performance and the minimum annulus friction loss characteristics of any aluminum screen. The screen characteristics are shown in Table 10.

Previous work has indicated that at these low flow rates, breakdown will not occur until the tank is nearly empty (very small puddle residual), even for very small annulus gaps. It was originally thought that the minimum annulus gap would be of the order of 0.74 cm (0.29 inch) equivalent gap. Reevaluation of the possible installation methods indicated that smaller equivalent annulus gaps might be possible. Thus, equivalent gaps of 0.74, 0.5, and 0.25 cm (0.29, 0.2 and 0.1-inch) were parametrically studied. The outflow safety factor (ratio of screen bubble point to maximum outflow

TABLE 9. – TVS/WSL TANKAGE CHARACTERISTICS

Propellant	Volume m^3 (ft^3)	L/D	Diameter m (ft)	Tank Wall Area m^2 (ft^2)	Equivalent 1% Annulus Gap cm(in.)	Outflow Baffle Manhole Diameter m (ft)
LH_2	70.8 (2,500)	2	3.78 (12.4)	89.6 (965)	0.79 (0.31)	0.91 (3)
LO_2	21.24 (750)	1	3.44 (11.3)	36.9 (397)	0.58 (0.23)	0.91 (3)

TABLE 10. – SCREEN CHARACTERISTICS

Mesh - 200 x 1400		
Wire Diameter - Shute/Warp - (0.0016/0.0028)		
Weight (Aluminum) - 0.259 kg/m^2 (5.3 lb/100ft^2)		
Performance	H_2	O_2
Bubble Point - cm (ft)	45(1.477)	20.2(0.663)
Flow-Through Coefficients		
A	0.977	0.895
B (ft)	0.6126(2.01)	0.6126(2.01)
Roughness Dimension - cm (in.)	0.00203(0.0008)	0.00203(0.0008)

pressure loss) for a puddle residual of about 0.014 m^3 (0.5 ft^3) is very insensitive to annulus gap, as shown in Figure 16. Therefore, outflow is not the controlling operating condition, which is, rather, the TVS flow. The TVS flow rate must be defined ch that adequate flow is circulated in the annulus to prevent boiling. This requires consideration of gap size and pumping power, as well as annulus flow reduction due to flow leakage through the screen from the annulus.

The general criteria are that for the LH_2 tank with low-density propellant, the minimum gap can be somewhat compromised to reduce TVS pumping power, which results in direct vent loss and weight penalty. In the LO_2 tank, on the other hand, because of the high-density propellant, the absolute minimum annulus gap and residual must be retained, even at the cost of extra pumping power, which incurs no boiloff penalty in the LO_2 tank (assuming the H_2 vent rate can handle the O_2 pump heat load).

CR54

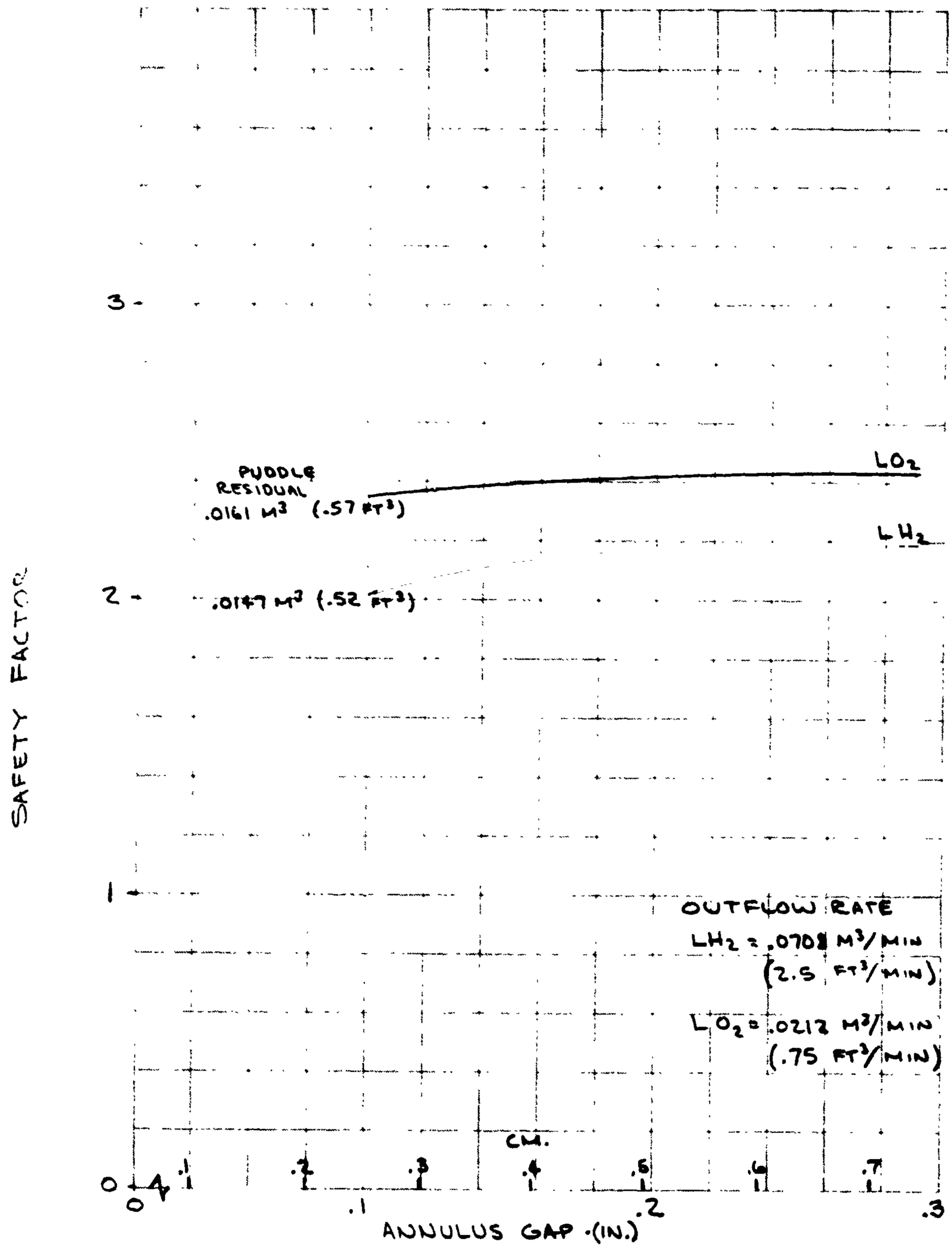

Figure 16. Outflow Safety Factor vs Annulus Gap

An analysis was performed to determine the required minimum flow necessary to remove the radiant heat flux without boiling. The heat flux is low enough to be in the free convection range at 10^{-5} g, and it is essential that the TVS flow against the gravitational buoyancy force not be so low that the flow stagnates. Sparrow and Gregg (ref. 16) have performed an analysis which considers the effects of buoyancy on forced convection flow and heat transfer. They found that the overall heat transfer can be found from the forced convection heat transfer within 5% (i. e., the buoyancy effects are less than 5% of the total) if:

$$Gr \leq 0.225\, Re^2 \tag{8}$$

The characteristic dimension, X, in the Grashof (Gr) and Reynolds (Re) numbers was chosen both to maximize the required flow rate for conservatism and to be representative of the vertical region of reduced flow. For the LH_2 tank, 6.1 m (20 ft) was used (which included the cylindrical length) while for the LO_2 tank, 1.22 m (4 ft) was used as the dimension characteristic of the reduced flow regime. The required flow rate fraction versus annulus gap is shown in Figure 17 for O_2 and H_2 TVS flow rates of 0.1% tank volume/minute to 1% tank volume/minute. Also shown in Figure 17 are the minimum flow rate fractions achieved, as computed by the annulus leakage flow computer code described in Appendix B. The circles indicate the gap where the required flow rate is achieved. Because of the flatness of the flow rate curve, reducing the nominal H_2 TVS flowrate from 1% to 0.1%/minute reduces the pump boiloff by about 6.3 kg, but increases gap residual by only about 5 kg. Since the H_2 system is rather insensitive to gap size, the lower flow rate was chosen to reduce pump boiloff, pump size, and power requirements, etc., while still retaining an achievable and small annulus gap. Therefore, a H_2 TVS flowrate of 0.1% tank volume/minute was selected, together with an equivalent annulus gap of 0.363 cm (0.143-inch), which can be achieved by stretching the screen panels between 0.08 cm (0.032 inch) high supports spaced a maximum of just under 30 cm apart for a total of 40 channel passes. For the O_2 tank, on the other hand, reducing the TVS flow from 1% to 0.1% increases the annulus residual by over 68 kg (150 lb). For this reason, the absolute minimum equivalent gap of 0.25 cm (0.1 inch) was chosen, which requires a TVS flow of 1% tank volume/minute (see Figure 17). This gap can be achieved by using 46 channel passes, giving a screen panel width of a little over 23 cm. As shown in the figure, the minimum flow fraction is 0.038 for the H_2 tank and 0.005 for the O_2 tank. This means that nearly all of the TVS flow leaves the screen annulus and circulates through the tank before reentering the screen, as shown ideally in Figure 18. This has a number of interesting system aspects, as follows:

A. The great bulk of the propellant is continuously mixed in the tank, tending to eliminate hot and cold spots.

B. Outflow during TVS flow is easily accommodated, since a small amount of extra propellant will enter the bottom of the screen for removal and outflow from the standpipe.

C. The pressurant bubble (if pressurized) or vapor bubble will tend to stay near the standpipe since the fluid will tend to flow from the top to the bottom as shown in Figure 18.

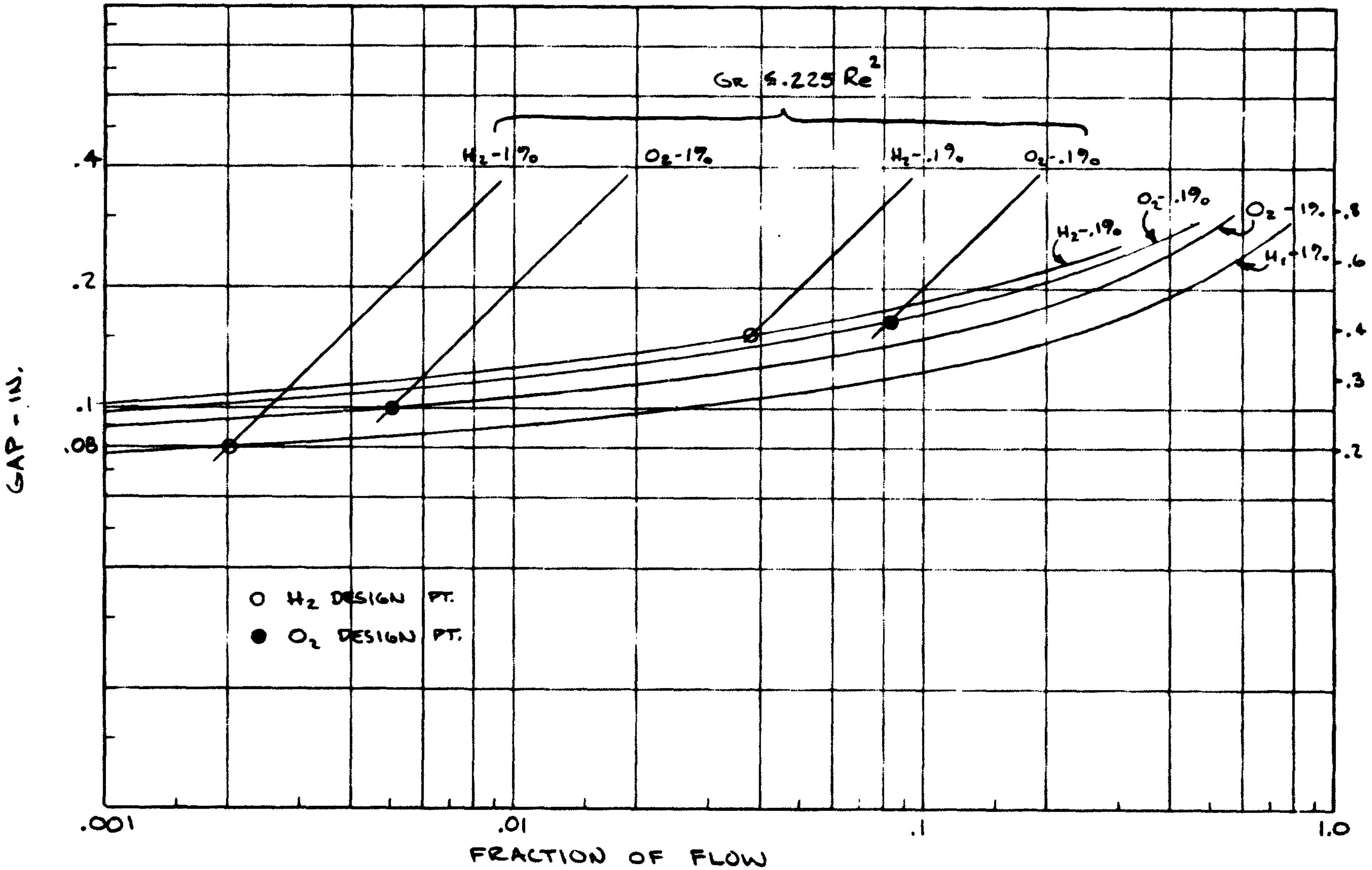

Figure 17. Required Annulus Gap vs TVS Flow Fraction

CR64

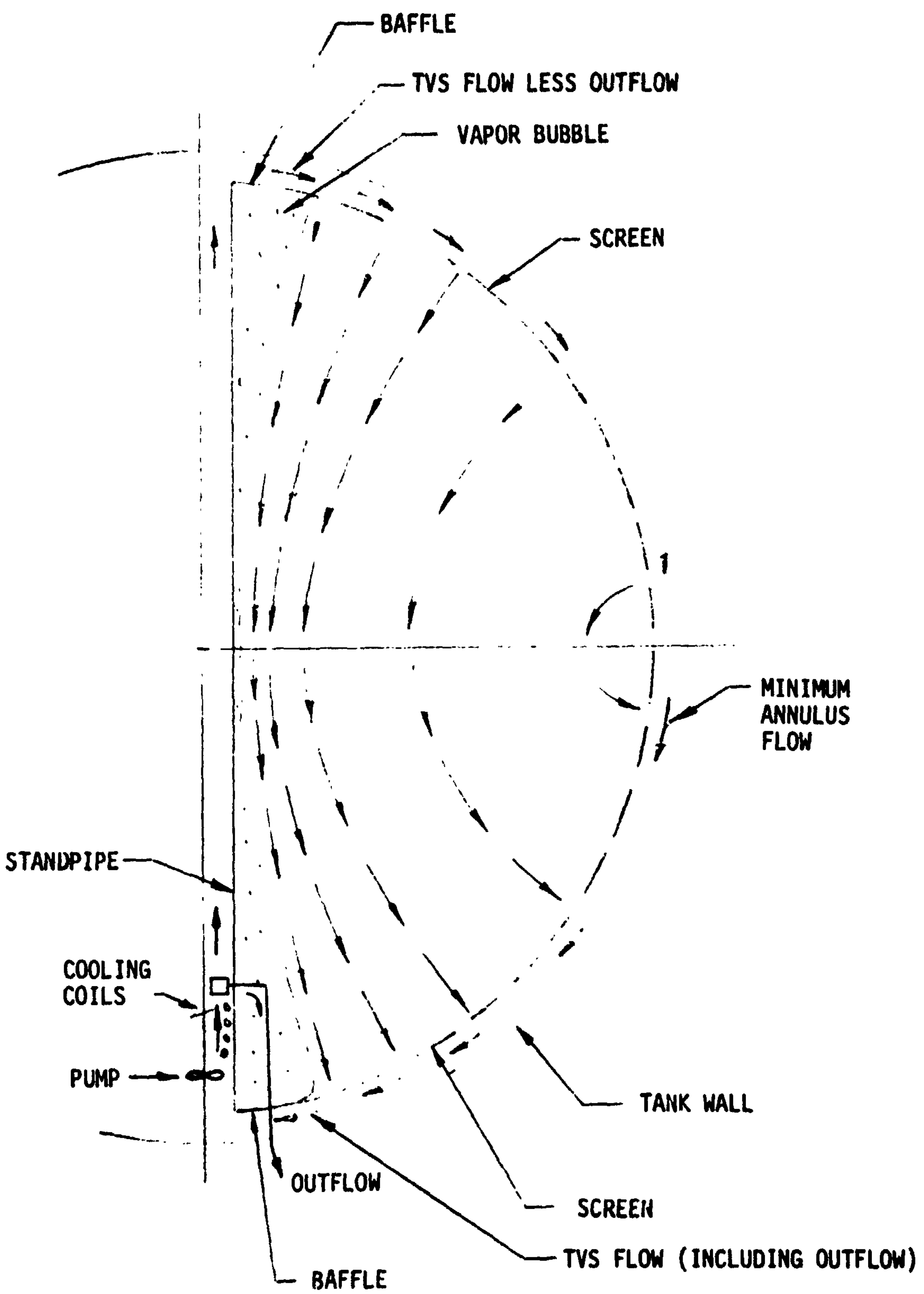

Figure 18. Idealized Liquid Flow Field in Tank

D. The pump head requirements consist only of the frictional loss along the standpipe, frictional loss along the baffle annulus, and integrated annulus friction loss. The dynamic head varies around the annulus, but is not lost in the closed flow path (and thus does not have to be made up by the pump). The entire bulk of liquid in the tank will be accelerated from rest up to the steady-state velocity field where the volumetric flow rate and pressure loss match the pump capability.

E. There is no overwhelming reason to have the pump flow in either direction. The pump flow direction was selected as up the standpipe only so that the flow goes from the pump to the cooling coils, with the pump motor potentially installed in the bottom baffle. This is so that in case of pump efficiency uncertainty, the flow can tend to be cooled down along the standpipe (in case of inadequate TVS cooling) before entering the annulus.

The TVS must remain operating during outflow because of the very long outflow time (16.67 hours), and the design TVS flow rates must be achieved during outflow when the outflow rate of 0.1% tank volume/minute is extracted from the standpipe. Therefore, during coast the TVS flow rate must be 0.2% tank volume/minute for the H_2 tank, and 1.1% volume/minute for the O_2 tank, which will give conservative performance. During outflow the TVS pump will pump 0.1% volume/minute or 1% volume/minute (for H_2 or O_2) out the top of the standpipe and 0.2% volume/minute or 1.1% volume/minute (for H_2 or O_2) into the bottom of the standpipe. The flow distribution in the design annulus during coast and outflow with the TVS operating is shown in Figure 19 for the O_2 and H_2 tanks.

With the TVS flowrate, direction, equivalent annulus gap and gap flow losses defined, the standpipe was then optimized for minimum weight. In the H_2 tank, the standpipe size is optimized by minimizing the sum of the standpipe weight, standpipe residual weight, and boiloff weight due to pump power input, as described previously in ref. 6. However, in the O_2 tank boiloff does not occur, since the H_2 vent gas is used to cool the O_2 tank and keep it vent-free. Instead, reducing the standpipe size and residual increases the O_2 pump power and O_2 tank heat load, which for a given H_2 vent rate, reduces the allowable heat flow through the O_2 MLI, which in turn increases the required O_2 MLI thickness and weight. Clearly a new optimum O_2 standpipe size can be found which minimizes the sum of standpipe weight, standpipe residual weight, and MLI weight. The O_2 pump power and O_2 tank heat load due to pressure loss around the annulus was not directly dependent on the standpipe diameter, did not enter this optimization, and will be accounted for later in the analysis. Similarly the pump/motor weight was a very small value, so that it too was ignored in the optimization, and will be accounted for later.

The O_2 standpipe optimization analysis is developed in Appendix C. Equation (C-15) resulted from this analysis; it was solved by iteration to find standpipe diameter, D_s, as a function of overall pump efficiency, η, with the other parameters known and input. The values are shown in Figure 20 for H_2 from the optimization from ref. 6 and for O_2 from equation (C-15) as the rather flat lines. Cross-plotted in Figure 20 are the functions for total pump size and efficiency versus standpipe diameter for

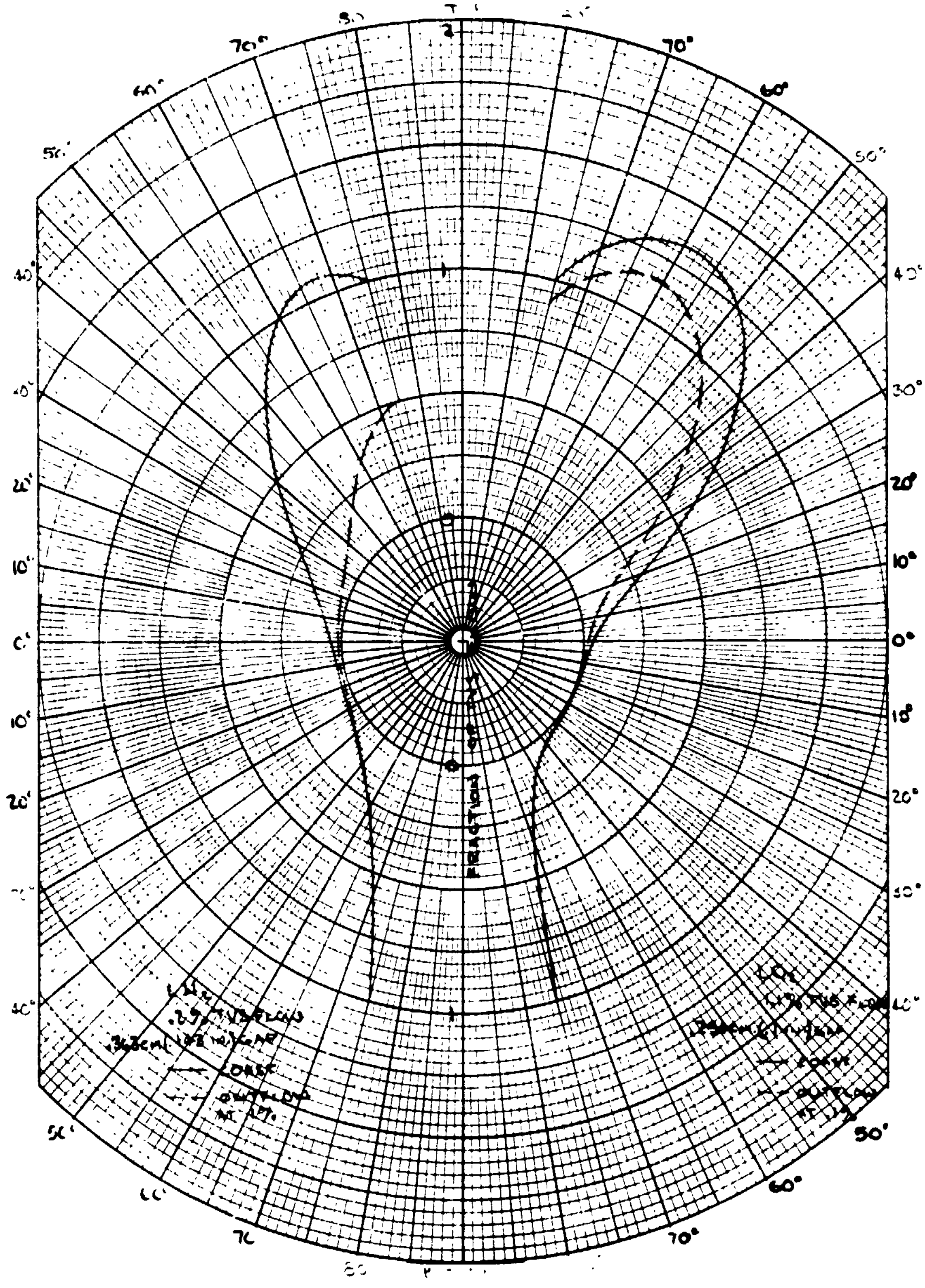

Figure 19. TVS/WSL Annulus Flow Distribution

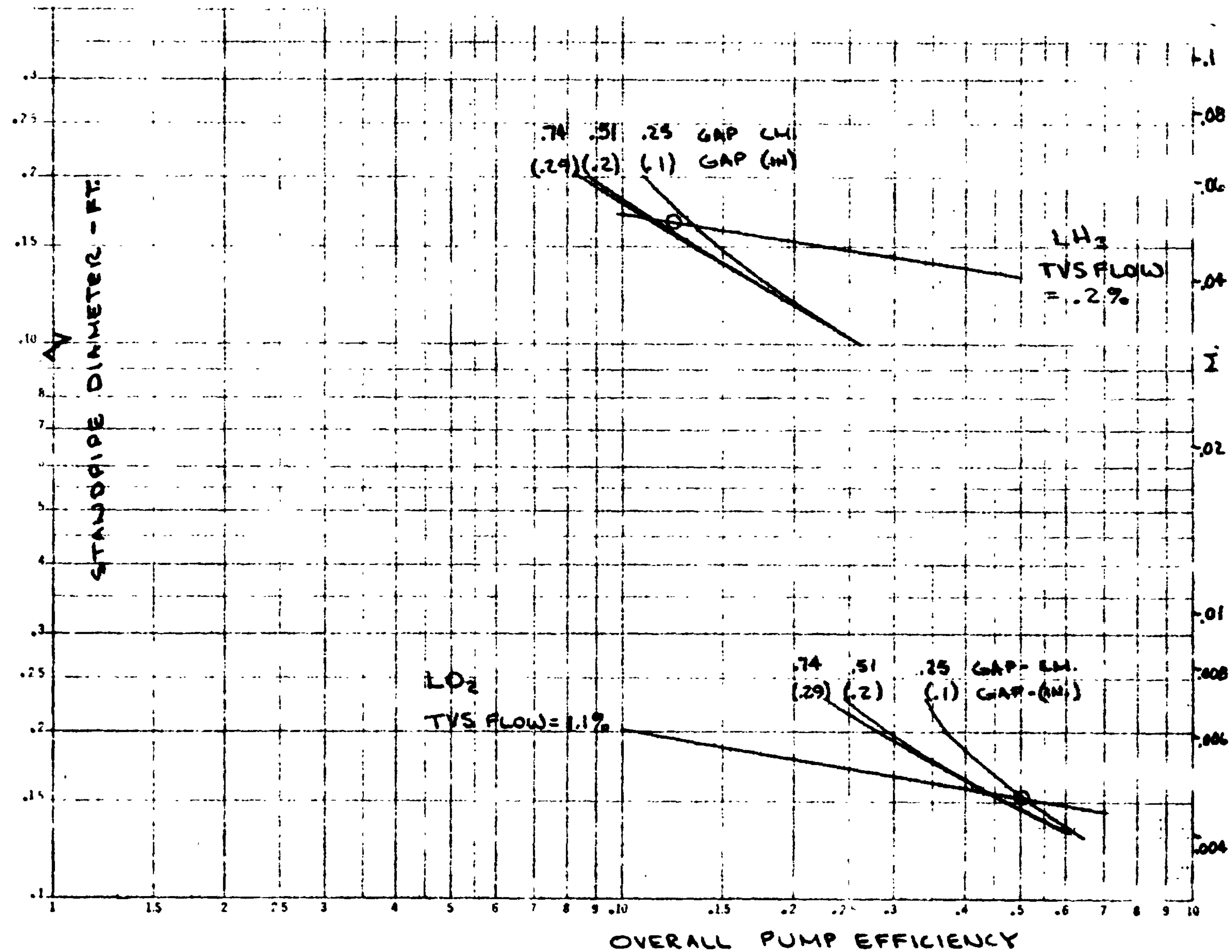

Figure 20. Optimum Standpipe Determination for 3-Day Mission

the total pump power (including standpipe head loss, annulus heat loss, etc.) as defined by the analysis of ref. 6. The circles indicate the optimum standpipe size, which is 0.051 m (2 inch) for H_2 and 0.047 m (1.84 inch) for O_2. With these values of standpipe diameter, the TVS pump parameters, system residuals, and hardware weights were found, using the pump analysis of ref. 6. The system parameters are summarized in Table 11.

It can be seen that the pump diameters are compatible with standpipe size, making installation design straightforward, and the pump operating parameters of rpm, head, efficiency etc. are reasonable. The O_2 pump power input requires that the O_2 tank have 0.915 cm (0.36 inch) of MLI weighing 9.4 kg (20.7 lb) to insure that the H_2 vent flow is adequate to cool the O_2 tank and keep it vent-free.

TABLE 11. – DESIGN TVS/WSL SYSTEM AND MIXER CHARACTERISTICS, 3-DAY MISSION

	H_2	O_2
TVS Pump Head - cm (ft)	12.516 (0.41063)	35.5037 (1.16482)
Annulus loss	(0.009744)	(0.0498)
Baffle loss	(0.014)	(0.12215)
Standpipe loss	(0.38688)	(0.99287)
Pump flowrate - m^3/min(ft^3/min)	0.1416(5)	0.2336(8.25)
Pump efficiency (%)	11.4	50.5
Pump input power (watts)	1.737	29.66
Pump boiloff - kg (lb)	1.28(2.82)	--
External boiloff - kg (lb)	64.4(141.9)	--
Pump speed (rpm)	1342	2284
Pump diameter - cm (ft)	6.04(0.198)	5.97(0.196)
Pump weight - kg (lb)	0.34(0.76)	0.34(0.75)
Motor weight - kg (lb)	0.03(0.07)	0.35(0.77)
Optimum Standpipe Diameter - cm (ft)	5.06(0.166)	4.66(0.153)
Standpipe residual - kg (lb)	1.0(2.3)	6.5(14.3)
Annulus Gap (Equivalent) - cm (in.)	0.363(0.143)	0.254(0.100)
Annulus residual - kg (lb)	22.3(49.1)	105.6(232.9)
Puddle residual - kg (lb)	1.0(2.2)	17.8(89.3)
Standpipe Weight - kg (lb)	3.0(6.7)	1.3(2.8)
Screen Weight - kg (lb)	23.3(51.3)	9.6(21.2)

The screen liner panels are assumed to be mechanically fastened to support angles which are in turn spot-welded to the pressure vessel, as shown in Figure 21.

The weight of the screen liner supports was found by assuming 1.9 x 0.63 x 0.08 cm (0.75 x 0.25 x 0.032 inch) angles as the support members, spaced at the previously mentioned channel widths, and with screen panels 1.22 m (4 ft) long. The combined weight of the supports and fasteners is more than 3-1/2 times the weight of the basic screen.

Cooled-Shield TVS/Partial Screen Liner System; 3-Day Transfer Mission. – When the TVS/WSL system weight analysis was completed, it was found that propellant residual and the WSL weight represented major weight penalties for the TVS/WSL which could perhaps be reduced by considering a partial WSL. It was further noted that the TVS flow was the controlling factor on the design of the WSL, therefore clearly the minimum partial screen liner would be designed only for outflow, with the TVS flow requirements eliminated. Use of a cooled shield TVS would eliminate TVS flow requirements and result in minimum flow passages; this system was, therefore, analyzed first. Initially it was assumed that the number of passes (channels) remained the same (40 for the LH_2 tank and 46 for the LO_2 tank), since that had given reasonable spacing and panel size. The safety factor for outflow was parametrically analyzed versus residual for flow channels 1/6, 1/8, and 1/10 of the full WSL panel width, and at annulus gaps of 0.25, 0.38, and 0.5 cm (0.1, 0.15, and 0.2 inch) for the LO_2 tank, and 0.36, 0.54, and 0.73 cm (0.143, 0.215, and 0.286 inch) for the LH_2 tank. The sum of puddle and channel residual for a safety factor of 2 during outflow at 0.1% tank volume/minute was plotted versus channel width and gap, as shown in Figures 22 and 23. The minimum residual occurs at about 1/8 channel width for both the LH_2 and LO_2 tanks, resulting in a channel which ranges from about 0.63 to 2.5 cm (0.25 to 1.0 inch) wide. Again, the channel height (gap) for minimum residual is 0.25 cm (0.1 inch) for LO_2, but the optimum gap for the LH_2 channel is 0.54 cm (0.215 inch).

The cooled-shield design parameters were evaluated. It was assumed that the shields were made of 1100 aluminum foil, to a minimum of 0.0127 cm (0.005 inch) thick, to which were bonded 1100 aluminum tubes, a minimum of 0.318 cm dia x 0.038 cm (0.125 inch dia x 0.015 inch) wall. Type 1100 aluminum has a conductivity of 260 joule/m-sec-°K (150 Btu/hr-ft-°R) at 17.2°K (31°R), and 306 joule/m-sec-°K (177 Btu/hr-ft-°R) at 75°K (135°R). It was assumed that the vented H_2 was expanded to 3.45 N/cm^2 (5 psi) (17.2°K) and boiled at essentially constant pressure in the H_2 shield.

The H_2 vent gas was assumed to be superheated at essentially constant pressure from 54.5°K (98°R) to 96.6°K (174°R) in the O_2 shield. The MLI on the H_2 tank had been previously optimized for the 3-day mission at 2.08 cm (0.82 inch) thick, with a H_2 vent rate of 0.725 kg/hr (1.6 lb/hr), and an MLI heat flux of 0.97 watt/m^2 (0.3075 Btu/hr-ft^2). This relatively high heat flux could only be absorbed by using rather close spacing of the cooling tubes on the 0.0127 cm thick shield (13.2 cm (5.2 inch) apart with 90 passes). This was arranged with 10 parallel flow passages so that the shield pressure drop was about 0.103 N/cm^2 (0.15 psi). The O_2 shield required 50 passes (at about 21.6 cm (8.5 inch) apart) and because of the very low density of the superheated H_2, the tubing diameter had to be 0.478 cm (0.188 inch) (compared to 0.318 cm (0.125 inch) diameter for the H_2 shield tubing) to limit the O_2 shield pressure drop to 0.234 N/cm^2 (0.34 psi).

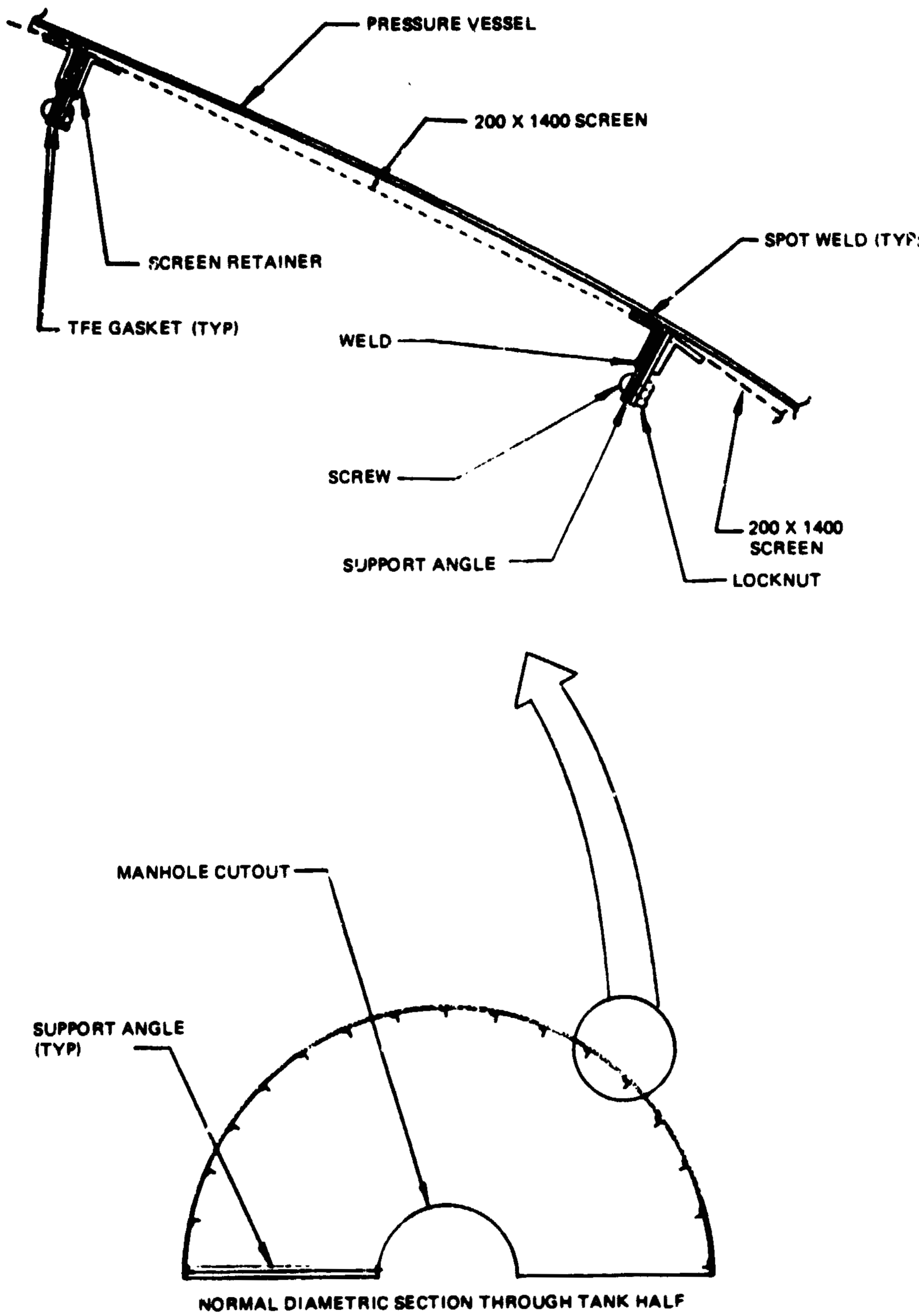

Figure 21. Screen Liner Mounting Method

CR64

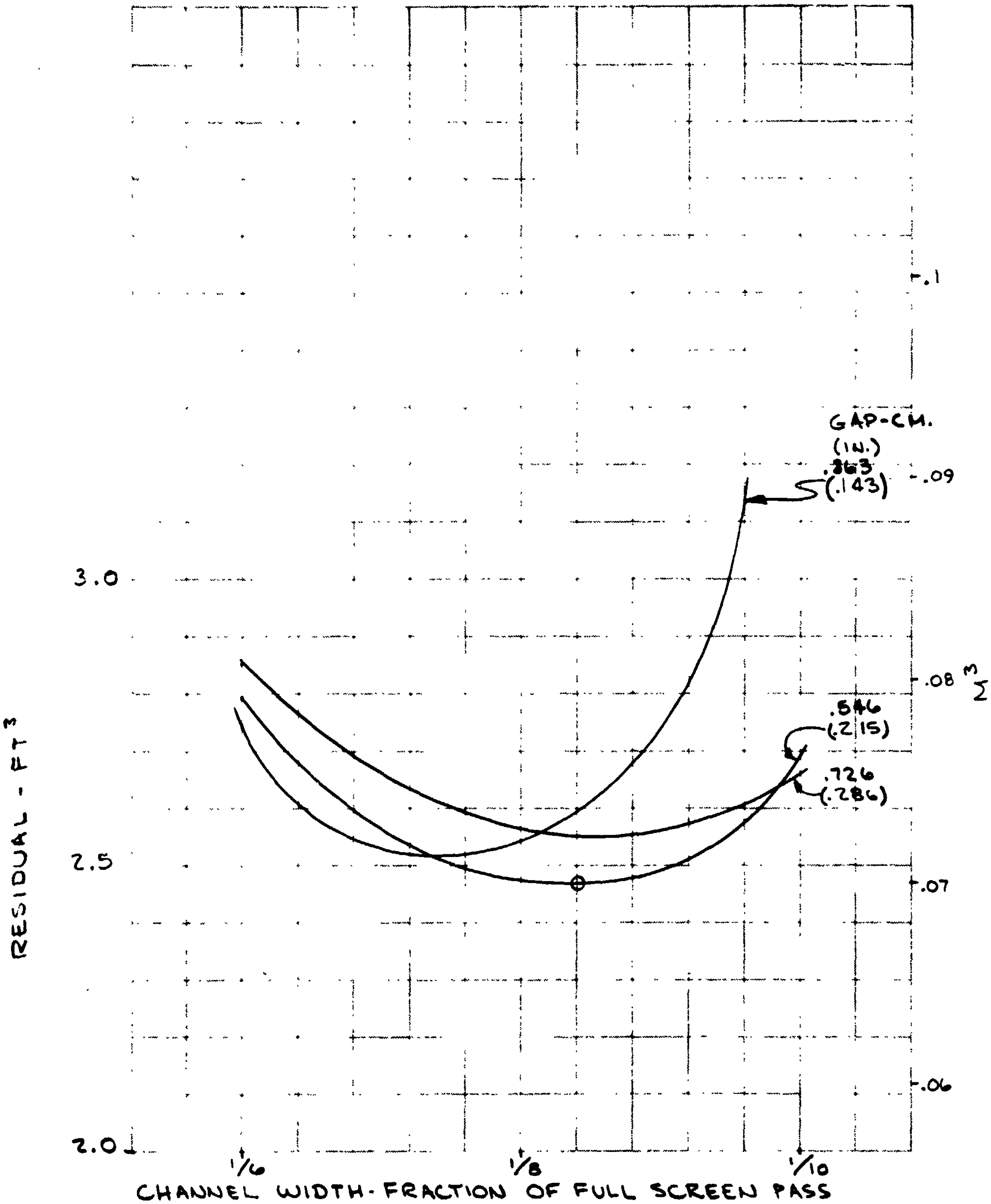

Figure 22. Optimum LH_2 Partial Screen Channel Gap and Width

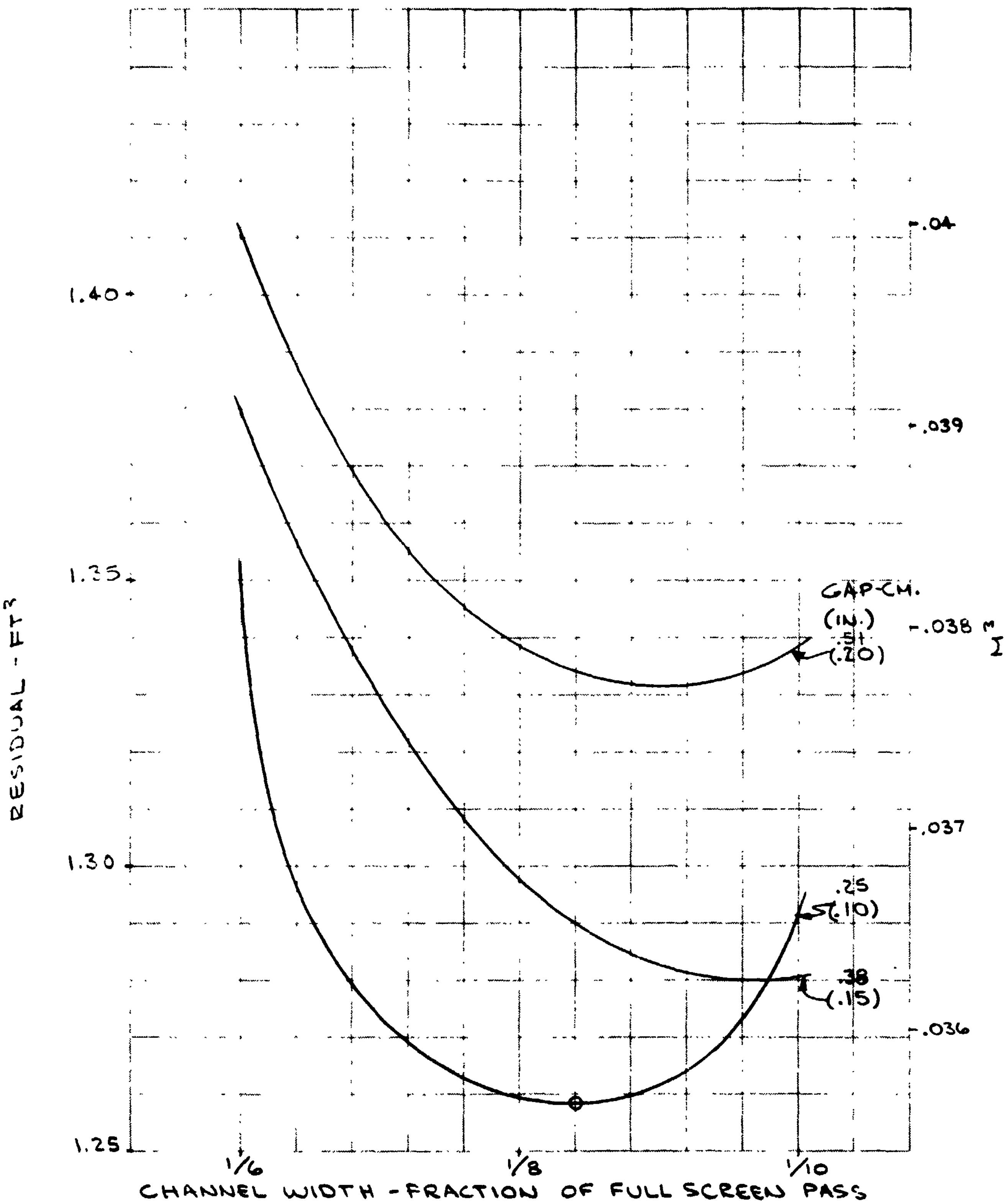

Figure 23. Optimum LO_2 Partial Screen Channel Gap and Width

The close spacing of the tubing in the shields was a consequence of the relatively high heat flux through MLI, and the need to use the thinnest possible shield to reduce weight. Fabricating such a shield for these large tanks would be a significant technical challenge, although MDAC has fabricated smaller shields, as shown in ref. 8. As also mentioned in ref. 8, use of the shield (perforated as is the MLI) to provide MLI support and a MLI purge annulus, eliminated the need for the aluminum mesh support, and saved over 22.8 kg (50 lb).

Weight Comparison and Other System Considerations; 3-Day Transfer Mission. — The final weight summary shown in Table 12 indicates that the cooled shield TVS/partial screen liner is 29% lower in weight than the TSPM and 11% lower than the TVS/WSL.

It is clear that there is no advantage in using a full WSL with a cooled shield TVS, since the full weight penalties of residual and cooled shield would be suffered. However, it is possible that a pumped TVS might be usable in conjunction with a partial WSL. In order for this approach to be feasible, the TVS must be able to cool the tank wall not covered by the partial WSL, and further, in order for this approach to be advantageous, it should show a weight advantage relative to the cooled shield system. The additional residual that could be accommodated (and still allow the pumped TVS to show a weight advantage) was about 34.4 kg (76 lb) (the difference between the cooled shield TVS system weight and the pumped TVS system weight). This indicated that the pumped TVS channel could be about 1.8 times as large as the channel in the cooled shield TVS system. This in turn indicated that the channel spacing, D_o, for 40 channels in the LH_2 tank would be 25.4 cm (10 inch) and for the 46 channels in the LO_2 tank, 18.5 cm (7.3 inches). Using the tank wall thickness and properties, and the shield equation

$$D_o^2 + \frac{4 D_o K}{h_i} - \frac{4 Kt \Delta T}{\dot{q}} = 0, \tag{9}$$

the required ΔT to transfer the incident heat flux, $\dot{q}$, could be found, which was up to 1.67°K (3.0°R) for the LH_2 tank at the tank midriff, and up to 17.2°K (31°R) at the tank midriff for the LO_2 tank. To prevent boiling in the tank, the fluid circulated by the TVS would have to be subcooled by the above temperature differences, which could not conceivably be done in the tank. Clearly, vented fluid could be expanded in a cooled shield, and temperature gradients like those above could be obtained in the isolated shield; however, subcooling temperature gradients like those mentioned could not be obtained with the channels in contact with the bulk fluid. Even using high conductivity tank material for the LO_2 tank required 9.5°K (17°R) subcooling, while costing over 56.6°kg (125 lb) in tank weight (due to reduced strength of the higher conductivity tank material).

In order to limit the required temperature gradient in the LO_2 tank to 0.061°K (0.11°R) (the incipient boiling point) the channel spacing for 46 channels would have to be only 0.02 cm (0.008 inch). This would save less

TABLE 12. – COMPARISON OF TSPM AND TVS/WSL WEIGHTS (KG) FOR 3-DAY MISSION

	TSPM	TVS/WSL	Cooled Shield TVS Partial Screen Liner
A. Tankage			
H_2	248.6	248.6	248.6
O_2	144.2	71.7	71.7
B. Pressurization System	24.8	24.8	24.8
C. Insulation			
H_2 MLI	52.0	52.0	52.0
O_2 MLI	11.4	9.4	8.6
Purge system			
Components	5.4	5.4	5.4
He bottle	47.6	47.6	47.6
He	6.0	6.0	6.0
Mesh	25.0	22.9	0
D. TVS			
H_2	4.7	0.8	42.5
O_2	1.1	1.1	18.7
Components	7.3	2.3	2.3
E. WSL and supports	0	153.2	123.3
F. Propulsion module	56.7	0	0
G. Propellant residual	163.3	154.3	44.2
H. Propellant boiloff	64.4	65.6	64.4
I. Propulsive propellant	272.2	0	0
J. Hardware			
Transfer and fill systems	91.5	91.5	91.5
Baffles	0	17.7	17.7
Standpipes	0	4.3	0
TOTAL	1226.2	979.2	869.3
(lb)	(2703.3)	(2158.9)	(1916.6)

than 0.23 kg of LO_2 residual compared to a full WSL, but would incur additional weight of screen supports to obtain this gap. Therefore, use of a partial screen liner in conjunction with a pumped TVS was simply not practical.

Tug-Scale Propulsion Module; 7-Day Restart Mission. – For the 7-day restart mission, the TSPM was assumed to be a Tug vehicle initially weighing 29,400 kg (65,000 lb). Typically, engine start propellants are provided by tank pressurization, providing the propellants are settled by using the auxiliary propulsion system. It was assumed that this technique was used for this mission, and the necessary settling propellants for six restarts was determined.

MDAC has developed a complete analysis of propellant settling (ref. 17) which has been correlated with experiment and which accounts for liquid fall; liquid turbulence dissipation; bubble formation, rise, and displacement; and laminar-wave energy dissipation; The equations have been programmed in a computer code, H470, which was used to predict the settling time and settling propellant weight for each of the six burns of the 7-day mission. Minimum settling propellant penalty occurs with minimum settling accleration, so for this study, a minimum settling thrust of 15.5 N (3.5 lb) (the same as for the 3-day mission TSPM) was arbitrarily selected. The maximum settling time occurs for settling of the LH_2 tank, since it is twice as long as the LO_2 tank.

The start-up characteristics of the RL-10 derivative engine are shown in Figure 24, and are as follows: 2224 N (500 lb) thrust is reached 0.2 second after restart and is maintained for about 1.8 seconds, after which the thrust climbs rapidly, reaching 90% of the rated 66,720 N (15,000 lb) thrust about 2.1 seconds after initiation of restart. During this time, the LH_2 restart flow rate is 2.12 kg/sec (4.666 lb/sec) (equivalent to 0.0437% tank vol/sec) and the LO_2 flow rate is 12.7 kg/sec (28 lb/sec) (0.0541% tank vol/sec). These values were used in the analysis.

The propellant loading for the TSPM is most important since it strongly influences the g-level occurring during the final restart. The propellant loading history for initially full tanks and for the mission shown in Table 3 resulted in 4300 kg (9500 lb) of residual following the final burn. It was felt that a more severe requirement for the system would be to initially off-load the tanks, so that following the last burn, 2% of the propellant would remain as residual/contingency. The propellant loading and usage history based on 2% residual is shown in Table 13.

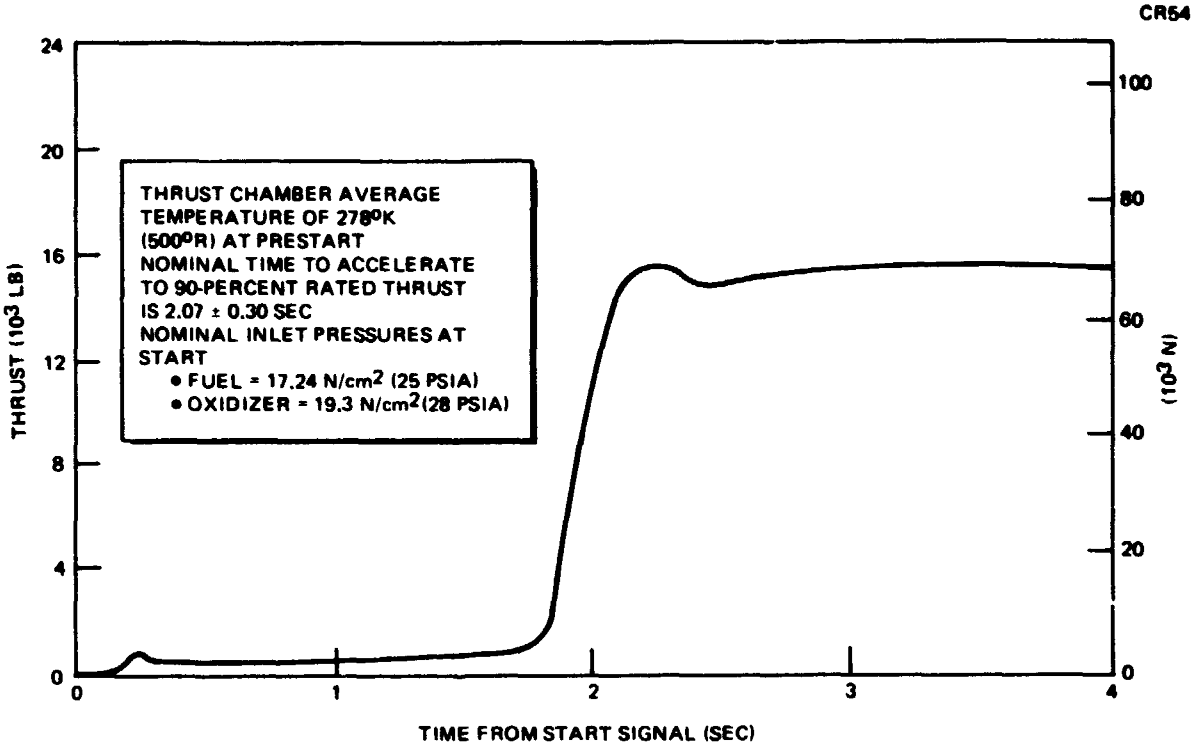

Figure 24. Estimated Tug Engine Start Transient Thrust vs Time

The TSPM has residual unavailable to the engine during high-g thrusting as a result of pull-through near the end of draining. Because of the high g-levels involved, it was not necessary to assume a conical-bottomed LO_2 tank to reduce residuals; rather, the LO_2 tank was assumed spherical with a resulting weight savings of 72.5 kg (160 lb). The pull-through height, h, for the TSPM was found from the correlation of ref. 18;

$$\frac{h}{D} = 0.43 \tanh \left[1.3 \left(\frac{V_m^{\ 2}}{gd} \right)^{0.29} \right] \tag{10}$$

where d is the drain diameter and D is the tank diameter. This equation was developed from experiments on flat bottom cylinders with center drains; however, the modified Froude number of equation (10) gives a good correlation for h in spherical tanks when the mean velocity, V_m, and the tank diameter are based on the wetted portion of the tank at pull-through, as shown in Figure 25.

From Figure 25,

$$V_m = \frac{\dot{Q}}{\pi r^2} \text{ where } D = 2r \tag{11}$$

TABLE 13. – CONSUMPTION, VENTING, AND SETTLING PROPELLANT HISTORY

	LH_2 (kg)	LO_2 (kg)
7-Day Mission		
Inert Weight = 3,586 kg (5,700 lb)		
Initial Propellants	3,377	19,714
174.74-Hour Venting	75	0
	(3,302)*	(19,714)
Settling for POI Burn	1	3
POI Burn	521	3,124
	(2,780)	(16,587)
1.92-Hour Venting	1	0
	(2,779)	(16,587)
Settling for TOI Burn	1	3
TOI Burn	1,257	7,544
	(1,521)	(9,040)
5.27-Hour Venting	2	0
	(1,519)	(9,040)
Settling for MOI Burn	3	19
MOI Burn	775	4,649
	(741)	(4,372)
11.15-Hour Venting	5	0
	(736)	(4,372)
Settling for TOI Burn	2	9
TOI Burn	355	2,134
	(379)	(2,229)
5.27-Hour Venting	2	0
	(377)	(2,229)
Settling for POI Burn	1	7
POI Burn	165	991
	(211)	(1,231)
3.02-Hour Venting	1	0
	(210)	(1,231)
Settling for Rendezvous Burn	1	6
	140	838
	(69)	(387)
5.23-Hour Venting	2	0
Residual Contingency (2%)	67	387

*Parentheses indicate residual at this point in mission

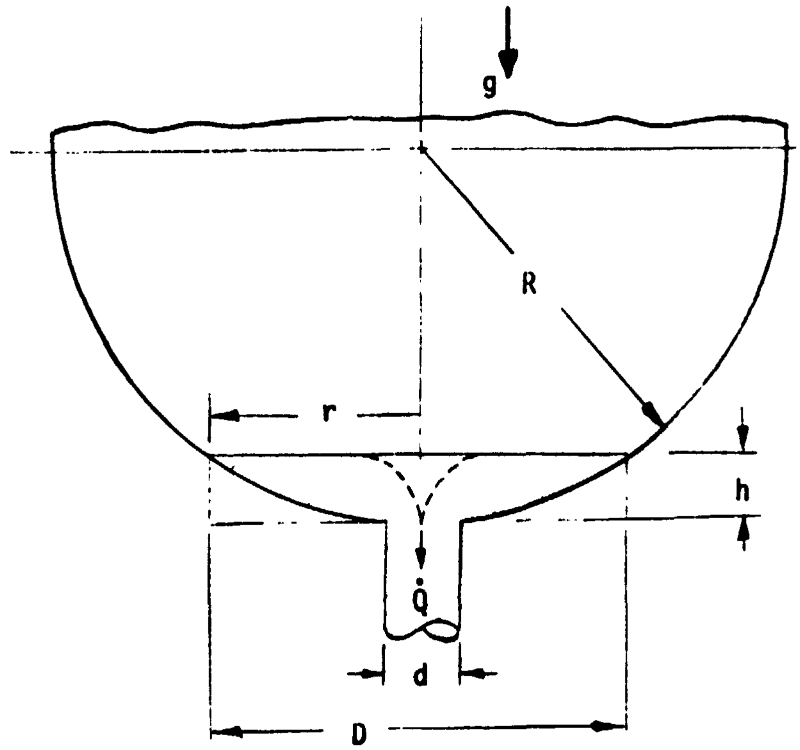

Figure 25. Draining Pull-Through Nomenclature

and r is related to the tank radius, R, and h by

$$r = (2\,R\,h - h^2)^{1/2} \tag{12}$$

Equations (10 through (12) were combined and solved for the pull-through height at the final burn termination and assuming burning of the residual, with acceleration, g, ranging from 22 to 25.8 m/sec^2 (72 to 84.5 ft/sec^2) for both the LO_2 and LH_2 tanks. The total unavailable residual due to pull-through was found to be 13.1 kg (29.0 lb) for the TSPM.

TVS/WSL System; 7-Day Restart Mission. During restart, the flow rates are quite high, and for the final burn, the propellant quantities are low, so that the final burn restart is the controlling design criteria for the screen device. Therefore, prior to the final rendezvous burn, the propellant quantity was 209 kg (461 lb) H_2 and 1228 kg (2714 lb) O_2, as shown in Table 13.

Since the rendezvous burn takes place in a 160-nmi orbit, it was assumed that a drag force had occurred to force the propellant away from the engine inlet at 10^{-6} g's. This gave Bond numbers of 1.48 for the LH_2 tank and 2.74 for the LO_2 tank. Assuming standpipe diameters of the order of 0.021 m (0.07 ft), the annulus ratio (ratio of standpipe diameter to tank diameter) was about 0.006. The contour of the interface in the tanks, based on these Bond numbers and annulus ratios, from the data of ref. 19 for a contact angle of 0°, is shown in Figure 26 for the rendezvous burn restart. Initially, when the engine flow is first started, but before the thrust reaches 2224 N (500 lb), the required flow must be lifted against 10^{-6} g's. The safety factor for this condition versus annulus gap is shown in Figure 27. For a safety factor of 2, the equivalent annulus gap required was 0.065 cm (0.27 inch) for the LH_2 tank and 0.4 cm (0.158 inch) for the LO_2 tank. When the 2224 N (500 lb) thrust comes on, the g-vector reverses, and breakdown would tend to occur near the bulk liquid (rather than at the outflow baffle, as was the case under a negative 10^{-6} g's) and the critical head which must be supported is the sum of the acceleration head imposed by the 2224 N (500 lb) thrust ($\sim$0.056 g's) and the dynamic head in the annulus where the bulk liquid interface is (see Figure 26). The safety factors based on these conditions are also shown in Figure 27, and indicate that the safety factor is dominated by g-level (and very insensitive to annulus gap or dynamic head), and that for the LH_2 tank the safety factor drops from 2.0 to 1.35, and for the LO_2 tank, from 2.0 to 1.65. The only practical way to increase the safety factor during the period of 2224 N (500 lb) thrust is to reduce the g-level by increasing the propellant load (namely, the residual/contingency, since the burn requirements are fixed). However, it would require more than 10% contingency to raise the LH_2 tank safety factor to 2. Since a safety factor of 2 is an arbitrary standard, increasing the contingency propellant was not a reasonable solution; rather, the system should have been designed to the initial conditions (the screen may not break down at 2224 N (500 lb) thrust anyway). Breakdown during this low thrust phase was academic since when full thrust was reached, after 2 seconds, the g-level will be 1.69 g's and the screen would certainly have broken down. An additional remaining question was whether there was enough propellant in the annulus to feed the engine if bubble ingestion did occur under the 2224 N (500 lb) thrust. With the above annulus gaps and flowrates, there was over 15 seconds of LH_2 and 8 seconds of LO_2 in the annulus. The time required for settling after full thrust is reached was about 0.7 second for the LH_2 tank and 0.3 second for the LO_2 tank (plus 2 seconds at 2224 N (500 lb) thrust). Thus there was ample reserve in the annulus to provide propellant to the engine, even if the 2224 N (500 lb) thrust induced breakdown.

During full thrust operation, the TVS pumps would be overpowered by the high outflow rates, and should be turned off. There would not be enough heat transferred into the tank during the short-duration burns to cause problems. Following the burn, in low-g (10^{-6} g's), the screen annulus would refill with propellant, aided by the TVS flow and heat exchanger, which would tend to condense any remaining vapor in the annulus. Since the annulus gap was defined by the outflow requirements, the TVS flow was analyzed to be the minimum necessary to prevent boiling in the given annulus, according to the criterion of Sparrow and Gregg (as described previously, ref. 16). The results are shown in Figure 28. It was found that for a given annulus gap, the minimum fraction of flow was nearly constant, as shown in Figure 28. The required TVS flowrates, defined by the ref. 16 requirements, were 0.011 m^3/minute (0.39 ft^3/minute) for the LH_2 tank and 0.0255 m^3/minute (0.9 ft^3/minute) for the LO_2 tank. With the annulus gaps and TVS flow rates defined, the optimum standpipe diameters were found, based on the analyses of ref. 6 and Appendix B for the LH_2 and LO_2 tanks, respectively, and are 0.02 m (0.8 inch) diameter for the LH_2 standpipe, and 0.022 m (0.875 inch) diameter for the LO_2 standpipe. With these values

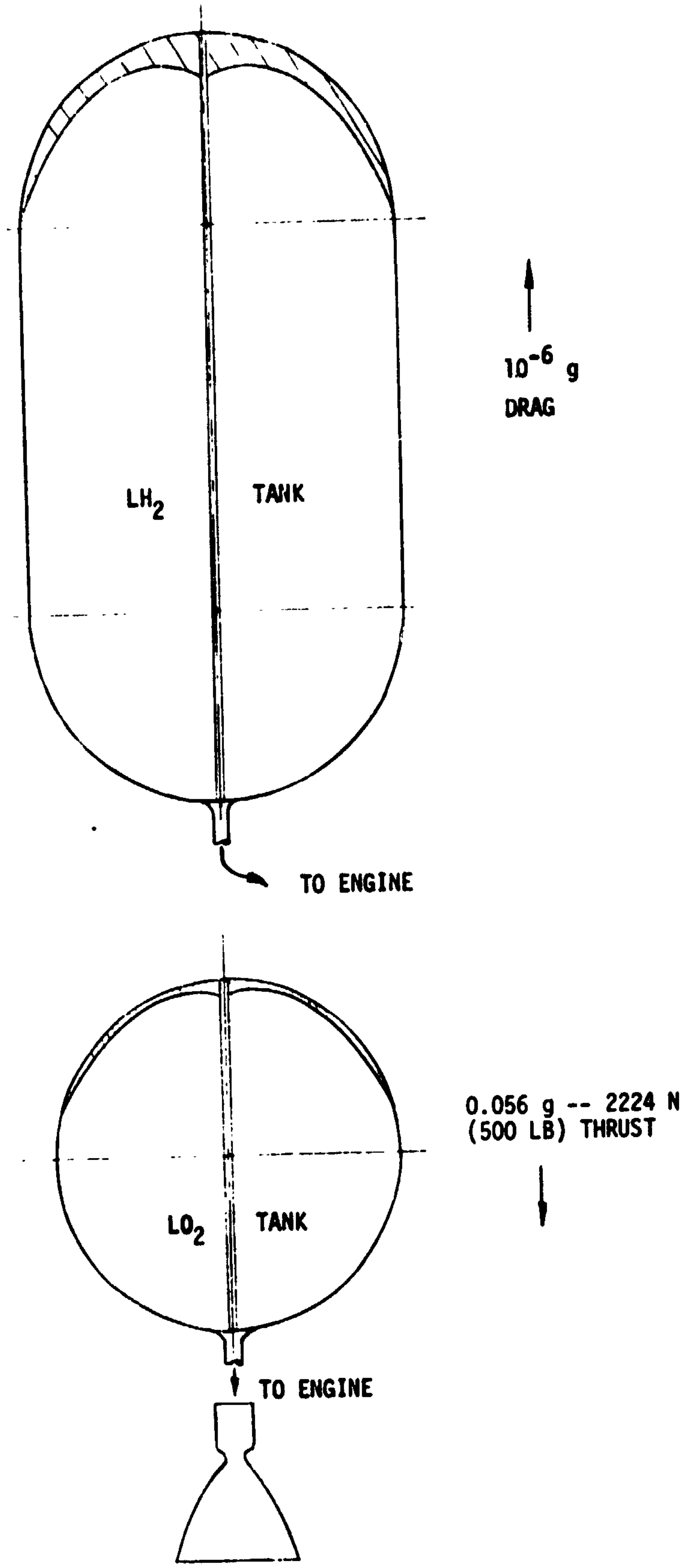

Figure 26. Propellant Interface Contours at Restart

CR54

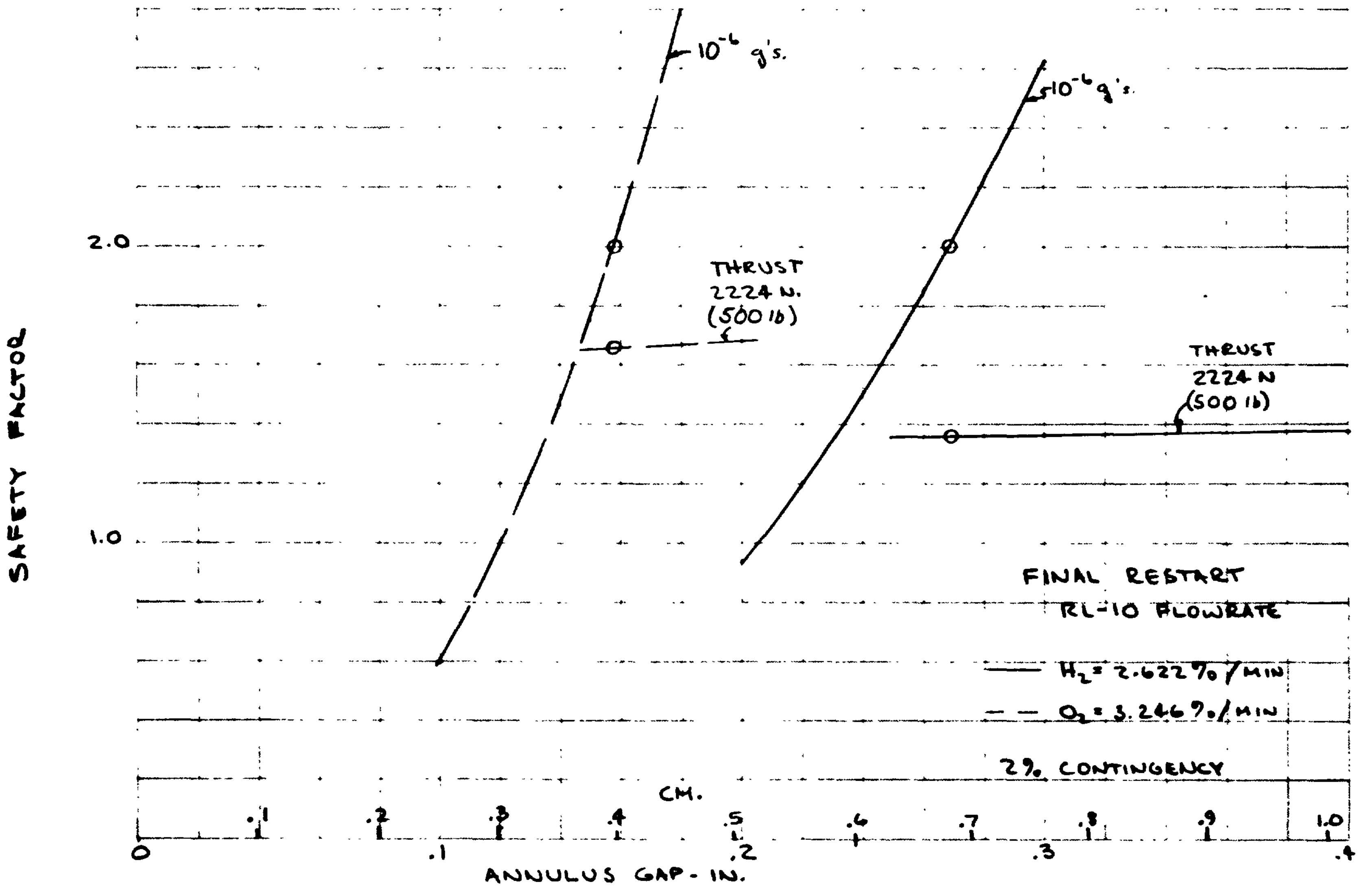

Figure 27. Annulus Gap vs Safety Factor for TVS/WSL for 7-Day Restart Mission

CR54

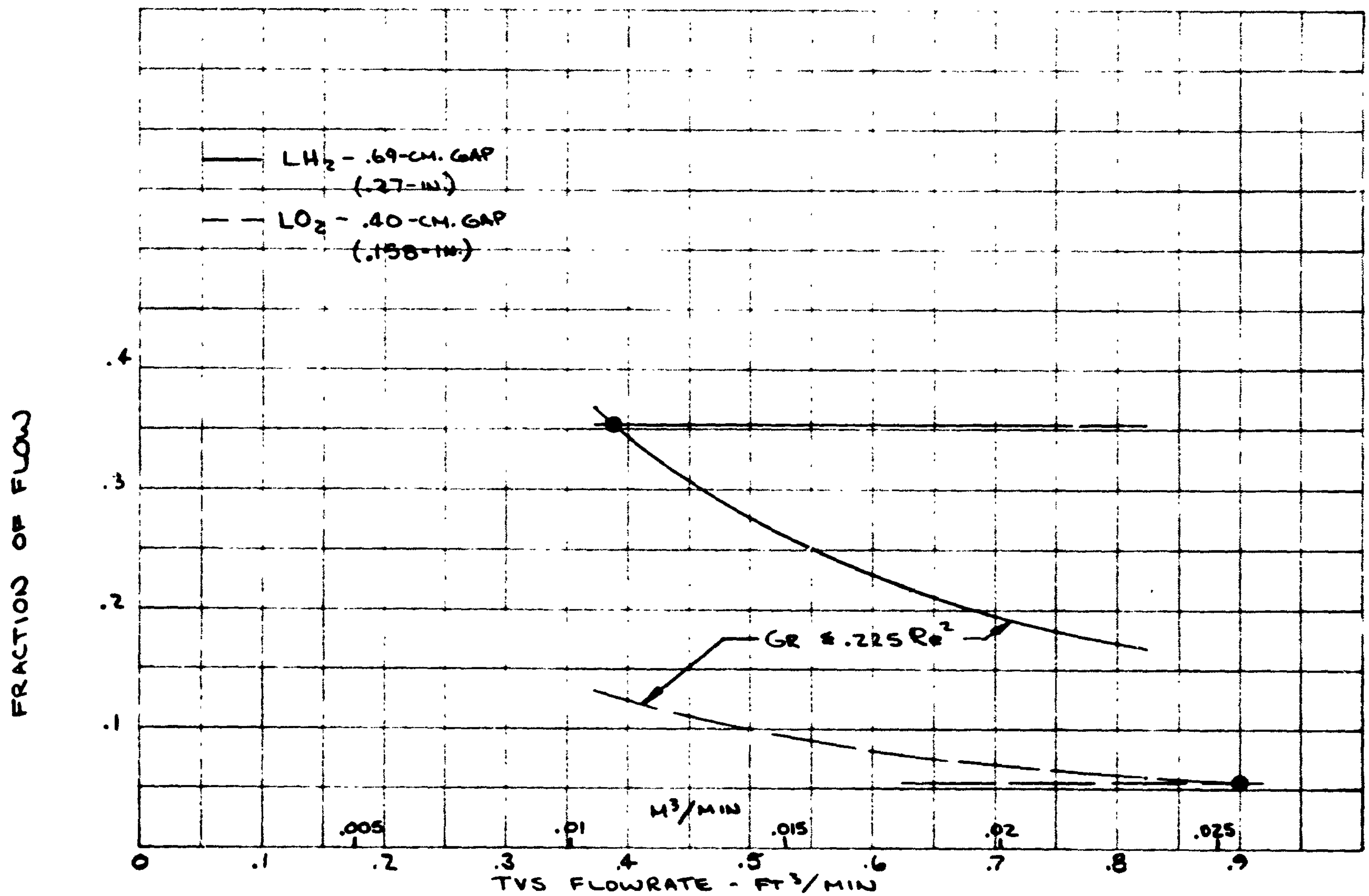

Figure 28. Required TVS Flowrate for 7-Day Restart Mission

of standpipe diameters, the TVS pump parameters, system residuals, and hardware weights were found, using the pump analysis of ref. 6. The results are shown in Table 14.

It can be seen that the pump diameters were reasonably compatible with the standpipe sizes, making installation design straightforward, and the pump operating parameters of rpm, head, efficiency, etc., were reasonable. The LH_2 pump input power was very small, but above the minimum feasible value of 0.1 watt. The LO_2 pump input power is too small to have a noticeable effect on the O_2 MLI thickness or weight for the TVS/WSL.

The TVS/WSL annulus (or standpipe) residual is not relevant because complete screen breakdown will occur under full 66,720 N (15,000 lb) thrust. The 2% residual/contingency of 452.7 kg (998.0 lb) is greater than the annulus residual and is all available to the engine during high-g thrusting except that trapped by the outflow baffle, as puddle residual (a total of 24.2 kg (53.4 lb)). This mass will be assessed to the TVS/WSL as a penalty.

TABLE 14.—DESIGN TVS/WSL SYSTEM AND PUMP CHARACTERISTICS FOR 7-DAY MISSION

	H_2	O_2
TVS Pump Head - cm (ft)	5.324 (0.17467)	12.2615 (0.40228)
Annulus loss	(0.000161)	(0.00108)
Baffle loss	(0.000190)	(0.00504)
Standpipe loss	(0.174321)	(0.39616)
Pump flowrate - m^3/min (ft^3/min)	0.011 (0.39)	0.0255 (0.9)
Pump efficiency (%)	3.53	16.34
Pump input power (watts)	0.186	3.45
Pump boiloff - kg (lb)	0.32 (0.7)	---
External boiloff - kg (lb)	88.9 (195.9)	---
Pump speed (rpm)	2531	3115
Pump diameter - cm (ft)	2.10 (0.069)	2.59 (0.085)
Pump weight - kg (lb)	0.029 (0.064)	0.047 (0.104)
Motor weight - kg (lb)	0.0021 (0.0047)	0.034 (0.075)
Optimum Standpipe Diameter - cm (ft)	2.04 (0.067)	2.23 (0.073)
Standpipe residual - kg (lb)	0.18 (0.4)	1.5 (3.3)
Annulus Gap (Equivalent) - cm (in.)	0.71 (0.28)	0.41 (0.16)
Annulus residual - kg (lb)	43.2 (95.3)	166.8 (367.7)
Standpipe Weight - kg (lb)	1.1 (2.4)	0.54 (1.2)
Screen Weight - kg (lb)	23.3 (51.3)	9.6 (21.2)

TABLE 15. - COMPARISON OF TSPM AND TVS/WSL WEIGHTS (KG) FOR 7-DAY MISSION

	TSPM	TVS/WSL
A. Tankage		
H_2	248.6	248.6
O_2	71.7	71.7
B. Pressurization system	24.8	24.8
C. Insulation		
H_2 MLI	88.2	88.2
O_2 MLI	14.6	14.6
Purge system		
Components	5.4	5.4
He bottle	47.6	47.6
He	6.0	6.0
Mesh	22.9	22.9
D. TVS		
H_2	3.4	0.5
O_2	1.1	0.5
Components	7.3	2.3
E. WSL and supports	0	124.9
F. Propulsion module	56.7	0
G. Propellant residual (2%)	(452.7)	(452.7)
(Unavailable residual)	13.1	24.2
H. Propellant boiloff	88.9	89.2
I. Propulsive propellant*	17.8	0
J. Hardware		
Transfer and fill systems	91.5	91.5
Baffles	0	17.7
Standpipes	0	1.6
TOTAL	809.6	882.2
(lb)	(1784.0)	(1945.2)

*Propellant required for ΔV at I_{sp} = 350 sec instead of I_{sp} = 460 sec (main engine)

Weight Comparison and Other System Considerations; 7-Day Restart Mission. – Since only the TVS/WSL puddle residual trapped by the outflow baffle was unavailable, trying to use a partial screen to reduce residual was pointless. Therefore, use of a partial screen liner was not practical for the 7-day coast/restart mission. Further, use of a cooled shield TVS showed no advantage, because, although a partial screen could be used, only the screen weight would be reduced (but the screen support weight would be essentially unchanged). Since the total cooled shield weight was 62.2 kg (135 lb), and the combined weight of screens, TVS and mesh MLI supports was 56.6 kg (125 lb), there was no way that use of a cooled shield could show a weight advantage. Therefore, the only two systems which were considered and compared were the TSPM and the TVS/WSL, shown in Table 15.

The weight of the WSL shown in the table was found using the same screen support configuration assumptions as for the 3-day mission; however, because fewer passes and supports are needed, the WSL weight was somewhat less than for the 3-day mission configuration.

It can be seen that the TSPM was 8.2% lighter than the TVS/WSL for the 7-day coast/restart mission. It can be concluded from this that the TVS/WSL was not used to its best advantage in a purely restart type of mission. However, the WSL system had the capability to perform this mission, and if a cooled shield TVS were used (at an additional weight penalty of perhaps 9 kg (20 lb)) restart could be accomplished with a completely passive system.

Life Support Power Supply Reactant System

Definition of the physical and operational characteristics of the baseline 0.5 m^3 (17.5 ft^3) supercritical cryogenic gas storage system (CGSS) was based on Reference 20. This design was developed for the Apollo Applications Program (AAP) and was an extension of the technology developed for the Apollo environmental control system/fuel cell supply system. The two propellant storage systems studied were for H_2 and O_2, and the system is shown in Figure 29.

Each storage tank consisted of two concentric shells, and the annular space between the shells was evacuated. There were two concentric, discrete, aluminum shields that acted as thermal-radiation barriers within the vacuum annulus. The innermost shield on both types of tanks (oxygen and hydrogen) had provisions for vapor cooling. The supply fluid passed through a tube that was brazed to this shield prior to exiting the dewar system, thus cooling the shield. This cooling made the shield more efficient in the interception of incoming heat. Part of the intercepted heat was absorbed by the exiting fluid and was carried out of the system.

The inside of the vacuum jacket, outside of the pressure vessel, and both shields were silver-plated for low emissivity. The shields were 0.05 cm (0.020 inch) thick and weighed 4.54 kg (10 lb) apiece.

The pressure vessel was supported by 16 radial bumpers – 8 bumpers on the bottom hemisphere and 8 bumpers on the top hemisphere. These bumpers were made of a low-thermal-conductivity material known as Kel-F.

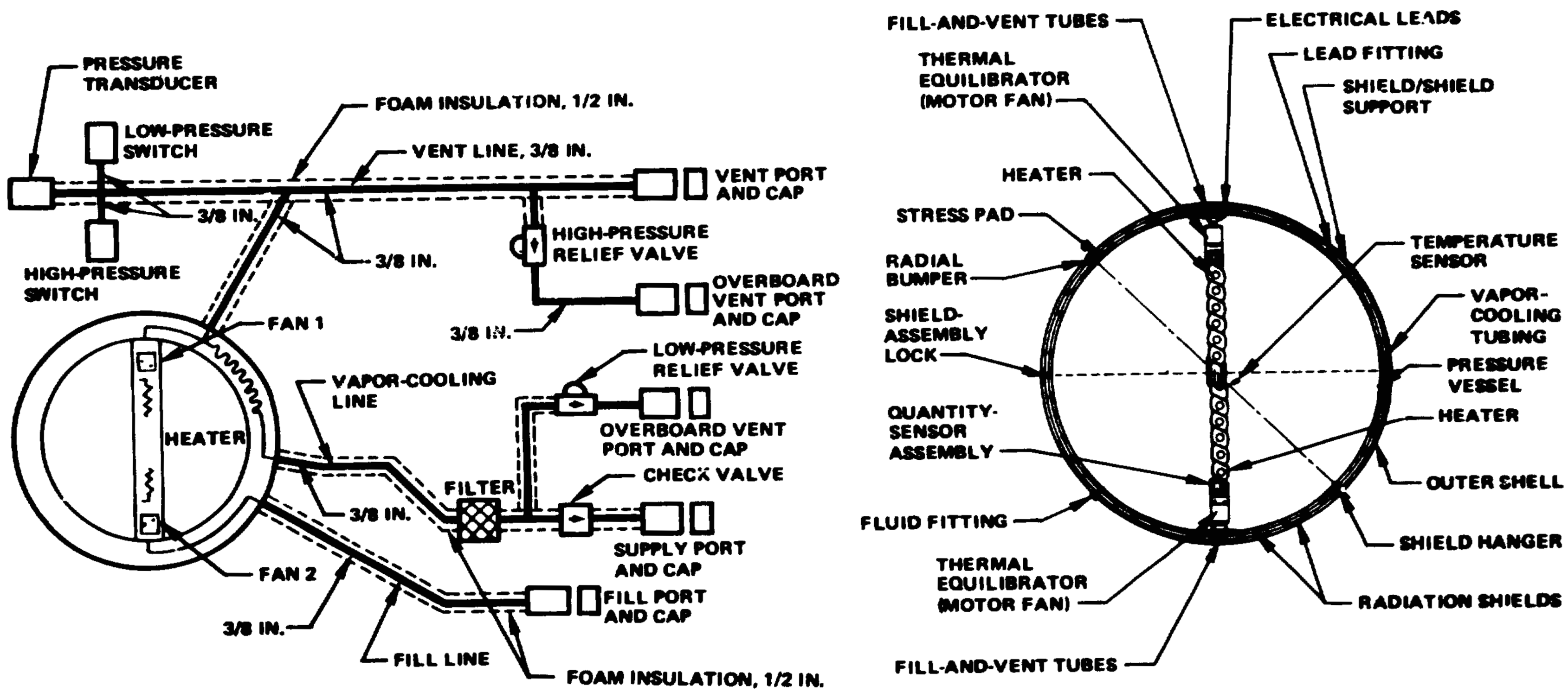

Figure 29. Supercritical Storage System

The pressure-vessel loads were transmitted through the bumpers to the mount structure. The fluid-equilibration-heater system consisted of a perforated cylindrical tube that had coiled electric heater elements fastened to the external surface of the tube. An electric motor-fan unit was mounted on each end of the tube; the unit was a source of convective heating of the fluid, and the unit maintained a homogeneous fluid mixture. The AAP fluid-equilibration-heater system was packaged with the quantity-measuring sensor within one cylindrical tube assembly, whereas the Apollo tanks involved two separate tube structures.

Following the accident on Apollo 13 involving an electrical short and explosion in the supercritical O_2 tank, NASA made the decision to eliminate the fans in supercritical O_2 tanks. For the AAP system, it was assumed that the fans were eliminated, but the heater increased slightly in size (in order to obtain sufficient expulsion heating power) with no net weight change.

The initial CGSS design necessitated that all three tank types operate at the nominal supercritical pressure of 620.6 N/cm^2 (900 psi), thus making use of common pressure vessels and relief valves. However, during the AAP CGSS contract, it was proved that Inconel 718, the pressure-vessel material, is susceptible to hydrogen embrittlement. A series of tests was conducted at NASA's Johnson Spacecraft Center (JSC) in support of the AAP CGSS effort. The results of these tests confirmed the findings of the contractor. However, through the JSC tests it was ascertained that there was a threshold limit to the hydrogen-embrittlement phenomenon. It was determined that Inconel 718 could be used for the hydrogen pressure vessel if the maximum pressure is less than 303.4 N/cm^2 (440 psi).

Reduction of the storage pressure for the H_2 system reduces the H_2 storage efficiency somewhat. Redesign of the H_2 pressure vessel to use, for example, 5 Al-2.5 Sn ELI Titanium, with its good cryogenic properties, could allow increase of the storage pressure back to 620.6 N/cm^2 (900 psia) with little or no increase in pressure vessel weight. However, this would only increase the available H_2 by less than 5%, and such a modest increase was assumed to not justify elimination of pressure-vessel commonality, or to justify the effort of redesign. Instead the values of CGSS weights and physical characteristics contained in ref. 20 were used. These are shown in Table 16 (taken directly from the reference). Use of the system for N_2 was not studied.

Supercritical CGSS; 30-Day Storage Mission. — The operational assumptions (see Table 16) for the 30-day storage mission were:

A. The pressure buildup time is 50 hours to the low pressure relief valve setting (293 N/cm^2 (425 psia) for H_2, 658.5 N/cm^2 (955 psia) for O_2) with an uncooled heat flux of 4.25 watts (14.5 Btu/hr) for H_2 and 11.72 watts (40 Btu/hr) for O_2. *

*The cooled heat flux was specified (Table 16); the uncooled heat flux was extrapolated by ratioing up the cooled heat flux by the same ratio specified for the Apollo CGSS (Table 9, pages 33 and 34, ref. 20).

TABLE 16a. - APOLLO APPLICATIONS PROGRAM CGSS WEIGHTS

Item	Oxygen tank	Hydrogen tank	Nitrogen tank
System weight			
CGSS assembly, lb	380	338	380
Dewar assembly, lb	283	283	283
Mount/interface structure, lb	74	32	74
External components, lb	10	10	10
Interface connections, lb	13	13	13
Major parts weight			
Pressure vessel, lb	182 to 185	182 to 185	182 to 185
Outer shell, lb	34.5	34.5	34.5

TABLE 16b. - STRUCTURAL CHARACTERISTICS OF THE AAP CGSS

Characteristic	Oxygen tank	Hydrogen tank	Nitrogen tank
Fluid			
Maximum fill, percent	98	98	98
Maximum fill quantity, lb	1221	76.6	868
Usable quantity, lb	1200	75.0	850
Residual quantity, lb	21	1.6	18
Flow rates at normal temperature and pressure			
Minimum normal, lb/hr	0.80	0.06	0.57
Maximum normal, lb/hr	8.0	0.60	8.0
Maximum heat leak at minimum *dQ/dM* for a 1500-hr mission, Btu/hr	28	5	25
Minimum *dQ/dM*, Btu/lb	35 at 900 psi	100 at 250 psi	44 at 900 psi
Maximum *dQ/dM*, Btu/lb	160 at 900 psi	275 at 250 psi	180 at 900 psi
Fluid pressure			
Normal operating range, psia	820 to 910	200 to 260	820 to 910
Minimum delivery, psia	150	100	150
Relief valves [a]			
High pressure			
Crack, minimum, psi	980	430	980
Full flow, maximum, psi	1020	440	1020
Reseat, minimum, psi	950	390	950
Low pressure			
Crack, minimum, psi	950	420	950
Normal flow, maximum, psi	975	430	975
Full flow, maximum, psi	1020	440	1020
Reseat, maximum, psi	920	400	920
Heater circuit			
High pressure			
Open, psia	910^{+0}_{-25}	260^{+0}_{-15}	910^{+0}_{-25}
Close, psia	845^{+25}_{-0}	220^{+15}_{-0}	845^{+25}_{-0}
Low pressure			
Open, psia	845^{+0}_{-25}	240^{+0}_{-15}	845^{+0}_{-25}
Close, psia	820^{+25}_{-0}	200^{+15}_{-0}	820^{+25}_{-0}
Operating fluid temperature, °F	−300 to 80	−425 to 80	−325 to 80
Servicing			
Fill time, hr	3.0	3.0	3.0
Chilldown time, hr	36.0	36.0	36.0
Top-off time, hr	3.0	3.0	3.0
Pressure buildup at normal temperature and pressure			
Standby time, minimum, hr	50	50	50
Heater time, maximum, hr	10	10	10

[a] Pressure above ambient pressure is defined as psi.

TABLE 16c. – ELECTRICAL AND INSTRUMENTATION CHARACTERISTICS OF THE AAP CGSS

Characteristic	Oxygen tank	Hydrogen tank	Nitrogen tank
Connectors	Hermetically sealed pin receptacle	Hermetically sealed pin receptacle	Hermetically sealed pin receptacle
Heaters			
Voltage, Vdc	28	28	28
Power, each, W	45	45	45
Number	8	1	8
Resistance per heater, nominal, ohms	15	15	15
Power, total, W	360	45	360
Motor fans			
Voltage at 400 Hz, Vac	115	115	115
Power, each, W	25	25	25
Number	2	2	2
Power, total, W	50	50	50
Pressure-gaging system			
Range, psia	0 to 1200	0 to 550	0 to 1200
Accuracy, percent full range	±2.5	±2.5	±2.5
Output voltage, Vdc	0 to 5	0 to 5	0 to 5
Output impedance, ohms	500	500	500
Power, W	0.35	0.35	0.35
Voltage, Vdc	28	28	28
Quantity-gaging system			
Range, percent full	0 to 100	0 to 100	0 to 100
Accuracy, percent of full range	±2.5	±2.5	±2.5
Output voltage, Vdc	0 to 5	0 to 5	0 to 5
Output impedance, ohms	500	500	500
Power, W	4.5	4.5	4.5
Voltage at 400 Hz, Vac	115	115	115
Temperature-gaging system			
Range, °F	−425 to 80	−425 to 80	−425 to 80
Accuracy, percent full range	±2.5	±2.5	±2.5
Output voltage, Vdc	0 to 5	0 to 5	0 to 5
Output impedance, ohms	500	500	500
Power, W	1.1	1.1	1.1
Voltage, Vdc	28	28	28
Ion pump power supply			
Power, W	10	10	10
Voltage, Vdc	28	28	28

TABLE 16d. – STRUCTURAL CHARACTERISTICS OF THE AAP CGSS

Item	Oxygen tank	Hydrogen tank	Nitrogen tank
Pressure vessel			
Material	Inconel 718	Inconel 718	Inconel 718
Ultimate strength, psi	180 000	180 000	180 000
Yield strength, psi	145 000	145 000	145 000
Safety factors			
Ultimate strength	2	4.5	2
Yield strength	1.5	3	1.5
Configuration	Spherical	Spherical	Spherical
Volume, ft^3	17.5	17.5	17.5
Outside diameter, in.	39.0	39.0	39.0
Wall thickness,[a] in.	$0.130^{+0.011}_{-0.017}$	$0.130^{+0.011}_{-0.017}$	$0.130^{+0.011}_{-0.017}$
Girth thickness, in.	0.141 ± 0.003	0.141 ± 0.003	0.141 ± 0.003
Weight, lb	182 to 185	182 to 185	182 to 185
Outer shell			
Material	6061 Al	6061 Al	6061 Al
Buckling-pressure differential at 140° F, minimum, psid	20	20	20
Configuration	Spherical	Spherical	Spherical
Outside diameter, in.	41.5	41.5	41.5
Wall thickness, in.	0.064	0.064	0.064
Weight, lb	34.5	34.5	34.5

[a] Tolerance varies along the meridian.

B. The low pressure relief valve vents through the cooled shield at the set pressure (293 N/cm^2 (425 psia) for H_2, 658.4 N/cm^2 (955 psia) for O_2) for 670 hours with a cooled heat flux of 1.46 watts (5 Btu/hr) for H_2 and 8.2 watts (28 Btu/Hr) for O_2.*

C. At 720 hours, usage begins. The usage rate is assumed as a constant weight flow rate demand based on the initial usable weight flowing for 10,000 minutes (0.01% tank volume/minute) or 0.2 kg/hr (0.45 lb/hr) for H_2; 3.27 kg/hr (7.2 lb/hr) for O_2.

D. Outflow drops the pressure from the relief valve pressure (293 N/cm^2 for H_2, 658.5 N/cm^2 for O_2) to the heater circuit (delivery) pressure (172.4 N/cm^2 (250 psia) for H_2, 608.1 N/cm^2 (882 psia) for O_2) in 4.1 hours for H_2 and 1.49 hours for O_2. At this time, the heaters come on with sufficient power demand (plus the external heat flux of 1.46 watts (5 Btu/hr) for H_2, 8.2 watts (28 Btu/hr) for O_2) to maintain a constant outflow rate at 172.4 N/cm^2 (250 psia) for H_2 (608.1 N/cm^2 (882 psia) for O_2).

E. When the outflow power demand exceeds the maximum power of the heaters near the end of outflow, they are shut off, and the tank pressure decays isentropically from 172.4 N/cm^2 for H_2 (608.1 N/cm^2 for O_2) to the minimum delivery pressure of 69 N/cm^2 (100 psia) for H_2 (103.4 N/cm^2 (150 psia) for O_2), at which time outflow ceases and the residual is 0.73 kg (1.6 lb) H_2 (9.53 kg (21 lb) O_2).

The assumed fluid characteristics were based on H_2 properties from ref. 21 and O_2 properties from ref. 22. During venting, the fluid mass and enthalpy were integrated over the storage time (670 hours) based on constant heat input (see B above) through the cooled shield. During outflow, the fluid mass and enthalpy were integrated over the outflow time based on constant outflow rate (see C above). The H_2 weight history is shown in Figure 30 for the 30-day storage mission, at the end of which 29 kg (63.9 lb) H_2 remain. During outflow, the power demand for the H_2 heater (not including the 1.46 watts (5 Btu/hr) external heat flux) is shown in Figure 31. The integrated heater energy required is 2,500 watt-hr. This energy requirement was converted to battery weight. Two kinds of batteries were investigated: nickel-cadmium with an energy storage capacity of 66.1 watt-hr/kg (30 watt-hr/lb) (ref. 23) and silver-zinc with an energy storage capacity of 143.3 watt-hr/kg (65 watt-hr/lb) (ref. 24). It is possible that the silver-zinc batteries may not have the long storage time needed for the long coast time mission, in which case the electrolyte may have to be added after coast. However, in order to present the supercritical system, with its large power requirements, in the best possible light, this minor problem was ignored, and a silver-zinc battery system was chosen.

The O_2 system weight history is shown in Figure 32 for the 30-day storage mission, at the end of which 496.6 kg (1094.8 lb) O_2 remain. During outflow, the power demand for the O_2 system heaters (not including 8.2 watts (28 Btu/hr) external heat flux) is shown in Figure 33. The integrated heater energy required is 18,200 watt-hr, which was also converted to silver-zinc battery weight.

*The cooled heat flux was specified (Table 16); the uncooled heat flux was extrapolated by ratioing up the cooled heat flux by the same ratio specified for the Apollo CGSS (Table 9, pages 33 and 34, ref. 20).

CR54

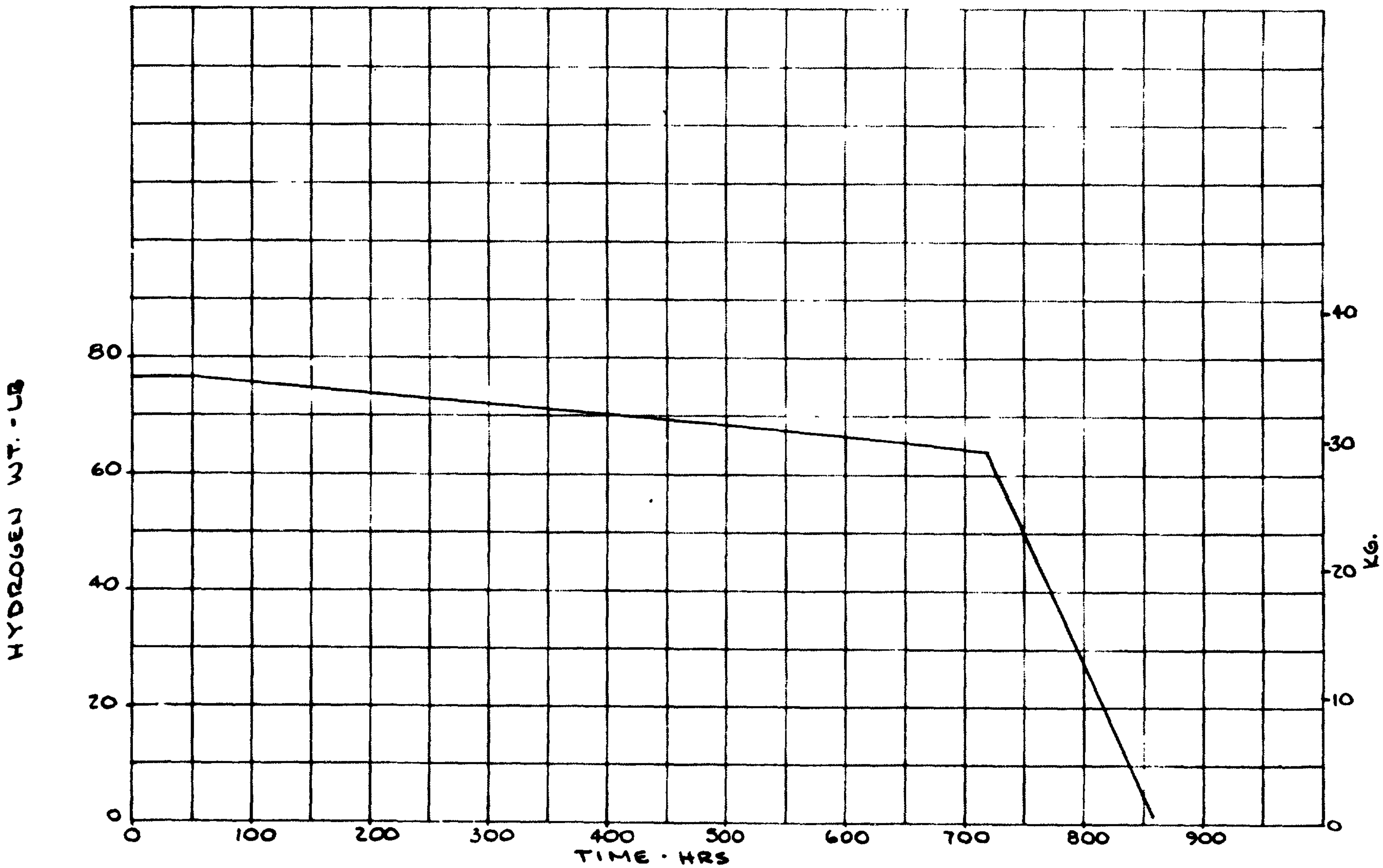

Figure 30. Hydrogen Weight History for 30-Day Storage

CR64

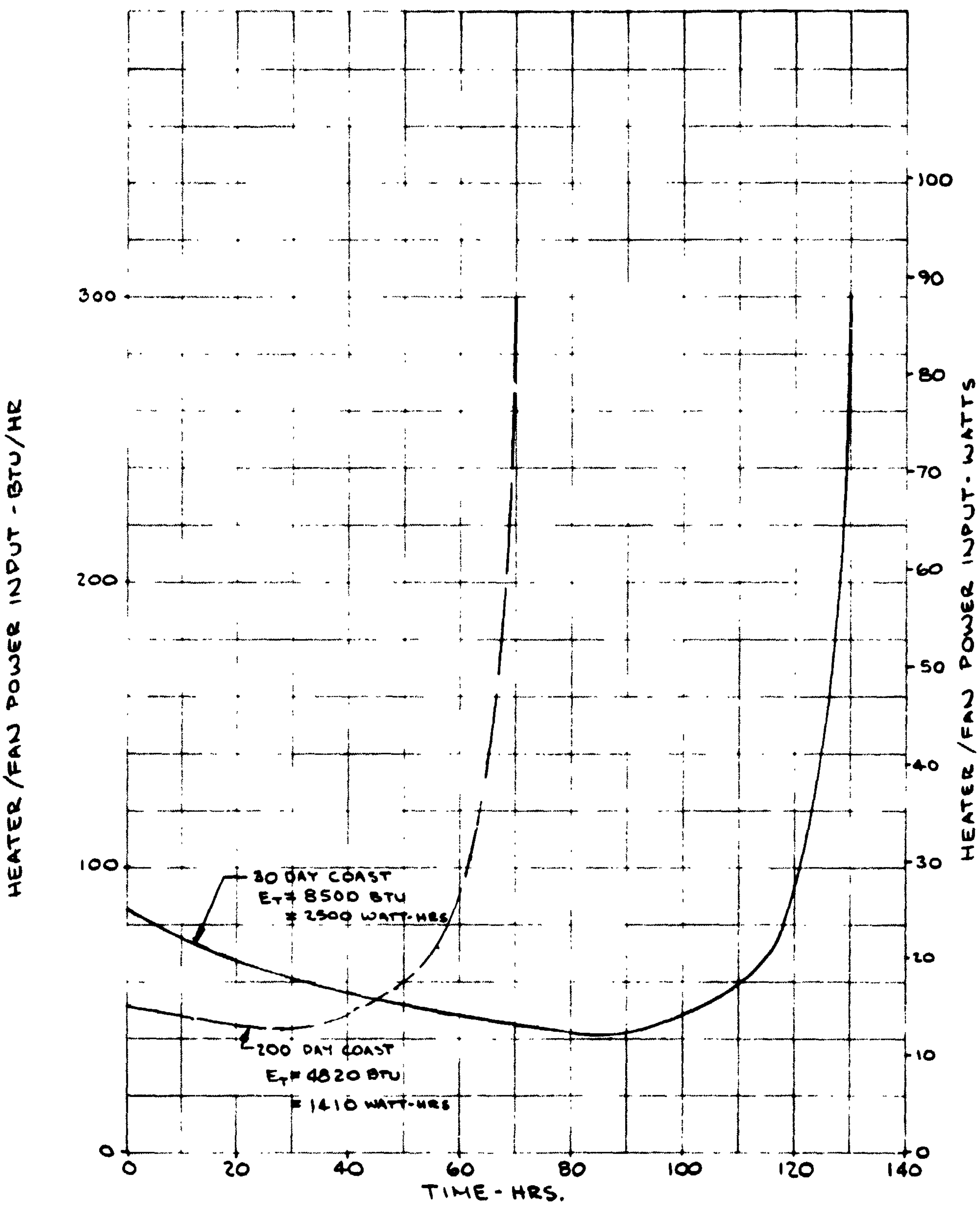

Figure 31. Hydrogen Power Requirements for Outflow

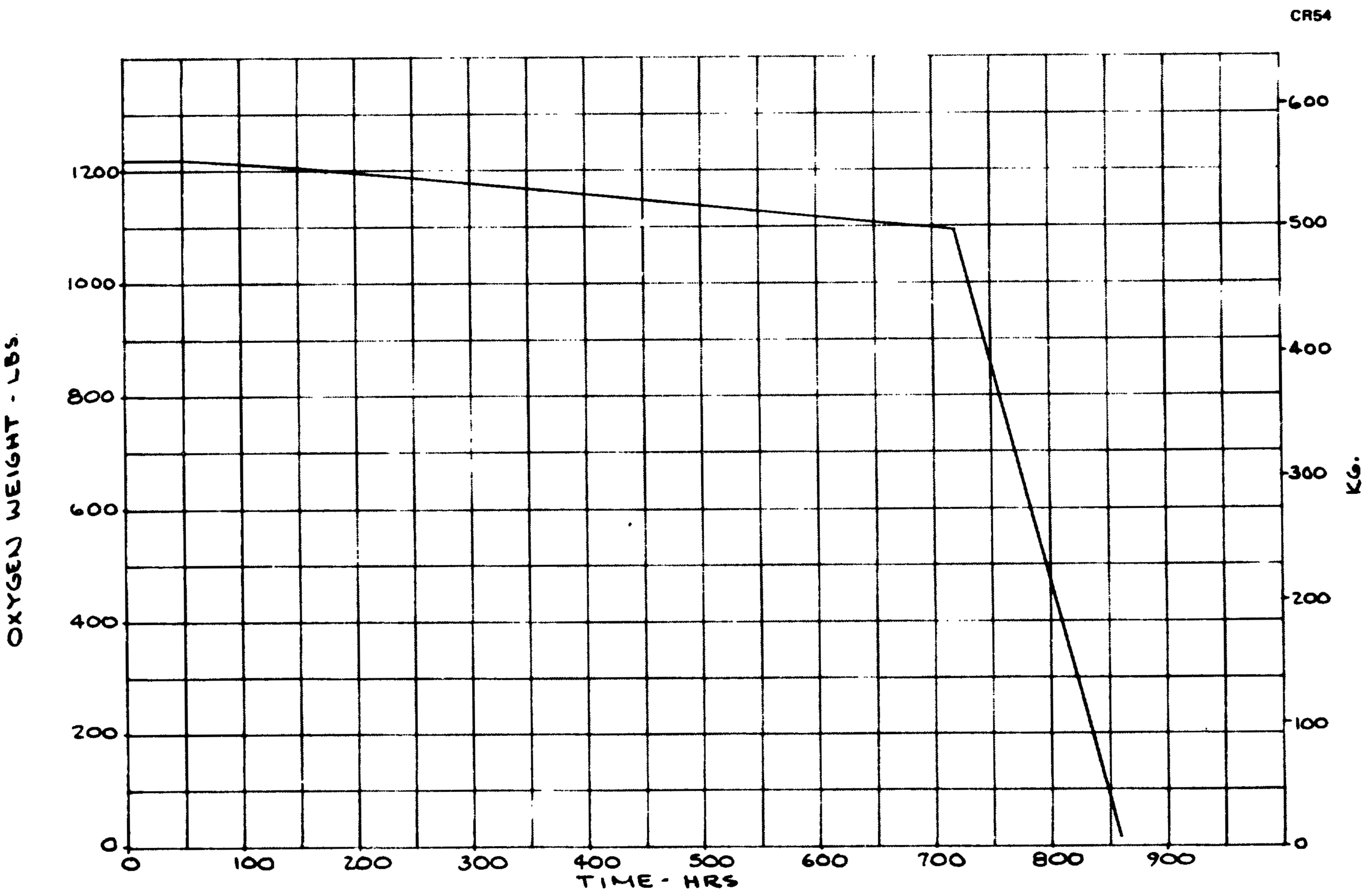

Figure 32. Oxygen Weight History for 30-Day Storage

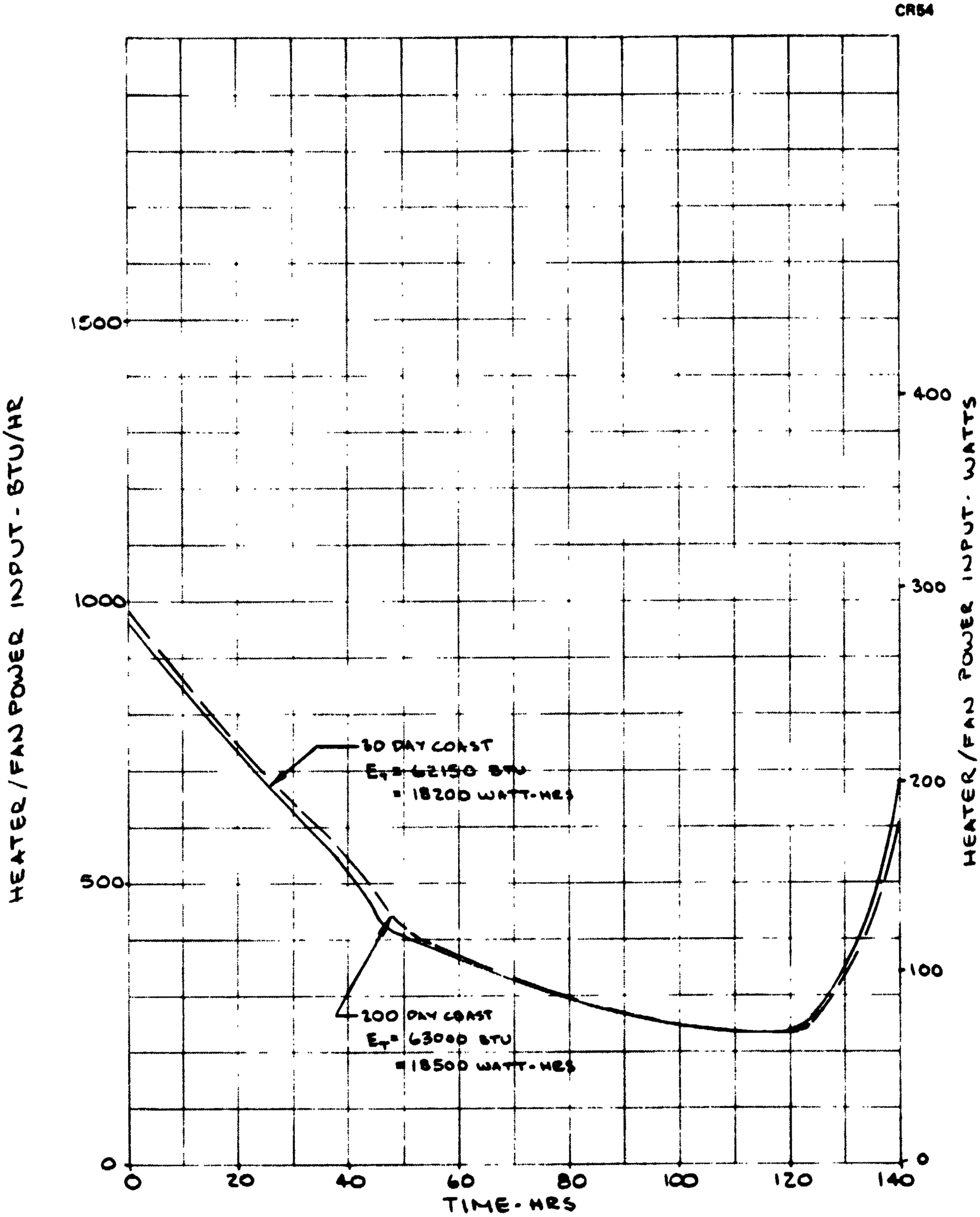

Figure 33. Oxygen Power Requirements for Outflow

Supercritical CGSS; 200-day Storage Mission. – Based on the boiloff resulting from the 30-day storage mission, it was clear that the thermal protection system employed was not adequate for the 300-day storage mission originally proposed (ref. 8). Therefore, initially, as proposed in ref. 8, MLI was added to the system to reduce the heat leak to more acceptable values. However, the radial bumper design utilized was not very efficient for very low heat leak design, so that despite the addition of MLI, substantial heat leak entered the system through conductive heat leak through the supports and plumbing. Therefore, initially an analysis was performed to determine the approximate amount of heat flux through the supports and plumbing. It was assumed that the amount conducted through the plumbing was small because long, small diameter, thin wall stainless steel tubing was used. It was further assumed that, because the O_2 temperature was below 110°K (200°R), the radiation heat flux, $\dot{Q}_{RAD}$, was essentially the same for both the O_2 and H_2 tanks. Finally, it was assumed that the conductive heat flux, $\dot{Q}_{COND}$, through the radial bumpers was proportional to the bumper area which in turn was proportional to the supported weight. The weight of internal tank components (heaters, fan, probes, etc.) was not known, so it was assumed that the supported weight was the sum of the pressure vessel plus propellant weights 118.4 kg (261 lb) for H_2, 637.8 kg (1406 lb) for O_2). Thus, for no cooling flow in the shields, the energy balance equations for the O_2 and H_2 tanks were solved simultaneously to yield:

$$\dot{Q}_{RAD} = 1.364 \text{ watts } (4.656 \text{ Btu/hr})$$

$$H_2 \quad \dot{Q}_{COND} = 2.883 \text{ watts } (9.844 \text{ Btu/hr})$$

$$O_2 \quad \dot{Q}_{COND} = 10.352 \text{ watts } (35.344 \text{ Btu/hr})$$

In order to check these values, the radiative heat flux was calculated for concentric spheres, ignoring small diameter differences in the shields, and assuming typical equal emissivities of 0.01 (ref. 25) for silver plating. The $\dot{Q}_{RAD}$ calculated in this fashion was 1.318 watts (4.5 Btu/hr) which is remarkably close to that found above.

When a cooled shield is placed within a nominal thickness of MLI, it not only absorbs additional heat, raising the shield exit temperature, but in so doing it also changes the temperature profile through the MLI, changing the transmitted heat flux. The MDAC Shield Analysis Computer Code P3513 was used to define the optimum shield location, and the reduction in MLI heat flux due to the presence of cooled shield(s), as a function of the heat short heat leak expressed as a fraction of the unshielded MLI heat flux. The analysis for one and two shields determined that the optimum dimensionless shield location within the MLI (X_1) was essentially unaffected by the amount of heat short heat leak. The variation in MLI heat flux for optimum shield location, as a function of heat short heat flux fraction is shown in Figure 34. The left hand side of Figure 34 is expanded for LH_2 and LO_2 in Figures 35 and 36, together with optimum shield location within the MLI. It will be noted that the second shield is much more efficiently utilized with the LH_2 system than with the LO_2 (because of the higher specific heat of H_2).

It was assumed that the MLI added for the long-coast-time mission was distributed about the cooled shield so that the minimum heat flux ratio would be obtained.

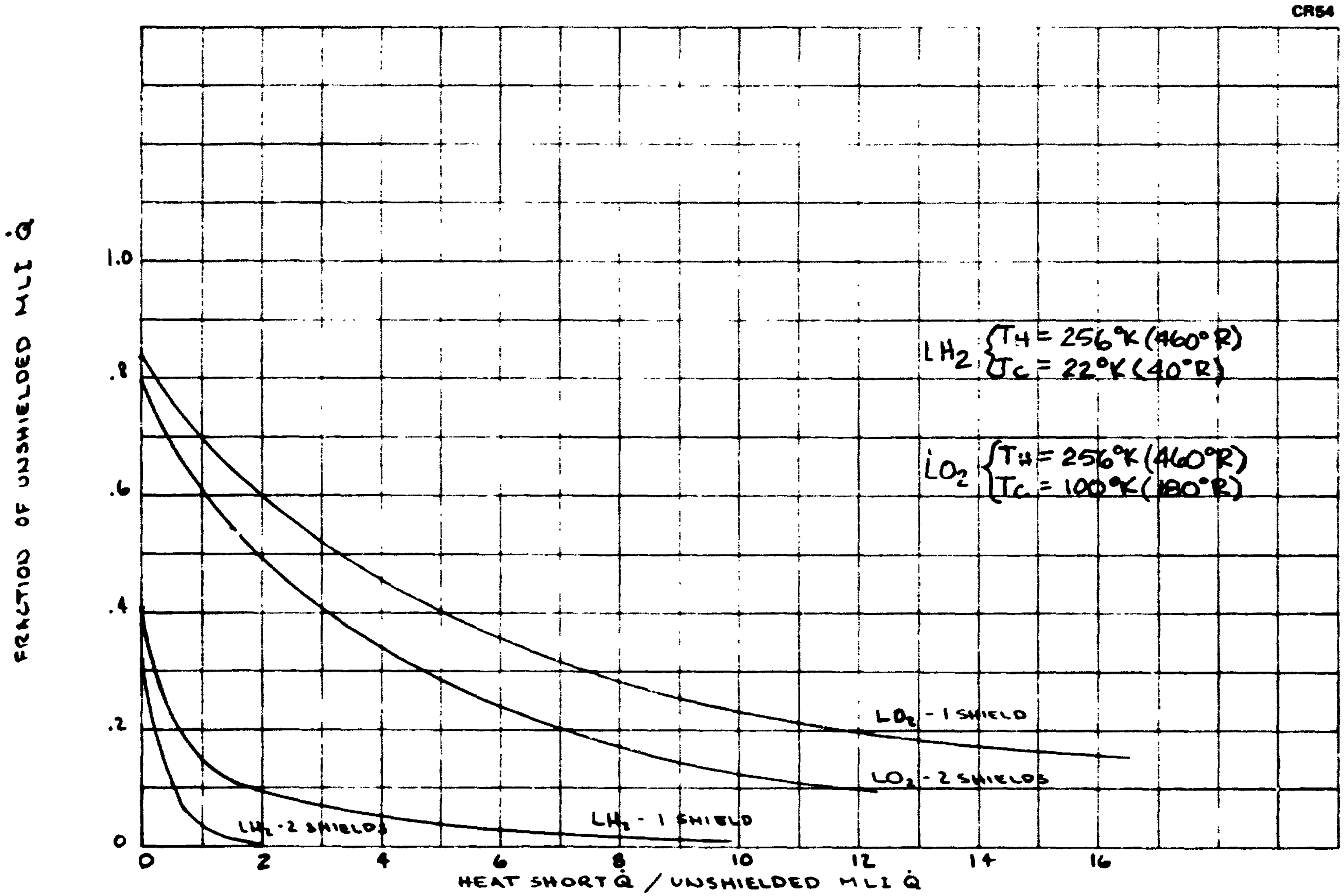

Figure 34. Shielded MLI Heat Flux as a Function of Heat Short Heat Leak

CR84

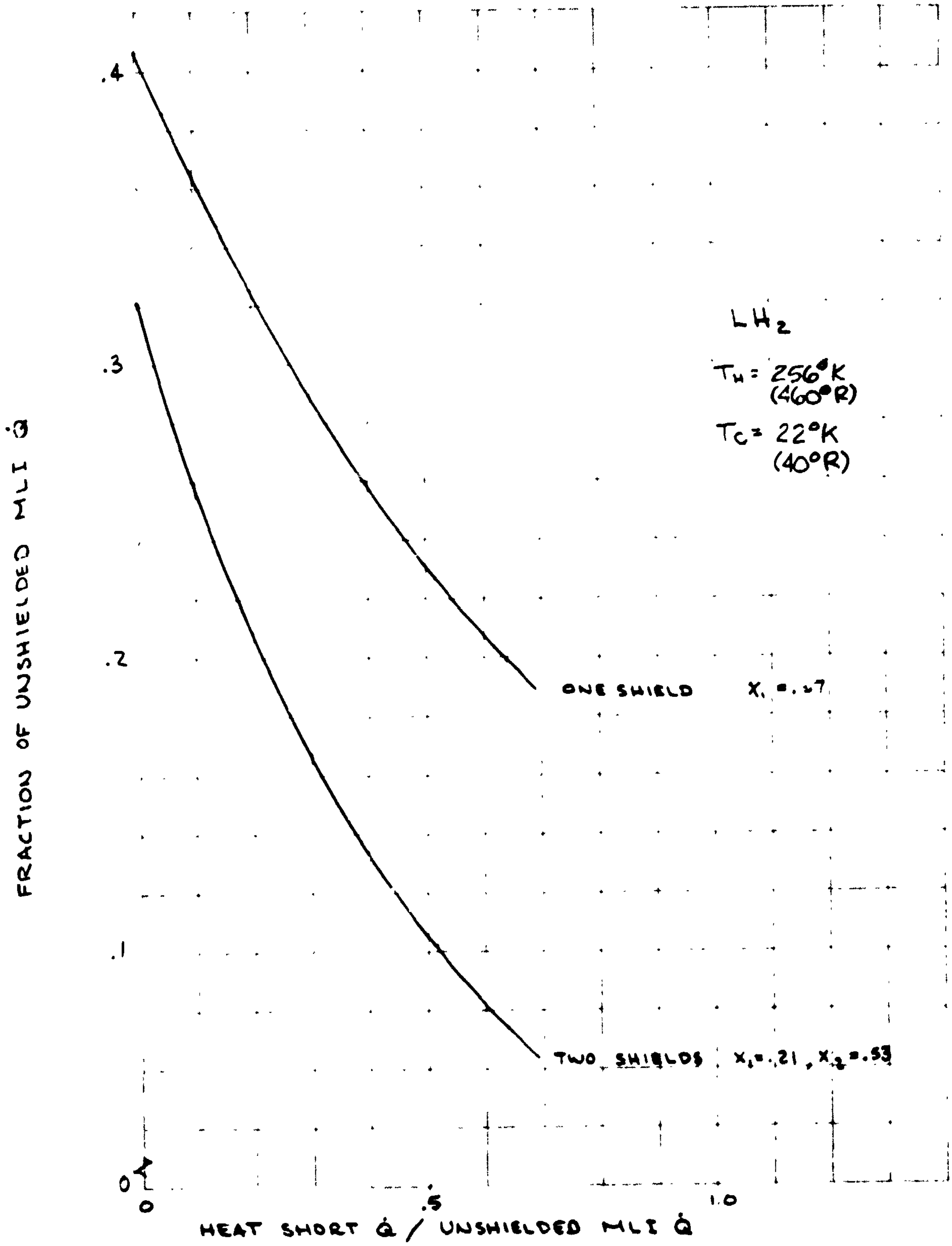

Figure 35. Shielded MLI Heat Flux as a Function of Heat Short Heat Leak – LH_2

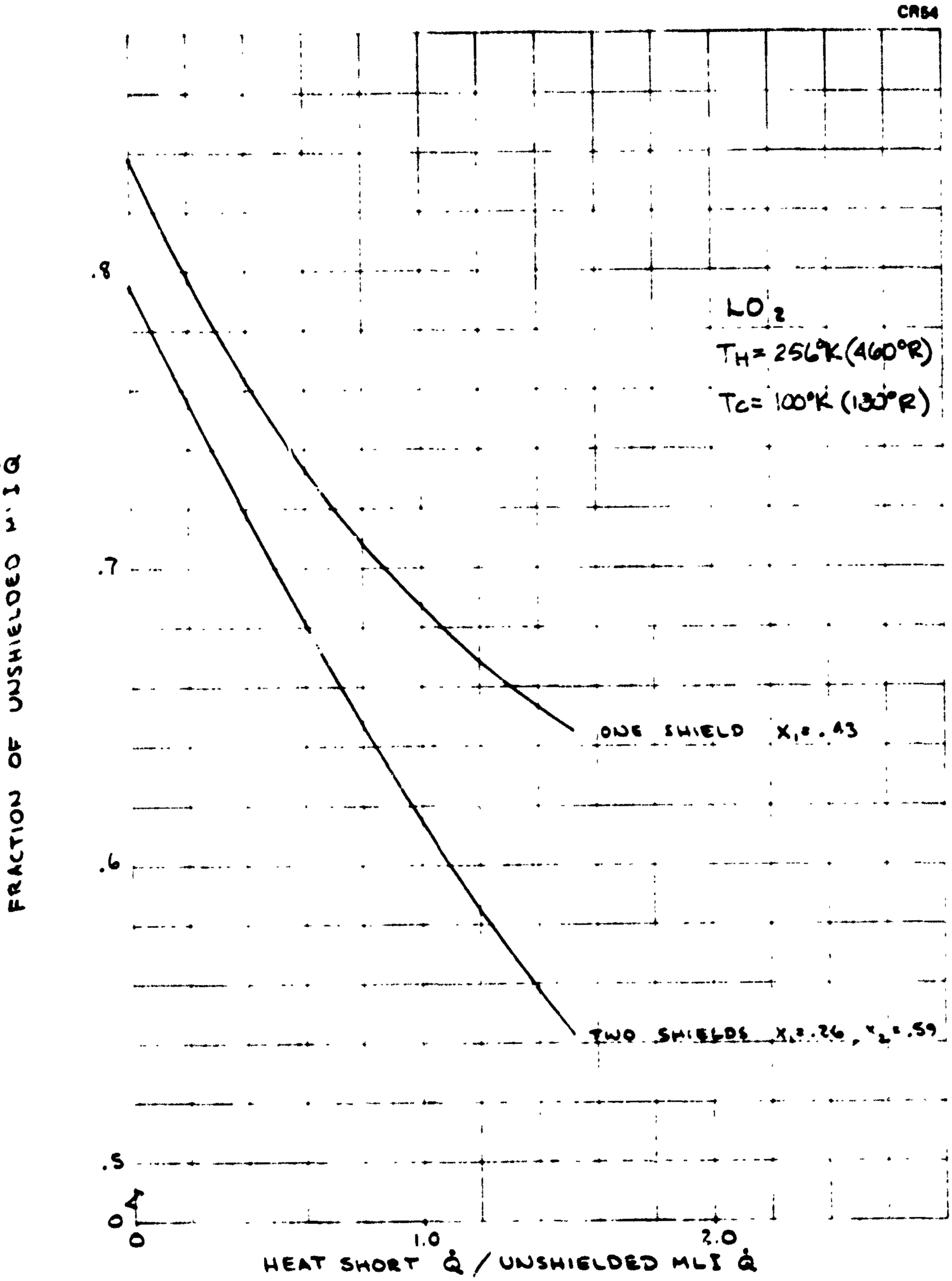

Figure 38. Shielded MLI Heat Flux as a Function of Heat Short Heat Leak – LO_2

In order to determine the optimum amount of MLI, previous analyses (ref. 6) have determined the minimum sum of boiloff weight and MLI weight, to minimize total system weight. However, for this analysis, it was specified that the various storage systems be compared on the basis of weight fraction, or ratio of delivered propellant weight to total loaded system weight. Therefore, the MLI thickness was selected to maximize the weight fraction. When the optimization was performed for the 300-day mission, the optimum insulation thickness was over 20 cm (8 inch) for the H_2 tank and over 28 cm (11 inch) for the O_2 tank. Note that this large MLI thickness resulted because of the two-fold effect of reducing first the MLI heat flux, but more importantly, reducing the conductive heat flux down the bumpers (which was about three times that of the MLI). This very long conductive length of the radial bumpers distorted the design of these supports such that it was not clear that the resulting bumpers would be structurally sound from a compression/buckling standpoint.

It was clear from the foregoing that the structural support and thermal control systems were inadequate for long-term storage missions, and that it would be necessary to redesign the thermal control system to reduce the conductive heat flux, and to determine a long-term mission time which would allow a reasonable overall system comparison.

The basic redesign scheme selected was to separate the pressure vessel from the bumpers and vacuum jacket during low-g flight and coast, thus changing the large conductive heat flux through the bumpers to much smaller radiation (with MLI installed in the vacuum annulus). This was done by installing small, wound fiberglass springs around each lower bumper (in eight places) and removing the bumpers in the upper hemisphere (which do not contribute structurally). A fiberglass stop was added to the top of the vessel, around the vent line, to locate the pressure vessel when lifted from the bumpers, as shown in Figure 37. In addition, the plumbing lines and shields would also tend to stabilize the vessel when it is separated from the bumpers in low-g coast. Because the structural details of the CGSS are not known from ref. 20, the proposed modifications described above were conceptual only, and would probably require development to assure structural/vibrational stability.

It was further assumed that the vacuum jacket and shield design size would be held constant for commonality with the original CGSS design, and only 2.5 cm (1 inch) of MLI would be used, which would be positioned around the cooled shield to minimize the heat flux. The calculated heat flux through the redesigned thermal control system is shown in Table 17.

With these values of heat flux, it was found that the H_2 tank was the limiting case for mission duration: after 200 days coast, 18.1 kg (40.0 lb) of H_2 remained; after 300 days coast, only 8.8 kg (19.5 lb) of H_2 remained. Therefore, the 200-day coast mission was selected for the long term mission for both the H_2 and O_2 systems for commonality (even though the O_2 system could easily coast for longer than 300 days).

The weight history of the H_2 for the 200-day mission is shown in Figure 38, and the power requirements during outflow were shown previously in Figure 31. The time to reach vent pressure at the reduced heat flux is 146 hours, followed by 4654 hours of venting, and then 85 hours of use.

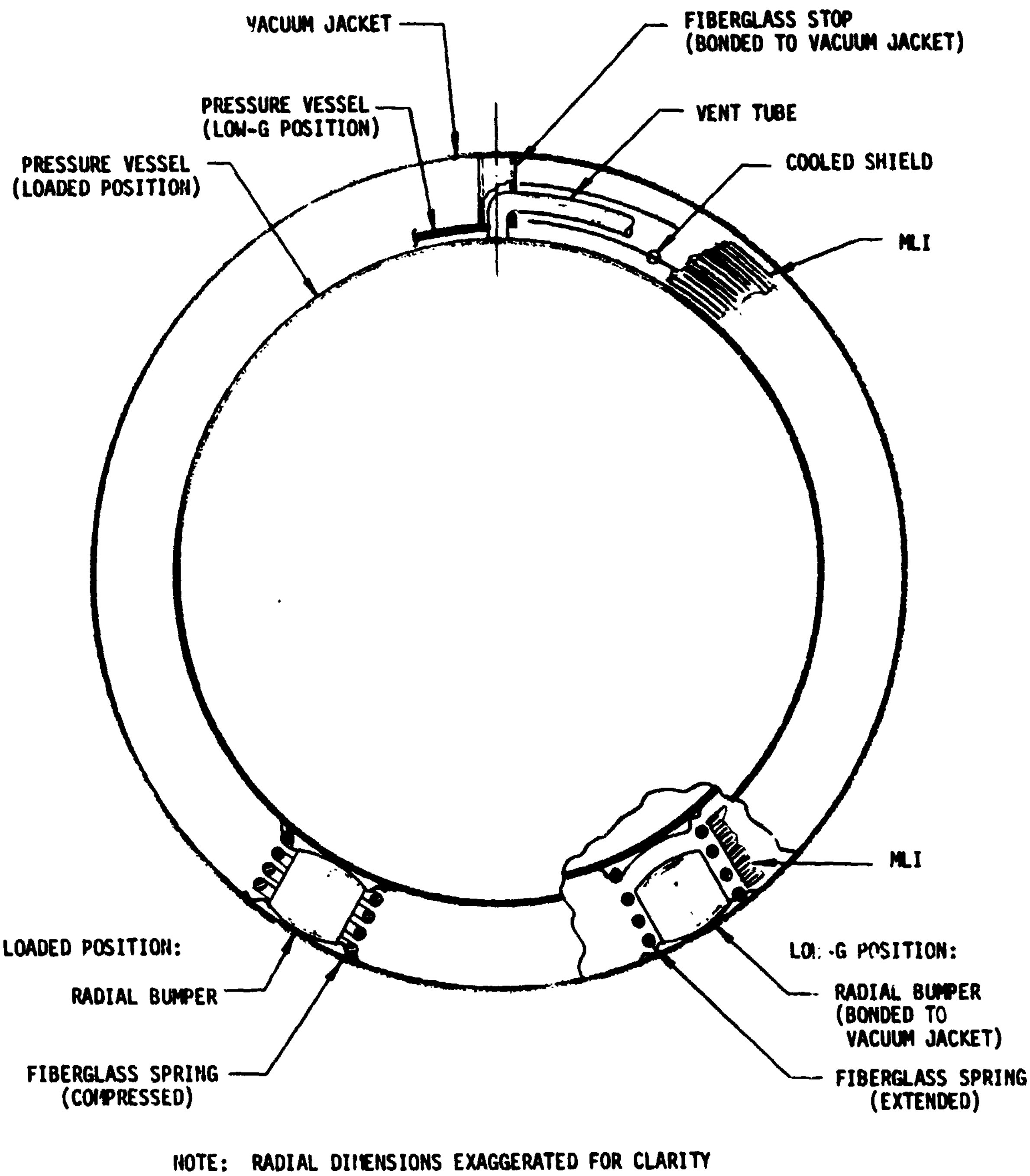

Figure 37. Modified Support System for Long-Term Mission

TABLE 17. - THERMAL CONTROL SYSTEM HEAT FLUX

	Supercritical Storage		TVS/WSL	
	H_2 (watt)	O_2 (watt)	H_2 (watt)	O_2 (watt)
30-Day Mission Total Heat Leak	1.46*	8.2*	0.809**	7.319**
Long-Term (200-Day) Mission				
Conduction Through Fiberglass Stop — K = 0.588 joule/m-sec-°K (0.34 Btu/hr-ft-°R)	0.110	0.073	0.110	0.073
Conduction Through Eight Fiberglass Springs	0.029	0.029	0.014**	0.029
Conduction Down Stainless Steel Vent and Fill Lines	0.141	0.094	0.141	0.094
Radiation from Eight Bumpers Bumper $\epsilon = 1.0$ Tank $\epsilon = 0.01$	0.125	0.661	0.062**	0.595**
Heat Flux Through 2.5-cm (1-in.) MLI with Cooled Shield	0.077	0.503	0.107	0.517
(With No Cooling)	(1.046)	(0.926)	(1.046)	(0.926)
TOTAL	0.482	1.360	0.434	1.308

*Defined by NASA SP-247
**Corrected for reduced bumper heat leak

Similarly, the weight history of the O_2 for the 200-day mission is shown in Figure 39, with 489.5 kg (1079.2 lb) remaining after coast, and the power required for outflow was shown previously in Figure 33. The time to reach vent pressure at the reduced heat flux is 328 hours, followed by 4472 hours of venting, and then by 147 hours of use.

The final weight summary for the supercritical CGSS will be compared with the TVS/WSL system in a subsequent section.

TVS/WSL System; 30-Day and 200-Day Transfer Missions. — For the supercritical system, the path for heat flux into the tank was not as important as the overall quantity since boiling did not occur. However, for the subcritical TVS/WSL system, the radiative and conductive heat flux had to be defined to determine if and where boiling may occur. If boiling occurred within the screen annulus in the vicinity of the ullage bubble, it was possible that with vapor on both sides of the screen, screen drying and breakdown would occur.

CR54

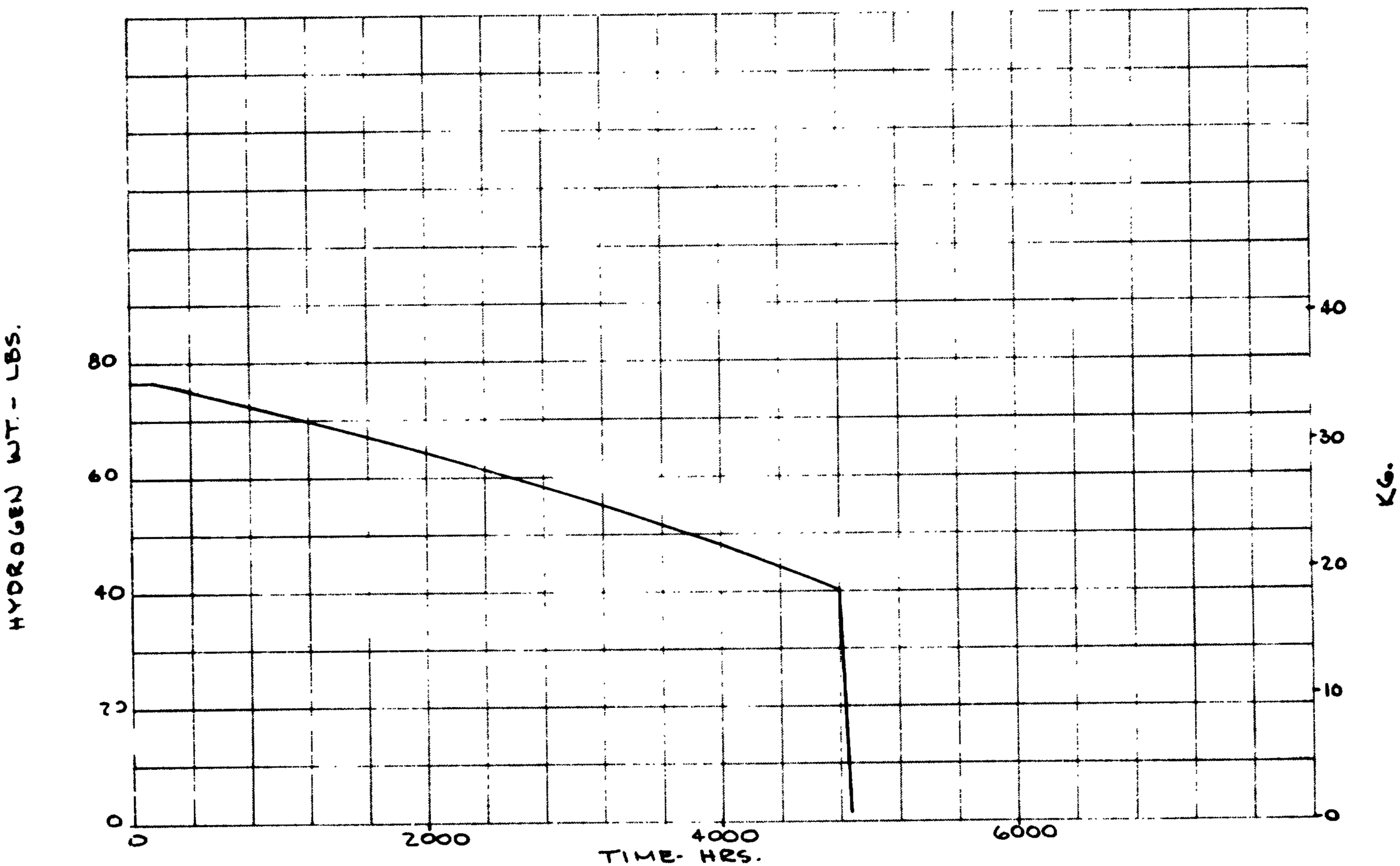

Figure 38. Hydrogen Weight History for 200-Day Storage

CR54

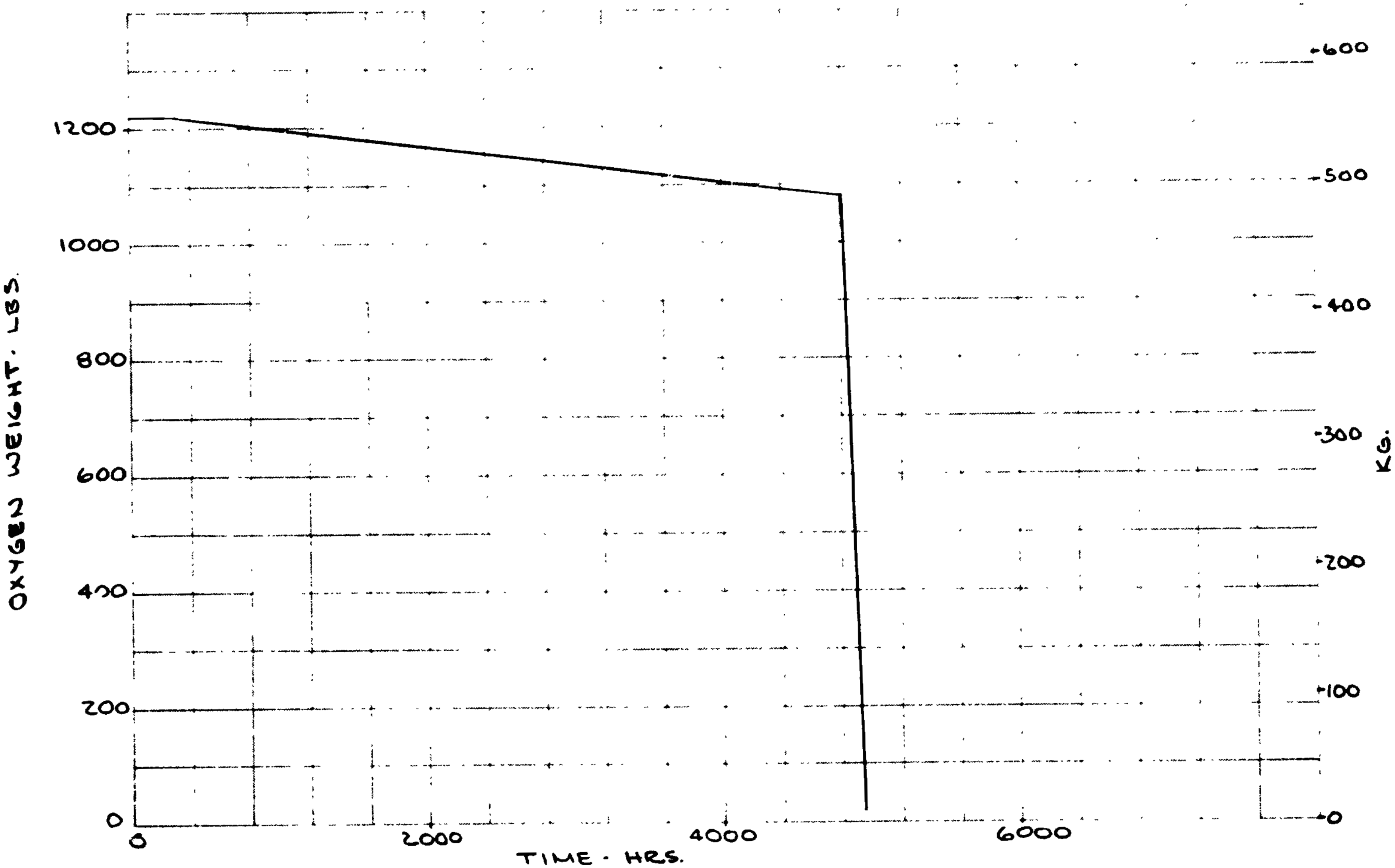

Figure 39. Oxygen Weight History for 200-Day Storage

It was assumed that the incipient boiling point (in terms of heat flux and ΔT) occurred at the intersection of the free convection curve at 10^{-5} g and the nucleate boiling curve, as shown in Figure 40. The boiling curves used for LH_2 and LO_2 were based on the Kutateladze correlation given in ref. 7, for a pressure of 27.6 N/cm^2 (40 psia). As discussed in ref. 8, 27.6 N/cm^2 (40 psia) was the tank pressure selected for the TVS/WSL system which would allow use of minimum gage (0.05 cm (0.020 inch)) 6063-T5 high conductivity aluminum alloy for the subcritical pressure vessel. The free convection curve was based on the vertical flat plate correlation (ref. 25):

$$Nu = 0.555 \, (Ra)^{1/4} \tag{13}$$

where Nu is the Nusselt number and Ra the Rayleigh number based on the hydraulic diameter (twice the annulus gap) for our system. The incipient boiling points shown are 0.0055°K (0.01°R) at 0.0473 watt/m^2 (0.015 Btu/hr-ft^2) for LH_2 and 0.0833°K (0.15°R) at 1.419 watt/m^2 (0.45 Btu/hr-ft^2) for LO_2. Shown for comparison are the 1-g incipient points: the value of 0.055°K (0.1°R) at 1-g for LH_2 generally agrees with the data of Drayer and Timmerhaus (ref. 26) who found incipient boiling points for LH_2 of 0.033°K (0.06°R) to 0.094°K (0.17°R).

The overall thermal control system for the two fluids and missions were analyzed to determine the resultant system heat fluxes. In determining the fluxes for the LH_2 tank, it was assumed that the size or number of bumpers could be reduced due to the reduction in supported weight caused by the use of low pressure tankage. The tank used for the TVS/WSL weighs 4.54 kg (10 lb) compared to 83.9 kg (185 lb) for the supercritical tankage. The total weight supported by the bumpers for the TVS/WSL is, therefore, about 46.3 kg (102 lb) compared to 122.9 kg (271 lb) for the supercritical system. Therefore, conservatively, the number of bumpers was halved: to 8 for the 30-day mission configuration, and to 4 for the 200-day mission configuration. Similarly, for the O_2 tank, the TVS/WSL supported weight is 548.9 kg (1210 lb) compared to 642.3 kg (1416 lb) for the supercritical system, or a ratio of 0.855. Thus, for the LO_2 system the number of bumpers was unchanged but the area was reduced by 10%. The resulting heat loads and flux for the H_2 and O_2 TVS/WSL are shown in Table 18.

The radiative flux was below the boiling point, but the flux in the vicinity of the bumpers could result in boiling. (The areas near the bumpers were approximate because of the uncertain temperature distribution caused by the bumper stress pads on the tank.) To avoid boiling, the possibility of circulating TVS mixer flow over these areas with sufficient velocity and forced convection coefficients to prevent boiling was investigated. It was found that boiling could not be suppressed for the 30-day configuration (conductive heat shorts) without exceeding the bubble point capability of the 200 x 1400 screen (the finest obtainable aluminum screen). For the 200-day configuration (radiative heat shorts) the boiling could be suppressed but at the cost of excessive pump "boiloff" penalty. Further, during outflow at 0.01% tank volume/minute boiling could occur in the absence of TVS mixer flow.

Since boiling near the heat shorts could not practically be suppressed, it was decided to configure the WSL so that boiling would not compromise the integrity or performance of the screen. In the vicinity of the bumper heat

CR54

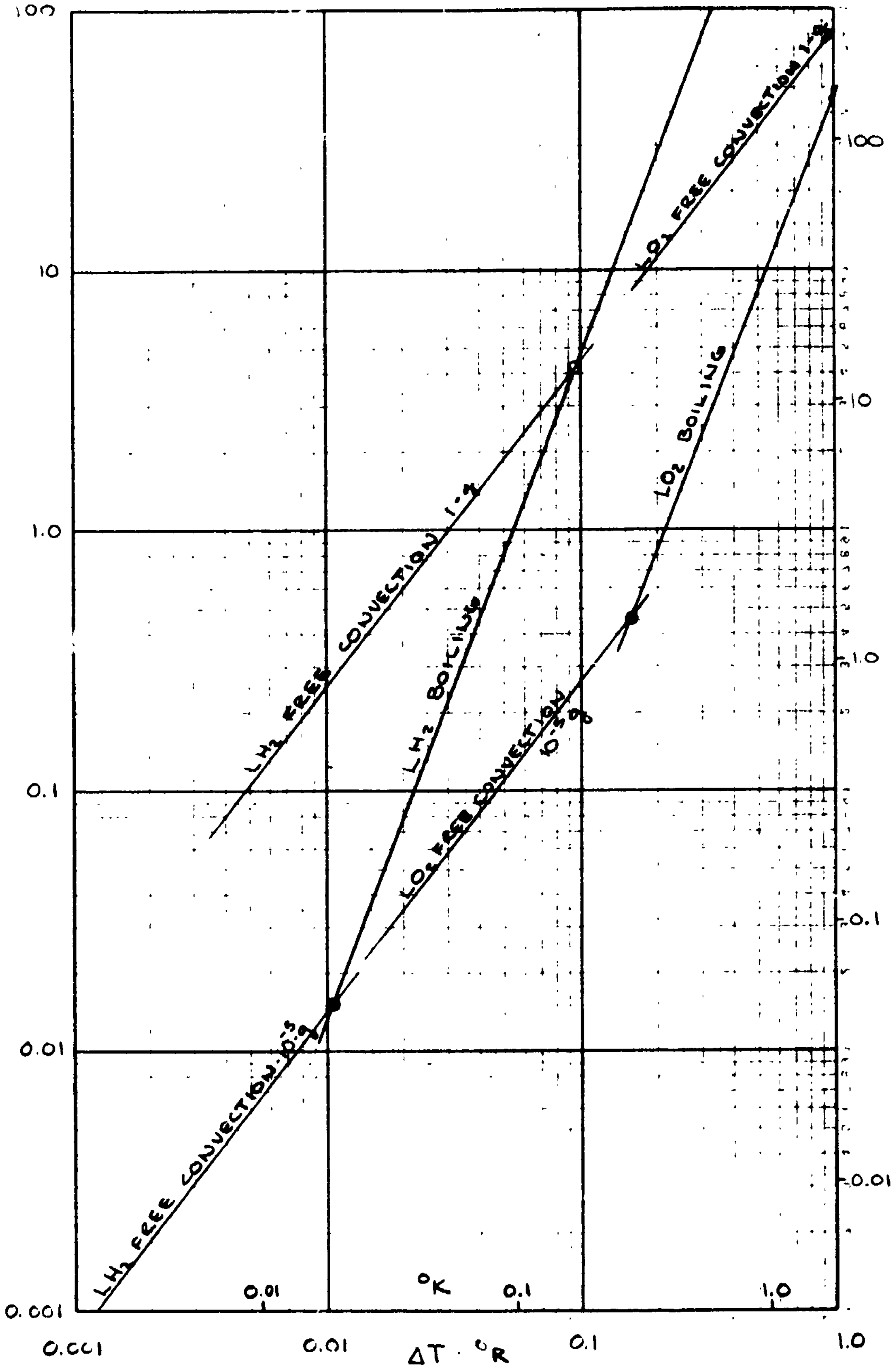

Figure 40. Incipient Boiling Points for LH2 and LO2

TABLE 18. – TVS/WSL HEAT LOADS AND HEAT FLUX WITH COOLED SHIELD

	$\dot{Q}$ (watt)	A (m^2)	$\dot{Q}/A$ (watt/m^2)
LH_2 – 30-Day			
External Radiation	0.154	3.02	0.051
16 Conductive Bumpers (Each)	0.0819	0.0011	74.4
LH_2 – 200-Day			
External Radiation	0.107	3.02	0.035
8 Radiative Bumpers Plus Spring (Each)	0.0193	0.0036	5.35
LO_2 – 30-Day			
External Radiation	0.317	3.02	0.105
16 Conductive Bumpers (Each)	0.4434	0.0055	80.6
LO_2 – 200-Day			
External Radiation	0.215	3.02	0.0713
8 Radiative Bumpers Plus Spring (Each)	0.0776	0.0177	4.39

shorts, solid aluminum sheet, 0.05 cm (0.020 inch thick), would be used in place of the screen panels so that vapor generation from boiling would not result in screen failure. As shown in Figure 41, the vapor would be confined to the solid channels, which would be used at four locations in the LH_2 tank and eight locations in the LO_2 tank. This would reduce the screen area available to outflow by 1/8 and 1/4, respectively, but this was not believed to be a problem with our configuration. The details of assembling the WSL in the tank were described generally in ref. 8. Because the pressure vessel was made of aluminum for minimum weight, aluminum screen was selected for the WSL to eliminate problems of differential contraction. The 200 x 1400 screen was selected for several reasons: It has the maximum bubble point obtainable with an aluminum screen (see screen performance in Table 19), which gives maximum protection against random acceleration perturbations during use. While lighter screens with adequate performance could be obtained, they would save, at most, a few tenths of a pound in this size system. This screen type is quite sturdy, easily fabricated, and resistant to wire separation or holing problems during fabrication and installation.

The screen was installed in the tank by mechanically fastening screen panels to angles spot welded to the tank wall as shown in Figure 41. The angles were 0.08 cm (0.032 inch) thick aluminum as shown. The number of screen passes was arbitrarily set at 32, which was a convenient multiple of the number of bumpers, and which gave panels about 10 cm (4 inch) (max)

TABLE 19. - PROPELLANT CHARACTERISTICS AND SCREEN PERFORMANCE PARAMETERS, TVS/WSL

	LH_2	LO_2
Propellant Characteristics		
Propellant Quantity - kg (lb) (Initial — Zero Ullage)	32.6 (71.8)	535.2 (1180)
Design Tank Pressure - N/cm^2 (psia)	27.6 (40)	27.6 (40)
Saturation Temperature - °K (°R)	24.2 (43.6)	101.1 (182)
Density - kg/m^3 (lb/ft^3)	65.7 (4.1)	1081.4 (67.5)
Heat of Vaporization - joule/kg (Btu/lb)	4.14×10^5 (178)	1.99×10^5 (85.5)
Surface Tension - dyne/cm (lb/ft)	1.29 (0.89×10^{-4})	10.6 (7.3×10^{-4})
Viscosity - $N\text{-}sec/m^2$ (lb/ft-sec)	1.0×10^{-5} (0.68×10^{-5})	15.3×10^{-5} (10.3×10^{-5})
Thermal Conductivity - joule/m-sec-°K (Btu/hr-ft-°R)	0.1116 (0.0645)	0.1358 (0.0785)
200 x 1400 Screen		
Bubble Point - cm (ft)	37.6 (1.233)	18.75 (0.613)
Flow-Through Coefficients		
A	0.91	0.838
B (ft)	0.6126 (2.01)	0.6126 (2.01)
Roughness Dimension - cm (in.)	0.00203 (0.0008)	0.00203 (0.0008)
Weight - kg/m^2 ($lb/100\ ft^2$)	0.259 (5.3)	0.259 (5.3)

by 63.5 cm (25 inch), which was a convenient handling size. When the screen panels were stretched between the angles as shown, using the 0.08-cm angle thickness as the minimum spacing, the equivalent annulus gap residual was 1.156% of tank volume. It was assumed that thin Teflon gaskets were used between the joints to assure leak-tightness, as shown in Figure 41. Because of the small tank size it would be impractical to assemble the screen inside the finished tank; therefore the screen would be installed in each tank half prior to the final tank girth weld. A gap of 2.5 cm (1 inch) (or less if electron-beam welding is used) would be left around the tank. The configuration of the baffle at the top of the tank is shown in Figure 42, and was made in two sections and tack-welded to the tank halves. When the tank halves were welded, the baffle halves would overlap as shown to prevent excessive leakage of the TVS mixer flow.

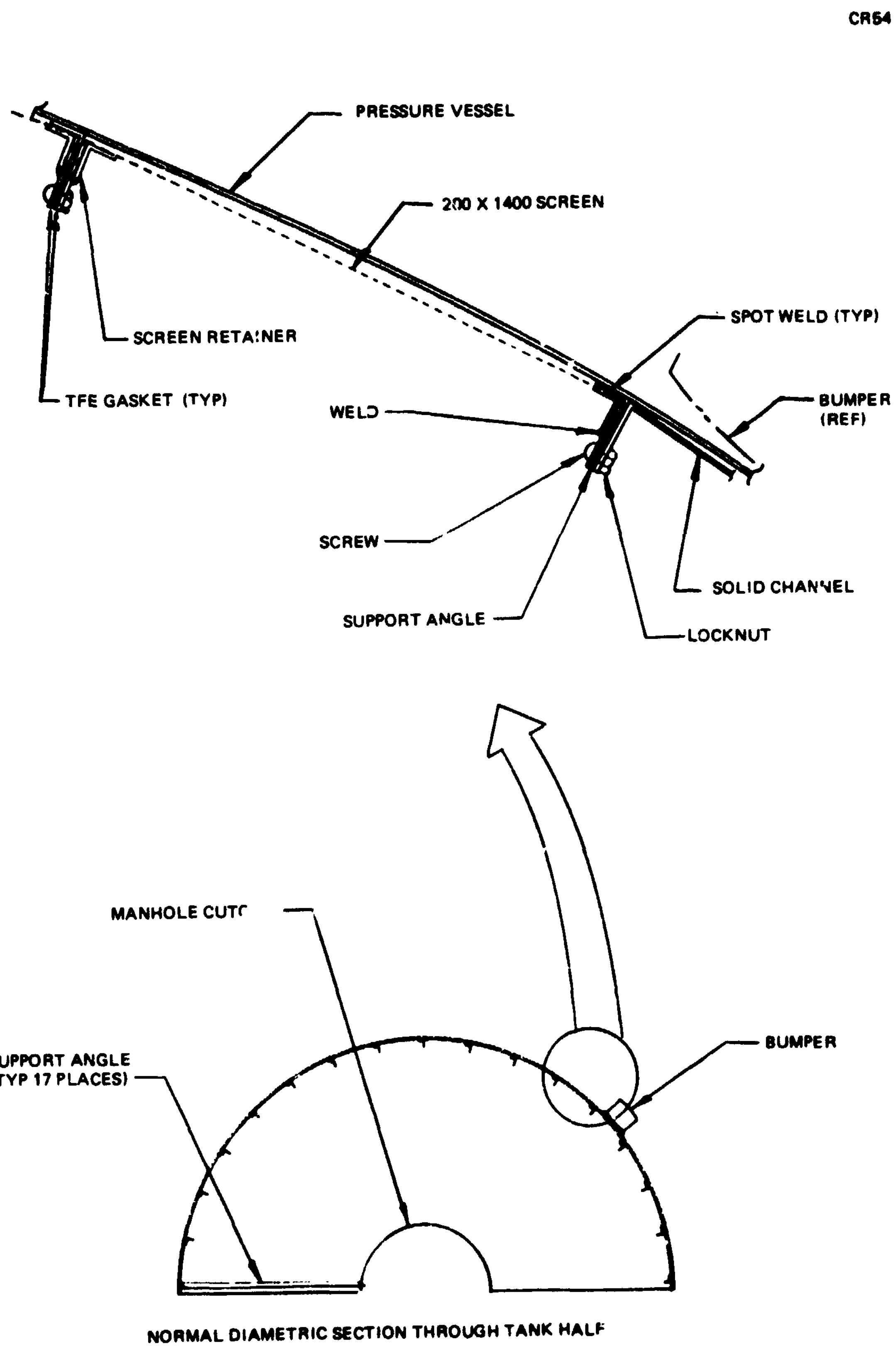

Figure 41. Screen Liner Mounting Method

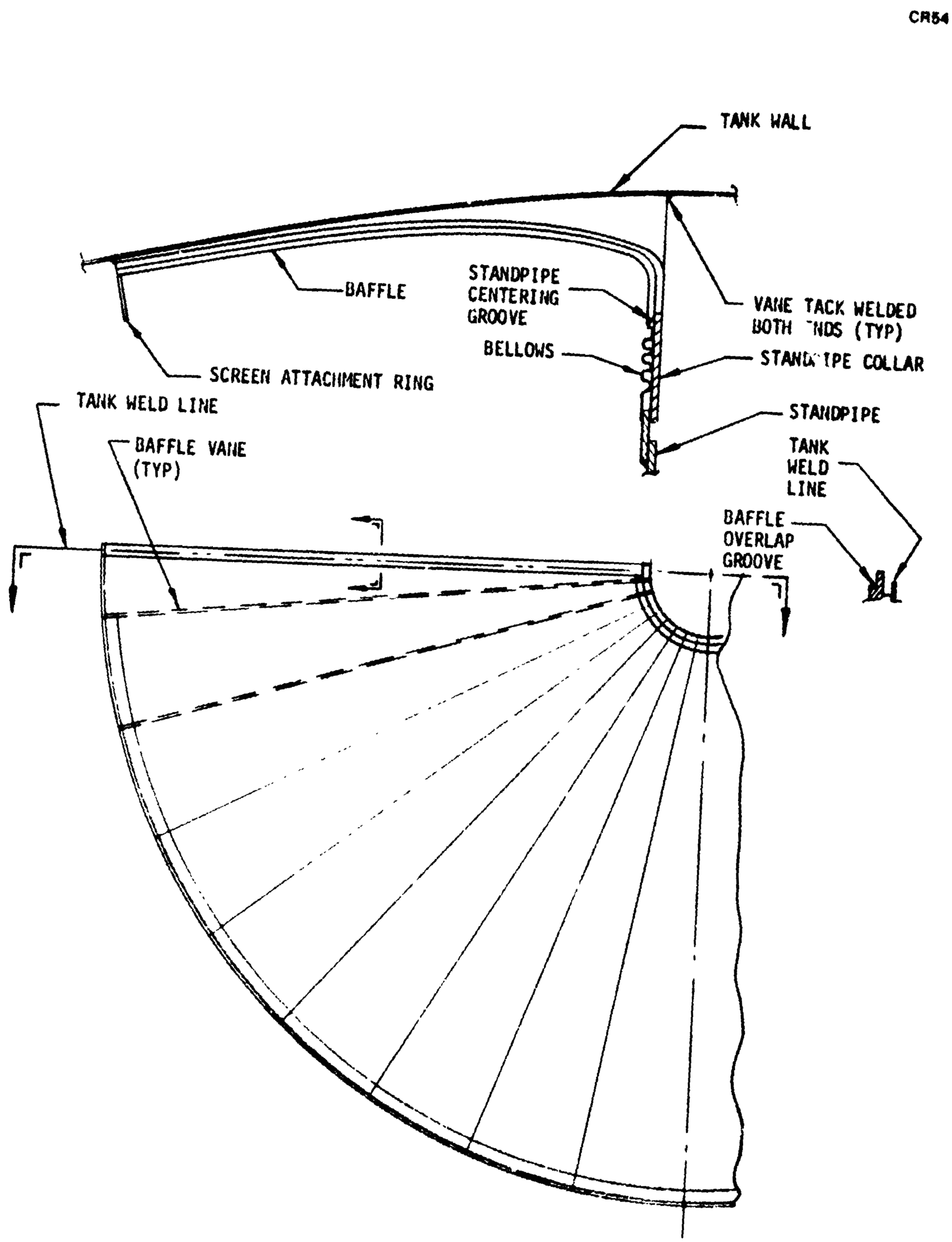

Figure 42. Tank Top Baffle Detail

Previous studies of the TVS/WSL cryogen storage system showed the TVS pump arranged to pump against the outflow direction (ref. 6). With reasonably rapid outflow (~1% tank volume/minute) unloading would be completed without requiring TVS flow for thermal control. However, the present outflow rate of 0.01% tank volume/minute was so slow that boiling would occur during the 100 hours required for outflow, and further, stagnant vapor areas could build up as shown in Figure 43. These stagnant areas could overflow the solid channels and result in screen breakdown. Therefore, it was proposed that the TVS pump be operated during outflow in order to provide the requisite thermal control. The TVS flow direction was arranged to go up the standpipe and down the wall. The outflow was removed from the cold, high pressure side of the pump, where liquid was always present, as shown schematically in Figure 44. Because the outflow rate was small compared to the TVS pump flow rate (~1%, as described below) the TVS pump flow distribution would not be noticeably affected by outflow.

During coast, the vent flow was expanded to low pressure and routed through the TVS heat exchanger and then the shield to provide TVS cooling and thermal protection. However, the LH_2 outflow rate was 16 to 56 times the vent flow rate (21 to 180 times for the LO_2) and routing the outflow through the shield would overload the shield flow capacity and raise the shield and vent heat exchanger pressure, reducing the vent ΔT and cooling capacity of the heat exchanger. To compensate for this, and provide adequate cooling during outflow, the outflow was expanded to a slightly lower pressure (dictated by the flow capacity of the shield) and routed through a secondary heat exchanger in parallel with the vent heat exchanger as shown in Figure 44. All of the outflow and vent flow was routed through the shield and used, resulting in no vent penalty during outflow. This large shield flowrate during outflow would also reduce the radiative heat flux to the tank to a very low value.

The TVS pump flowrate was defined to determine the pump energy input to the tank and resulting "boiloff" attributable to the TVS. Initially the TVS flow was assumed to be sufficient so that the drag on a hemispherical bubble near the heat shorts would exceed the bubble surface tension force when the bubble radius equalled half the annulus gap. This criterion resulted in a TVS mixer flow of 64% tank volume/minute in a larger-than-necessary annulus gap (2+%) which in turn resulted in excessive LH_2 mixer boiloff (24.7 kg, 54.5 lb) in 30 days. This was unacceptable; therefore, the mixer flowrate was arbitrarily selected at 1% tank volume/minute, and the flow and pressure distribution in the annulus was determined using the analysis of Appendix B.

It was found, for the minimum gap of 0.08-cm (0.032-inch), that the minimum flow in the annulus, at approximately the tank midrift was about 10^{-5} times the design flowrate (see Figure 45). At a gap of 0.16 cm (0.064 inch), the minimum annulus flow was about 0.04 times the design flowrate. In order to define the minimum required flow in the annulus to insure that forced convection heat transfer was dominant, and that the flow does not stagnate in low-gravity because of adverse buoyancy forces, the criterion of Sparrow and Gregg (ref. 16) was used:

$$Gr \leq 0.225\, Re^2 \tag{14}$$

If this is met, buoyancy effects are less than 5% of the total heat transfer, and the forced convection component dominates.

CR54

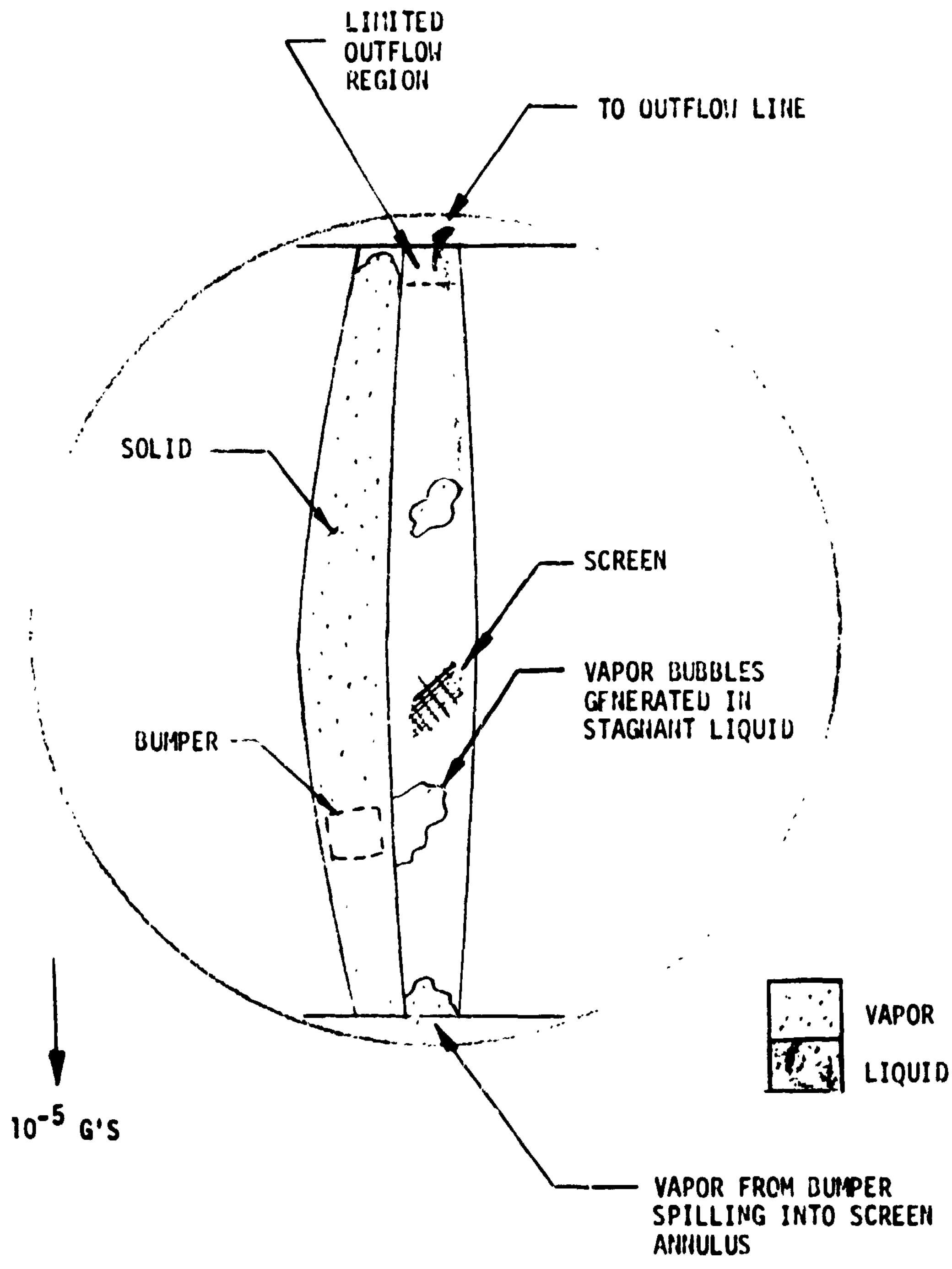

Figure 43. Vapor Generation During Long Outflow Without TVS Pump Operating

CR54

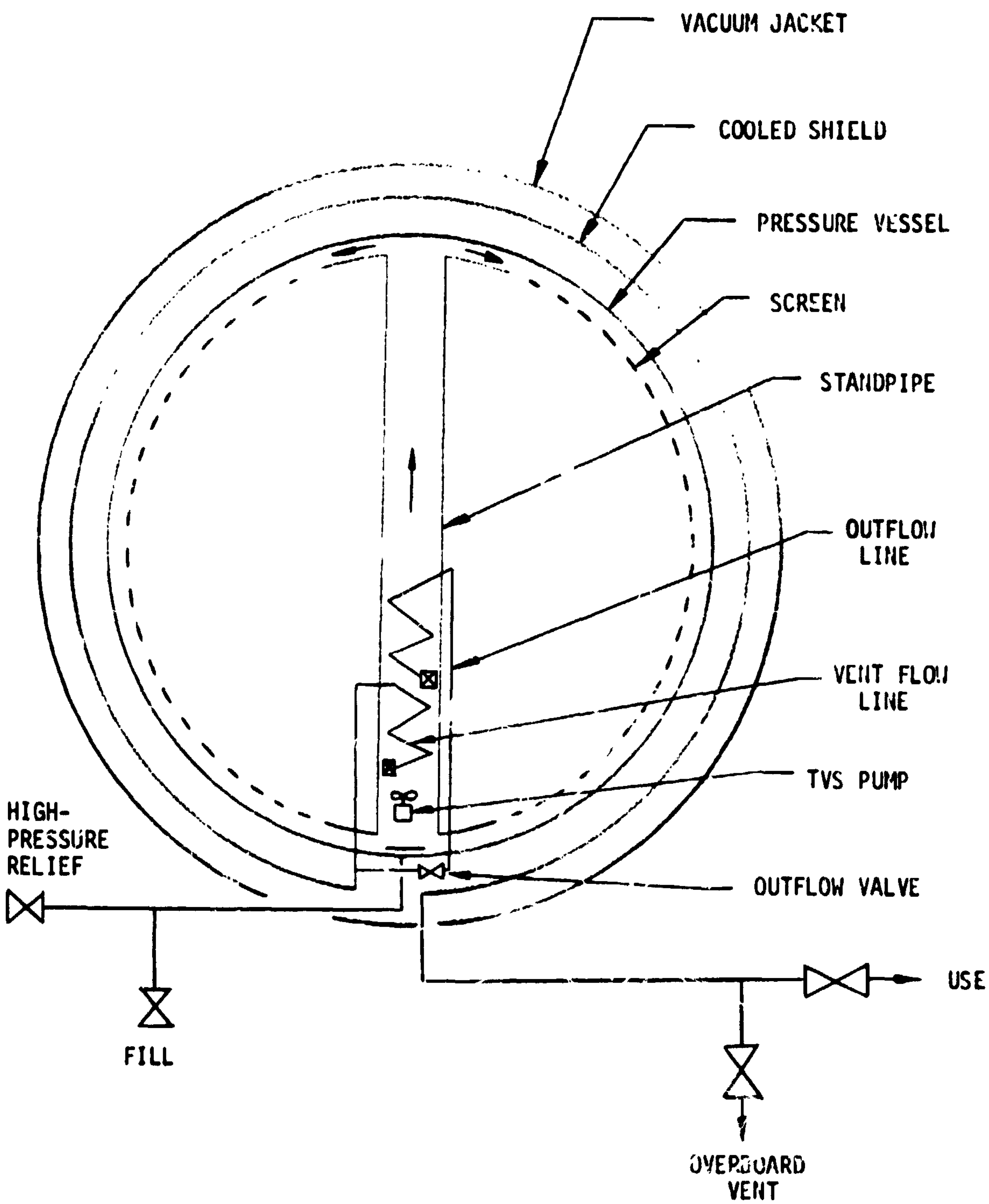

Figure 44. TVS/WSL Operational Schematic

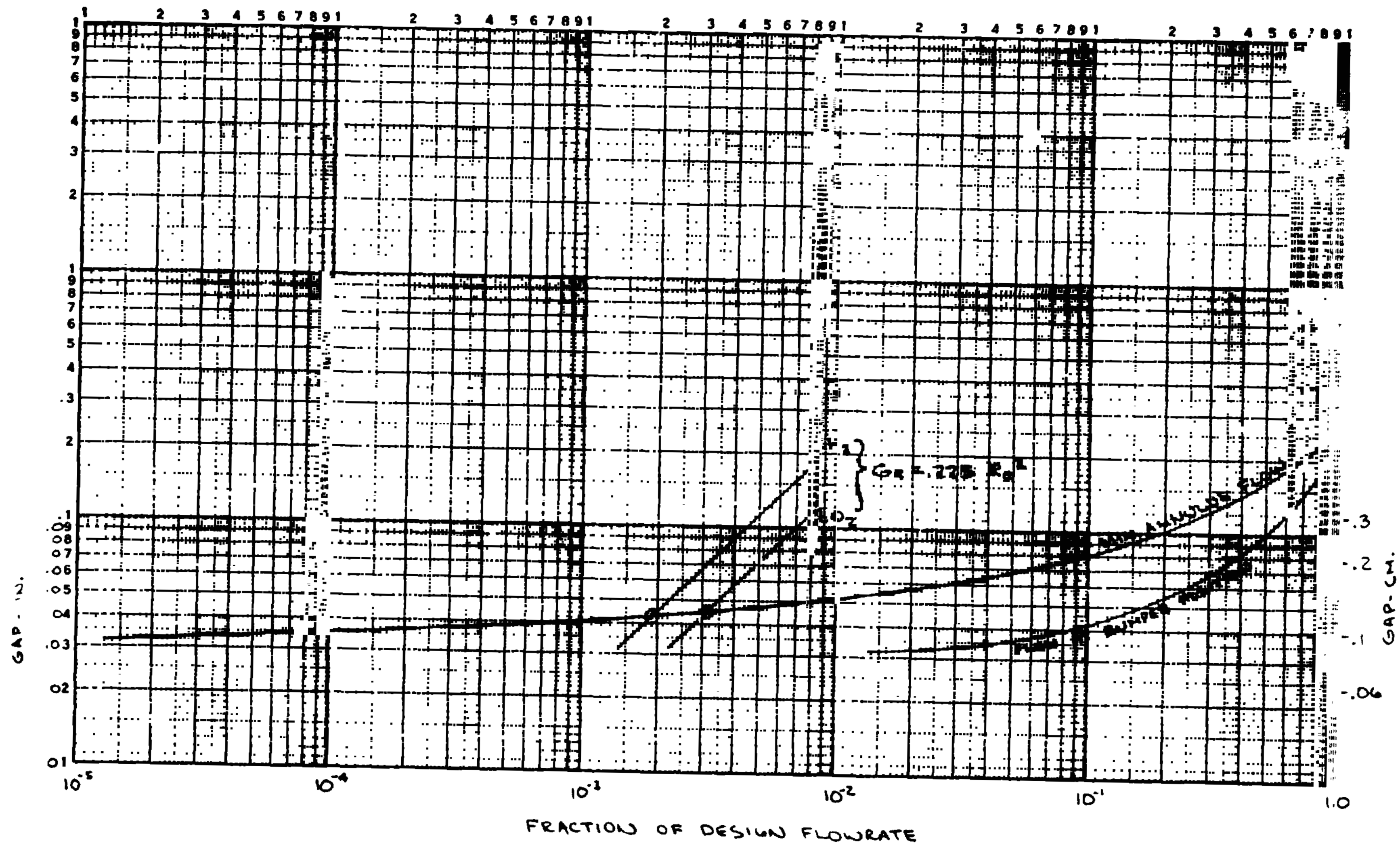

Figure 45. Annulus Flow vs Annulus Gap

Equation (14) was used as the criterion to determine the flowrate based on the velocity in the Reynolds number, assuming a characteristic (vertical) distance of 0.3 m (1 ft) in the Grashof and Reynolds numbers. A dimension of 0.3 m was representative of the length of the region of reduced flow. This criterion is shown in Figure 45 for both the LH_2 and LO_2. Where equation (14) crosses the minimum annulus flow curve defines the required gap: 0.109 cm. (0.043 inch) for LH_2 and 0.114 cm (0.045 inch) for LO_2. The minimum flow was 0.0019 of the design flowrate (0.005 m^3/minute) for the LH_2 and 0.0031 of the design flowrate for the LO_2.

The flow in the vicinity of the bumpers (in the screened channels) was more than 10% of the design flowrate (see Figure 45), tending to reduce the bumper heating problem, especially since more than 60% of the flow entering the vicinity (± 5°) of the bumpers would leave through the screen.

With the pressure distribution in the annulus and tank specified, the temperature distribution was analyzed. The critical problem was to determine if the radiative heat flux to the reduced annulus flow would increase the temperature of the minimum annulus flow above saturation, leading to bubble generation within the annulus. Fortunately, for the worse case of the 200-day mission, the radiative heat flux was a small fraction of the total tank heat input. The subcooling produced by the TVS heat exchanger is thus 0.00492°K (0.00885°R) for the LH_2 tank plus a mean pressure equivalent subcooling of 0.00005°K (0.00009°R). With full flow in the annulus, the temperature increase due to radiative heat flux was 0.000153°K (0.000276°R). Because this radiative heat flux was evenly distributed around the tank, the mean integrated flow in the annulus must be 0.0309 of the design flowrate. The actual integrated annulus flow was computed to be 0.235 of the design flowrate, for a margin of 7.6. A similar calculation for the LO_2 tank resulted in a mean integrated annulus flow requirement of 0.142 of the design flowrate. The actual integrated annulus flow for the LO_2 tank was computed to be 0.2425 of the design flowrate for a margin of 1.7. Therefore, the TVS has adequate thermal margin at the gaps previously defined for the LH_2 and LO_2 tanks.

Based on the criterion of 0.1 watt minimum input power, the LH_2 TVS/WSL system was analyzed at a minimum gap of 0.109 cm (0.043 inch). The optimum standpipe diameter in terms of minimum pump boiloff and standpipe residual weight was found to be 0.032 m (0.105 ft) for the 200-day mission and 0.023 m (0.076 ft) for the 30-day mission (as shown in Figure 46). For both of these, the pump size was below the minimum power. It was determined that the most efficient way to increase the power was to increase the head rise by reducing the standpipe diameter. This had the dual favorable effect of reducing standpipe weight and residual, and requiring higher pump speeds which were more easily obtained. Accordinly, the standpipe diameter was reduced to 0.0127 m (0.0417 ft) which gave an input power of just over 0.1 watt (as shown in Table 20).

The LO_2 system was analyzed and the optimum standpipe size is also shown in Figure 46. The system characteristics are shown in Table 20. Since the pump input power was above the minimum, the optimized system was selected.

An analysis was performed to define the pressurization requirements and the TVS cooling requirements during outflow. Initially it was thought that TVS

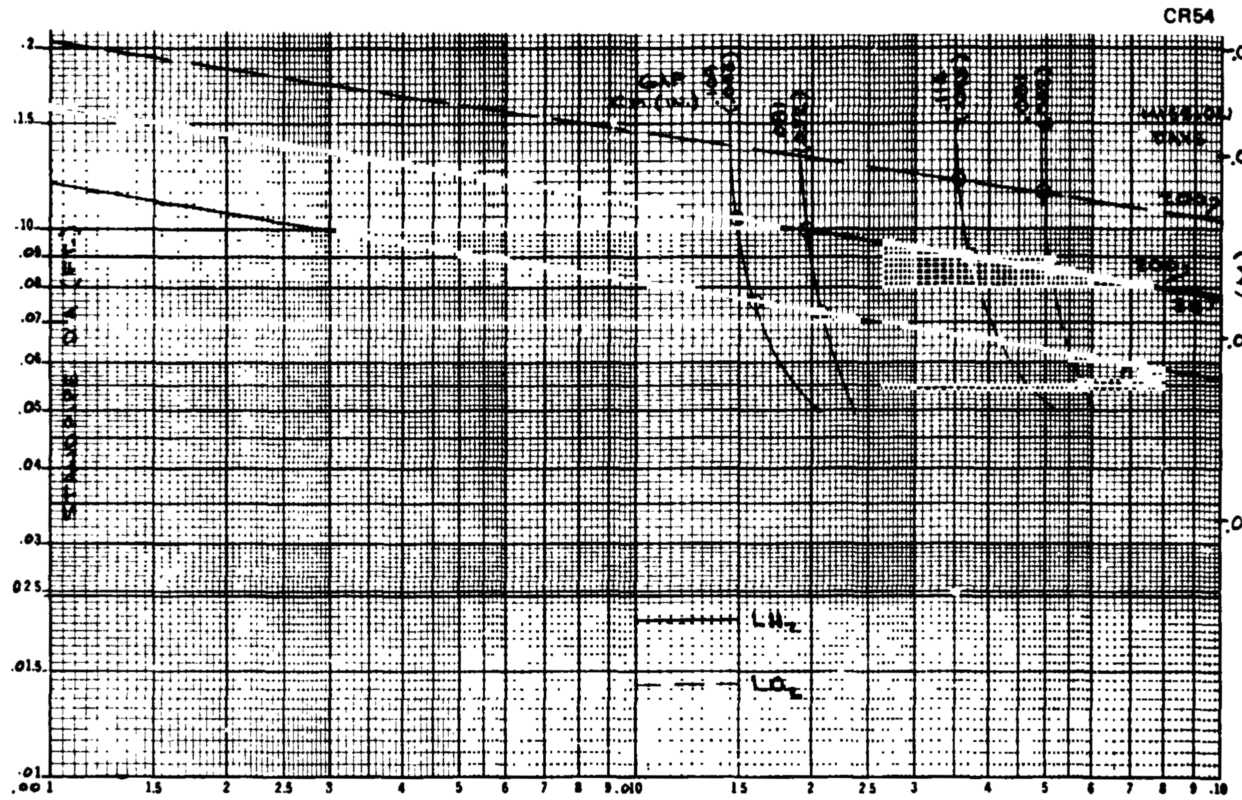

OVERALL PUMP EFFICIENCY

Figure 46. Optimum Standpipe Determination

cooling during outflow could be eliminated, and the heat input from the pump and heat leaks used to help pressurize the tank during outflow. However, all of these heat leaks would occur within the annulus or standpipe, so that vaporization bubbles that occur would be trapped by the screen, and would eventually dry out the TVS flow passage. Before this happened, the increasing vapor fraction in the standpipe would reduce the outflow rate taken from the standpipe. Therefore, it was clear that the TVS cooling process must be continued during outflow to insure that subcooled-to-saturated fluid is available for outflow. This would be done with an auxiliary outflow heat exchanger as described previously.

With the TVS operating during outflow, more flow (the amount of outflow) would leave the bulk fluid through the bottom baffle, than would enter the bulk from the top baffle. Thus, the static pressure in the bulk would slowly decrease during outflow. This would cause slow vaporization and cooling of the bulk liquid during outflow, and these vapor bubbles would be confined to the bulk (since they could not penetrate the screen). The cooled liquid would enter the screen, pass through the standpipe and annulus, mix with the other bulk fluid, etc., so that the entire tank contents would uniformly and steadily cool down during outflow. As the tank cooled, the tank pressure would drop to about 12 N/cm^2 (17.5 psia) for the LH_2 tank, and to about 22.8 N/cm^2 (33 psia) for the LO_2 tank. Whether pressures this low could be tolerated would depend on the LH_2/LO_2 user requirements. For purposes of this analysis, it was decided to not include pressurization system weights as part of the TVS/WSL system. In the absence of user interface requirements,

TABLE 20. – DESIGN TVS/WSL SYSTEM AND MIXER CHARACTERISTICS

	LH_2		LO_2	
	30-Day	200-Day	30-Day	200-Day
TVS Pump Head – cm (ft)	4.88 (0.16)	4.88 (0.16)	0.853 (0.028)	0.762 (0.025)
Pump flowrate – m^3/min (ft^3/min)	0.005 (0.175)	0.005 (0.175)	0.005 (0.175)	0.005 (0.175)
Pump efficiency (%)	2.57	2.57	3.68	3.57
Pump input power (watts)	0.1012	0.1012	0.2015	0.1897
Pump boiloff – kg (lb)	0.64 (1.40)	4.23 (9.32)	2.63 (5.79)	16.49 (36.36)
External boiloff – kg (lb)	5.06 (11.16)	14.15 (31.20)	96.67 (213.12)	81.87 (180.48)
Pump speed (rpm)	3542	3542	952	888
Pump diameter – cm (ft)	1.433 (0.047)	1.433 (0.047)	2.225 (0.073)	2.256 (0.074)
Pump weight – kg (lb)	0.0119 (0.0262)	0.0119 (0.0262)	0.033 (0.0730)	0.035 (0.0771)
Motor weight – kg (lb)	0.001 (0.0023)	0.001 (0.0023)	0.005 (0.0106)	0.005 (0.0105)
Optimum Standpipe Diameter – cm (ft)	1.271 (0.0417)*	1.271 (0.0417)*	2.743 (0.090)	3.658 (0.120)
Annulus Gap (Equivalent) – cm (in.)	0.109 (0.043)	0.109 (0.043)	0.114 (0.045)	0.114 (0.045)

* Not optimum - required for minimum power

it was felt that other alternatives, such as increasing tank pressure, could be employed if higher delivery pressure was required. The final manhole assembly design for the TVS/WSL is shown in Figure 47. The basic manhole attachment method used a Marman-type clamp, and was sealed with either an O-ring or an indium-wire seal ring. The screen annulus flow path was sealed by compression-deflection between two thin metal rings, as shown. It should be noted that the static pressure was higher outside the annulus, so that any leakage would be into the annulus. However, the leakage would be downstream of the screen, and the subcooling from the heat exchanger, and the long mixing zone in the standpipe would tend to eliminate any vapor bubbles which might leak in. With the TVS flow up the standpipe, the pump heat input would be directly cooled by the heat exchanger, and the long standpipe mixing length would tend to eliminate hot and cold spots in the flow before encountering the screen.

The pump/motor was attached to the lower baffle, which was contoured to give constant dynamic pressure from the screen to the standpipe, and was attached to the manhole by vanes for structural integrity. The heat exchanger section of the standpipe was enlarged somewhat to reduce pressure loss around the heat exchanger. The outside of the heat exchanger section was insulated with 0.64 cm (0.25 inch) of polyurethane foam to prevent condensation and heat transfer from the bulk propellant to the colder vent fluid. The complete TVS/WSL weight analysis was completed and is discussed in the next section.

Supercritical CGSS and TVS/WSL Weight Comparison. — The weight summaries comparing the supercritical and TVS/WSL systems for both propellants and both missions are shown in Table 21. The table shows that the TVS/WSL is markedly superior to the supercritical system for 30 days, but the LH_2 TVS/WSL is slightly lower in performance than the supercritical system for the 200-day mission, due solely to large boiloff losses caused by the inefficiency of the thermal control system (and the TVS pump). For a somewhat shorter mission (~170 days), the TVS/WSL system would again be superior, as shown in Figure 48, which plots performance ratio versus mission coast time for the high-performance bumper thermal control system. It can also be seen from Table 21 that elimination of the LH_2 TVS pump boiloff for the 200-day mission would increase the performance ratio by nearly 50%; for all of the other systems the TVS pump boiloff was not too significant. For this reason, the vapor-cooled shield TVS concept was studied only for the LH_2 tank and for the 200-day mission.

It will also be noted from Table 21 that the weight of the screen (WSL) and the annulus residual were essentially insignificant for both the LH_2 and LO_2 TVS/WSL systems. It is possible that a partial screen could save a few pounds in the LO_2 system, but the bulk of the weight of the WSL system was in the supports, which would probably not change for a partial screen. Therefore for this small-scale system, use of a partial screen was not analyzed.

LH_2 Cooled-Shield TVS/WSL Comparison; 200-day Transfer Mission. — For the internal mixer TVS, the heat through the heat shorts and the heat through the MLI cannot be distinguished, since both are mixed internally and vent fluid is extracted to cool all of the fluid in the tank. On the other hand, for a cooled-shield TVS, any heat entering the tank through heat shorts cannot be removed, since the cooled shield is external to the tank. In addition, although the mixer TVS can be overdesigned and run intermittently (for example,

CR54

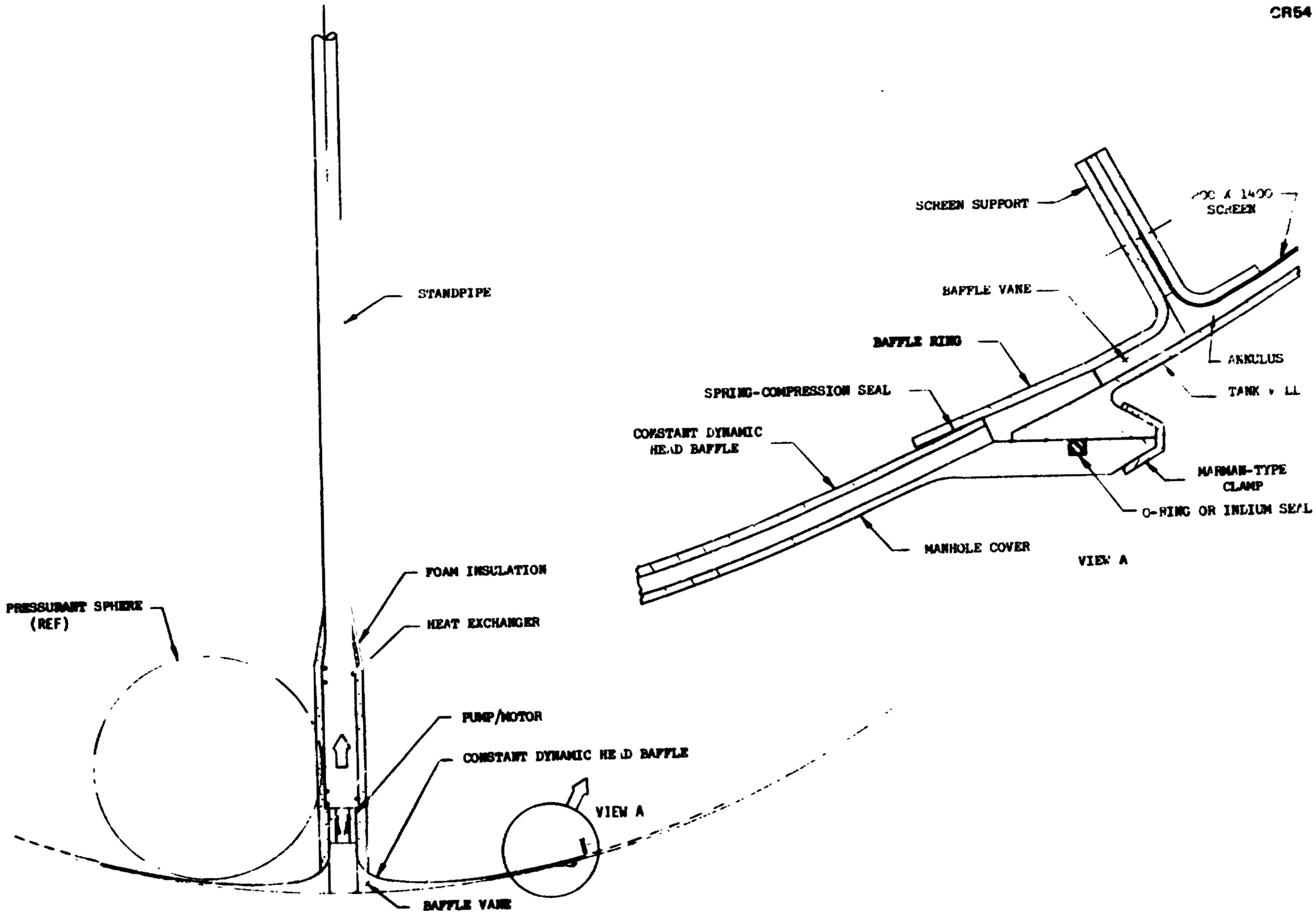

Figure 47. TVS/WSL Manhole Assembly Concept

ORIGINAL PAGE IS
OF POOR QUALITY

TABLE 21. – TOTAL WEIGHT SUMMARY (KG)

	30-Day				200-Day			
	Supercritical		TVS/WSL		Supercritical		TVS/WSL	
	H_2	O_2	H_2	O_2	H_2	O_2	H_2	O_2
A. Thermal Control System								
A1 Vacuum jacket	15.6	15.6	15.6	15.6	15.6	15.6	15.6	15.6
A2 V-C shields	9.0	9.0	9.0	9.0	9.0	9.0	9.0	9.0
A3 MLI	0.0	0.0	0.0	0.0	4.8	4.8	4.8	4.8
B. Tankage	83.9	83.9	4.6	4.6	83.9	83.9	4.6	4.6
C. Batteries	17.6	127.1	0.6	1.2	9.9	129.1	3.4	6.5
D. Hardware	44.7	63.7	49.5	68.9	44.7*	63.7*	49.5	69.0
D1 TVS pump/HEX			0.1	0.1			0.1	0.1
D2 Standpipe			0.1	0.2			0.1	0.3
D3 WSL			1.2	1.6			1.2	1.6
D4 WSL supports/baffles			9.3	9.3			9.3	9.3
D5 Other hardware			38.8	57.7			38.8	57.7
E. Total System	170.8	299.3	79.3	99.3	167.9	306.1	86.9	109.5
+ Propellant	34.7	553.9	32.6	535.3	34.7	553.9	32.6	535.3
	205.5	853.2	111.9	634.6	202.6	860.0	119.5	644.8
(lb)	(453.1)	(1881.0)	(246.7)	(1399.1)	(446.7)	(1896.[illegible])	(623.4)	(1421.5)
F. Total Propellant	34.7	553.9	32.6	535.3	34.7	553.9	32.6	535.3
G. Propellant Residual	0.7	9.6	1.2	12.3	0.7	9.6	1.2	12.8
G1 Annulus			0.4	7.1			0.4	7.1
G2 Standpipe			(0.01)	0.6			(0.01)	1.1
G3 Vapor			0.8	4.6			0.8	4.6
H. Propellant Boiloff	5.8	57.2	5.7	98.0	16.6	64.3	22.4	130.2
H1 Pump			0.6	2.6			4.2	16.5
H2 External			5.1	5.4			18.2	113.7
I. Deliverable Propellant	28.2	487.1	25.7	425.0	17.4	480.0	9.0	392.3
(lb)	(62.3)	(1073.8)	(56.6)	(936.7)	(38.4)	(1058.2)	(19.8)	(864.8)
J. Performance Ratio	0.1375	0.5709	0.2294	0.6697	0.0860	0.5581	0.0751	0.6083

* Not increased to reflect sma[illegible] increase in supported weight

ORIGINAL PAGE IS
OF POOR QUALITY

CR54

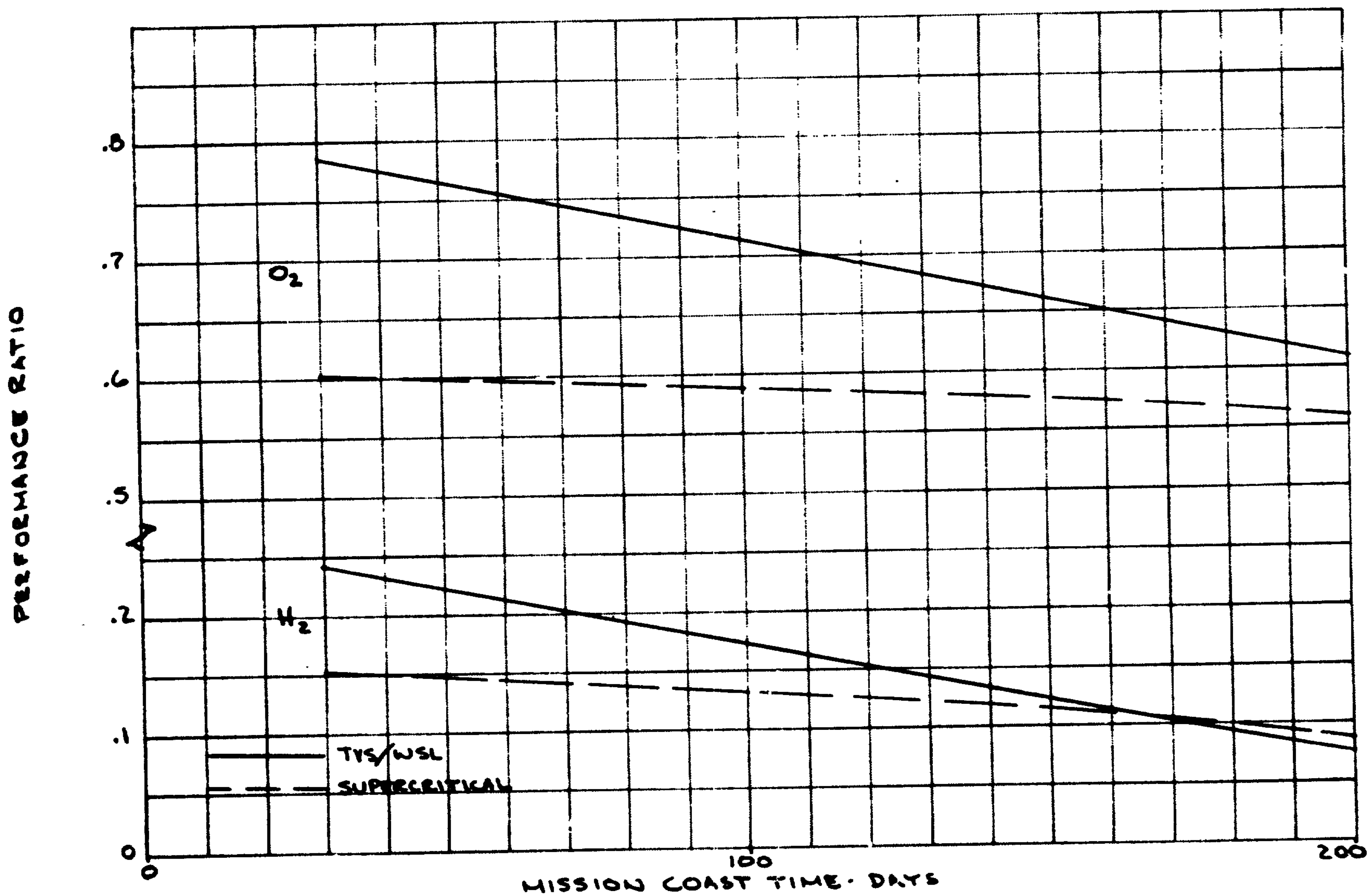

Figure 48. Performance Ratio for High-Performance MLI/Bumper System

to maintain tank pressure within set limits), the cooled shield TVS must operate continuously (since it is intercepting heat - and heat not intercepted cannot be subsequently removed). In order for the tank pressure to be maintained constant when using a cooled shield TVS, the heat leak to the tank must vaporize exactly enough propellant to displace the liquid required for vent outflow. To minimize the vent rate, the heat short heat leak to the tank must be minimized. This is normally accomplished by 1) using long thin low-conductivity supports and fluid tubing, and 2) where possible, shorting the heat leaks directly to the cooled shield instead of to the tank. In the second case, however, care must be taken not to overload the cooling capacity of the cooled-shield TVS.

Previously, the thermal control system was modified to provide long-term storage capability. The basic, well-developed tank support bumper system and vacuum jacket/cooled shield thermal protection system were retained, and the modifications only included reducing the bumper conductive heat leak by lifting the tank off the bumpers in low-g flight, and adding a maximum of one-inch of MLI (to minimize vacuum jacket and support changes). These thermal control system modifications had minimum overall system impact and gave adequate-to-marginal thermal performance for the 200-day coast mission (as described above). However, if the heat short heat leak from this modified LH_2 storage system (0.327 watt (1.117 Btu/hr)) entered a tank equipped with a cooled-shield TVS, all of the LH_2 would be vented in about 600 hours. Even if the radiative flux from the bumpers, and conductive flux along the plumbing lines were shorted to the cooled-shield TVS, the remaining conductive heat leak of 0.1245 watt (0.425 Btu/hr) would vent all of the LH_2 in about 1,550 hours.

Clearly, in order to obtain a 200-day coast capability with the cooled-shield TVS storage system, fundamental redesign of the thermal control system was necessary. This redesign would not only require minimization of the direct heat flux to the tank, but also control of where the heat input occurs, so as to prevent vapor generation within the acquisition screen. In addition, the heat leaks to the tank and to the cooled shields must be balanced to provide the proper operating characteristics and efficient use of cooling fluid.

The assumed redesign technique was to change the method of tank support to minimize the support heat leak, and is shown in Figure 49. The assumed support shown was a very long, thin-walled epoxy-resin/fiberglass tube enclosed in an evacuated tube through the tank. The support cross section was sized to support the loaded tank under 3 g's in tension (this support was especially appropriate for low-density LH_2). The side loads were taken by a spider of three thin steel cables, of maximum length, top and bottom. The support was made of 141 weave S-glass, 1.27-cm (0.5 inch) diameter with 0.025 cm (0.01 inch) wall (the thinnest wall which could be conventionally fabricated). The heat leak down the support tube was 0.00073 watt (0.0025 Btu/hr), and through the three steel wire supports 0.0078 watt (0.0266 Btu/hr).

Several layers of MLI were used between the support and the tank tube to minimize radiant heat leak. The support heat leak was insulated from the liquid in the WSL annulus, so that bulk liquid evaporation occurred. The wire support heat leak at the bottom of the tank was shorted to the boiler shield at the shield outlet from the tank. The wire support at the tank top could be shorted to the boiler shield since a high conductivity short would occur between

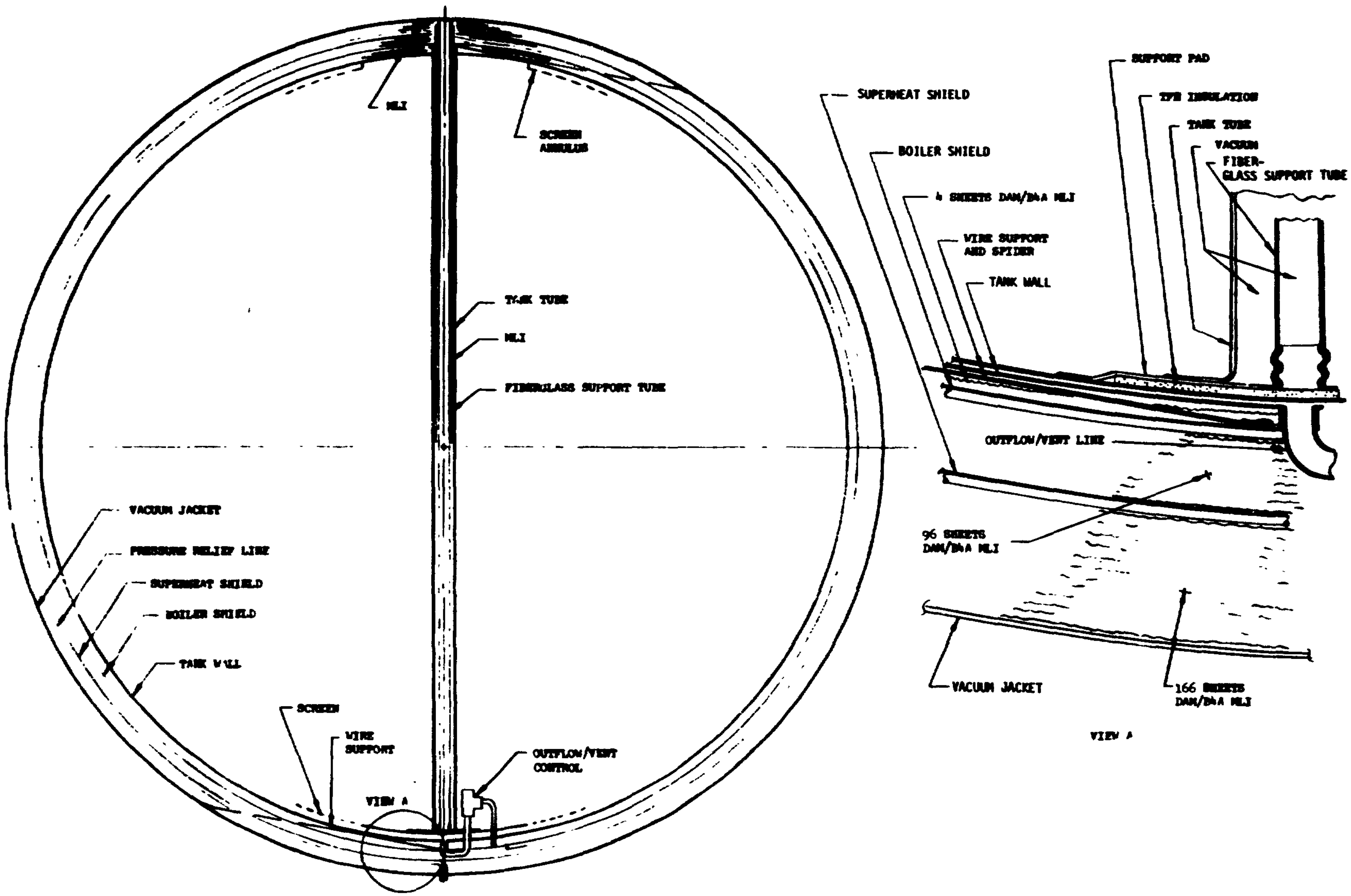

Figure 49. Ultra-High-Performance Thermal Control System with Cooled Shield TVS/WSL

the "warm" end of the shield and the tank, which could a .versely affect boiler thermal performance. Therefore, the top wire support heat leak went directly to the tank, but was restricted to a region of the tank where bulk evar... tion was permissible. This was achieved by removing the WSL at the t... tank where the baffle was in the TVS/WSL system, which would n. affect puddle residual following outflow (but would slightly decrease annulus resid..l).

The pressure relief line was shorted to both shields, and went completely around the tank. The outflow went through the shield system. Thus, the only heat leak to the tank was 0.00073 + 0.0078 = 0.00853 watt (0.0291 Btu/hr) which would result in a LH_2 vent rate of 0.00144 kg/hr (0.00318 lb/hr) (to maintain constant tank pressure). With this vent rate, the maximum heat flux which could be absorbed by the boiler shield was 0.1658 watt (0.566 Btu/hr). Of this, 0.00448 watt (0.0153 Btu/hr) entered through the relief plumbing, and 0.0078 watt (0.0266 Btu/hr) from the bottom wire supports; thus 0.1535 watt (0.524 Btu/hr) could enter through the MLI.

To determine the required MLI thickness, Figure 35 was used to define the unshielded MLI heat flux for both one and two shields (plus the boiler shield). The required MLI thickness for one shield plus boiler was 6.76 cm (2.66 inch); for two shields plus boiler, it was 5.23 cm (2.06 inch). The difference in MLI weight between the two thicknesses was 2.38 kg (5.25 lb).

It was assumed that for 2.5 cm (1 inch) of MLI plus a total of two shields, that the vacuum jacket size would not have to be increased. Because of the extra MLI needed for one shield plus boiler, the vacuum jacket weight would increase by 4.08 kg (9.0 lb); for two shields plus boiler, the vacuum jacket weight would increase by 2.9 kg (6.4 lb). Thus, the total penalty for one shield plus boiler was 2.38 + 4.08 = 6.46 kg (14.25 lb); for two shields plus boiler, the weight penalty was the shield weight of 4.54 + 2.9 = 7.44 kg (16.4 lb). This assumed that the shield thickness was 0.05 cm (0.020-inch) weighing 4.54 kg (10.0 lb). MDAC has fabricated cylindrical shields only 0.0127-cm (0.005-inch) thick, which would weight only 1.13 kg (2.5 lb); however, there may be severe fabrication problems with such thin spherical shields, and therefore, the thicker, but well-developed, 4.54-kg (10-lb) shields were used for this study. The lowest weight system using these shields was to use a boiler plus a single shield with 6.76 cm (2.66 inch) of MLI. This would also simplify shield installation problems as well.

With this baseline design and heat flux definition, the boiler shield configuration, using 1100 aluminum, was defined: with a single pass of 0.318-cm (0.125-inch) diameter – 0.0127-cm (0.005-inch) wall tubing up the shield (see Figure 49), the maximum shield temperature difference would be 0.47°K (0.84°R) at the equator. This meant that the fluid in the boiler only had to be expanded to 24 N/cm^2 (36.25 psia) to provide adequate cooling. The outflow could also be routed through the boiler at the same pressure and temperature by using a larger shield outlet flow control valve. At the higher outflow rate, the maximum shield temperature differences would be reduced to 0.24°K (0.44°R), which would not significantly affect shield thermal performance. The maximum pressure drop through the shield tubing for outflow is 0.0028 N/cm^2 (0.004 psi); during venting the pressure drop would be much less.

The system weight analysis for the cooled shield TVS H_2 system is shown in Table 22. In order to compare the performance of the three concepts, it was assumed that the same ultra-high-performance thermal control system was used, including the thicker MLI of 6.76 cm (2.66 inches) and a total of two shields. For the TVS/WSL, the central standpipe would be annular, surrounding the support tube and tank tube, which adds a few tenths of a kg., but which should not affect the fluid dynamic operation of the system. Note that the cooled-shield TVS eliminated the top baffle which saves 0.68 kg (1.5 lb) compared to the TVS/WSL. The most significant hardware difference between the two concepts was the requirement for 3.45 kg (7.6 lb) of batteries to provide power to the TVS pump.

A very interesting difference appeared in the boiloff for the two concepts. The cooled-shield TVS had a boiler shield and only one superheat shield and had a boiloff of 6.94 kg (15.3 lb). The TVS/WSL had the boiler (heat exchanger) inside the tank and two superheat shields outside the tank. In addition, because of the pump boiloff (which acted as heat short boiloff), the TVS/WSL had excess flow through the two shields which reduced the external heat leak boiloff to 3.58 kg (7.9 lb), which, plus the 4.26 kg (9.4 lb) pump boiloff, gave 7.85 kg (17.3 lb) of total boiloff, only 0.91 kg (2.0 lb) more than the cooled-shield TVS concept. Thus, the TVS pump/heat exchanger system effectively compensated for itself by reducing the external heat leak.

As shown in Table 22, the cooled-shield TVS/WSL concept had superior performance. In addition, this system had a number of operational advantages over the TVS/WSL. None of the heat transfer processes in the cooled-shield TVS were g-dependent, since they consisted of conductive heat leaks, conduction in the cooled shield, forced convection in the shield tubing, and radiation through the MLI. In the TVS/WSL, on the other hand, while none of the heat transfer processes were directly g-dependent, the internal flow which caused forced convection was pumped by the TVS pump. Unless the annulus and standpipe were completely full of fluid, the TVS pump did not have enough head capability to move the fluid in one g. In addition, the pressure and flow field in the annulus would be different in one g than in low g, which would directly affect the forced convection process. Thus, it may not be possible to verify the thermal performance of the TVS/WSL in one-g testing even with the tank 100% full. The most significant operational advantage of the cooled-shield TVS was that the system was completely passive and the conductive heat transfer processes driving the system performance were easily analyzed. The TVS pump, conversely, was an active unit near the limits of the state of the art, and in which small deviations in pump performance (efficiency) could have significant effects on overall system performance (pump boiloff).

Based on performance advantages and operational verification capability, the cooled-shield TVS/WSL was recommended for the life support power systems storage system application.

Shuttle Fuel Cell Reactant Supply System

The TVS/WSL and a cooled-shield TVS/WSL were compared on the basis of weight with a supercritical power reactant storage assembly (PRSA) being developed for the Space Shuttle by Beech Aircraft under subcontract to Rockwell International. The systems were compared for the baseline 7-day

TABLE 22. – TOTAL WEIGHT SUMMARY (KG), HIGH PERFORMANCE SYSTEMS FOR H_2 TANK AND 200-DAY MISSION

	Cooled-Shield TVS	TVS/WSL	Supercritical
A. Thermal Control System			
A1 Vacuum jacket	19.7	19.7	19.7
A2 V-C shields	9.1	9.1	9.1
A3 MLI	11.3	11.3	11.3
B. Tankage	4.6	4.6	83.9
C. Batteries		3.4	19.1
D. Hardware	44.2	45.1	35.6
D1 TVS pump/HEX	–	0.1	
D2 Standpipe	0.2	0.3	
D3 WSL	1.2	1.2	
D4 WSL supports/baffles	8.6	9.3	
D5 Other hardware	34.2	34.2	
E. Total System	88.9	93.2	178.7
+ Propellant	32.6	32.6	34.7
	121.5	125.8	213.4
(lb)	(267.8)	(277.3)	(470.5)
F. Total Propellant	32.6	32.6	34.7
G. Propellant Residual	1.2	1.2	0.7
G1 Annulus	0.4	0.4	
G2 Standpipe	–	(0.01)	
G3 Vapor	0.8	0.8	
H. Propellant Boiloff	6.9	7.9	3.9
H1 Pump		4.3	
H2 External		3.6	
I. Deliverable Propellant	24.5	23.5	30.1
(lb)	(53.9)	(51.9)	(66.4)
J. Performance Ratio	0.2013	0.1872	0.1411

Shuttle mission which would require two each of the H_2 and O_2 fuel cell reactant supply units, and the extended 30-day Shuttle mission which would require eight each of the H_2 and O_2 units. Therefore, just the basic units were compared on the basis of weight, and the total weight differences for the two missions were obtained by multiplying by two and eight respectively.

The basic groundrules for the analysis were that the usable quantity of reactant would be kept constant for all three systems, and the thermal control system would remain the same for all systems. However, as was the case in the previous section, it was found that the thermal control system had to be modified for the cooled-shield TVS to allow proper system operation, as discussed in subsequent sections.

Power Reactant Storage Assembly (PRSA). – The design features and requirements of the Space Shuttle fuel cell reactant supercritical storage and supply system were defined in refs. 27 and 28. The hydrogen PRSA consisted of a 0.2845-cm (0.112-inch) thick 2219 aluminum pressure vessel with an inside radius of 52.725 cm (20.758 inch). The pressure vessel was surrounded by an 0.038-cm (0.015 inch) vapor-cooled aluminum shield integrated with MLI, and further surrounded by a vacuum shell of 2219 aluminum.

The oxygen PRSA consisted of an 0.1956 cm (0.077-inch) thick Inconel 718 pressure vessel with an inside radius of 42.461 cm (16.717 inch). The pressure vessel was surrounded by MLI and a vacuum shell of 2219 aluminum, but did not have a vapor-cooled shield, since the minimum dQ/dm requirement could be met without one. The PRSA performance parameters (from ref. 27) are shown in Table 23. The average flow profiles required to supply the fuel cells are shown in Figure 50. The fuel cells operated at 41.4 N/cm^2 (60 psia), and the excess O_2 in the two PRSA's (~41 kg (90 lb)) was used for cabin atmosphere makeup at 10.3 N/cm^2 (15 psia). The fuel cells and PRSA's operated continuously during the 7-day mission. The weight breakdown of the PRSA's is shown (compared to the TVS/WSL) in Table 28 in a subsequent section in which the system weight comparisons are presented.

TVS/WSL System. – In order to design an equivalent subcritical TVS/WSL storage and supply system, a number of assumptions were made: (1) The maximum outside diameter of the pressure vessels was kept constant so as not to perturb the size, configuration, or weight of the thermal control system (vacuum jacket, MLI, and vapor-cooled shield); (2) the subcritical pressure vessels were made from minimum-gage (0.04 cm, 0.016 inch) 2219 aluminum; (3) the weight of the pressure vessel support fitting allowances varied with the supported load and inversely with material strength.

With these assumptions, and assuming 41.7 kg (92 lb) H_2 and 354.3 kg (781 lb) O_2, the maximum pressure allowed by density considerations was 22.4 N/cm^2 (32.5 psia) for the H_2 tank, and 23.5 N/cm^2 (34.1 psia) for the O_2 tank; therefore, the subcritical operating pressure was set at 20.7 N/cm^2 (30 psia). At this pressure the 0.04-cm (0.016-inch) thick tanks had a margin 1.5 to 2.0 times the safety factor used for the supercritical 2219 aluminum H_2 tankage. The weights of the subcritical pressure vessels were 4.45 kg (9.8 lb) for H_2 and 3.58 kg (7.9 lb) for O_2. The pressure vessel volumes were 0.623 m^3 (22 ft^3) for H_2 and 0.324 m^3 (11.45 ft^3) for O_2.

TABLE 23. – PRSA PERFORMANCE PARAMETERS

	Oxygen	Hydrogen
Fluid Quantity – kg (lb) per tank		
Minimum initial fill	354.3 (781.0)	41.7 (92.0)
Minimum usable (mission requirements)	321.0 (707.7)	37.4 (82.5)
Fluid Allowances – kg (lb) per tank		
Depletion unbalance	7.2 (15.9)	0.9 (1.9)
Post-loading venting	0.7 (1.5)	0.0 (0.0)
24-hour hold	3.2 (7.0)	0.3 (0.8)
Initial fill error	10.9 (24.0)	1.3 (2.8)
Residual	10.6 (23.4)	1.7 (3.8)
Prelaunch usage	0.7 (1.5)	0.1 (0.2)
Fluid Densities – kg/m^3 (lb/ft^3)		
Minimum initial conditions after fill (normal operating pressure)	1113.4 (69.5)	68.9 (4.3)
Flow Rates – kg/hr (lb/hr) per tank		
Minimum normal (without venting)	0.28 (0.618)	0.032 (0.070)
Maximum normal continuous**	6.3 (13.9)	0.79 (1.74)
Maximum for 2 minutes*	10.3 (22.8)	1.48 (3.27)
Fluid Pressure***		
Max relief full flow (tank) – N/cm^2 (psia)	724 (1050)	231 (335)
Max relief full flow (tank) – N/cm^2 (psig)	714 (1035)	221 (320)
Minimum relief valve crack – N/cm^2 (psig)	707 (1025)	214 (310)
Minimum relief valve reseat – N/cm^2 (psig)	686 (995)	210 (305)
Caution and warning high – N/cm^2 (psia)	685 ± 4 (994 ± 6)	205 ± 2 (297 ± 3)
Maximum normal operating – N/cm^2 (psia)	655 (950)	197 (285)
Heater off – N/cm^2 (psia)	638 ± 4 (925 ± 6)	183 ± 2 (265 ± 3)
Heater on – N/cm^2 (psia)	603 ± 4 (875 ± 6)	162 ± 2 (235 ± 3)
Minimum normal operating – N/cm^2 (psia)	586 (850)	148 (215)
Caution and warning low – N/cm^2 (psia)	521 ± 4 (756 ± 6)	133 ± 2 (193 ± 3)
Minimum operating, interface (residual) – N/cm^2 (psia)	138 (200)	103 (150)

* Pressure decay below the minimum normal operating pressure within the single-phase region is permitted for this flow rate.

** The PRSA stored fluid pressure shall be no less than the minimum normal operating pressure with the maximum normal continuous flow rates, except in the pressure decay density region.

*** Relief valves utilize ambient pressure reference. Caution and warning and heater control transducers utilize absolute pressur references.

CR54

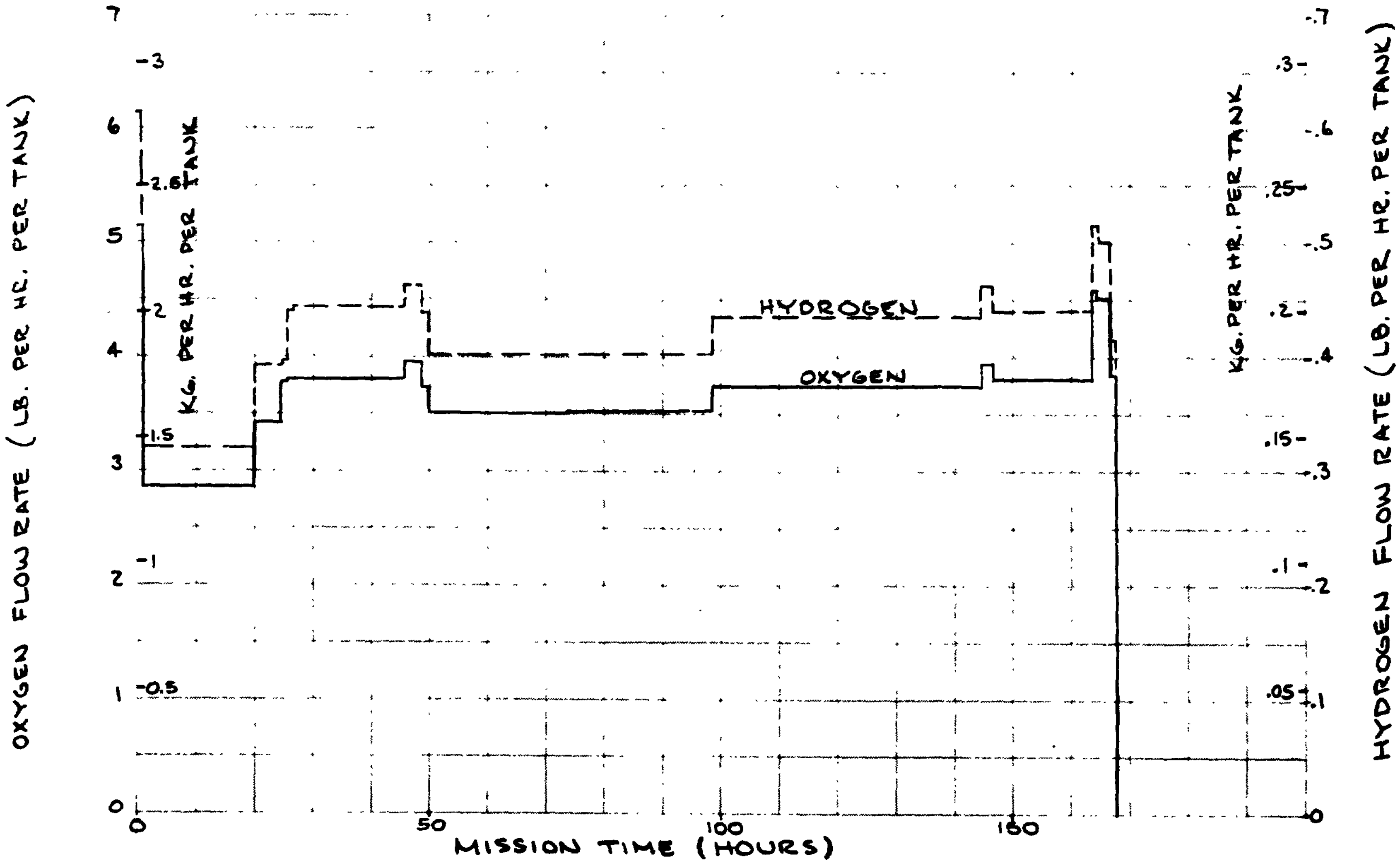

Figure 50. Average Flow Profile

The supercritical PRSA's would supply fuel cells which operated at 41.4 N/cm^2 (60 psia). In order to use subcritical supply tankage at 20.7 N/cm^2 (30 psia), the fuel cells had to be operated at 10.3 N/cm^2 (15 psia) (to allow adequate expansion and cooling margin for the subcritical TVS). This lower fuel cell pressure caused a minor voltage degradation, as shown in Figure 51. This could be overcome by adding two additional cells weighing 1.36 kg (3.0 lb) total. This penalty was not assessed to the TVS/WSL system; however, because the lower power requirements of the TVS, compared to the supercritical PRSA heaters, would save at least 6.35 kg (14.0 lb) of fuel cell reactants. It was noted that the excess O_2 could still be used for atmosphere makeup at 10.3 N/cm^2 (15 psia).

In the detailed design of an experimental tank with a complete WSL, described in Appendix A, it was found that a pleated screen was a very desirable method of installing a WSL in a small diameter tank. Accordingly, a complete pleated screen liner (200 x 1400 aluminum Dutch twill) was assumed for the TVS/WSL, configured as designed for the experimental tankage in Appendix A. The pleated screen residual, and annulus pressure and flow distribution were evaluated using the analyses described in Appendix D. The required screen pleat height and number, and baffle spacing, and the optimum standpipe diameter were determined by the TVS flowrates, which were very much larger than the outflow rates. The TVS flowrates were parametrically varied and optimized for pleat configurations from 0.318 cm (0.125 inch) to 0.792 cm (0.312 inch) pleat heights, according to two criteria – (1) absolute minimum TVS pump power (0.1 watt) and (2) currently obtainable minimum TVS pump power (1 watt). From ref. 9, substantial

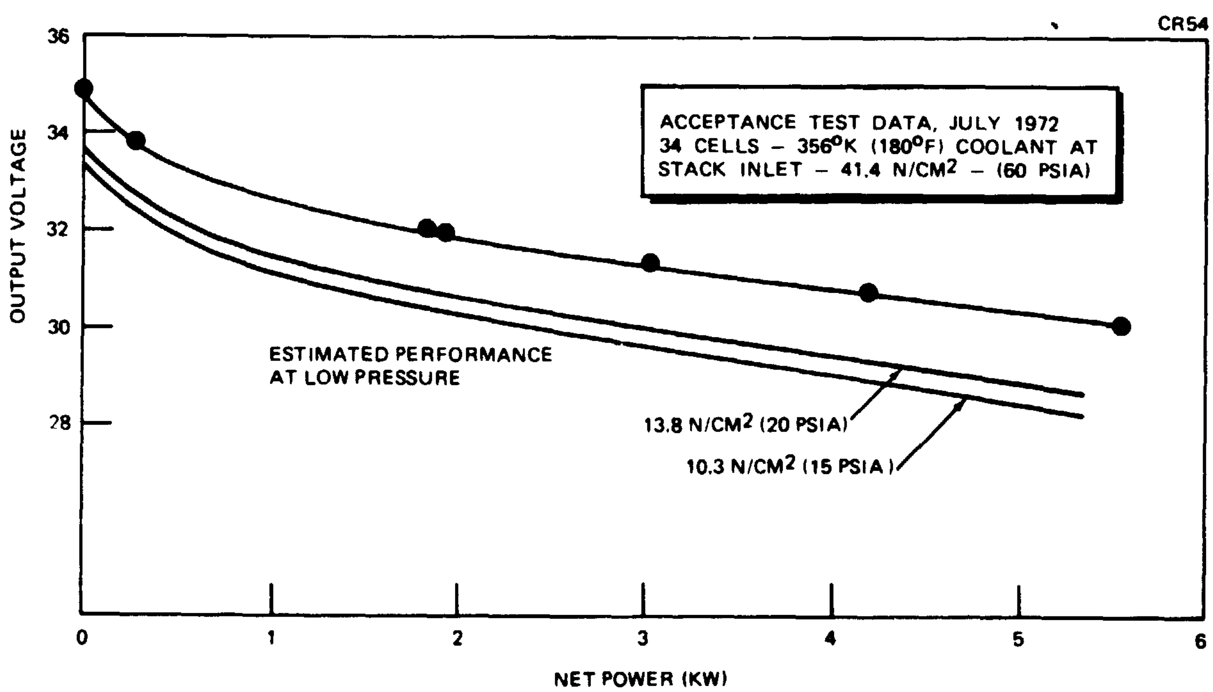

Figure 51. Output Voltage Characteristic of PC17A-2 (DM-2) Fuel Cell

development would be required to achieve 0.1-watt pumps for LH_2 and LO_2, while pumps currently exist which can be operated at about 1-watt input power. The characteristics of the TVS pump for the two power levels are shown in Table 24. The 1-watt pumps did not impose a significant weight penalty on the system, especially since the pump heat load, together with the external heat load, could be absorbed by the vaporized outflow in a TVS heat exchanger in the standpipe. Therefore, the "external and pump boiloff" were not real penalties to the system. Further, it was found that the 1-watt pumps allowed use of a smaller pleat height and equivalent annulus gap, with a net savings of 0.91 kg (2.0 lb) of residual in the O_2 tank. For these reasons, the 1-watt pumps were recommended for the Shuttle TVS/WSL system.

The minimum vent flow requirement was about 40 times less than the maximum outflow requirement (see Table 23), and therefore it was not considered feasible to integrate the vent flow and outflow into one system (because of the difficulty of controlling such a wide flow variation) nor was it feasible to use the outflow for TVS cooling because of the flow uncertainties. Instead, a parallel vent/outflow system was designed (Figure 52) with only the minimum vent flow being throttled to 13.8 N/cm^2 (20 psia) and used for TVS cooling. The vent flow was routed to the downstream side of the outflow regulator (which maintained 13.8 N/cm^2 (20 psia) supply to the fuel cells, further regulated to operate at 10.7 N/cm^2 (15 psia.) Outflow requirements above the minimum flow were supplied by demand through the outflow regulator which opened (or closed) as needed to maintain 13.8 N/cm^2 (20 psia) at the system outlet. The outflow was not expanded but simply flowed out along the cooled shield, ganged together with the vent flow line. The TVS heat exchanger was assumed to be 0.318-cm (0.125-inch) diameter 0.025-cm (0.01-inch) wall aluminum tubing. The laminar forced convection heat transfer coefficient inside the tube was controlling, since the pumped flow up the standpipe was highly turbulent with a much larger heat transfer coefficient. Table 25 shows the important TVS parameters. The TVS heat exchanger area was determined so that internal two-phase heat transfer occurred between a vent fluid quality of 5%, after expansion, and a quality of 85%, which marks transition from annular flow to mist flow (ref. 15). Lee Co. Viscojet fluid expanders were identified which would give the correct vent flow rates when expanding from 20.7 N/cm^2 (30 psia) to 13.8 N/cm^2 (20 psia). The weight of the TVS heat exchangeer system is trivial, as shown in Table 25, and was accounted for in the weignt comparison shown below.

The pressurant assumed was helium gas, stored at ambient conditions — 2[illegible] °K (400°R) and 2070 N/cm^2 (3000 psia) — which minimized problems of helium fill and system checkout operations, compared to cold helium storage.

The helium could, however, be used cold in the H_2 and O_2 tanks by being cooled to the tank temperature in an in-tank heat exchanger, as shown in Figure 52 Using the sensible heat of the helium to vaporize propellant to provide tank pressurization, reduced the helium required by a factor of 4 in the H_2 tank, and by 40% in the O_2 tank. Thus the helium required was only 0.82 kg (1.8 lb) (total for one H_2 and one O_2 tank) which could be stored in a 0.34-m (1.12-ft) diameter titanium sphere weighing 5.44 kg (12.0 lb). Because of the very low use rates, the helium would be expanded isothermally from 2070 N/cm^2 (3000 psia) to 207 N/cm^2 (300 psia). The in-tank heat exchangers would tend to be immersed in liquid, and were located where they were furthest from the screen.

TABLE 24.— DESIGN TVS/WSL SYSTEM AND PUMP CHARACTERISTICS, 7-DAY MISSION

	H_2		O_2	
	0.1 watt	1.0 watt	0.1 watt	1.0 watt
TVS Pump Head - cm (ft)	1.14748 (0.037647)	8.03340 (0.263563)	0.28203 (0.009253)	1.48081 (0.048583)
Annulus loss	(0.007908)	(0.094593)	(0.001791)	(0.02175)
Baffle loss	(0.007368)	(0.129725)	(0.001066)	(0.016785)
Standpipe loss	(0.022371)	(0.039245)	(0.006396)	(0.010048)
Pump flowrate – m^3/min (ft^3/min)	0.0224 (0.792)	0.106 (3.74)	0.0058 (0.206)	0.0324 (1.145)
Pump efficiency (%)	2.65	8.81	2.69	8.57
Pump input power (watt)	0.1	1.06	0.11	1.00
Pump boiloff – kg (lb)*	0.1506 (0.332)	1.496 (3.297)	0.328 (0.723)	3.0 (6.61)
External boiloff – kg (lb)*	2.891 (6.373)	2.891 (6.373)	19.11 (42.13)	19.11 (42.13)
Pump speed (rpm)	562	1113	385	566
Pump diameter – cm (ft)	4.39 (0.144)	5.85 (0.192)	3.17 (0.104)	4.94 (0.162)
Pump weight – kg (lb)	0.16 (0.36)	0.32 (0.70)	0.077 (0.17)	0.213 (0.47)
Motor weight – kg (lb)	0.003 (0.007)	0.02 (0.045)	0.005 (0.010)	0.03 (0.067)
Optimum Standpipe Diameter – cm (ft)	3.26 (0.107)	5.18 (0.17)	2.44 (0.08)	4.21 (0.138)
Standpipe residual – kg (lb)	0.06 (0.13)	0.15 (0.33)	0.44 (0.97)	1.31 (2.88)
Annulus Gap (Equiv) – cm (in.)	0.361 (0.142)	0.280 (0.114)	0.361 (0.142)	0.280 (0.114)
Annulus residual – kg (lb)	0.86 (1.90)	0.69 (1.52)	9.12 (20.1)	7.3 (16.1)
Standpipe Weight – kg (lb)	0.26 (0.57)	0.44 (0.97)	0.15 (0.33)	0.28 (0.61)
Screen Weight – kg (lb)	1.21 (2.67)	1.21 (2.67)	0.79 (1.74)	0.79 (1.74)
Pleat height – cm (in.)	0.742 (0.312)	0.635 (0.25)	0.792 (0.312)	0.635 (0.25)
Number of pleats	420	525	340	425

*Equivalent heat input

CR54

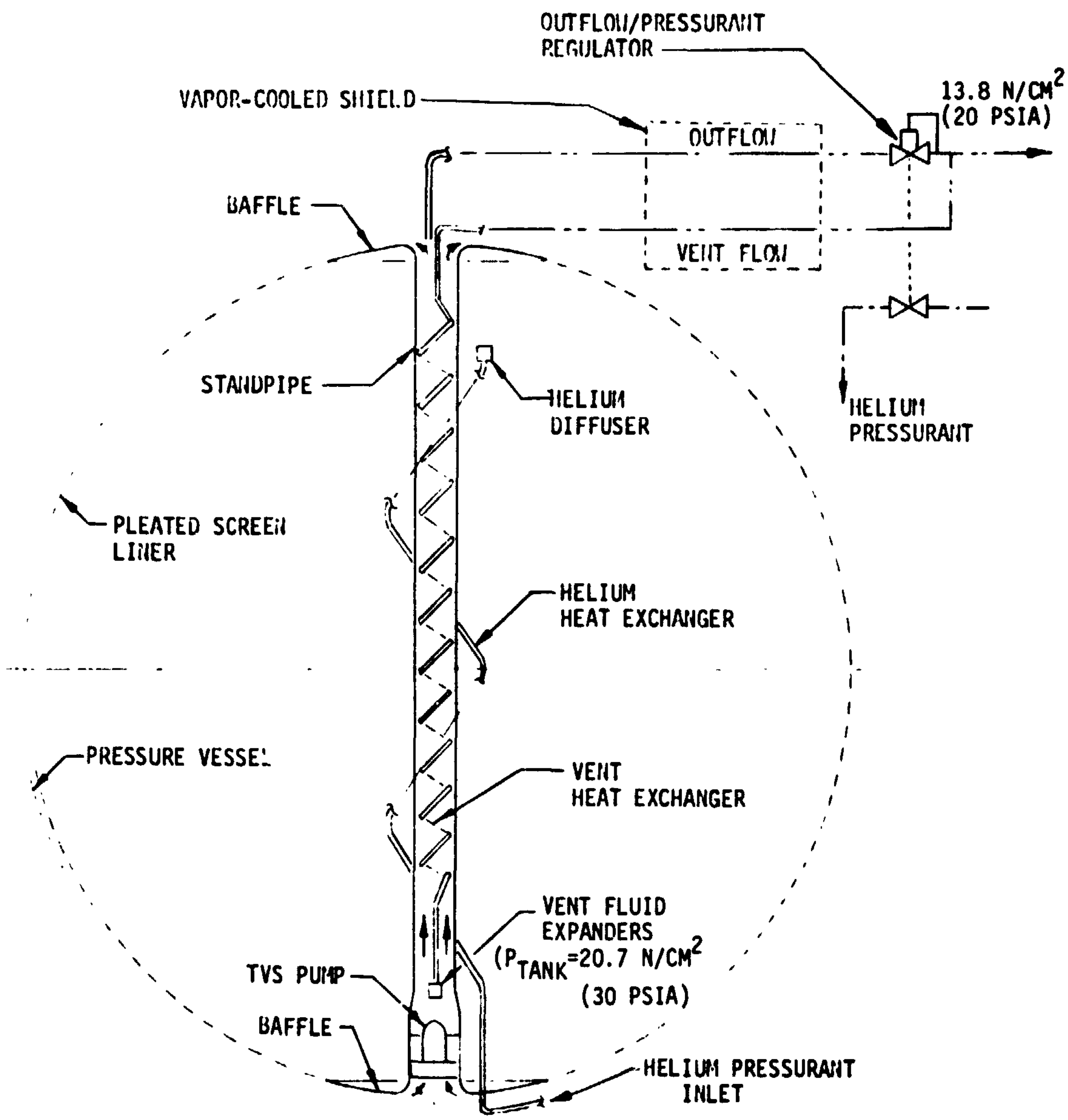

Figure 52. Vent/Outflow/Pressurization System Configuration

TABLE 25. – TVS HEAT EXCHANGER PARAMETERS

Parameter	H_2	O_2
Flow Rate – kg/hr (lb/hr)	0.032 (0.07)	0.28 (0.618)
Heat Transfer Coefficients – joule/ m^2-sec-°K (Btu/hr-ft^2-°R)		
Inside	123.98 (21.85)	137.03 (24.15)
Outside	1055.9 (186.1)	847.1 (149.3)
Overall	110.93 (19.55)	117.96 (20.79)
Tube Diameter by Wall Thickness – cm (in.)	0.318 x 0.025 (0.125 x 0.01)	0.318 x 0.025 (0.125 x 0.01)
Temperature Difference – °K (°R)	1.58 (2.85)	4.17 (7.5)
Tube Length – cm (in.)	222.3 (87.5)	189.5 (74.6)
Coil Diameter – cm (in.)	3.8 (1.5)	3.18 (1.25)
Number of Coils	18.5	19
Tube Weight – kg (lb)	0.016 (0.035)	0.014 (0.03)
Fluid Expander Viscojet P/N	13VC1, 13VC4 parallel	13AVC3 + 13AVC0 (series)
Viscojet Weight (TOTAL) – kg (lb)	0.027 (0.06)	0.027 (0.06)

The in-tank heat exchanger was analyzed, and it was found that about 30 cm (1 ft) of 0.318 cm (0.125-in) diameter tubing was all that would be required to cool the helium to propellant temperature. However, 60 to 90 cm of tubing would be used as shown typically in Figure 52. Control of the very low helium flow rates could be a problem, but it was envisioned that the same regulator controlling the propellant outflow could simultaneously control the helium inflow (Figure 52). This would require some component development, and, although the idea appears feasible, was not further pursued in this study.

The problem of low-g gaging of the propellant quantity was addressed. With supercritical tankage this problem is obviated because a capacitance probe can conveniently determine the single phase density and convert it to propellant mass. Such a probe would not work with a subcritical two-phase fluid in low-g, however, because liquid would stay in the capacitance probe (the minimum energy configuration) and thus the system would always indicate "full". However a propellant mass gaging system has been developed by the General Nucleonics Division (GND) of Tyco Laboratories which could be used in zero-g (ref. 29).

GND has been supplying mass quantity and density gaging systems to the government and industry since 1966. The aircraft oil quantity gaging system, for example, has been in use on over three thousand aircraft throughout the world for approximately ten years. They have also developed a liquid mass quantity gage for use in the space environment. The specific gaging system required was to provide continuous telemetry output signals, indicating the total pounds of hydrazine fuel remaining in each of three tanks on the spacecraft. The initial capacity of each tank was approximately 41 kg (90 lb) of hydrazine. The gaging system provided a very accurate reading, was non-contacting and light, and had a low power drain. Accuracy values for the current application were ± 3% of full volume near full tank, improving to ± 0.3% of full volume near empty tank. The gage was installed completely external to the tank being gaged; in fact it did not even come into physical contact with the tank. The complete gaging system for a single tank weighed less than 1.4 kg and the worst case power drain was less than 1.75 watts.

The gaging system was a mass quantity measuring device, and being mass sensitive, it could measure any type of liquid once it had been calibrated for that liquid. Further, the measurement was independent of liquid density changes in the fluid due to temperature effects and/or aeration of the fluid. Also, within a defined error envelope, the mass quantity measurement could be made independent of the tank attitude with respect to gravity forces, and independent of the fluid location within the tank in a zero gravity environment.

The gage was comprised of three assemblies, a radioactive source assembly, a detector assembly, and an electronics unit. When installed, the source assembly was typically located near one side of the tank and the detector assembly was located on the opposite side of the tank. The electronics unit could be located in any convenient place and was connected to the detector assembly through a low capacity coaxial cable. For application to the TVS/WSL, the source and detectors could be mounted from the girth ring supporting the vacuum jacket, thus being outside the MLI blanket. The source assembly configuration would be a small diameter tube containing a small quantity of Krypton-85, an inert radioactive gas. In the TVS/WSL application, it was a 0.318-cm (0.125-inch) diameter aluminum tube, 190-250 cm (75-100 inch) in length containing 500 millicuries of Krypton-85 (2.5 millicuries gamma equivalent), and weighing about 0.05 kg (0.1 lb).

The detector assembly contained an extremely reliable and ruggedized Gieger-Muller (GM) tube in an assembly that was approximately 0.85-cm (0.33 inch) in diameter and 19 cm (7-1/2 inch) long. This was the same detector assembly that was used in the aircraft oil quantity gaging systems. The detector assembly, in addition to meeting the requirements for spacecraft application and qualification, had passed all of the requirements of MIL-0-38338 which included temperature extremes of 233°K to 478°K (-40°F to + 400°F) and vibration levels at the resonant frequency of the GM tube center wire (anode) of 20 g's. All detector assemblies were subjected to 100% environmental testing prior to acceptance which included vibration, temperature, and operating voltage extremes. Two detector assemblies per tank would weigh about 0.11 kg (0.25 lb).

The electronics unit supplied the anode voltage to the detector, processed the detector output pulses, and supplied the measurement output voltage from the gage to the telemetry system. The unit weighs 1.2 kg (2.65 lb).

The characteristics of the system are shown in Table 26. The system accuracy was comparable to that required of the capacitance probe in the PRSA (see Table 22) and the weight was probably less than that of the capacitance probe. It appears that this completely developed and qualified system could be directly used for the subcritical TVS/WSL.

Cooled-Shield TVS/WSL System. —The problem of replacing the TVS pump system with a cooled-shield TVS was addressed. This would be desirable in that rotating machinery in the tank would be eliminated, along with a costly development program for the pump. Use of a cooled-shield TVS for tank thermal control would require that the heat input to the tank be carefully controlled in order to maintain tank pressure constant during outflow at the minimum outflow rate. The direct heat input to the tanks would have to be limited to 0.145 watts (0.495 Btu/hr) for the H_2 tank, and 0.125 watts (0.425 Btu/hr) for the O_2 tank. The heat inputs into the PRSA's were 2.05 watts (7 Btu/hr) for the H_2 tank, and 6.44 watts (22 Btu/hr) for the O_2 tank. It was not known what proportion of the heat input came through the MLI (and which could be stopped) and what proportion entered through direct heat shorts to the tank. The tank support system and MLI system for the PRSA were not then designed (effort was then being expended on pressure vessel development) and no details of these systems were available. Therefore, a completely new tank support and MLI/shield system was designed for the cooled shield TVS/WSL system, patterned after the fiberglass support tube and guy-wire system shown in Figure 49. The support system was designed to the critical loading g-levels given in ref. 27, and the system design parameters are shown in Table 27. The support tube was an epoxy/141 S-glass laminate with an ultimate strength of 137,900 N/cm^2 (200,000 psi) (LH_2) to 155,138 N/cm^2 (225,000 psi) (LO_2), and the guy wires were high strength stainless steel (17-7 PH) with an ultimate strength of 137,900 N/cm^2 (200,000 psi). The MLI system was designed to provide the maximum heat flux which could be absorbed by the vent fluid boiling within the shield. Note that because a cooled shield was used on the O_2 tank, the MLI requirements were minimal. The MLI assumed was double-aluminized-mylar with B4A dacron net spacers at 40 layers/cm (100 layers/inch). The cooled shields

TABLE 26. – GAGING SYSTEM SPECIFICATIONS

Type	Noncontacting nucleonic mass quantity gage.
Accuracy	Nominally 3 to 0.3% of full volume over the environmental conditions, including zero gravity.
Weight	Less than 1.36 kg (3.0 lb)
Volume	System – approximately 983 cm^3 (60 $in.^3$) Electronics unit – approximately 787 cm^3 (48 $in.^3$)
Input Power	Nominal 25 VDC unregulated (18 to 32 VDC). Power drain less than 1.75 watts under any and all environmental conditions.
Output	0.0 VDC full to 5.0 VDC empty (calibrated).
Parts	Established reliability (ER) and JAN-TXV parts.
Radioactive Source	Krypton-85, 500 millicuries (2.5 millicuries gamma equivalent).
Safety	Meets the radiation safety requirements of the State of California, the Atomic Energy Commission, and MIL-0-38338.
Reliability	Calculated MTBF in excess of 25,000 hours.
Qualification Environments	Temperature: -40°C to 204.4°C (-40°F to 400°F), detector -1.1°C to 7.1°C (30°F to 160°F), electronics Pressure: To 10^{-5} mm Hg. Humidity: To 95%. Vibration: 20 g's. EMI: MIL-STD 461 for ID equipment. Shock: MIL-STD 810, Method 516, Procedure III.

were assumed to be 0.0381-cm (0.015-inch) thick 1100 aluminum with 0.318-cm (0.125-inch) diameter x 0.025-cm (0.01-inch) wall vent flow tubing in one pass. All of the MLI and shield design parameters were easily achievable. The pressurization and gaging systems were identical to those evaluated for the TVS/WSL. The total system weight comparison is presented in the following section.

TABLE 27. – COOLED SHIELD TVS TANK SUPPORT AND THERMAL CONTROL SYSTEM PARAMETERS

	H_2	O_2
Tank Support System		
Fiberglass Support Tube		
Diameter – cm (in.)	1.27 (0.5)	1.27 (0.5)
Wall thickness – cm (in.)	0.025 (0.01)	0.038 (0.015)
Heat flux – watts (Btu/hr)	0.00069 (0.00236)	0.00104 (0.00356)
Max stress – N/cm^2 (psi) (3.3 g's – tank full)	16,686 (24,200)	77,224 (112,000)
Safety factor	9.1	2.0
Weight (including end fittings) – kg (lb)	0.04 (0.09)	0.05 (0.1)
Guy Wires (4)		
Diameter – cm (in.)	0.076 (0.03)	0.152 (0.06)
Length – cm (in.)	36.8 (14.5)	30.5 (12.0)
Heat flux – watts (Btu/hr)	0.01 (0.0343)	0.0387 (0.132)
Maximum stress – N/cm^2 (psi) (0.75 g's – tank full)	48,780 (70,748)	84,584 (122,674)
Safety factor	2.83	1.63
Weight (including end fittings) – kg (lb)	(0.01)	0.032 (0.07)
MLI		
Thickness – cm (in.)	1.07 (0.42)	0.15 (0.06)
Area – m^2 (ft^2)	3.86 (41.6)	2.56 (27.6)
Weight – kg (lb)	2.9 (6.3)	0.8 (1.7)
Heat flux – watts (Btu/hr)	3.0 (10.28)	12.6 (43.02)
Cooled Shield TVS		
Thickness – cm (in.)	0.038 (0.015)	0.038 (0.015)
Area – m^2 (ft^2)	3.86 (41.6)	2.56 (27.6)
Tube spacing – cm (ft)	69.2 (2.27)	37.2 (1.22)
Tube length – cm (ft)	557.8 (18.3)	688.8 (22.6)
Total weight – kg (lb)	4.3 (9.4)	2.9 (6.4)

System Weight Comparison. – The unit weight comparison for the PRSA, the TVS/WSL, and the cooled-shield TVS/WSL is shown in Table 28. The weight of the screens, baffles, and screen assembly rings for the WSL's were defined based on the pleated screen assembly design shown in Appendix C. The standpipe would not be required for the cooled-shield TVS, but would be retained to surround the fiberglass support tube. The screen pleat height

TABLE 28. – WEIGHT SUMMARY (KG), SHUTTLE FUEL CELL REACTANT SUPPLY

	PRSA		TVS/Pleated WSL		Cooled-Shield TVS/Pleated WSL	
	H_2	O_2	H_2	O_2	H_2	O_2
1. Pressure vessel	33.5	42.5	4.4	3.6	4.4	3.6
2. Outer shell	19.8	11.4	19.8	11.4	19.8	11.4
3. Girth ring	20.7	18.7	20.7	18.7	20.7	18.7
4. Suspension straps	6.5	7.0	6.5	0	0.2	0.2
5. Vapor-cooled shield	4.1	0.0	4.1	0	4.3	2.9
6. MLI	1.7	1.6	1.7	[illegible]	2.9	0.8
7. Quantity probe – temperature sensor and internal plumbing	3.2	3.0	3.2	3.0	3.2	3.0
8. Internal heater, mounting structure, and temperature sensor	1.7	3.4	0.0	0.0	0.0	0.0
9. Electrical harness and Vac-ion pump	3.4	3.4	3.4	3.4	3.4	3.4
10. Screen, baffles, standpipe, and support rings	0.0	0.0	2.2	1.5	2.2	1.5
11. TVS, pump, motor, HEX	0.0	0.0	0.5	0.4	0.0	0.0
12. Pressurization system (total), He sphere and support divided equally	0.0	0.0	5.0	4.8	5.0	4.8
13. Total system	94.6	91.0	71.5	55.4	66.1	50.3
14. Total propellant	41.8	354.3	42.1	354.3	41.9	354.3
Depletion unbalance	0.9	7.2	0.7	7.2	0.7	7.2
Post-loading venting	0.0	0.7	0.0	0.7	0.0	0.7
24-hour hold	0.4	3.2	0.4	2.7	0.4	2.7
Initial fill error	1.3	10.9	1.3	10.9	1.3	10.9
Prelaunch usage	0.1	0.7	0.1	0.7	0.1	0.7
Residual						
Annulus, puddle, standpipe (liquid)	0.0	0.0	0.9	8.8	0.7	7.5
Vapor residual	1.7	10.6	1.3	0.8	1.3	0.8
15. Usable propellant	37.4	321.0	37.4	322.5	37.4	323.8
Space Shuttle weight savings						
7-day mission (lb)			117.4 (258.8)		139.0 (306.4)	
30-day mission (lb)			469.6 (1035.2)		556.0 (1225.6)	

could be reduced, thus reducing the annulus residual, but it was of a convenient fabrication size at 0.64 cm (0.25 inch), and since the residual was minimal, and not critical, it was left the same. The baffles, also not needed, were retained to distribute the support loads to the pressure vessel. Thus the weight of item 10 of Table 28 was conservatively kept constant compared to the TVS/WSL.

The weights of items 7 and 9 were held the same for all three systems. In actuality, the weights for these items would almost certainly be reduced for the TVS/WSL, and cooled shield TVS/WSL, so that the weights shown are conservative for these two systems. Table 28 indicated that for the 7-day Shuttle mission, using two H_2 and two O_2 tanks, the TVS/WSL would save 117 kg (258 lb) relative to the PRSA, and for the 30-day extended mission, 470 kg (1033 lb) of weight savings. The cooled-shield TVS/WSL was even lighter than the TVS/WSL and would save 139 kg (305 lb) compared to the PRSA for the 7-day baseline mission and 556 kg (1220 lb) for the extended 30-day mission.

Spacelab Atmosphere Supply System

The Spacelab atmosphere supply system analyzed consisted of high-pressure 2070 N/cm^2 (3000 psi) N_2 and O_2 gas stored in 0.64-cm (0.25-inch) wall, 53.3-cm (21-inch) diameter high-strength maraging steel spheres, and regulated to low pressure for atmosphere makeup. Details of the system were found in ref. 30. The baseline system was sized for a 3-man crew for 7 days. There were some considerations for tieing the Spacelab atmosphere supply system into the Shuttle life support and fuel cell reactant supply systems (for O_2 only) for supplemental supply for longer missions and for backup.

Extension of the mission to 30 days would require quadrupling the baseline storage requirements. This study analyzed and defined the weight comparison between a subcritical cooled shield TVS/pleated screen liner system and the high pressure gas atmosphere supply system for the Spacelab 30-day extended mission. The capacities of the subcritical tanks were determined based on supplying four times the usable capacity of the gas storage system (30-day mission requirements) plus 9% residual/unavailable (estimates based on Shuttle fuel cell reactant supply system study above) plus 5% initial ullage. The characteristics of the tanks (both high pressure and subcritical) are shown in Table 29.

For commonality of construction, the subcritical O_2 tank was arbitrarily made the same size as the N_2 tank, with the result that it was slightly over-sized for the O_2 requirements. The O_2 and N_2 systems were made identical and interchangeable. At an operating pressure of 27.6 N/cm^2 (40 psia), a tank wall thickness of 0.025 cm (0.01 inch) resulted in a safety factor of 3.1 for the 2219 aluminum subcritical tanks. A basic assumption was that the thermal protection system to be used would be identical in concept to that used in the Shuttle fuel cell reactant supply. This system consisted of a vacuum jacket, girth ring, suspension tube/guy wire supports, vapor-cooled shield TVS integrated with MLI, and a similar vent/outflow/pressurization system to the Shuttle TVS/WSL described previously.

The vacuum jacket weight was conservatively ratioed from the Shuttle system size by the diameters squared, and the girth ring and internal plumbing weight by the ratio of diameters. A common MLI system was designed for use on either O_2 or N_2 tank. The MLI was optimized based on the minimum N_2 flow requirements of 1.055 kg/day (2.325 lb/day) for leakage makeup (rather than the leakage/breathing O_2 requirements of 2.807 kg/day (6.189 lb/day)), and gave 0.5 cm (0.2 inch) of double-aluminized mylar/B4A dacron net MLI, weighing 0.59 kg (1.3 lb). The low-pressure controls and distribution system weight was kept the same as for the gas system, and the electrical harness and Vac-ion pump weights were assumed to be the same as for the Shuttle system.

TABLE 29. – TANKAGE CHARACTERISTICS; SPACELAB ATMOSPHERE SUPPLY AND 30-DAY MISSION

	N_2	O_2
High-Pressure Gas		
Tank ID – cm (in.)	53.3 (21.0)	53.3 (21.0)
Volume – m^3 (ft^3)	0.0795 (2.806)	0.0795 (2.806)
Pressure – N/cm^2 (psia)	2069 (3000)	2069 (3000)
Capacity, total – kg (lb)	17.56 (38.72)	22.91 (50.51)
Capacity, usable – kg (lb)	15.68 (34.57)	20.76 (45.77)
Weight – kg (lb)	49.14 (108.33)	49.14 (108.33)
Subcritical Liquid		
Tank ID – cm (in.)	56.34 (22.18)	56.34 (22.18)
Volume – m^3 (ft^3)	0.0936 (3.306)	0.0936 (3.306)
Pressure – N/cm^2 (psia)	27.6 (40)	27.6 (40)
Wall thickness – cm (in.)	0.025 (0.01)	0.025 (0.01)
Capacity, total – kg (lb)	68.6 (151.3)	96.6 (212.9)
Weight – kg (lb)	1.0 (2.2)	1.0 (2.2)
Vacuum Shell OD – cm (in.)	76.2 (30.0)	76.2 (30.0)

The pleated screen liner (200 x 1400 aluminum) was constructed identically to the Shuttle system except that the pleat height was reduced to 0.478 cm (0.188 inch). Because of the low use rates, there was no problem found with safety factors during outflow in low-g. The total system weight summary and comparison is shown in Table 30. The liquid fill errors and depletion unbalances were assumed at the percentages of the Shuttle system. The venting/prelaunch usage and 24-hour hold quantities were based on 24-hour crew consumption with no atmosphere leakage. Table 30 indicates that for the 30-day mission, 349 kg (770 lb) out of 442 kg (975 lb) of inert system weight would be saved by u ing subcritical storage with a cooled shield TVS/WSL.

TABLE 30. – WEIGHT SUMMARY (KG), SPACELAB ATMOSPHERE SUPPLY AND 30-DAY MISSION

		High-Pressure Gas Storage		Cooled-Shield TVS/WSL	
		N_2	O_2	N_2	O_2
1.	Pressure vessel(s)*	196.5	196.5	1.0	1.0
2.	Hi-pressure regulators	9.1	9.1	0.0	0.0
3.	Lo-pressure controls and distribution	15.4	15.4	15.4	15.4
4.	Outer shell	0.0	0.0	7.2	7.2
5.	Girth ring	0.0	0.0	12.5	12.5
6.	Suspension system	0.0	0.0	0.2	0.2
7.	Cooled-shield TVS	0.0	0.0	1.4	1.4
8.	MLI	0.0	0.0	0.6	0.6
9.	Quantity gaging and internal plumbing	0.0	0.0	2.0	2.0
10.	Electrical harness and Vac-ion pump	0.0	0.0	3.4	3.4
11.	Screen, baffles, and support rings	0.0	0.0	0.6	0.6
12.	Pressurization system	0.0	0.0	2.2	2.2
13.	Total	221.0	221.0	46.5	46.5
14.	Total system (lb)	442.0 (975.0)		93.0 (205.0)	
15.	Net weight savings (lb)	349.0 (770.0)			
16.	Total propellant	70.3	91.6	68.6	96.6
	Depletion unbalance	0.0	0.0	1.4	2.0
	Venting and 24-hour hold	0.0	0.0	1.0	0.0
	Initial fill error	0.7	0.9	2.0	2.9
	Prelaunch usage	0.0	2.5	0.0	2.5
	Residual				
	Annulus (liquid)	0.0	0.0	1.7	2.4
	Vapor	7.5	8.6	0.4	0.3
17.	Usable propellant	62.1	79.6	62.1	86.5

*Four pressure vessels required for each gas

HEAT TRANSFER EFFECTS EXPERIMENTAL STUDY

When fine mesh screen acquisition systems are used for orbital transfer of LH_2 and other cryogens, there has been concern with the effects of heat transfer, from pressurizing gas or tank wall, on the screen retention capability, characterized by bubble point. Although considerable previous work has identified a potential problem with heat transfer effects, there have been no hard design data generated. Under Contract NAS8-27685 (ref. 31) and MDAC IRAD programs (ref. 32), three different methods of evaluating screen heat transfer effects were tested, with mixed results: two of the three methods of ref. 31 showed serious bubble point degradation with LH_2; one showed no degradation; and the ref. 32 tests with LN_2 showed no bubble point degradation.

Martin Marietta has recently completed a program to evaluate heat transfer effects (ref. 33). Unfortunately, the experimental program was not designed to yield quantitative design data. The program did demonstrate that with a 63.5-cm (25-inch) diameter spherical tank with 8 channels formed of two layers of 325 x 2300 screen, LH_2 could be successfully expelled against one-g using GHe or GH_2 pressurant at temperatures up to 311°K (560°R). Because all of the previous results may be highly configuration-dependent, it was the objective of our test program to use a carefully designed experimental apparatus, fabricated under an MDAC IRAD program, to evaluate many different screens (weaves, materials, and bubble points) with LH_2 and with both GHe and GH_2 pressurant, over a wide range of screen heat flux simulating that anticipated in vehicle applications.

Screen Selection

The eight screens originally selected included all of the screens studied under Contract NAS3-15846, except the 40 x 40 and 60 x 60 square-weave screens. These screens were eliminated because of the very low value of bubble point obtainable in LH_2. Because of developments in the analytical studies described above, further screen substitutions were made: a pleated 325 x 2300 stainless steel screen was substituted for the 500 x 500, so that a pleated and unpleated screen of the same mesh were compared directly. The pleats were 0.478 cm (0.188 inch) deep by 3.15 pleats/cm (8 pleats/inch), which was typical of the pleat configurations defined for potential systems in the analytical studies. Also, because of the desirability of using aluminum screens and tankage, aluminum 200 x 1400 was compared directly to stainless steel 200 x 1400, and aluminum 120 x 120 with stainless 120 x 120 (150 x 150 could not be obtained in aluminum) while the heavy and low performing 50 x 250 and 24 x 110 screens were eliminated.

The two aluminum screens selected were tested directly with the same mesh screens of the same wire size in 304 stainless steel. This was done to isolate heat retention degradation effects, if any, due to large differences in screen wire conductivity at LH_2 temperature. There were provisions to install two screens side-by-side within the test apparatus. The screen area exposed to heat flux was 10.4 cm x 10.4 cm (4.1 inch x 4.1 inch), except for the stainless 200 x 1400 screen which was 9.53 cm x 9.53 cm (3.75 inch x 3.75 inch) (due to a slightly undersized specimen). The screens were cleaned and bonded to stainless steel specimen holders with LH_2-compatible polyurethane adhesive. Each specimen was tested in isopropyl alcohol to determine its actual bubble point, and to ensure the bonding integrity. The alcohol bubble point data are shown in Table 31, compared to the predicted and actual LH_2 bubble point data. It was noted that the bubble point for the pleated 325 x 2300 screen was about that expected for 325 x 2300, while the bubble point for the plain 325 x 2300 was lower than expected. The reason for this is not known, however, MDAC experience with extremely fine-mesh screens indicates that bubble point variations of 10% are not abnormal. The four double screen specimens are shown in Figure 53, with the 325x2300 screens shown in detail in Figure 54.

Test Setup

Important features of the test apparatus and setup were: (1) the gas pressure was imposed on the screen mechanically and exactly, and the problem of measuring very low pressures in LH_2 was obviated; (2) the condition of screen breakdown (bubble penetration) was automatically determined and could also be observed visually; (3) extremely accurate calibrated and guarded heaters were used to impose heat flux; (4) the LH_2 under the screen could be slightly superheated or subcooled relative to saturation; (5) a calibrated flow of GHe in addition to GH_2 pressurization could be imposed on the screen; (6) gas temperatures were measured with accurate platinum resistance thermometers; and (7) two screen specimens could be tested with one experimental setup.

The internal apparatus is shown in Figure 55, and an external view of the dewar, showing the windows, is shown in Figure 56. The test apparatus arrangement is shown schematically in Figure 57. The operation of the apparatus was straightforward: with LH_2 supported with surface tension forces by the horizontal screen, both the plunger and the space above the LH_2 were purged with GH_2 (plus GHe if desired) and the plunger immersed in the LH_2 to the desired liquid head. With the plunger clear of liquid, a 0.1 ohm carbon resistor level sensor inside the plunger showed "gas." The heater was energized and, when the screen "failed" (permitted gas flow), the liquid dropped sharply away from the screen, and gas rushed from the plunger through the screen. Simultaneously, liquid surged into the plunger, covering the level sensor, which indicated screen breakdown.

The gas flow passages are shown approximately to scale in Figure 58. The GHe (if any) and GH_2 vaporized from the screen were continuously vented as shown. The gas could only exit from the vicinity of the screen through the slot shown, where the gas temperature was measured. The needle valve shown connected the plunger to the screen gas space (and another valve isolated the plunger from the other screen gas space).

The guarded heaters used were International Thermal Instrument Company Heat Flux Standards, 10-cm (4-inch) square, which consisted of a heat flux gage sandwiched between two electric heaters. Each heater was energized by a variable dc power supply capable of 40 VDC and 4 amps. The heaters were energized simultaneously so that the heat flux gage indicated zero; when this occurred all of the energy of the lower heater was directed into the GH_2,

TABLE 31. — HEAT TRANSFER SPECIMEN BUBBLE POINT

Test Setup	Mesh	Material	Weave	Isopropyl Alcohol Bubble Point cm H_2O (in. H_2O)	Predicted* LH_2 Bubble Point cm LH_2 (in. LH_2)	Actual LH_2 Bubble Point cm LH_2 (in. LH_2)
1-1	325 x 2300	304 SS	Twilled Dutch (pleated)	71.1 (28.0)	85.3 (33.6)	63.5 (25.0)**
1-2	325 x 2300	304 SS	Twilled Dutch	61.0 (24.0)	73.2 (28.8)	57.7 (22.7)
2-1	200 x 1400	304 SS	Twilled Dutch	36.8 (14.5)	44.2 (17.4)	42.7 (16.8)
2-2	200 x 1400	Aluminum	Twilled Dutch	36.3 (14.3)	43.7 (17.2)	42.7 (16.8)
3-1	720 x 140	304 SS	Reverse Dutch	26.7 (10.5)	32.0 (12.6)	29.7 (11.7)
3-2	165 x 800	304 SS	Twilled Dutch	22.1 (8.7)	26.7 (10.5)	27.2 (10.7)
4-1	120 x 120	304 SS	Twilled square	6.4 (2.5)	7.6 (3.0)	6.9 (2.7)
4-2	120 x 120	Aluminum	Twilled square	6.4 (2.5)	7.6 (3.0)	7.6 (3.0)

* Extrapolated from isopropyl alcohol data

** Apparatus limit

CR54

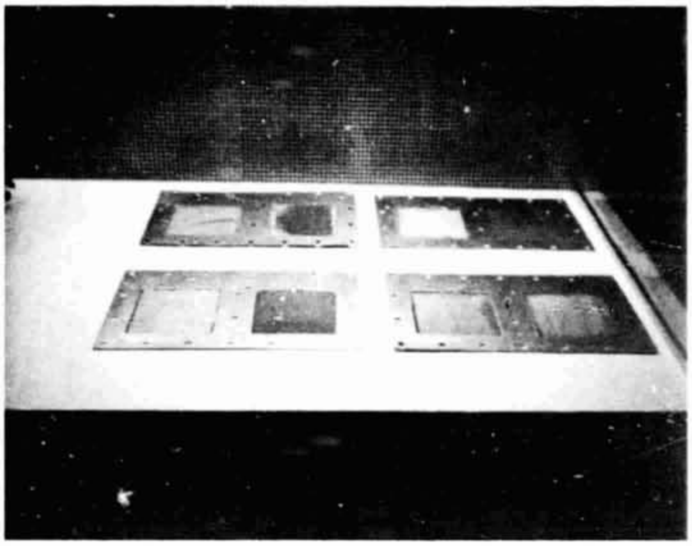

Figure 53. Screen Test Specimens

CR54

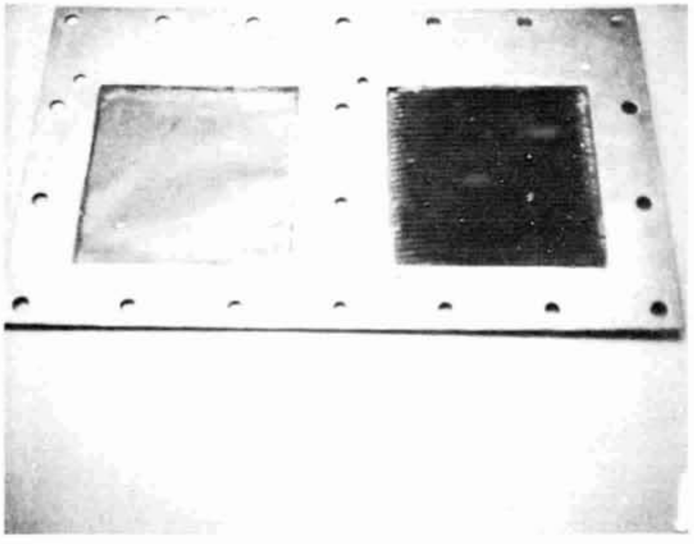

Figure 54. Detail of 325 X 2300 Screen Specimens

CR54

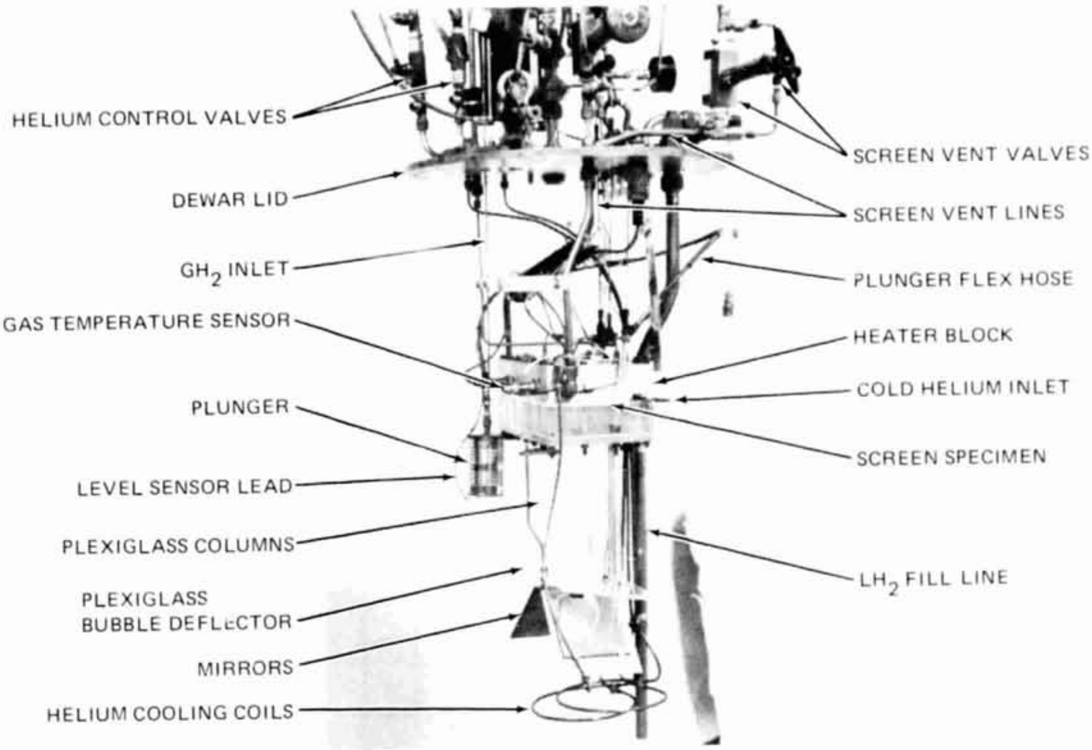

Figure 55. Screen Heat Transfer Test Apparatus

CR54

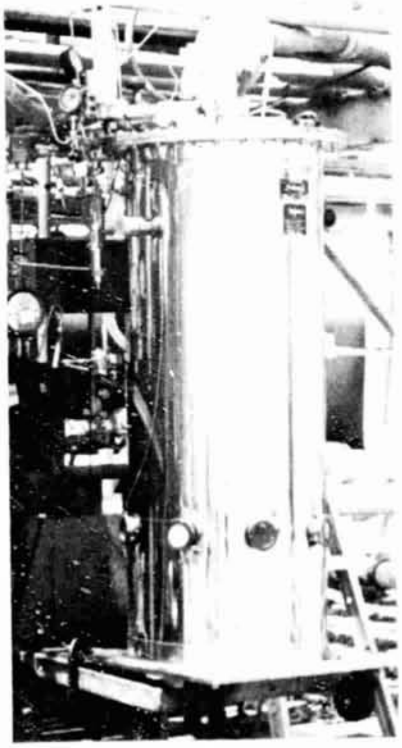

Figure 56. LH_2 Test Dewar

CR54

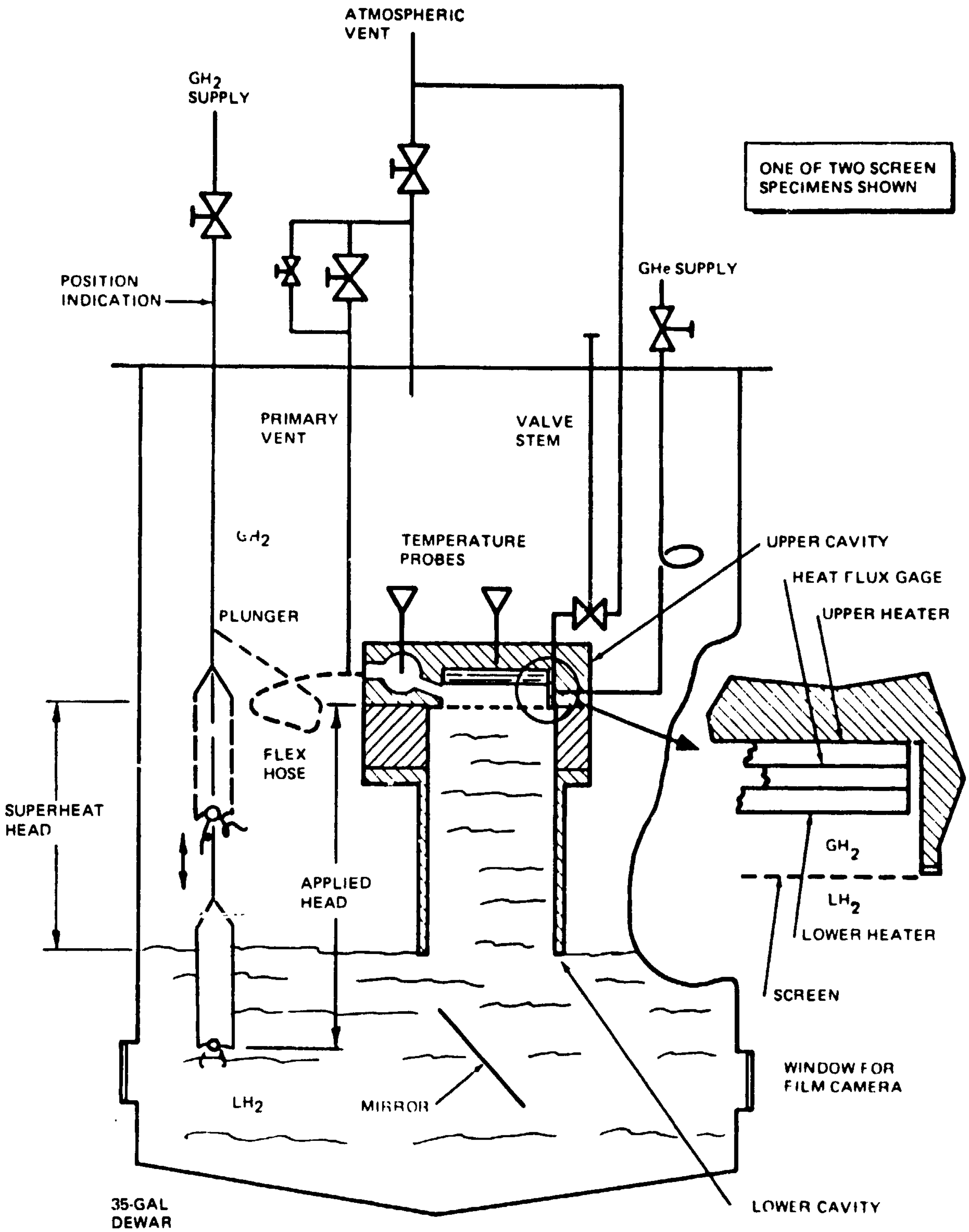

Figure 57. Test Apparatus Arrangement

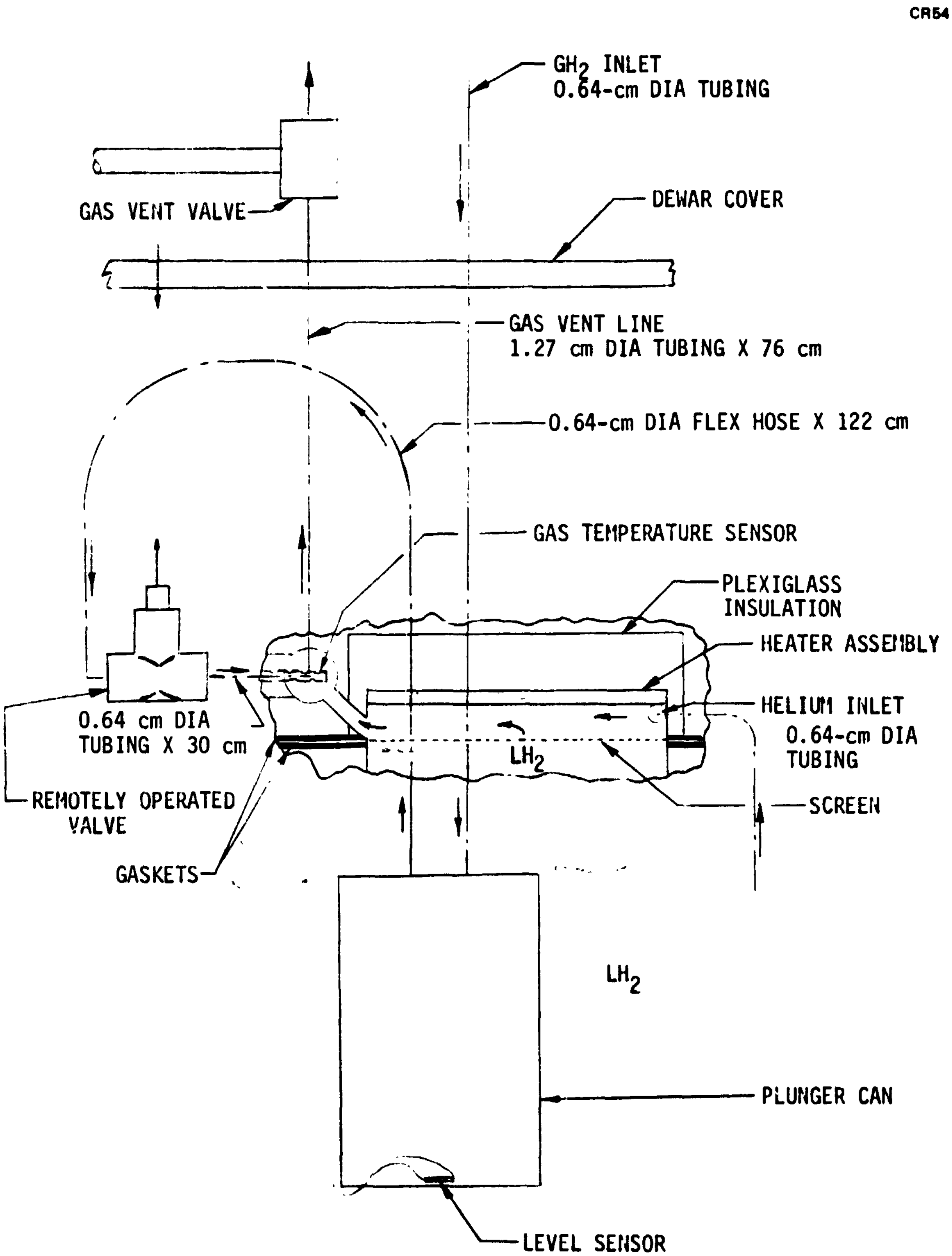

Figure 58. One-Half-Scale Detail of Apparatus Gas Passages

GHe, and LH_2 in the vicinity of the screen. The heaters and screen were surrounded by plexiglass, which acted as an insulator. The power (voltage and amperage) to the lower heater, together with other data (see Table 32) were recorded on a Mark 200 8-channel Brush Recorder. The plunger level sensor was indexed to screen position, and measured with a scale mounted on top of the dewar. The estimated accuracy of plunger position (and bubble point) measurement was ±0.25 cm (0.1 inch). The liquid level was observed visually through a window in the dewar to an estimated accuracy of ±0.64 cm (0.25 inch). As noted in Table 32, certain instrumentation failed during testing. The liquid temperature recording pen broke prior to testing — however, the dewar was kept at atmospheric pressure during testing, and therefore the liquid temperature was kept at 20.28°K (36.5°R) (within the accuracy of the sensor). The thermocouples recording the heat flux gage temperature failed during testing on both heaters. However, these data would only be used to correct the heat flux measurement for temperature variations. Since the heat flux gage was used as a nullmeter, and kept at zero, the gage temperature was not critical.

When desired, GHe was introduced through a calibrated rotameter, with gage-indicated back pressure, then through a 1.8-m (6-ft) length of 0.64-cm (0.25-inch) diameter copper tubing immersed in LH_2, where it was chilled to LH_2 temperature, and then to the opening above the screen. The length of the plexiglass columns shown in Figure 55, which allow liquid level to be lower than the screen, was modified during the test program depending on the specimen tested, as discussed in the next section. These columns also indicated when the screen failed to rewet by allowing gas to bubble out of the bottom of the columns instead of from the plunger (which was placed below the columns). The plexiglass barrier under the columns (see Figure 55) prevented bubbles (caused by boiling on the dewar bottom) from entering the columns, reaching the screen, and potentially causing screen breakdown.

Test Procedure

The dewar was slowly chilled down and filled with LH_2 (to avoid thermal stresses and cracking of the plexiglass) to a level above the heater block (see Figure 55). Because of vapor bubbles while filling, the LH_2 level usually stabilized at or slightly below the block when fill was terminated. The screen was wetted and the cavity filled with LH_2 by pressurizing the dewar and outflowing through the screen gas vent. The dewar vent was then opened, and the dewar kept at atmospheric pressure while testing. The degree of superheat was determined by converting the observed liquid head to an equivalent superheat temperature. The GH_2 flow was initiated to the plunger (set at 33 cm (13 inch) of head for the initial test with 325 x 2300 screen) until the plunger was clear with the level sensor indicating "gas." The cylindrical columns were observed to insure that no gas was bubbling from below them. With no heat flux, the plunger was slowly lowered until the level sensor indicated "liquid," signifying screen breakdown. With GH_2 flow terminated, the screen was rewetted and refilled by pressurization and outflow, as above, and

TABLE 32. – HEAT FLUX TEST INSTRUMENTATION

Channel	Parameter	Instrument	Range	Comments
1	Heater Current	DC power supply	0-10 amps	Maximum current – 4.2 amps
2	Heater Voltage	DC power supply	0-50 VDC	Maximum voltage – 40 volts
3	Gas Temperature	CEC 361449-0100 1380Ω – 0°C (32°F)	0-262.3Ω 0-78°K (0-140°R)	
4	Liquid Temperature	CEC 361449-0101 1380Ω – 0°C (32°F)	0-100Ω 0-49°K (0-89°R)	Recorder pen failed during test
5	Heater Temperature	Cu-CN thermocouple	-7 - +3 mV 0-344°K (0-620°R)	Failed prior to test
6	Heat Flux	ITI heat flux standard	-5 - +5 mV	
7	Insulation Temperature	Cu-Cn thermocouple	-7 - +3 mV 0-344°K (0-620°R)	
8	Liquid Level	0.1Ω carbon resistor	gas-liquid	

the plunger was then set at approximately three-fourths of the unheated bubble point, as shown in Table 33, and cleared with GH_2. The heaters were energized, and the heater next to the screen was brought slowly up to full power, with the heat flux gage indicating essentially zero. The heaters were kept at full power until the gas temperature reached about 45-55°K (80-100°R), at which time the plunger was slowly lowered, increasing the applied head, until breakdown occurred. The plunger was returned to the level shown in Table 33, and the screen rewetting and refilling cycle repeated. With GHe flow as a test parameter, the plunger was first cleared with GH_2 as above, and the GHe flow was then imposed. The plexiglass columns were visually checked to ensure that the screens remained wetted. The heaters were then energized and the plunger lowered as above.

Test Results and Analysis

The procedure described above necessitated considerable practice to achieve good results. A total of 58 test sequences were performed which resulted in 35 properly performed tests. In the case of the 120 x 120 screens, the bubble point capability was so low that it was very difficult to clear the plunger without also failing the screen. It was also impossible to initiate GHe flow with these screens, because the local GHe pressure above the screen was apparently sufficient to induce breakdown. A total of 14 test sequences with the 120 x 120 screen produced only five proper tests. The test results are summarized in Table 34, which shows the data taken at breakdown. The initial heat flux to the screen was usually higher than the value shown at breakdown. The values shown are quite large, however, and are certainly representative of the largest heat flux which would be anticipated to occur in a vehicle LH_2 tank. The heat flux to the screen was determined from an energy balance, where the GH_2 evaporation rate from the screem, $\dot{m}$, is found from.

$$V \cdot A = (\dot{m}\, C_{p_{H_2}} + \dot{m}_{He}\, C_{p_{He}})(T_{GAS} - T_{LH_2}) + \dot{m}\, h_{VAP} \qquad (15)$$

where

$V \cdot A$ = heater output at breakdown (volts-amperes)

$\dot{m}_{He}$ = GHe flow rate

h_{VAP} = LH_2 heat of vaporization

C_{pHe} = GHe specific heat

C_{pH_2} = GH_2 specific heat

The net heat transfer to the screen, $\dot{Q}$, is then

$$\dot{Q} = \dot{m}\, h_{VAP} \qquad (16)$$

and the heat flux is $\dot{Q}$ divided by the screen area.

TABLE 33. — SCREEN BUBBLE POINTS AND HEAD SETTINGS

Test Setup	Screen	Unheated Bubble Point cm LH_2 (in. LH_2)	Initial Head Setting With Heat Flux cm LH_2 (in. LH_2)	Plexiglass Column/Block Length Below Screen cm (in.)
1-1	325 x 2300 pleated	63.5 (25.0)	45.7 (18.0)	30.5 (12.0)
1-2	325 x 2300	57.7 (22.7)	45.7 (18.0)	30.5 (12.0)
2-1	200 x 1400	42.7 (16.8)	33.0 (13.0)	30.5 (12.0)
2-2	200 x 1400 aluminum	42.7 (16.8)	33.0 (13.0)	30.5 (12.0)
3-1	720 x 140	29.7 (11.7)	17.8 (7.0)	15.2 (6.0)
3-2	165 x 800	27.2 (10.7)	17.8 (7.0)	15.2 (6.0)
4-1	120 x 120	6.9 (2.7)	3.6-4.3 (1.4-1.7)	6.6 (2.6)
4-2	120 x 120 aluminum	7.6 (3.0)	3.6-4.3 (1.4-1.7)	6.6 (2.6)

TABLE 34. – HEAT TRANSFER TEST DATA

Test	Screen Specimen	Liquid Level Below Screen cm (in.)	Heat Flux to Screen watt/m² (Btu/hr-ft²)	m_{H_2} kg/hr (lb/hr) Evaporated	m_{He} kg/hr (lb/hr)	LH_2 Bubble Point cm (in.)	T_{GAS} °K(°R)	Comments
1	1-1	20.3(8.0)	0	0	0	63.5(25.0)	25.8(46.4)	
2	1-1	21.8(8.6)	8884(2818)	0.782(1.723)	0	57.2(22.5)	~59.4(107)	T_{GAS} off-scale
3	1-1	17.8(7.0)	6346(2013)	0.558(1.230)	0.635(1.400)	58.2(22.9)	~77.8(140)	T_{GAS} off-scale
4	1-1	21.8(8.6)	4536(1439)	0.339(0.879)	1.031(2.274)	53.3(21.0)	60.9(109.6)	
5	1-1	25.4(10.0)	3323(1054)	0.292(0.644)	1.260(2.778)	55.9(22.0)	67.3(121.1)	
6	1-2	5.1(2.0)	0	0	0	57.7(22.7)	22.0(39.6)	
7	1-2	7.6(3.0)	10261(3255)	0.901(1.987)	0	45.7(18.0)	38.7(69.7)	Possible bubble under screen
8	1-2	10.2(4.0)	6428(2039)	0.566(1.247)	0	53.3(21.0)	74.4(133.9)	
9	1-2	11.4(4.5)	5375(1705)	0.472(1.040)	0.423(0.932)	52.6(20.7)	69.5(125.1)	
10	1-2	14.2(5.6)	2049(637) 0	0.176(0.389) 0	1.546(3.408)	51.3(20.2)	69.9(125.9)	Good steady state data
11	2-1	12.7(5.0)	0	0	0	42.7(16.8)	20.3(36.5)	
12	2-1	15.2(6.0)	10041(3185)	0.738(1.628)	0	37.3(14.7)	50.7(91.3)	
13	2-1	19.1(7.5)	8427(2673)	0.619(1.365)	0	37.3(14.7)	64.6(116.2)	
14	2-1	20.3(8.0)	9136(2898)	0.672(1.482)	0.557(1.229)	40.6(16.0)	47.1(84.7)	
15	2-1	22.9(9.0)	4423(1403)	0.324(0.715)	1.263(2.785)	42.4(16.7)	63.2(113.7)	
16	2-2	11.4(4.5)	0	0	0	42.7(16.8)	23.5(42.3)	
17	2-2	12.7(5.0)	7074(2244)	0.622(1.372)	0	43.2(17.0)	64.6(116.2)	
18	2-2	14.0(5.5)	4754(1508)	0.418(0.922)	0.480(1.058)	40.6(16.0)	74.4(133.9)	
19	2-2	15.2(6.0)	5454(1730)	0.481(1.060)	0.697(1.537)	42.9(16.9)	60.4(108.7)	
20	2-2	22.9(9.0)	0	0	1.937(4.271)	33.0(13.0)	31.8(57.3)	Failed with He flow – no $\dot{Q}$
21	2-2	25.4(10.0)	5400(1713)	0.475(1.048)	1.143(2.520)	33.0(13.0)	52.2(94.0)	
22	3-1	8.9(3.5)	0	0	0	30.5(12.0)	38.1(68.5)	Not completely chilled
23	3-1	10.2(4.0)	0	0	0	29.7(11.7)	42.5(76.5)	Not completely chilled
24	3-1	12.7(5.0)	6671(2116)	0.587(1.293)	0	29.7(11.7)	69.9(125.9)	Not completely chilled
25	3-1	10.2(4.0)	6132(1945)	0.540(1.190)	0.520(1.147)	29.5(11.6)	59.9(107.9)	
26	3-1	10.2(4.0)	4698(1576)	0.438(0.966)	1.240(2.734)	30.5(12.0)	54.2(97.6)	
27	3-2	10.2(4.0)	0	0	0	27.2(10.7)	23.5(42.3)	
28	3-2	8.9(3.5)	6967(2210)	0.612(1.350)	0	27.4(10.8)	66.8(120.3)	
29	3-2	10.2(4.0)	7563(2399)	0.664(1.464)	0.480(1.058)	26.7(10.5)	49.7(89.4)	
30	3-2	12.7(5.0)	6428(2039)	0.566(1.247)	1.103(2.432)	27.2(10.7)	48.2(86.7)	
31	4-1	0.0	0	0	0	6.9(2.7)	20.3(36.5)	
32	4-1	0.0	8263(2621)	0.727(1.603)	0	6.9(2.7)	49.4(89.0)	
33	4-2	0.0	0	0	0	7.6(3.0)	20.3(36.5)	
34	4-2	0.0	12046(3821)	1.059(2.335)	0	3.6(1.4)	26.5(47.7)	Possible bubble under screen
35	4-2	0.0	8427(2673)	0.742(1.635)	0	7.0(2.75)	49.4(89.0)	

It will be noted from Table 34 that there was no noticeable effect of liquid level on bubble point. Although the potential for obtaining superheated liquid under the screen exists immediately after filling of LH_2 up to the screen, evaporation at the screen will probably quickly cool the LH_2 and achieve local saturation. The trend of bubble point with imposed heat flux is shown in Figures 59 through 62 for the four specimen pairs. Note from Figure 59 that the bubble point-heat flux trends were the same for the pleated and plain 325 x 2300 screens. There were two anomalous tests shown: test 7, which indicated failure at the preset head of 45.7 cm (18 inch) at maximum heater power, and test 34, which also failed at the preset head of 3.6 cm (1.4 inch) at maximum heater power. When these tests were repeated, tests 8 and 35, failure did not occur until substantially higher heads. It is possible that the premature failure was caused by a bubble trapped under the screen, which caused failure at maximum heater power. With GHe flow of the same order as the GH_2 evaporation rate (0.5-1 kg/hr (1-2 lb/hr)), the bubble point was essentially unaffected. However, when high GHe flow rates were imposed, two other premature failures occurred, tests 20 and 21 (Figure 60). Referring back to Figure 58, it is clear that with very high GHe flow (test 20) there was sufficient restriction in the screen vent line that the local head above the screen was 5-7.5 cm (2-3 inch) above that at the plunger, resulting in an apparent reduction in bubble point by that amount. However, this was a spurious effect due to apparatus limitations. This effect can also be seen (Figure 59) in the other high flow rate GHe test (No. 10). Test 10 was interesting from another standpoint: at approximately two-thirds of full power to the heater, the evaporation rate at the screen dropped to zero, i.e., the GHe flow was absorbing all of the heater power. When the heater power was increased to the maximum, evaporation at the screen reoccurred, but at a fairly low rate. In fact, it can be seen from Table 34, that the screen heat flux was reduced with increasing GHe flow, since heating the GHe was absorbing a great deal of the heater power. Figures 60 and 62 show that there was no essential difference between stainless and aluminum screens in response to heat flux.

Figures 59-62 indicate that with the exception of the anomalous tests discussed above the maximum bubble point degradation due to heat flux was 12.5 percent. This indicates that the fine-mesh screens customarily used for acquisition devices are excellent wicks (evaporators) and are able to absorb large heat fluxes and high temperatures without significant bubble point degradation.

CR54

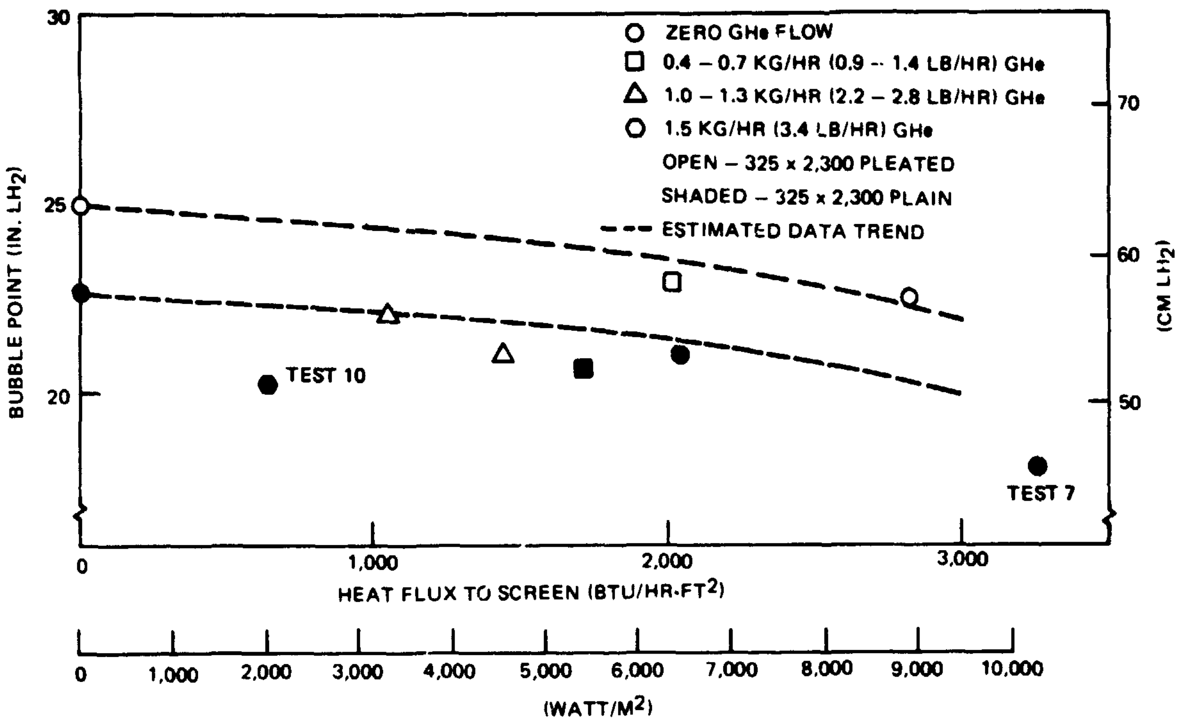

Figure 59. Screen Bubble Point Dependence on Heat Flux – Specimen 1

CR54

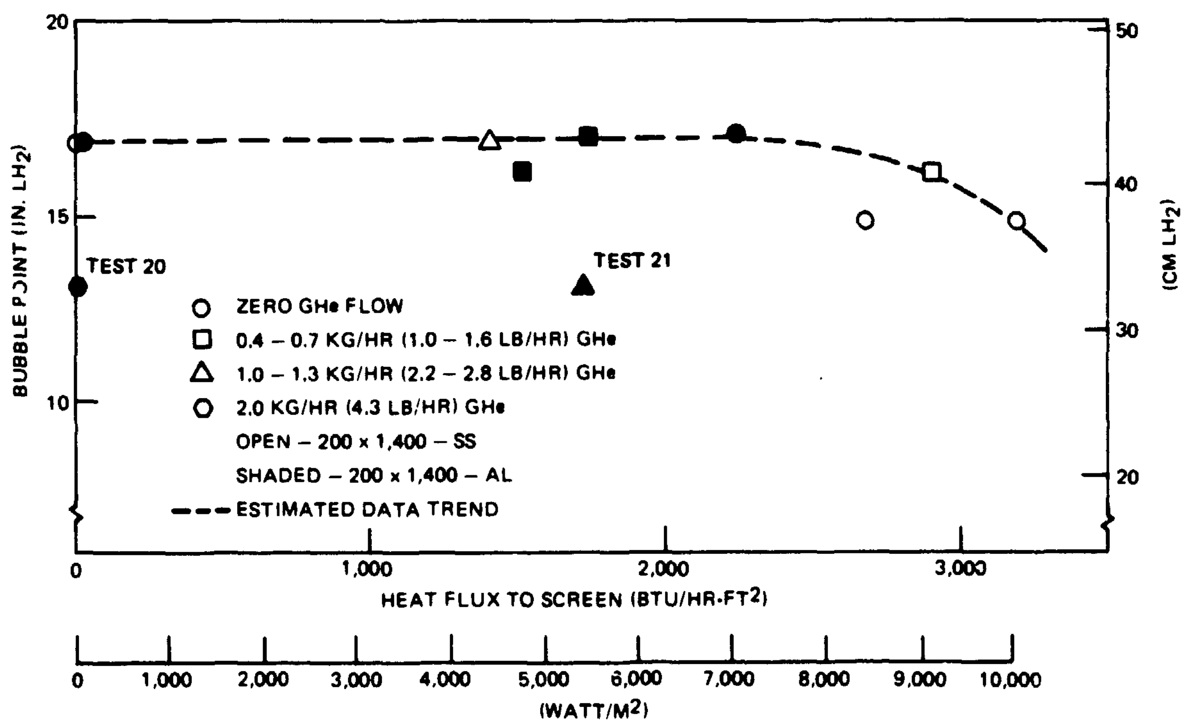

Figure 60. Screen Bubble Point Dependence on Heat Flux – Specimen 2

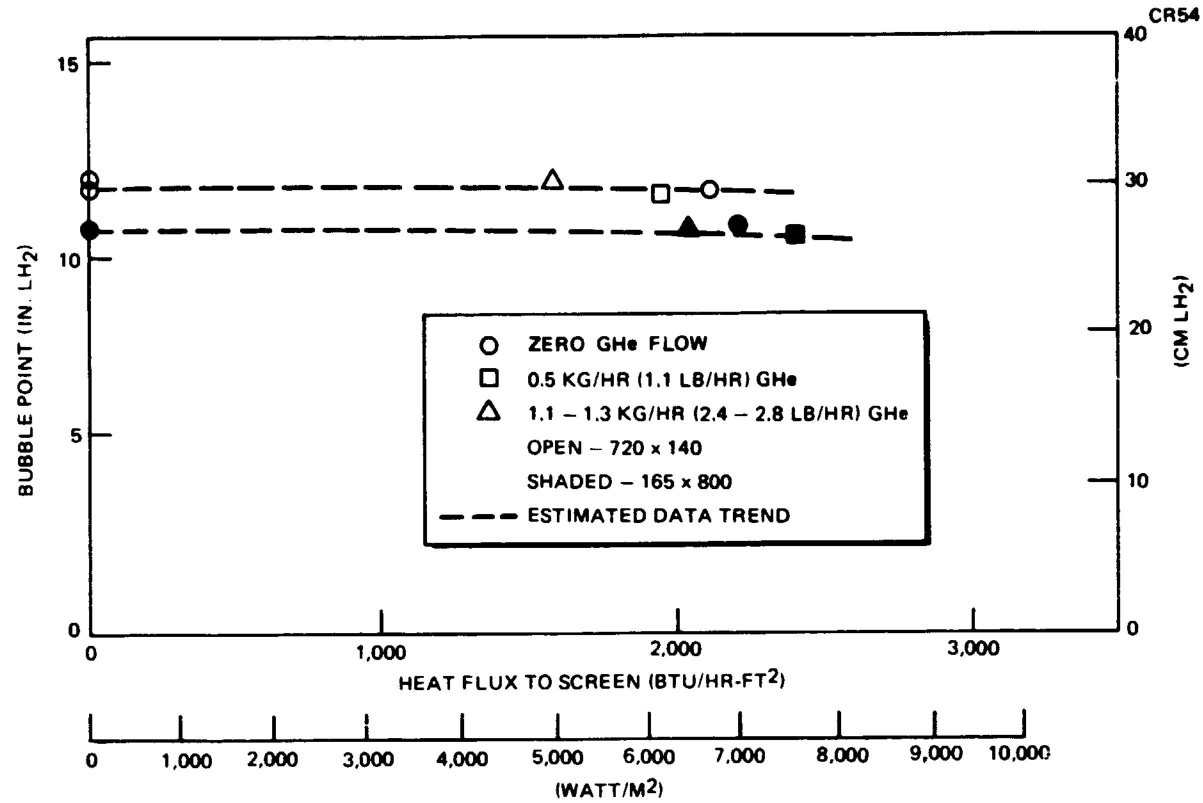

Figure 61. Screen Bubble Point Dependence on Heat Flux – Specimen 3

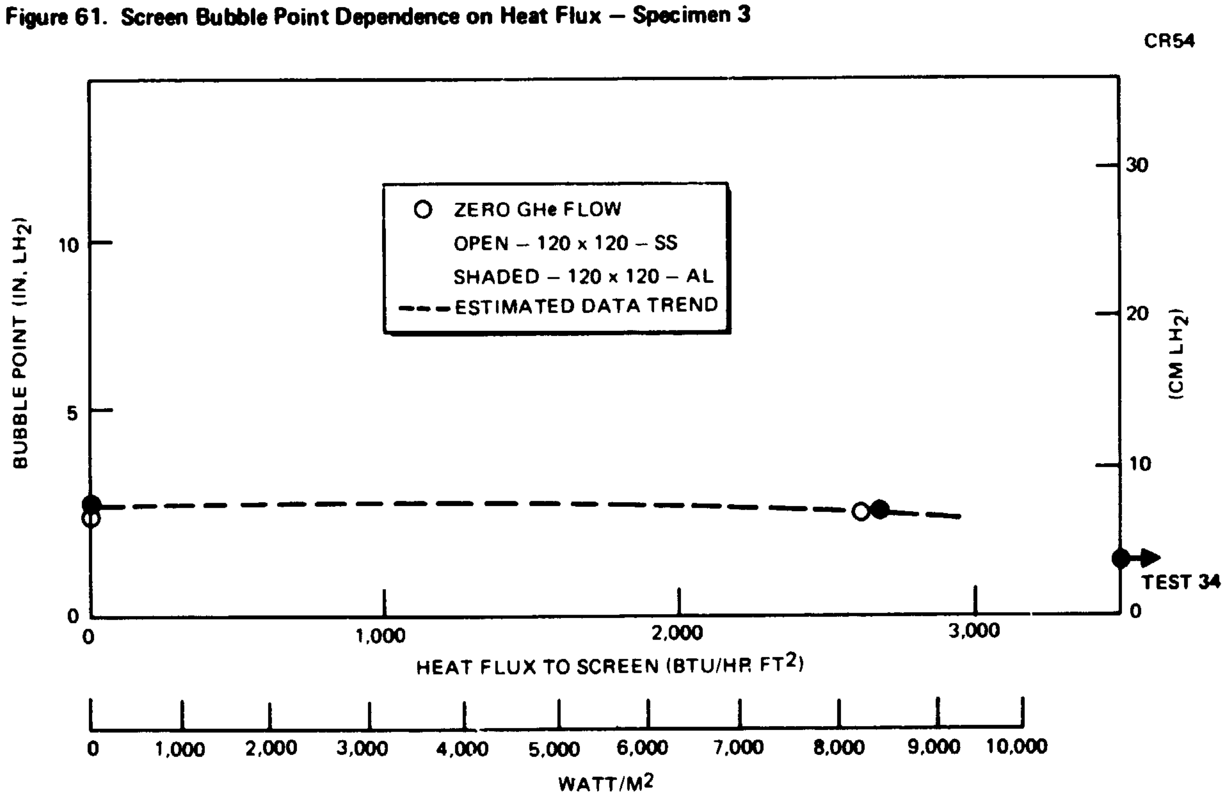

Figure 62. Screen Bubble Point Dependence on Heat Flux – Specimen 4

CONCLUSIONS

The principal conclusions drawn from the analytical studies were that with the exception of propulsive stages the TVS/WSL cryogen storage and transfer systems were highly efficient compared to other orbital storage and transfer methods:

A. Compared to a propulsively-accelerated Tug-scale module for orbital transfer of LH_2 and LO_2, a TVS/WSL saved 20% of the inert transfer-sensitive weight, and the cooled-shield TVS/partial WSL saved 29%.

B. Compared to small-scale supercritical storage and transfer systems for life-support and H_2/O_2 fuel cell reactant supply, the TVS/WSL and cooled-shield TVS/WSL were up to 40% more efficient. For the Space Shuttle Fuel Cell Reactant Supply System, use of a TVS/WSL or cooled-shield TVS/WSL would save up to 139 kg (306 lb) for the 7-day baseline mission, and up to 556 kg (1225 lb) for the extended 30-day mission, compared to the current supercritical design.

C. Compared to high pressure gas storage for the Spacelab atmosphere makeup supply, use of cooled-shield TVS/WSL would save 349 kg (770 lb) out of 442 kg (975 lb) of inert system weight for a 30-day mission.

D. Compared to a propulsively accelerated Tug-scale module with a multiple engine-restart-mission, either the TVS/WSL or cooled-shield TVS/WSL was 8% heavier.

E. Further potential current applications for the cooled-shield TVS/WSL include common self-contained cryogen storage and supply system for He, H_2, O_2, and N_2 for use in mission-peculiar Spacelab or Shuttle experiments requiring cryogens, or complete proof-of-concept experiment to verify thermodynamic/fluidynamic feasibility while providing backup use capability to existing Shuttle/Spacelab systems.

For nearly all of the systems studied, the TVS pumps were at or near the minimum feasible input power level of 0.1 watt, which may lead to problems of fabricability, reliability, and indeterminate efficiency and performance. Replacement of the TVS pump with a completely passive cooled-shield TVS could eliminate potential problems of small pumps, and result in greater system efficiency, but will require use of extremely high performance thermal control systems.

The screen LH_2 heat transfer experimental study, covering eight screens ranging from 325 x 2300 to 120 x 120, indicated (1) a maximum degradation in bubble point of 12.5% at screen heat fluxes of up to 9450 watt/m^2 (3000 Btu/hr-ft^2); (2) no observable effect of LH_2 superheat; (3) no observable effect of helium flowrates of the same order as the LH_2 evaporation rate – at high relative helium flowrates, apparatus flow restriction resulted in a decrease in observed bubble point; and (4) no observable effect of screen material on bubble point performance with heat transfer. Similar trends in bubble point degradation were observed for the pleated and plain screens.

APPENDIX A
SUB-SCALE SYSTEM DETAIL DESIGN

The objective of this effort was to design a 51-cm (20-inch) spherical tank containing a screen acquisition device suitable for testing with liquid nitrogen (LN_2) in the NASA LeRC Zero-Gravity Facility. A secondary objective was to develop the techniques necessary to fabricate, clean, and check out a representative screen acquisition device for a small-scale cryogenic tank.

Design Requirements

The basic design requirements for the tank were that it be interchangeable with an existing bare tank which was installed within a vacuum jacket and mounted on a drop test apparatus used for zero-gravity inflow/venting experiments with LN_2. Therefore the inlet and vent fluid connections and tank diameter were required to be identical to those shown in NASA Drawing CR634476. It was also required that the tank (pressure vessel) be identical to the previous tank, i.e., fabricated from 0.02 to 0.03-cm (0.008 to 0.012-inch) thick AM350 (SCT-850) stainless steel. Other design specifications for the tank apparatus are shown in Table 35. It was also required that the vent system be arranged so that the screen annulus, or the tank interior, could be selectively vented.

Screen Device Design

The screen selected was 325 x 2300 Dutch twill woven from 0.0015/0.001 304 ELC stainless steel. Of the screens currently and conveniently available, this screen had the maximum bubble point, maximum resistance to flow through the screen, and minimum resistance to annulus flow. This screen material was completely compatible with the AM 350 pressure vessel. The original conceptual design of the tank, including a partial screen liner acquisition system, is shown in Figure 63.

The partial screen liner would be configured as eight channels, with eight spaces between channels. The screen panels covering the channels would be about 2.5 cm (1 inch) wide at the inflow baffle, about 10 cm (4 inches) wide at the girth, and about 30 cm (1 foot) long. The screen panels would be welded to bracing angles which would be fastened to support angles bonded to the pressure vessel interior.

The inflow baffle would be about 12.7 cm (5 inches) in diameter with a flow splitting cone as shown. The 1/4 ratio of baffle diameter to tank diameter had been shown to give minimal residual for outflow, and good annular direction to inflow. The upper baffle would be about 30 cm (12 inches)

PRECEDING PAGE BLANK NOT FILMED

TABLE 35. – DESIGN SPECIFICATIONS

1. The experimental tankage shall conform to the envelope defined by the existing tankage as shown on the enclosed NASA Drawing CR634476. The design shall meet the following environmental requirements:

   a. Vacuum exterior, interior working pressure of 17.24 N/cm^2 (25 psia) with a safety factor of 2.

   b. Shock loading averaging 35 g's for 120 milliseconds with a peak load of 50 g's.

   c. Cooling from room temperature to liquid nitrogen temperature in 2 seconds.

2. The following Quality Assurance Controls are recommended as specification guides to potential fabricators.

   a. Material Specification:

      Stainless Steel Bar per Fed. Spec. QQ-S763d, 304L, Condition A, Cold Finished.

      Cold Rolled Stainless Steel Sheet per MIL-S-8840 (AM-350) or per AMS 5548E (AM-350).

   b. Heat Treat Stainless Steel AM-350 per MIL-H6875F (SCT-850).

   c. Fluorescent Penetrant inspect per MIL-I-6866, Type 1, Method A, Water Washable, use Tracer Tech No. P-134 or app'd equal (No cracks allowed).

   d. Cleaning Specification:

      Prior to assembly, use cleaning procedure for screens established under Contract NAS3-15846.

      Use Trichloroethane per Fed. Spec. O-T-620 before joining pressure vessel halves.

      For final cleaning, immerse twice in Freon per NASA Spec. No. 237A. Drain thoroughly and dry after final rinse.

   e. Inert Gas Tungsten arc weld per MIL-W-8611A using welding rod per MIL-R-5031B (308 S. S.), Class 1.

   f. Resistance weld per MIL-W6858C, Class B.

   g. Visually inspect braze under 10 to 30 magnification (no cracks allowed).

   h. Pressure test and leakage test per print. (Dwg. No. CR634476).

   i. Place clean plastic caps on external openings.

   j. Identify assembly by marking with Monode Electrolyte Process or other acceptable electro-chemical-etching process.

   k. Package assembly in contamination barrier per Para. 3.3.2 of MIL-M-9950 (USAF). Polyethylene bag to be free of oils and foreign materials. Seal, tag and identify with assembly part number.

CR54

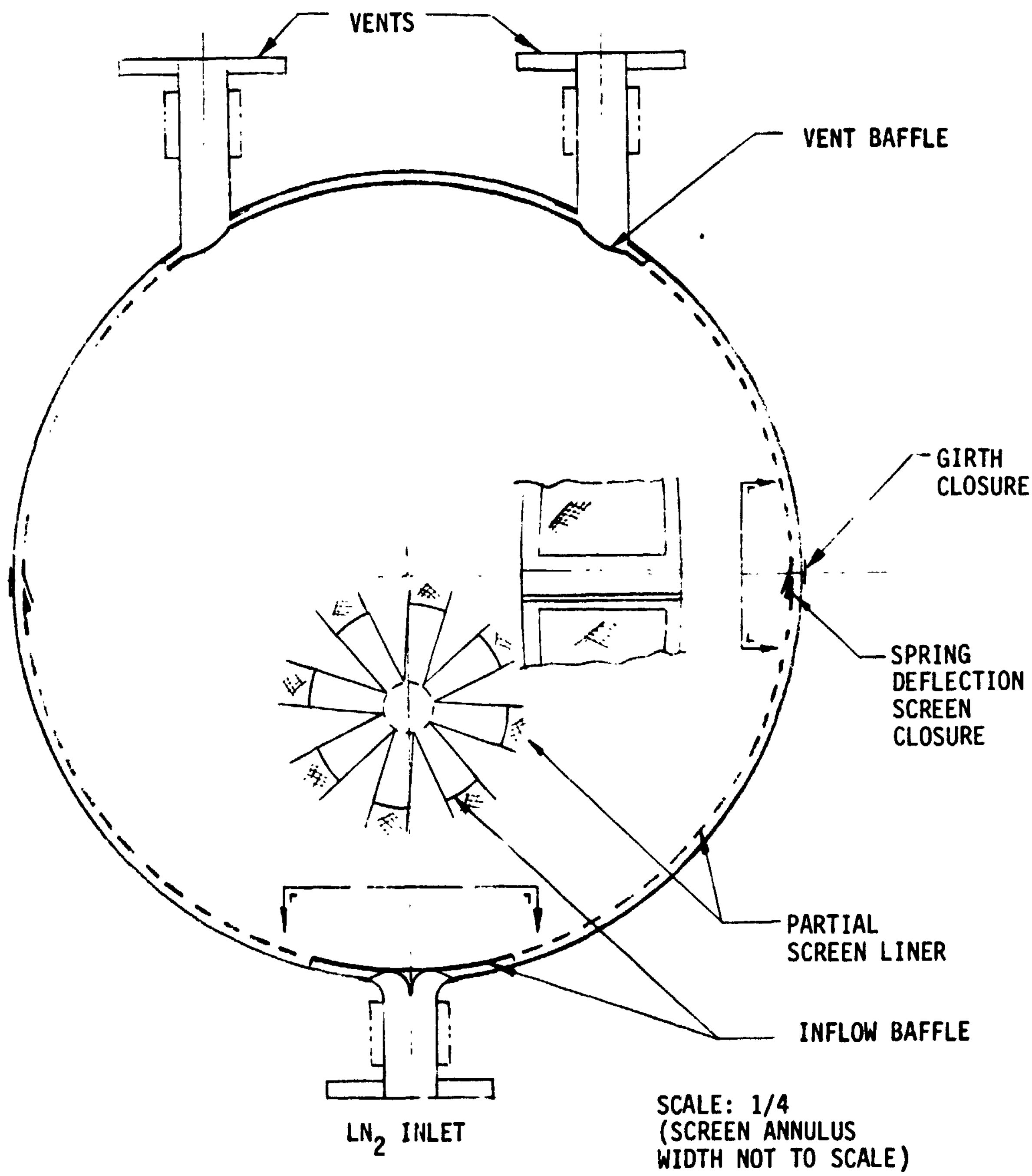

Figure 63. Conceptual Tank Configuration

diameter and would include the two vents, so that by using Teflon sleeves, either the connected channel annulus, or the internal tank, or both could be vented. The screen channel halves could be sealed at the girth by pressure deflection of thin sections, oriented in the direction as shown to minimize leakage during inflow

Implementation of this conceptual design required definition of certain critical design details, which included: (1) screen, screen support, and tankage bonding technique; (2) vent and baffle arrangement to provide selective venting options; and (3) screen sealing and closure method at the tank girth. A number of potential fabricators were contacted to definitize these fabrication techniques. With the tank parting plane and girth ring perpendicular to the inlet, it was determined that the screen support angles could not be welded to the tank, because the very thin 0.02-0.03-cm (0.008-0.012-inch) tank would warp badly and could not be reliably joined. Two methods to avoid this problem were investigated: (1) to bond all joints with cryogenic and vacuum compatible epoxy adhesive to avoid welding warpage, and (2) to reorient the tank parting plane to pass through the inlet, so that welding would not warp the tank near the parting plane joint. The first method, bonding, was extensively evaluated with screen system and tankage vendors, and was eventually rejected for two reasons: (1) no reliable technique for insuring a leak tight joint for the screen closure at the girth could be devised, and more importantly (2) the epoxy bonding technique was not representative of the methods which would probably be used for an actual flight system (which would require quality control and uniformity to withstand vibration, and other qualifying environments). The second method, girth reorientation and welding, was also extensively evaluated, and was retained as a viable candidate, although the fabrication would be quite complex and require considerable tooling, especially for seam-welding of the screen panels to the tank shells.

While discussing screen fabrication methods with a screen vendor, a complete pleated screen liner was exhibited, as shown typically in Figure 64. These liners were formed into spheres or ellipsoids, and because of the pleating, were very sturdy and self-supporting. They could be made so that they have virtually a net fit inside the pressure vessel, but without being physically attached to it. The fabrication problems and expense using the pleated liner would be greatly minimized, and the resulting system would be strong, clean and simple, and would potentially be representative of a flight-type system. The screen device could be tested for integrity and bubble point (a problem with the welded partial liner system) and could be easily integrated with the inlet and vent baffles (as shown for example in Figure 64). In order to determine if the full pleated screen would be competitive from a system standpoint, a system weight and residual analysis was performed to compare the full pleated liner with the partial wall screen liner. The results are shown in Table 36, which indicates that while the pleated liner has more residual weight, the screen/support weight is substantially less, so that for the 51-cm (20-inch) diameter experimental tank, the pleated liner system shows a net weight savings relative to the partial wall screen liner. Whether this would be true for an actual flight-type system was not known, but the pleated liner would certainly appear to be competitive. The residual shown in Table 36 was for a net fit of the liner within the tank; if a gap of 0.05 cm (0.020 in.) existed between liner and tank, an additional 0.607% residual would occur.

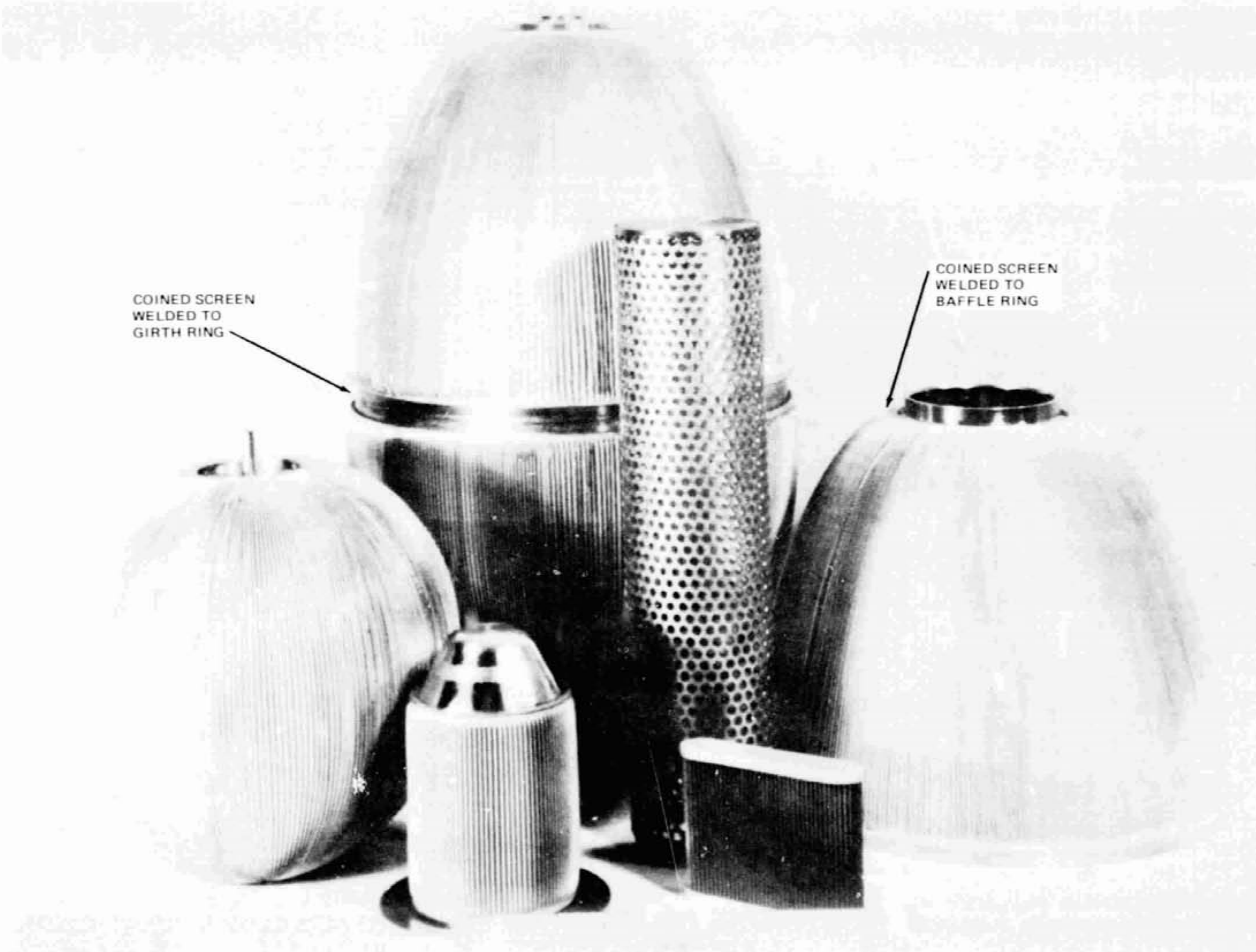

Figure 64. Pleated Screens

TABLE 36. – WEIGHT ANALYSIS OF PLEATED LINER VS PARTIAL LINER, 50.8-cm (20-IN.) DIAMETER TANK

	Pleated Liner	Partial Liner
Residual		
Screen	1.501%	1.576%
Baffle	0.361%	0.282%
Total	1.862%	1.858%
Equivalent weight of LN_2 – kg (lb)	0.90 (1.99)	0.90 (1.98)
Component weight – kg (lb)		
Tank and inlets	2.05 (4.52)	2.05 (4.52)
Baffles	0.38 (0.84)	0.29 (0.64)
Screen	0.93 (2.04)	0.19 (0.41)
Supports	0.50 (1.10)	2.86 (6.30)
Screen closure	0.64 (1.42)	0.16 (0.36)
TOTAL	4.50 (9.92)	5.55 (12.23)

Design of the experimental tankage to include a complete pleated liner was selected and recommended to NASA who approved this design concept. The selected pleat dimensions were 0.318 cm (0.125 inch) deep by 500 total pleats (about 12 pleats/cm at the 12.7-cm (5-inch) baffle). The pleats were oriented in the direction of the shute wires. The ends of the formed pleated hemispheres were required to be coined, so that they could be welded to rings, at the girth and baffle locations, which would subsequently be welded together to form the complete sphere (see, for example, Figure 64). The bubble point requirements for the complete welded screen assembly were set at 35.6 cm (14 inches) of water using ACS reagent grade isopropyl alcohol, corrected to standard conditions.

Sub-Scale System Design

A number of other design areas were investigated and resolved while defining the tank design, as described below.

It was found that the SCT-850 heat treat of the AM350 stainless steel material (originally required by NASA LeRC for purposes of commonality with the previous tank) was subject to severe stress corrosion, and in fact this heat treatment was prohibited by NASA MSFC. Other heat treat methods, annealing and double-aging, were investigated. The strength characteristics of AM-350 for the three heat-treat conditions are shown in Table 37. The strength and safety factor at 17.24 N/cm^2 (25 psia) was adequate for all three methods. Therefore it was decided to double-age the material if a welded tank joint was used (see below). If the optional braze joint was used, double-aging could not be used (it would melt the braze material), and just the annealed strength was allowed.

The tank inlet and vent outlets used bellows to allow adjustment when installing the tank inside the vacuum jacket, and the bellows had to be sufficiently stiff to resist the deceleration loads on the tank following the zero-gravity drop test. Since the tank with the screen liner would weight 4.5 kg (9.9 lb) compared to 2.0 kg (4.4 lb) for the original base tank, the bellows spring rate was increased by the same margin by increasing the bellows wall thickness from 0.0127 cm (0.005 inch) to 0.0178 cm (0.007 inch),

The vent outlets were designed to use Teflon sleeves to allow selective venting of the annulus volume, the interior tank volume, or both. The pressure vessel was designed to allow the use of a burn-down welded joint or an alternate overlapping braze joint. These details are shown in the final delivered drawing (see Figure 65). The notes in Figure 65 indicate the various process information needed to satisfy the design specifications of Table 35.

TABLE 37. – AM 350 STRENGTH PROPERTIES

	UTS N/cm^2 (psi)	Yield N/cm^2 (psi)	Safety Factor 17.24 N/cm^2 (25 psid)
Hard			
SCT-850	127,560 (185,000)	103,400 (150,000)	8.32
Annealed			
811°K (1000°F)	81,360 (118,000)	66,200 (96,000)	5.31
Double-Aged	113,800 (165,000)	93,000 (135,000)	7.42

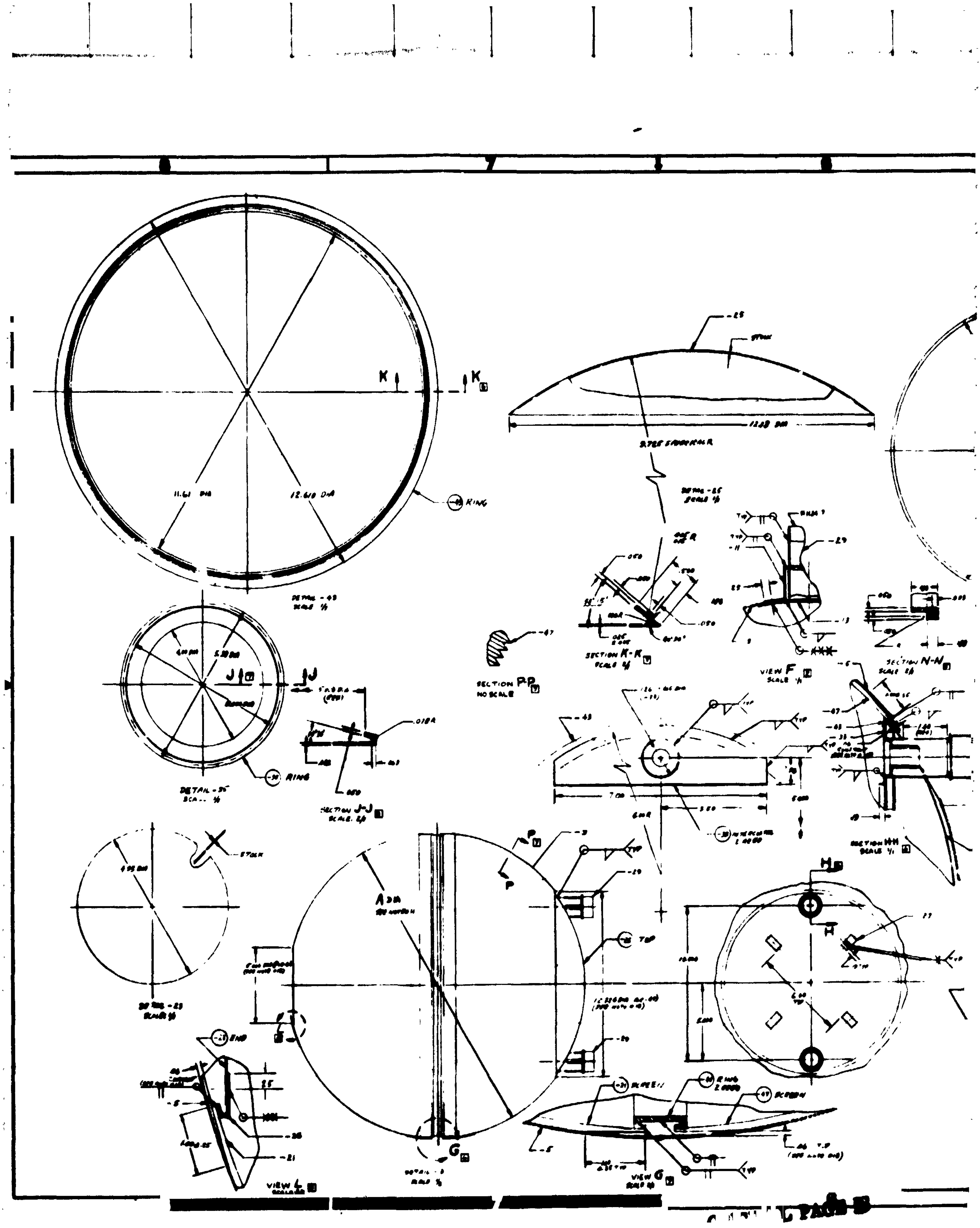

DETAIL -43
11.61 DIA
12.610 DIA
RING
DETAIL -25
12.28 DIA
SECTION K-K
SECTION P-P
NO SCALE
VIEW F
SECTION N-N
SECTION J-J
DETAIL -35
RING
SECTION H-H
STOCK
TYP
SCREEN
VIEW L
VIEW G

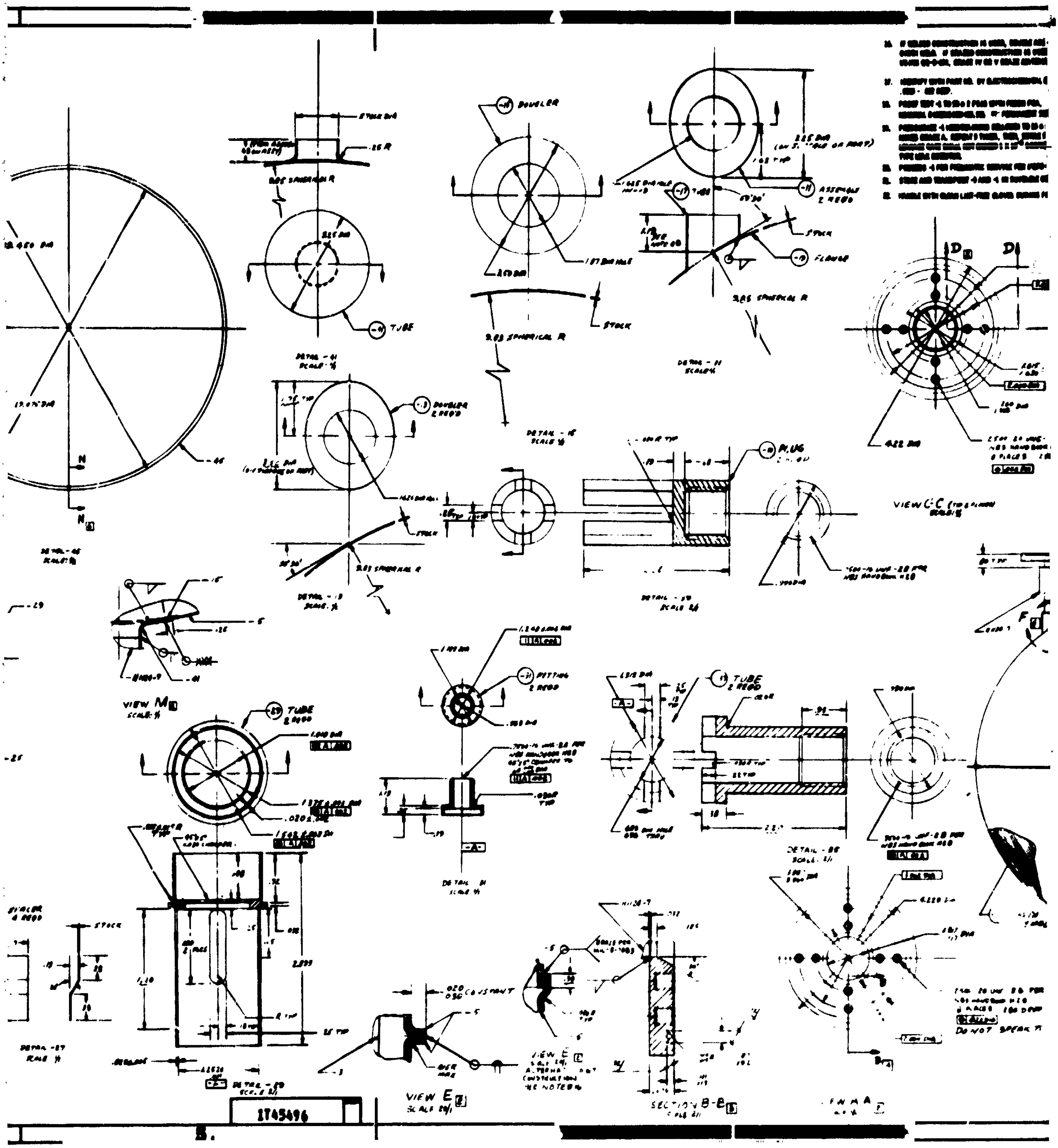

FOLDOUT FRAME 2

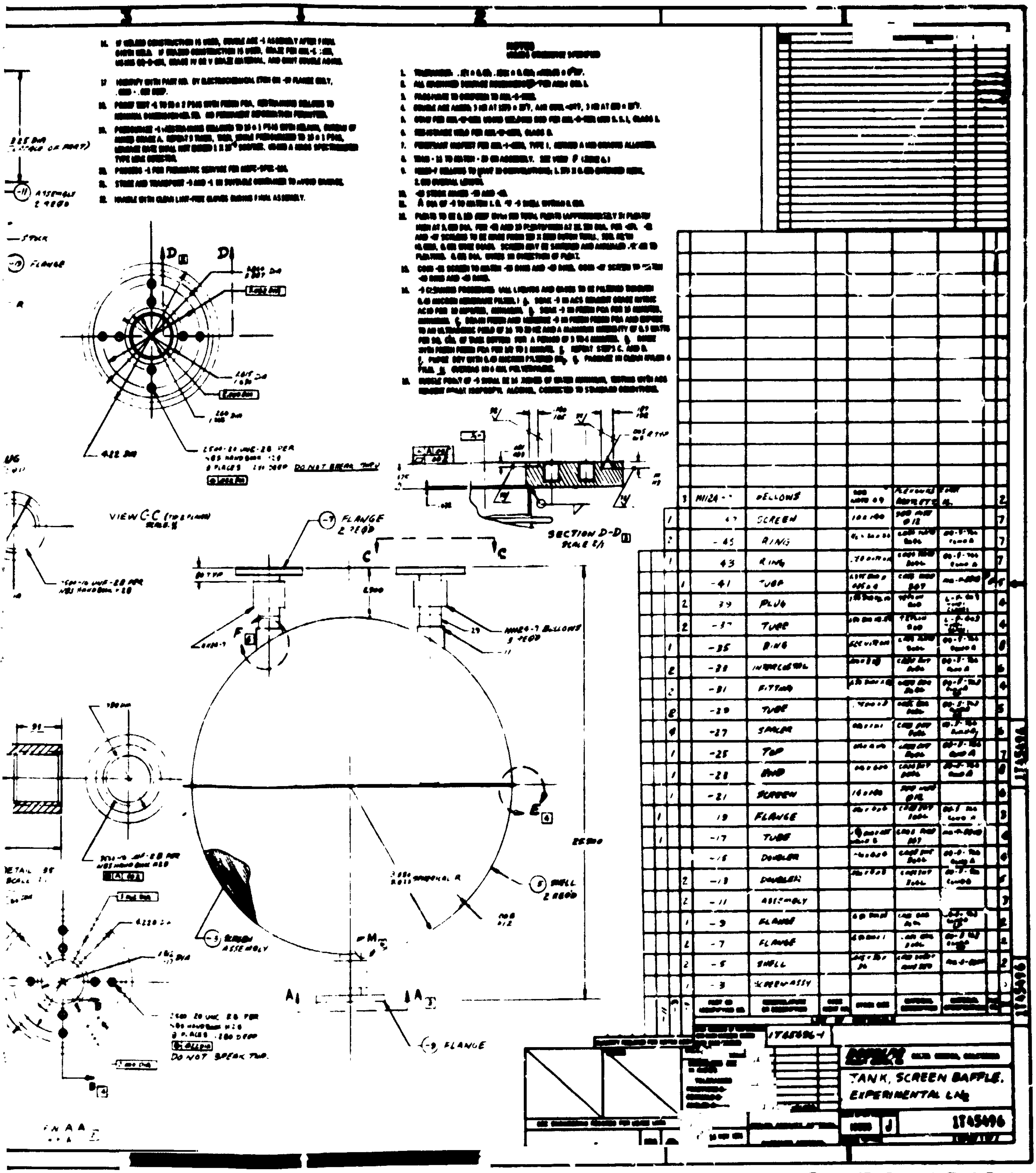

Figure 65. Subscale Tank Design

FOLDOUT FRAME 5

APPENDIX B
ANNULUS PRESSURE AND FLOW DISTRIBUTION ANALYSIS

In order to define pressurization requirements, TVS flow direction, and pump head rise requirements, a complete system pressure and temperature analysis was performed. Unlike previous analyses of the TVS/WSL flow (ref. 6) which assumed that all TVS flow was confined to the annulus, this analysis accounted for leakage of the TVS flow through the screen. The flow model is shown in Figure 66. The pump provides a design flowrate, Q, with a static pressure rise which drops due to standpipe friction to P1 which, with the standpipe dynamic head, PD1, gives a total pressure of P1 + PD1. The frictional pressure loss along the baffle, P2, plus the dynamic pressure change due to deceleration of the fluid along the baffle defines the static pressure at the baffle outlet:

$$P3 = P1 + PD1 - P2 - PD3 \tag{B-1}$$

The internal static pressure, P0, was assumed constant, ignoring the very small head variation due to the 10^{-5} g field. The static pressure difference between P3 and P0 will cause flow, Q1, through the screen area defined by the incremental angle, T1. The correlation from Reference 6, using this nomenclature is:

$$P3 - P0 = AV + BV^2 \tag{B-2}$$

where V is the approach velocity to the screen, and A and B are experimentally determined constants.

$$V = \frac{\sqrt{A^2 + 4B\,(P3 - P0)} - A}{2B} \tag{B-3}$$

and the flowrate through the screen is:

$$Q1 = V \cdot 2 \cdot \pi\,(D/2 - S)^2\,(\sin T2 - \sin(T2 - T1)) \tag{B-4}$$

where D is the tank diameter. The flow entering the next incremental annular segment is:

$$Q2 = Q - Q1 \tag{B-5}$$

The frictional static pressure loss along the screened annulus, P8, is given by the correlation from ref. 6. The pressure drop is thus:

$$P8 = \frac{6\,\mu\,Q2}{\rho\,g_c\,\pi\,S^3}\,\ell n\left[\tan\frac{(T2 + \pi/2)}{2}\bigg/\tan\frac{(T2 - T1 + \pi/2)}{2}\right]$$
$$+ \frac{1}{16\left(\log\dfrac{7.4}{e/S}\right)^2 g_c S}\left(\frac{Q2}{2\pi S}\right)^2\frac{2}{D}\,(\tan T2 - \tan(T2 - T1)) \tag{B-6}$$

PRECEDING PAGE BLANK NOT FILMED

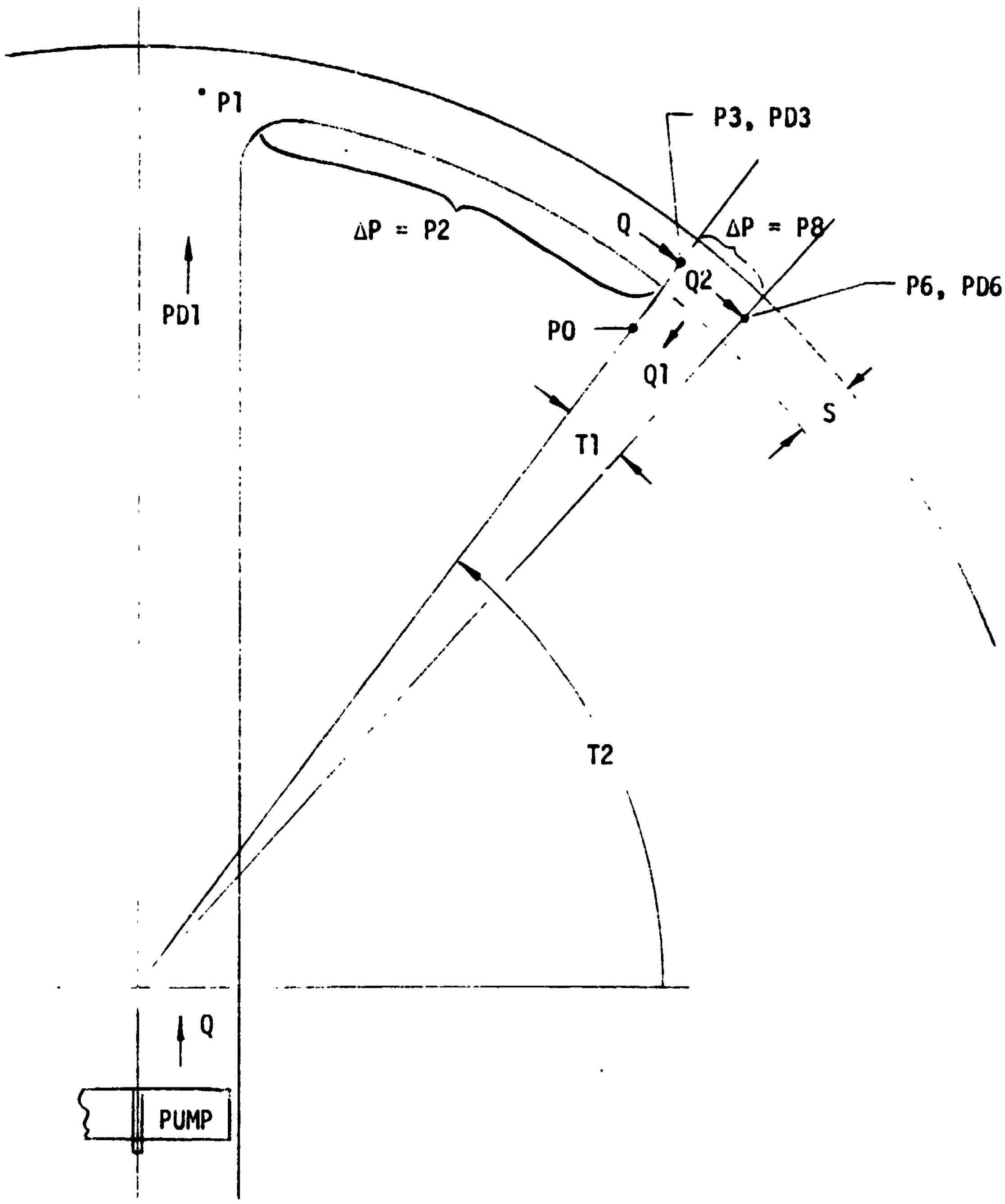

Figure 66. Annulus Leakage Flow and Pressure Distribution Model

The dynamic pressure, PD6, after the incremental angle T1 is related to the dynamic pressure. PD3, by:

$$PD6 = PD3 \left[\frac{Q2}{Q} \frac{\cos T2}{\cos (T2 - T1)} \right]^2 \qquad \text{(B-7)}$$

The static pressure after the incremental angle T1 is thus:

$$P6 = P3 + PD3 - P8 - PD6 \qquad \text{(B-8)}$$

The pressure and flow conditions for the next incremental angle are thus defined. All of the parameters of the analysis are known except for the internal pressure, P0. The equations above were programmed on the MDAC Direct Access Computing System, and were arranged to solve for the flowrate and pressures for each incremental angle. With an incremental angle of 1°, the internal pressure, P0, was iterated until the flowrate leaving the screen annulus at the bottom baffle was identical to the flowrate entering the annulus at the top baffle (the design flowrate); at this point the flow and pressure distribution at 1° increments along the annulus were output.

APPENDIX C

UNVENTED LO_2 TANK STANDPIPE OPTIMIZATION ANALYSIS

In a vented tank, the standpipe size is optimized by minimizing the sum of the standpipe weight, standpipe residual weight, and boiloff weight due to pump power input, as described previously in ref. 6. However, in the O_2 tank boiloff does not occur, since the H_2 vent gas is used to cool the O_2 tank and keep it vent-free. Instead, reducing the standpipe size and residual increases the O_2 pump power and O_2 tank heat load, which for a given H_2 vent rate, reduces the allowable heat flow through the O_2 MLI, which in turn increases the required O_2 MLI thickness and weight. Clearly a new optimum O_2 standpipe size can be found which minimizes the sum of standpipe weight, standpipe residual weight, and MLI weight. The O_2 pump power and O_2 tank heat load due to pressure loss around the annulus was not directly dependent on the standpipe diameter, did not enter this optimization, and will be accounted for later in the analysis. Similarly the pump/motor weight was a very small value, so that it too was ignored in the optimization, and will be accounted for later.

The weight of the standpipe residual, in terms of the standpipe diameter, D_s, and length, L, is:

$$W_1 = \frac{\pi D_s^2 L}{4} \rho \tag{C-1}$$

The weight of the standpipe depends on the thickness of the standpipe and the material. Since there is essentially no pressure load on the standpipe the thickness criterion used was that specified by NASA MSFC as minimum handling gage for ducting in the Space Shuttle. The thickness in meters (inches) for aluminum is

$$\begin{aligned} t_{MIN} &= 0.00076 + 0.036\, D_s \\ (t_{MIN} &= 0.030 + 0.036\, D_s) \end{aligned} \tag{C-2}$$

Multiplying the thickness by the density of aluminum gives, for standpipe weight

$$W_2 = \pi D_s L (A_1 + B_1 D_s) \tag{C-3}$$

where

$$A_1 = 2.1 \text{ and } B_1 = 99.5$$

PRECEDING PAGE BLANK NOT FILMED

It has been shown (ref. 6) that essentially all of the input power to the pump/motor is dissipated to the LH_2. The input power is:

$$P_i = \frac{\dot{Q} \rho H 60}{\eta J} \tag{C-4}$$

where J is the energy conversion, and η is the overall efficiency. The fluid power is $\dot{Q} \rho H$, where $\dot{Q}$ is the volumetric flowrate and H is the pressure drop down the standpipe. This head loss is:

$$H = f \frac{L}{D_s} \frac{V^2}{2 g_c} \tag{C-5}$$

In terms of the volume flowrate, $\dot{Q} = VA$, or

$$V = \frac{\dot{Q}}{A} = \frac{\dot{Q} \cdot 4 \cdot 60}{\pi D_s^2} \tag{C-6}$$

The friction factor, f, is a function of Reynolds number, Re. For our flow conditions, the flow is turbulent and the standpipe hydraulically smooth so that the correlation of Blasius (ref. 6) is suitable, or:

$$f = \frac{0.316}{Re^{0.25}} \tag{C-7}$$

or, since

$$Re = \frac{4 \rho \dot{Q}}{\pi \mu D_s}, \quad f = \frac{0.316 \, D_s^{0.25}}{(4 \rho \dot{Q}/\pi\mu)^{0.25}} \tag{C-8}$$

It has been shown that the Blasius correlation is accurate to within 5 percent for Re from 3,000 to 300,000.

Combining Equations (C-5), (C-6), and (C-8) gives:

$$H = \frac{0.316 \, L \, (\dot{Q} \cdot 4/\pi)^2}{(4 \rho \dot{Q}/\pi\mu)^{0.25} \, 2 g_c \, D_s^{4.75}} \tag{C-9}$$

Equation (C-9) can be simplified in terms of the important variable:

$$H = \frac{H'}{D_s^{4.75}} \quad \text{where } H' = \frac{0.316 \, L \, (\dot{Q} \cdot 4/\pi)^2}{(4 \rho \dot{Q}/\pi\mu)^{0.25} \, 2 g_c} \tag{C-10}$$

The allowable heat capacity of the H_2 vent fluid is the weight flowrate of the H_2, $\dot{W}_{H_2}$, times the heat capacity h_g, and the allowable heat leak, $\dot{Q}$ through the MLI is:

$$\dot{Q} = \dot{W}_{H_2} h_g - P_i - P_o \qquad \text{(C-11)}$$

where P_o is the external heat leak through all of the heat shorts to the O_2 tank. The MLI thickness, ℓ, is:

$$\ell = \frac{KA\,(12)\,\Delta T}{\dot{Q}} \qquad \text{(C-12)}$$

and the MLI weight is (ref. 14):

$$W_3 = 0.145\ \ell\ A \qquad \text{(C-13)}$$

Combining equations (C-1), (C-3), (C-4), (C-10), (C-11), (C-12), and (C-13) gives the total weight in terms of D_s

$$W_T = \pi L A_1 \cdot 144\, D_s + [\tfrac{\pi}{4} L \rho + \pi L B_1 \cdot 144]\, D_s^{\,2}$$

$$+ \frac{0.145\ KA^2\,(12)\,\Delta T}{\dot{W}_{H_2} h_g - P_o - \dfrac{\dot{Q}\,\rho\,H' \cdot 60}{\eta\, D_s^{\,4.75}\ 778}} \qquad \text{(C-14)}$$

Differentiating with respect to D_s and equating to zero gives:

$$0 = A_2 + B_2 D_s + \frac{4.75\, E_2\, D_s^{\,3.75}}{D_2 D_s^{\,4.75} - C_2} - \frac{4/75\, D_2\, E_2\, D_s^{\,8.5}}{(D_2 D_s^{\,4.75} - C_2)^2} \qquad \text{(C-15)}$$

where

$$A_2 = \pi L A_1 \cdot 144$$

$$B_2 = 2\,[\pi L\,(\rho/4 + B_1 \cdot 144)]$$

$$C_2 = \frac{\dot{Q}\,\rho\,H' \cdot 60}{\eta\ 778}$$

$$D_2 = \dot{W}_{H_2} h_g - P_o$$

$$E_2 = 0.145\ KA^2\,(12)\,\Delta T$$

Equation (C-15) can be solved for the optimum D_s in terms of the other known parameters as a function of η.

APPENDIX D
PLEATED SCREEN ANNULUS RESIDUAL AND PRESSURE DISTRIBUTION ANALYSIS

An analysis was performed to determine the residual and flow-loss characteristics of the pleated screen liner configured as shown in Figure 67. The recommended practice for pleating of the screen is to provide a sufficient number of pleats so that the included pleat angle is not greater than 60° at the maximum girth of the tank (liner) (see Figure 67). This equilateral triangle configuration provides exceptional rigidity and stiffness to the liner. This criterion defines the minimum number of pleats required, N, as a function of pleat height, S_1, and tank (liner) diameter, D, as follows:

$$N = \frac{\pi D}{S_1} \tag{D-1}$$

At the baffle ends of the liner, the same number of pleats are squeezed closer together by the baffle diameter, giving a more acute and stiffer triangle (see Figure 67). The annulus residual associated with the pleated liner is that trapped between the liner and the tank, since, during outflow, the gas/liquid interface is maintained by the screen pores until screen breakdown at propellant depletion. The area under each triangle is:

$$\frac{\pi D'}{2N}\left(\sqrt{S_1^{\,2} - \left(\frac{\pi D'}{2N}\right)^2}\right) \tag{D-2}$$

or, for $D' = 2R \sin\theta$ and for N triangles, the total area between the pleated screen and the tank wall is:

$$\begin{aligned} A &= \pi R \sin\theta \sqrt{S_1^{\,2} - \left(\frac{\pi R \sin\theta}{N}\right)^2} \\ &= \pi R S_1 \sin\theta \sqrt{1 - \left(\frac{\pi R}{S_1 N} \sin\theta\right)^2} \end{aligned} \tag{D-3}$$

Integrating the area from the top baffle to the bottom baffle gives the trapped volume:

$$\overline{V}_1 = \int_{\theta_1}^{\theta_2} AR\, d\theta = \int_{\theta_1}^{\theta_2} \pi R^2 S_1 \sin\theta \sqrt{1 - k^2 \sin^2\theta}\; d\theta \tag{D-4}$$

where $k = \pi R / S_1 N$

PRECEDING PAGE BLANK NOT FILMED

CR54

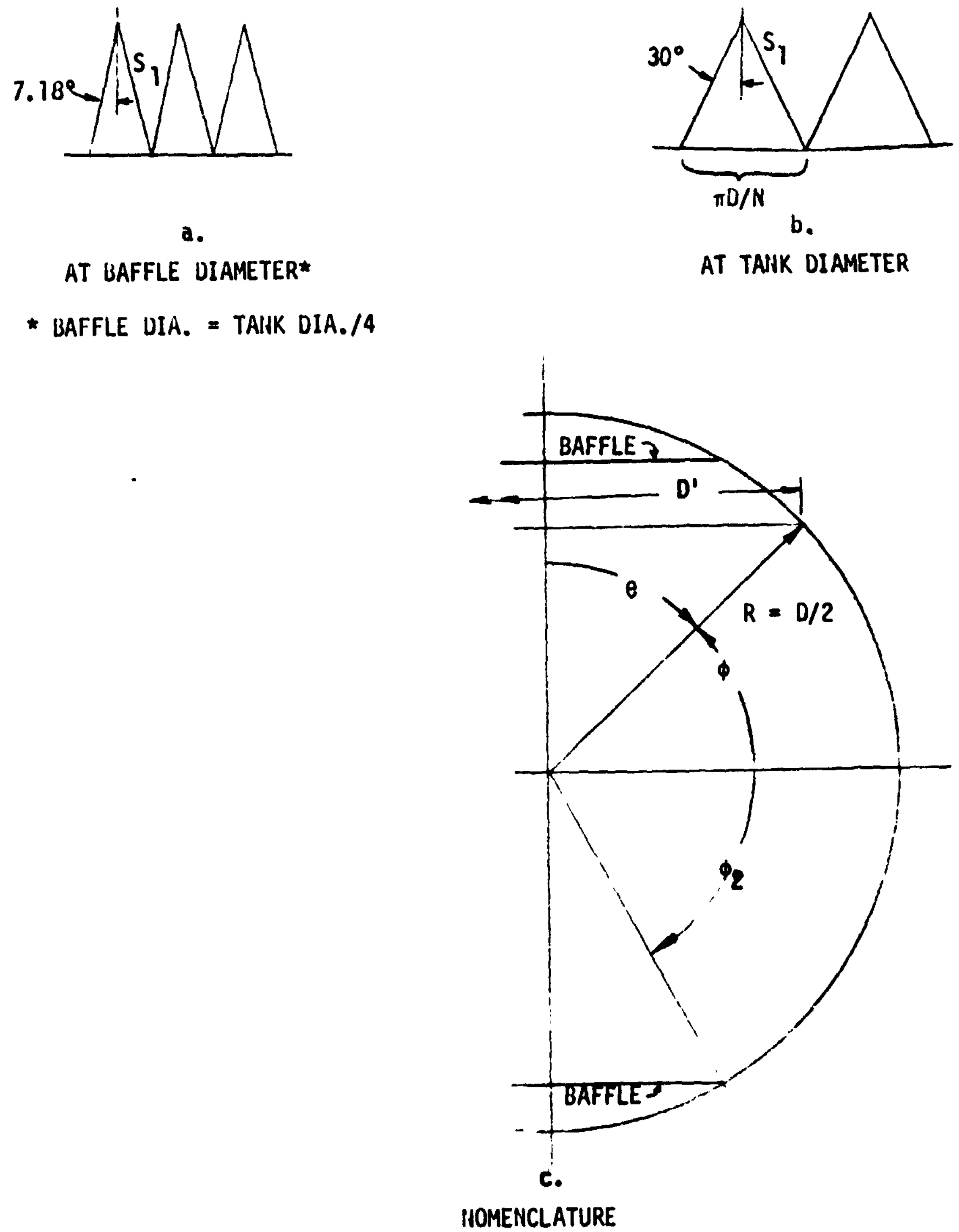

Figure 67. Pleated Screen Configuration

This yields:

$$\bar{V}_1 = \pi R^2 S_1 \left[-\frac{1}{2} \cos\theta \sqrt{1 - k^2 \sin^2\theta} \right.$$

$$\left. - \frac{1 - k^2}{2k} \ell n \left(k \cos\theta + \sqrt{1 - k^2 \sin^2\theta} \right) \right]_{\theta_1}^{\theta_2} \tag{D-5}$$

If the liner has a cylindrical section (where $L \equiv L_{liner}/D$), then for $L > 1$, the residual volume in this section is

$$\bar{V}_2 = (L - 1) D \pi R S_1 \sqrt{1 - k^2} \tag{D-6}$$

These residuals, plus that trapped by the baffles (assuming a baffle gap of S):

$$\bar{V}_3 = 2 \pi R^2 S \left[(1 + \cos\theta_2) + (1 - \cos\theta_1) \right] \tag{D-7}$$

plus the puddle and standpipe residuals, gives the total residual.

The pressure (head) loss for flow through the pleated screen liner is determined from the same correlation as for the plain screen liner:

$$H = A_1 V + B_1 V^2 \tag{D-8}$$

where V is the screen approach velocity $V = \dot{Q}/A_2$ with A_2 the screen flow area, and $\dot{Q}$ the volume flowrate. For relatively low flowrates through fine Dutch Twill pleated screens, the area A_2 is the total area of screen exposed to the flow (ref. 34) or:

$$A_2 = (T - \theta_1)(D/2 - S_1/2) N \cdot S_1 \cdot 2 \tag{D-9}$$

where T is the angle to the liquid interface.

The head loss for the flow along the annulus between the pleated liner and the tank wall was determined in the same way as for the plain screen liner, and a modified Moody correlation was assumed. From Eckert and Irvine (ref. 35) the laminar friction factor, f, is related to the Reynolds number Re, by:

$$f = \frac{C}{Re} \tag{D-10}$$

and for isosceles triangles with apex angles ranging from 14° to 60°, the average value of C is 53 (as compared to C = 96 for a thin annulus). In the turbulent regime, the shape of the flow passage does not affect f except as it affects the hydraulic diameter, D_h, and:

$$f = \frac{1}{4\left(\log \frac{3.7}{e/D_h}\right)^2} \tag{D-11}$$

where e is the roughness dimension of the screen. As was done for the plain screen liner, the laminar and turbulent friction factors were added to give:

$$f = \frac{53}{Re} + \frac{1}{4\left(\log \frac{3.7}{e/D_h}\right)^2} \tag{D-12}$$

Since

$$f = H_f \Big/ \frac{L}{D_h} \frac{V^2}{2g_c} \quad \text{and} \quad Re = \rho \frac{VD_h}{\mu} \tag{D-13}$$

then

$$H_f = 53 \frac{\mu}{\rho} \frac{L}{D_h^2} \frac{V}{2g_c} + \frac{LV^2}{8\left(\log \frac{3.7}{e/D_h}\right)^2 g_c D_h} \tag{D-14}$$

The hydraulic diameter of the triangular passages varies along the flow path:

$$D_h = \frac{4 \text{ Area}}{\text{Circumference}} = \frac{4S_1 \cos\alpha \, \pi D \cos}{2N \quad 2S_1 + \left(\frac{\pi D \cos\phi}{N}\right)}$$

$$= \frac{2S_1 \, \pi D \cos\phi \, \cos\alpha}{2S_1 \, N + \pi D \cos\phi} \tag{D-15}$$

For our system (see Figure 67), $\cos\alpha$ varies only from 0.9922 ($\alpha = 7.18°$) to 0.866 ($\alpha = 30°$) and therefore an average value of 0.93 was used for $\cos\alpha$.

The flow velocity along the triangle is:

$$V = \frac{2\dot{Q}}{DS_1 \, \pi \cos\phi \; 0.93} \tag{D-16}$$

The length along the flow path is $L = D/2\, d\phi$ and the log term in equation (D-14) is a weak function of D_h and, for ease of later integration, a mean value of this term was used:

$$\left[\log\left(\frac{3.7}{e/D_h}\right)\right]^2 = 6.6046 \tag{D-17}$$

Substituting for L and equations (D-15), (D-16), and (D-17) in Equation (D-14) gives:

$$H_f = \int_{-\phi_1}^{\phi_2} \frac{53\,\mu}{4 g_c \rho}\, D \left[\frac{N}{\pi D\ 0.93 \cos\phi} + \frac{1}{2S_1\ 0.93}\right]^2 \frac{2\dot{Q}}{D S_1 \pi\ 0.93 \cos\phi}\, d\phi$$

$$+ \frac{D}{16\,(6.6046) g_c}\left[\frac{N}{\pi D\ 0.93 \cos\phi} + \frac{1}{2S_1\ 0.93}\right]\left[\frac{2\dot{Q}}{D S_1 \pi\ 0.93 \cos\phi}\right]^2 d\phi$$

(D-18)

Expanding and collecting terms gives:

$$H_f = a\int_{-\phi_1}^{\phi_2} \frac{d\phi}{\cos^3\phi} + b\int_{-\phi_1}^{\phi_2} \frac{d\phi}{\cos^2\phi} + c\int_{-\phi_1}^{\phi_2} \frac{d\phi}{\cos\phi} \tag{D-19}$$

where:

$$a = \frac{53\mu}{2 g_c \rho}\ \frac{N^2\dot{Q}}{0.93^3\ \pi^3\ S_1\ D^2} + \frac{N\dot{Q}^2}{4\,(6.6046) g_c\ 0.93^3\ \pi^3\ D^2\ S_1{}^2}$$

$$b = \frac{53\mu}{2 g_c \rho}\ \frac{N\dot{Q}}{0.93^3\ \pi^2\ D S_1{}^2} + \frac{\dot{Q}^2}{8\,(6.6046) g_c\ 0.93^3\ \pi^2\ D S_1{}^3}$$

$$c = \frac{53\mu}{8 g_c \rho}\ \frac{\dot{Q}}{0.93^3\ \pi\ S_1{}^3}$$

Integrating

$$\int_{-\phi_1}^{\phi_2} \frac{d\phi}{\cos^3\phi} = \frac{\sin\phi}{2\cos^2\phi}\Bigg|_{-\phi_1}^{\phi_2} + \frac{1}{2}\int_{-\phi_1}^{\phi_2} \frac{d\phi}{\cos^2\phi}$$

$$\int_{-\phi_1}^{\phi_2} \frac{d\phi}{\cos^2\phi} = \tan\phi\Bigg|_{-\phi_1}^{\phi_2}$$

$$\int_{-\phi_1}^{\phi_2} \frac{d\phi}{\cos\phi} = \ell\eta\tan\left(\frac{\pi}{4}+\frac{\phi}{2}\right)\Bigg|_{-\phi_1}^{\phi_2} \qquad \text{(D-20)}$$

so that:

$$H_f = \frac{a}{2}\left(\frac{\sin\phi_2}{\cos^2\phi} + \frac{\sin\phi_1}{\cos^2\phi_1}\right) + \left(\frac{a}{2}+b\right)(\tan\phi_2 + \tan\phi_1)$$

$$+ c\left(\ell\eta\left[\tan\frac{(\phi_2+\pi/2)}{2} \Big/ \tan\frac{(\pi/2-\phi_1)}{2}\right]\right) \qquad \text{(D-21)}$$

The pertinent equations were programmed for the MDAC Direct Access Computing System, and were used to determine Safety Factor and residual during outflow and annulus TVS flow and pressure distribution for the pleated liner in the same fashion as was shown in Appendix B for a plain liner.

REFERENCES

1. S. C. DeBrock et al: A Survey of Current Developments in Surface Tension Devices for Propellant Acquisition. AIAA Paper No. 70-685, June 1970.

2. H. L. Paynter and G. R. Page: Final Report, Acquisition/Expulsion System for Earth Orbital Propulsion System Study. Vol. II, Cryogenic Design. MMC Report MCR-73-97, October 1973.

3. B. R. Bullard: Wall-Mounted Heat Exchanger Characterization. NASA CR-134536, January 1975.

4. W. H. Sterbentz: Liquid Propellant Thermal Conditioning System. Lockheed Missiles and Space Company, Report LMSC K-07-68-2 (NASA CR-72365), August 1968.

5. J. A. Stark and M. H. Blatt: Cryogenic Zero-Gravity Prototype Vent System. General Dynamics/Convair Report GDC-DD967-006, October 1967.

6. E. C. Cady: Study of Thermodynamic Vent and Screen Baffle Integration for Orbital Storage and Transfer of Liquid Hydrogen. McDonnell Douglas Astronautics Company Report MDC G4798 (NASA CR-13448[illegible]), August 1973.

7. E. G. Brentari et al: Boiling Heat Transfer for Oxygen, Nitrogen, Hydrogen, and Helium. NBS Technical Note No. 317, September 1965.

8. E. C. Cady: Design and Evaluation of Thermodynamic Vent/Screen Baffle Cryogenic Storage System. Vol. I, Technical Proposal. McDonnell Douglas Astronautics Company Report MDC G4805P, September 1973.

9. Personal communication between E. C. Cady, MDAC, and J. R. Hamm and G. H. Caine, Sundstrand Corporation.

10. R. E. Sexton: In-Space Propellant Logistics. Vol. II, Technical Report. North American Rockwell Report SD 72-SA-0053-2, June 1972.

11. T. M. Lovrich and S. H. Schwartz: Development of Thermal Stratification and Destratification Scaling Concepts. Vol. I. McDonnell Douglas Astronautics Company Report MDC G4753, July 1973.

12. J. R. Van Hook and L. J. Poth: A Study of Cryogenic Fluid Mixing Techniques. General Dynamics Report FZA-450-1, 15 September 1970.

13. G. H. Caine and A. V. Pradhan: Pumps or Fans for Destratification of Hydrogen Liquid and Gas. Advances in Cryogenic Engineering, Plenum Press, New York, 1968. Volume 13, P. 728

14. D. R. Krause: Development of Lightweight Material Composites to Insulate Cryogenic Tanks for 30-day Storage in Outer Space. McDonnell Douglas Astronautics Company Report MDC G2742, June 1972.

15. J. B. Blackmon: Design, Fabrication, Assembly, and Test of a Liquid Hydrogen Acquisition Subsystem. McDonnell Douglas Astronautics Company Report MDC G5360, May 1974.

16. E. M. Sparrow and J. L. Gregg: Buoyancy Effects in Forced Convection Flow and Heat Transfer. Transactions of the ASME, Journal of Applied Mechanics, Sect. E, Vol. 81, 1959, PP. 133-135.

17. J. B. Blackmon, J. N. Castle, and B. R. Heckman: Propellant Settling. Douglas Aircraft Company Report DAC-62263, May 1968.

18. D. F. Gluck et al: Distortion of a Free Surface During Tank Discharge. Journal of Spacecraft and Rockets, November 1966; Vol. 3, No. 11, P. 1691-1692.

19. T. L. Labus: Liquid-Vapor Interface Configuration in Annular Cylinders. NASA TM X-1973, March 1970.

20. M. L. Davis et al: The Development of Cryogenic Storage Systems for Space Flight. NASA SP-247, 1970.

21. H. M. Roder and R. D. Goodwin: Extended Tables of Provisional Thermodynamic Functions for Para Hydrogen. NBS Report 7220, January 1962.

22. L. A. Weber: Thermodynamic and Related Properties of Oxygen from the Triple Point to 300°K at Pressures to 330 Atmospheres. NBS Report 9710, June 1968.

23. C. J. Menard: High Energy Density Nickel-Cadmium Batteries. IECEC Paper No. 729020, 1972.

24. J. K. Wilson et al: High Energy Density Long-Life Secondary Silver-Zinc Batteries. IECEC Paper No. 709067, 1970.

25. F. Kreith: Principles of Heat Transfer — Second Edition. International Textbook Co., 1965.

26. D. E. Drayer and K. D. Timmerhaus: An Experimental Investigation of the Individual Boiling and Condensing Heat Transfer Coefficients for Hydrogen. Advances in Cryogenic Engineering, 1962; Vol. 7, P. 401-412.

27. Procurement Specification: Storage Assembly, Power Reactant — Orbiter. Rockwell Document No. MC282-0063, Rev. C., 21 June 1974.

28. Personal Communication between E. C. Cady, MDAC, and Robert Antell, PRSA Subsystem Manager, Rockwell International.

29. Personal communication between E. C. Cady, MDAC, and Keith Pearson, Director of Engineering, General Nucleonics Division of Tyco Laboratories.

30. Proposal for the Spacelab Design and Development Contract to ESRO/ESTEC. RFP A0/600. Volume 1, Technical. 16 April 1974.

31. G. W. Burge and J. B. Blackmon: Study and Design of Cryogenic Propellant Acquisition Systems — Volume II, Supporting Experimental Program, Final Report. NAS8-27685. McDonnell Douglas Astronautics Company Report MDC G5038, December 1973.

32. J. N. Castle: Heat Transfer Effects on Bubble Point Tests in Liquid Nitrogen. McDonnell Douglas Astronautics Company Report MDC G2653, January 1973.

33. Acquisition System Environmental Effects Study, Final Report, NAS8-30592. Martin Marietta Report MCR-75-21, May 1975.

34. J. R. Buckingham: Final Report, Shuttle Filter Study — Volume I. Wintec Report No. WDB2000, June 1974.

35. E. R. G. Eckert and T. F. Irvine: Incompressible Friction Factor. Transition and Hydrodynamic Entrance Length Studies of Ducts with Triangular and Rectangular Cross-Sections. WADC Technical Report 58-85 (ASTIA Document No. AD151027), April 1957.